AD-A077 895 ILLINOIS UNIV AT URBANA-CHAMPAIGN ELECTROMAGNETICS LAB F/G 20/3
INVESTIGATION OF TRANSFORM TECHNIQUES FOR SOLVING ELECTROMAGNET--ETC(U)
DEC 79 R MITTRA , S W LEE , W L KO N00014-75-C-0293
UNCLASSIFIED UIEL-79-13 NL

1 OF 2
AD A077895

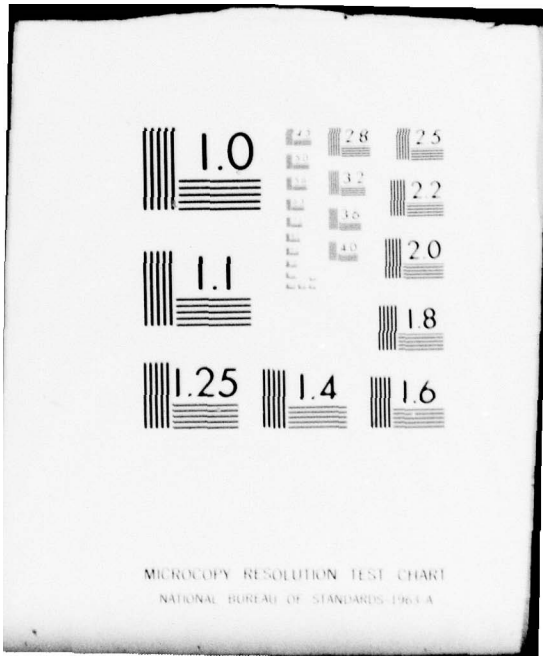
1.0
1.1
1.25
1.4
1.6
2.8
3.2
3.6
4.0
2.5
2.2
2.0
1.8
MICROCOPY RESOLUTION TEST CHART
NATIONAL BUREAU OF STANDARDS 1963-A

ELECTROMAGNETICS LABORATORY
TECHNICAL REPORT NO. 79-13

December 1979

LEVEL II

INVESTIGATION OF TRANSFORM TECHNIQUES FOR SOLVING ELECTROMAGNETIC RADIATION AND SCATTERING PROBLEMS

Technical Report

R. Mittra

S. W. Lee

W. L. Ko

ELECTROMAGNETICS LABORATORY
DEPARTMENT OF ELECTRICAL ENGINEERING
ENGINEERING EXPERIMENT STATION
UNIVERSITY OF ILLINOIS AT URBANA-CHAMPAIGN
URBANA, ILLINOIS 61801

Supported by
Contract No. N00014-75-C-0293
Office of Naval Research
Department of the Navy
Arlington, Virginia 22217

UNCLASSIFIED

SECURITY CLASSIFICATION OF THIS PAGE (When Data Entered)

REPORT DOCUMENTATION PAGE		READ INSTRUCTIONS BEFORE COMPLETING FORM
1. REPORT NUMBER	2. GOVT ACCESSION NO.	3. RECIPIENT'S CATALOG NUMBER
4. TITLE (and Subtitle) INVESTIGATION OF TRANSFORM TECHNIQUES FOR SOLVING ELECTROMAGNETIC RADIATION AND SCATTERING PROBLEMS		5. TYPE OF REPORT & PERIOD COVERED Technical Report December 1979 6. PERFORMING ORG. REPORT NUMBER EM 79-13; UILU-ENG-79-2560
7. AUTHOR(s) R. Mittra, S. W. Lee and W. L. Ko		8. CONTRACT OR GRANT NUMBER(s) N00014-75-C-0293
9. PERFORMING ORGANIZATION NAME AND ADDRESS Electromagnetics Laboratory Department of Electrical Engineering University of Illinois, Urbana, IL 61801		10. PROGRAM ELEMENT, PROJECT, TASK AREA & WORK UNIT NUMBERS
11. CONTROLLING OFFICE NAME AND ADDRESS Office of Naval Research Department of the Navy Arlington, Virginia 22217		12. REPORT DATE December 1979 13. NUMBER OF PAGES 132
14. MONITORING AGENCY NAME & ADDRESS(if different from Controlling Office)		15. SECURITY CLASS. (of this report) UNCLASSIFIED 15a. DECLASSIFICATION/DOWNGRADING SCHEDULE

16. DISTRIBUTION STATEMENT (of this Report)

Distribution Unlimited. Reproduction in whole or in part is permitted for any purpose of the United States Government.

17. DISTRIBUTION STATEMENT (of the abstract entered in Block 20, if different from Report)

18. SUPPLEMENTARY NOTES

19. KEY WORDS (Continue on reverse side if necessary and identify by block number)

high-frequency diffraction; antennas; GTD; and Fourier transform.

20. ABSTRACT (Continue on reverse side if necessary and identify by block number)

In this project, we attack electromagnetic scattering and the diffraction problems by using a spectral domain formulation, which generally yields accurate results in a numerically efficient manner. Several published papers are attached in which the research was supported by this project.

DD FORM 1 JAN 73 1473 EDITION OF 1 NOV 65 IS OBSOLETE

UNCLASSIFIED

SECURITY CLASSIFICATION OF THIS PAGE (When Data Entered)

(17) UIEL-79-13

UILU-ENG-79-2560

Electromagnetics Laboratory Report No. 79-13

(6)

INVESTIGATION OF TRANSFORM TECHNIQUES FOR SOLVING ELECTROMAGNETIC RADIATION AND SCATTERING PROBLEMS

(9) Technical Report

(10) R. Mittra
S. W. Lee
W. L. Ko

(12) 137

(11) December 1979

Office of Naval Research
Department of the Navy
Arlington, Virginia 22217

(15) Contract No. N00014-75-C-0293

Electromagnetics Laboratory
Department of Electrical Engineering
Engineering Experiment Station
University of Illinois at Urbana-Champaign
Urbana, Illinois 61801

408 192 1/6

TABLE OF CONTENTS

		Page
I.	INTRODUCTION AND REVIEW OF RESEARCH ACCOMPLISHED DURING THE PRESENT GRANT PERIOD.	1
II.	PROPOSED EFFORT FOR THE NEXT GRANT PERIOD	3
	A. Application of the Spectral Domain Approach to Canonical-Type Problems.	3
	B. Application of Spectral Domain Approach to Complex Structures . .	4
	C. Analysis of Frequency Selective Surface Using the Spectral Domain Approach	5
III.	ATTACHMENTS	10
	A. Solution of Electromagnetic Scattering and Radiation Problems Using a Spectral Domain Approach - A Review By R. Mittra, W. L. Ko and Y. Rahmat-Samii*	
	B. Penetration of an EM Wave into a Cylindrical Cavity and the Current Induced on a Wire Inside By E. K. Yung, S. W. Lee and R. Mittra	
	C. Accuracy Test for High-Frequency Asymptotic Solutions By R. Mittra and M. Tew	
	D. Source Radiation in the Presence of Smooth Convex Bodies By R. Mittra and S. Safavi-Naini	
	E. Accuracy Tests and Iterative Procedures for High Frequency Asymptotic Solutions - a Spectral Domain Approach By R. Mittra and M. Tew	
	F. An Integral E-Field Accuracy Test for High Frequency Asymptotic Solutions By M. Tew and R. Mittra	
	G. Transform Approach to Electromagnetic Scattering By R. Mittra, W. L. Ko, and Y. Rahmat-Samii	

*Each attachment has its own pagination.

I. INTRODUCTION AND REVIEW OF RESEARCH ACCOMPLISHED DURING THE PRESENT GRANT PERIOD

During the present grant period, we have made considerable progress in developing the Spectral Domain Approach for solving radiation and scattering problems. The fundamental concepts of the Spectral Domain Approach for solving electromagnetic problems have been described in an invited paper entitled, "Transform Approach to Electromagnetic Scattering," which will soon appear in Proceedings of the IEEE. In this paper we have also illustrated a number of important applications of the spectral approach and have demonstrated the accuracy and reliability of this method by solving problems that are not tractable with Keller's GTD. The reliability of the method derives from the fact that the boundary condition check is built-in in the procedure for constructing the solution. The spectral approach can also be used to verify the accuracy of any given solution, regardless of how the solution was derived. We have described this work in a chapter of a book on "Classical Wave Scattering," which is to be published by Academic Press. This chapter deals with the topic of accuracy tests for asymptotic solutions using the spectral domain approach. We have also presented the material described in the above two publications in a NATO Advanced Study Institute in England in August of 1979.

The problem of radiation from sources located on smooth convex surfaces has been discussed in two publications. One of these is an invited paper in the Hans Bremmer 75th Anniversary issue of Radio Science and the other is a paper submitted for possible publication in the Transactions of IEEE Antenna and Propagation Society. Other publications that have either appeared during the year 1979 or prepared for publication

during the present grant period are attached herewith. Six symposium presentations describing the results of spectral domain analysis have been presented at domestic and international technical meetings.

II. PROPOSED EFFORT FOR THE NEXT GRANT PERIOD

During the next grant period, we propose to investigate three different aspects of the spectral domain approach for solving electromagnetic radiation and scattering problems. As indicated in Section I, we have made considerable progress during the last grant period toward developing the spectral domain approach, and have demonstrated its usefulness by solving a number of problems which are not tractable using Keller's GTD. During the next grant period, we propose to investigate additional canonical geometries for which the GTD solution is either unavailable or unreliable. We also propose to apply the spectral domain technique to a number of complex structures in order to fully develop an appreciation of the scope and limitations of the approach. Finally, during the present grant period we have discovered that the spectral domain approach has an inherent potential for solving a new class of problems which cannot be accurately solved either via the asymptotic techniques, e.g., GTD, or by the low-frequency techniques. We provide brief descriptions of the proposed efforts in these three areas in the paragraphs below.

A. Application of the Spectral Domain Approach to Canonical-Type Problems

Having demonstrated the usefulness of the spectral approach to the finite strip problem, we propose to extend the approach to the more complex problems of the curved strip, strips of finite thickness, and plates with sharp or curved corners (see Fig. 1). Preliminary analysis of the curved strip has shown that its GTD solution can be inaccurate for certain angles of observation, particularly when these are away from the direction of specular reflection. We propose to employ the spectral approach to

derive expressions for the scattered field that make express use of the available GTD solutions but do not suffer from their deficiencies. The results obtained will be useful for many complex, curved-surface, scattering structures with edges, e.g., reflector antennas. We will discuss some of these applications in Section B below.

Returning to the canonical-type problems, the next modification of the thin edge problem we wish to consider is the thick strip problem which cannot be handled using the conventional GTD because the typical thickness of the strip is on the order of one wavelength or less. However, in the spectral approach we can begin with the thin strip solution and incorporate it into the transform method to derive an accurate solution to the thick strip problem in a systematic manner.

The third problem in this category that we propose to consider is that of scattering by a plate with either sharp or rounded corners. Recently, a number of corner diffraction coefficients have been proposed for handling the sharp corner problem. The spectral domain approach is not only able to verify the validity and accuracy of these solutions but to systematically refine them as well.

Before closing this section, we would like to point out an important and unique characteristic of the spectral approach, viz., it provides a built-in boundary condition check not available in any other high frequency technique. Thus, the solution generated via the spectral domain approach is always reliable and does not require the use of independent checks for its validation.

B. Application of Spectral Domain Approach to Complex Structures

It is always desirable to consider the application of a solution technique to practical geometries that are not just test or canonical problems, though

the latter are useful in their own right in the early developmental stages of any new method.

Consequently, the second class of problems we propose to consider has relatively more complex geometries, those which require the use of the canonical solution developed during the first stages of the proposed effort. The types of geometries we propose to consider are those for reflector antennas, masts and struts of rectangular and circular cross section, leaky-wave radiators comprising metal strips on a dielectric substrate, planar waveguides for optical and quasi-optical wave propagation, and microstrip-type antennas. At the end of the first grant period, we expect to have the necessary tools for attacking all of the problems listed above. For instance, for the reflector antenna problem we would use the solution for the curved surface with edges. For the mast scattering problem, we can make use of an efficient and accurate procedure for calculating the scattered far field that employs a combination of equivalent Huyghens' source and Fourier transform techniques. For the microstrip and leaky-wave radiation problems, the spectral domain approach offers a very convenient representation for the Green's function, i.e., for the problem of a current source located above, or inside, the dielectric substrate. The solution to the above class of radiation problems is derived by applying the Galerkin method in the Fourier transform domain.

C. Analysis of Frequency Selective Surfaces Using the Spectral Domain Approach

Frequency selective surfaces find important applications in antenna radomes, Cassegrainian-type reflector antennas, and gratings and filters for optical, infra-red and millimeter waves. As shown in Fig. 3, a typical example of such a surface is a perforated metal sheet placed on a dielectric support. In the past, the analysis of such a screen has been carried out

using the moment method or the mode-matching method, both of which are useful for solving the problem when the cell size of the mesh is on the order of a wavelength or less. Beyond that, the matrix size required to solve the problem can become prohibitively large, and the computer cost as well as storage requirements make these approaches impractical to apply to the problem under consideration.

During the present grant period, we have discovered that the spectral domain approach offers an extremely accurate and efficient way for attacking the problem of a periodic array of apertures with or without a dielectric substrate. We have established that the spectral approach can handle upward of 2^{11} (= 2048) unknowns*, which in the case of the present problem are the complex Floquet space harmonic amplitudes. We can determine these many unknowns accurately with only 5 to 6 seconds of CPU time on the CDC Cyber 175 computer. In contrast, a matrix approach for determining 2000 unknowns is estimated to require 8 hours of computer time! An added advantageous feature of the spectral approach is that the reliability of the solution is guaranteed, since the boundary condition check is built-in the algorithm for constructing the solutions.

We propose to analyze the various, frequency-selective surfaces with parameter choices that would make them suitable for different applications, e.g., filters, radomes and reflectors mentioned earlier in this section.

---

*Note that using the usual guideline of unknowns per wavelength, a $4\lambda \times 4\lambda$ cell size would require 1024 unknowns for each of the two components of the current or aperture field, and hence the total number of unknowns would be 2048.

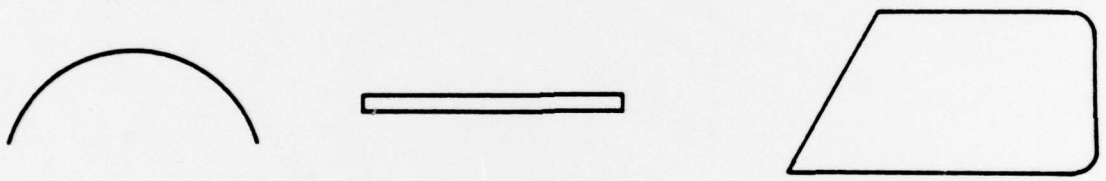

(a) Curved edge

(b) Thick strip

Plate with sharp
and rounded corners

Fig. 1. Canonical type geometries.

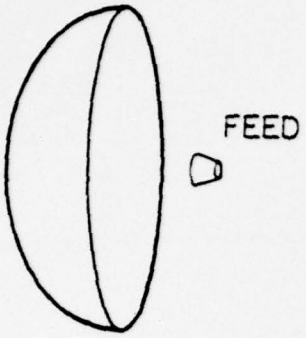

(a) Reflector antenna

(b) Scattering by a mast

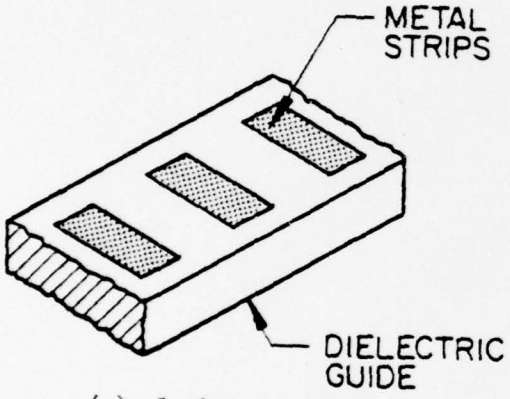

(c) Leaky wave antenna

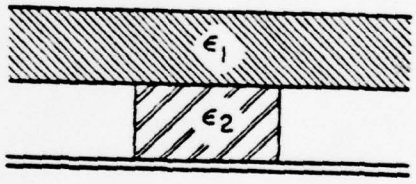

(d) Quasi-optical waveguide

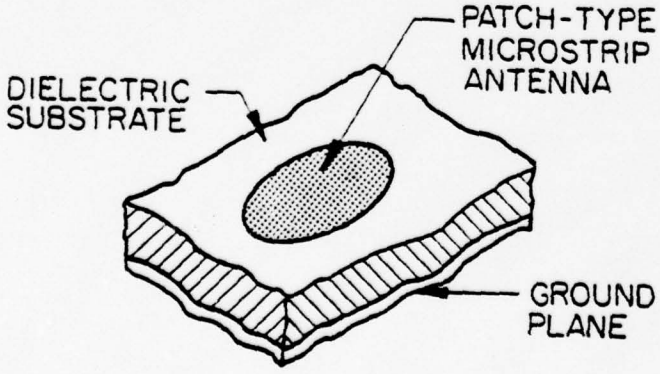

(e) Microstrip antenna problem

Fig. 2. Problems to be solved using the spectral domain approach.

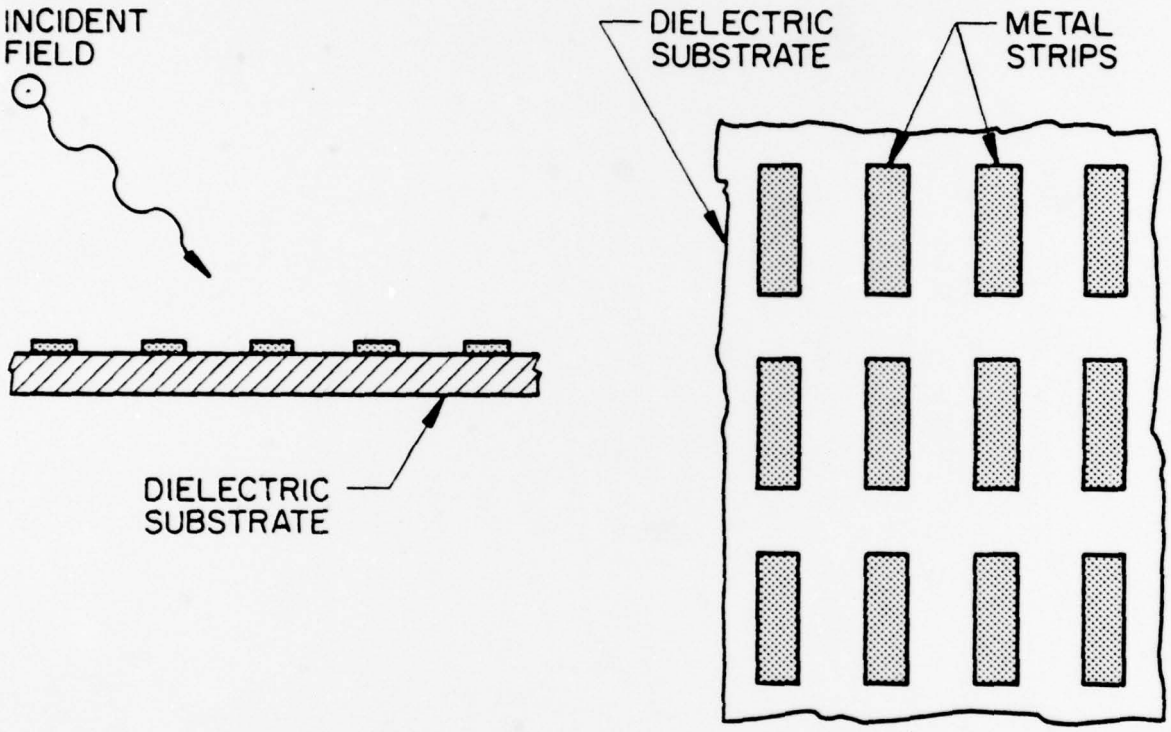

(a) Side view

(b) Top view

Fig. 3. Periodic mesh on a dielectric substrate with application to radomes, optical gratings and reflector antennas.

III. ATTACHMENTS

A

WAVE MOTION 1 (1979) 95–106.

SOLUTION OF ELECTROMAGNETIC SCATTERING AND RADIATION PROBLEMS USING A SPECTRAL DOMAIN APPROACH—A REVIEW

R. MITTRA, W.L. KO and Y. RAHMAT-SAMII*
Electrical Engineering Department, University of Illinois, Urbana, Il 61801, U.S.A.

Received 3 April 1978, revised 4 September 1978

In this paper we present a brief review of some recent developments on the use of the spectral-domain approach for deriving high-frequency solutions to electromagnetics scattering and radiation problems. The spectral approach is not only useful for interpreting the well-known Keller formulas based on the geometrical theory of diffraction (GTD), it can also be employed for verifying the accuracy of GTD and other asymptotic solutions and systematically improving the results when such improvements are needed. The problem of plane wave diffraction by a finite screen or a strip is presented as an example of the application of the spectral-domain approach.

1. Introduction

Asymptotic solutions of differential equations are extremely useful in many branches of mathematical physics. In electromagnetics, these solutions are constructed [1] directly from the solution of Maxwell's equations and are valid in the high-frequency regime, i.e. $k \to \infty$, where k ($= 2\pi/\lambda$) is the wave number and λ is the wavelength of the incident illumination. An alternate approach to the solution of Maxwell's equations for electromagnetic scattering problems entails the initial step of converting the partial differential equations into an integral equation via the use of the Green's function. Such an equation is self-contained, since the boundary conditions are already "built-in" during the process of its derivation. However, at high frequencies, where the characteristic dimension of the scatterer becomes very large compared to the wavelength, numerical solution of the integral equation becomes very unwieldy if not impractical, because the size of the matrix equation [2] for the unknown surface current on the scatterer becomes prohibitively large. Thus, an asymptotic solution based on GO (geometrical optics), or its refined version GTD (geometrical theory of diffraction), is widely used in the high-frequency regime [3–7]. The ray methods, which encompass GO and GTD, find extensive applications, not only in electromagnetics and acoustics, but in other fields of wave propagation as well.

However, these methods, although extremely useful, have certain limitations which must be fully appreciated by the user in order to assess their applicability to the specific problem. The original form of the Keller GTD formulas needs modifications at shadow boundaries [4,8], which separate the lit and shadow regions and in the neighborhood of caustics where the rays intersect each other, e.g., in the neighborhood of the focus of a parabolic reflector illuminated by a plane wave. Finally, it is difficult to estimate the accuracy of the GTD solution for a given problem; no systematic approach for improving the solution has been available within the framework of the ray methods, except via the use of multiply diffracted

* Currently with NASA Jet Propulsion Laboratory, California Institute of Technology, Pasadena, California 91103.

rays, a process which can lead to a divergent series.

In this paper, we illustrate the application of a recently-developed method, called the "spectral domain" technique [8–10], that views the asymptotic method from a different perspective. The spectral approach, which is based on a combination of Fourier transform and integral equation techniques, regards the high frequency asymptotic solution for electromagnetic scattering as an asymptotic evaluation of the integral representation for the scattered field, which may be expressed as an integral over the Fourier spectrum of the surface current distribution on the scatterer. Strictly speaking, such an interpretation of the asymptotic solution is not geometric in nature; however, it has been shown [8, 9] that the GTD solution, where valid, is indeed identifiable with the asymptotic result derived from the evaluation of the transform integral. One also finds that the integral representation provides a uniform solution for the field even at shadow boundaries and caustic regions where GTD formulas need modification. Furthermore, systematic improvement of the GTD solution is possible in the spectral domain by combining the GTD approach with the integral-equation formulation. An example of such a procedure for refining GTD solutions via the use of the spectral domain approach is included in the paper. A unique advantage of the method is that it provides a convenient accuracy test for the solution, a feature that is unavailable in other asymptotic techniques for solving high-frequency scattering problems.

It should be pointed out that the spectral approach does not gain these advantages over the conventional GTD methods without some cost. The beauty and simplicity of Keller's geometric interpretation of wave propagation at high frequency in terms of the ray picture, and the "local" character of the propagation of fields are no longer present in the integral representation, until after the spectral integral has been asymptotically evaluated. On the other hand, it is well-recognized that the difficulties in the GTD formulas are encountered precisely in the situations where the local character of the field propagation breaks down. Consequently, and non-unexpectedly, an integral over a wider region of the scatterer, rather than just the neighbourhood of the specular reflection points, or edge points, contributes to the scattered far field, a phenomenon which is in line with spectral domain interpretation of high-frequency diffraction phenomena.

2. Spectral domain approach to verification and refinement of asymptotic solutions

One of the most challenging problems in the solution of high-frequency scattering analyses is the establishment of the accuracy of the results and the refinement of the solution when the need for its improvement is clearly indicated. The difficulty in verifying whether the asymptotic expression, typically derived from the GTD approach, does indeed solve the boundary value problem under consideration stems primarily from the fact that there is no obvious way to "build in" the boundary conditions in solution procedures based on ray methods. Another reason is that the high-frequency solutions are often constructed for the radiated far fields, whereas the application of the boundary conditions clearly requires the near-field information. In contrast, the integral-equation formulation for the scattering problem is based directly on the application of the boundary condition and, consequently, the boundary-condition check is redundant for this approach. However, the conventional moment-method solution of integral equations is limited strictly to the low-frequency and resonance regions as the matrix size becomes unmanageably large beyond the resonance region.

In this section we will briefly outline a spectral-domain method for bridging the two approaches, viz., the integral-equation and asymptotic techniques. The hybrid method has the desirable feature that it not only verifies the accuracy of the ray

solutions but provides a systematic means for improving the solution for a large class of problems of practical interest. This fact will be illustrated via a typical example, viz., plane-wave diffraction by a strip. Other cases have also been treated and may be found in [10–13].

2.1. Development of spectral-domain formulation of the integral equation and its approximate solution

The key to combining the asymptotic solution with the integral-equation formulation lies in recognizing the fact that the Fourier transform of the induced current on a scatterer is directly related to the scattered far field and that a good approximation to this scattered field is often available from any asymptotic methods, e.g., GTD. To take advantage of these facts we choose to work with the "Fourier-transformed" or "spectral-domain" version of the integral equation rather than with the conventional spatial-domain counterpart. We begin, however, with the conventional electric-field integral equation (E-equation) for a perfectly conducting scatterer:

$$(\mathbf{G} * \boldsymbol{J})_t = -\boldsymbol{E}^i_t,$$
$$\mathbf{G} = (\mathbf{I} + k^{-2}\nabla\nabla)\, e^{ik|\boldsymbol{r}-\boldsymbol{r}'|}/(4\pi|\boldsymbol{r}-\boldsymbol{r}'|) \tag{1}$$

where $\mathbf{G}$ is the Green's dyadic, $\mathbf{I}$ is the unit dyad and $J(\boldsymbol{r}')$ is the unknown induced surface current density. The subscript t signifies the tangetial component of the field on the surface S of the scatterer, $\boldsymbol{E}^i$ is the incident electric field on the scatterer, and "$*$" symbolizes the convolution operation.

As a preamble to Fourier transforming (1), we first extend it over all space. To this end we define a truncation operator $\theta(\boldsymbol{A})$,

$$\theta(\boldsymbol{A}) = \int \boldsymbol{A}_t \delta(\boldsymbol{r} - \boldsymbol{r}_s)\, d\boldsymbol{r}, \quad \boldsymbol{r}_s \in S, \tag{2}$$

where δ is the Dirac delta function. Let $\hat{\theta}(\boldsymbol{A})$ be defined as the complementary operator

$$\hat{\theta}(\boldsymbol{A}) = \boldsymbol{A} - \theta(\boldsymbol{A}). \tag{3}$$

We can then rewrite (1)

$$\mathbf{G} * \boldsymbol{J} = \theta(-\boldsymbol{E}^i) + \hat{\theta}(\mathbf{G} * (\theta \boldsymbol{J})) \tag{4}$$

for all space.

As indicated above, in contrast to (1), (4) is valid at all observation points whether on or off the surface S. Note that the integral equation (1) is embedded in (4) and that we have made use of the obvious identity $\theta \boldsymbol{J} = \boldsymbol{J}$. We have also dropped the subscript t in writing (4), because by referring to (2) we observe that the θ operator selects the tangential component of the function in its argument.

Next we Fourier transform (4) by introducing the transform relationships

$$\tilde{F}(\boldsymbol{k}) = \int_{-\infty}^{\infty} F(\boldsymbol{r})\, e^{-i\boldsymbol{k}\cdot\boldsymbol{r}}\, d\boldsymbol{r} = \mathcal{F}[F(\boldsymbol{r})] \tag{5a}$$

and

$$F(\boldsymbol{r}) = \left(\frac{1}{2\pi}\right)^3 \int_{-\infty}^{\infty} \tilde{F}(\boldsymbol{k})\, e^{i\boldsymbol{k}\cdot\boldsymbol{r}}\, d\boldsymbol{k} = \mathcal{F}^{-1}[\tilde{F}(\boldsymbol{k})] \tag{5b}$$

with $\sim$ on top denoting the transformed quantities.

The transformed version of (4) reads

$$\tilde{\mathbf{G}}\tilde{\boldsymbol{J}} = -\tilde{\boldsymbol{E}}_1 + \tilde{\boldsymbol{F}} \tag{6}$$

where $\tilde{\boldsymbol{F}} = \mathcal{F}[\hat{\theta}(\mathbf{G} * (\theta \boldsymbol{J}))]$ and $\tilde{\boldsymbol{E}}_1$ is the transform of the tangential component of the incident field truncated on S. Note that the convolution operation in (4) is transformed into an algebraic product upon Fourier transformation.

A formal solution to (6) can now be written as

$$\tilde{\boldsymbol{J}} = \tilde{\mathbf{G}}^{-1}(-\tilde{\boldsymbol{E}}_1 + \tilde{\boldsymbol{F}}). \tag{7}$$

Equation (7) implies that if we had available the Fourier transform of the scattered electric field, we could construct the solution for the induced surface current density in the transform domain by adding it to $-\tilde{\boldsymbol{E}}_1$, which is known, and by performing an algebraic division represented by $\tilde{\mathbf{G}}^{-1}$. In practice, of course, $\tilde{\boldsymbol{F}}$ is not known and must be solved for along with $\tilde{\boldsymbol{J}}$ if (7) is to be used in the form as shown. However, instead of using this

form, we proceed to derive an iterated form of the equation as shown below:

$$\tilde{\boldsymbol{J}}^{(n+1)} = \tilde{\mathbf{G}}^{-1}(-\tilde{\boldsymbol{E}}_1 + \tilde{\boldsymbol{F}}^{(n)}) \tag{8}$$

which indicates the $(n+1)$th approximation of $\tilde{\boldsymbol{J}}$ can be derived from the nth approximation for $\tilde{\boldsymbol{F}}$. We next show how $\tilde{\boldsymbol{F}}^{(n)}$ itself can be derived from $\tilde{\boldsymbol{J}}^{(n)}$. To this end, we use the identity

$$\tilde{\boldsymbol{F}} = \mathcal{F}[\mathcal{F}^{-1}[\tilde{\mathbf{G}}\tilde{\boldsymbol{J}}] - \theta(\mathcal{F}^{-1}[\tilde{\mathbf{G}}\tilde{\boldsymbol{J}}])] \tag{9}$$

which may be verified by writing (9) as

$$\tilde{\boldsymbol{F}} = \mathcal{F}[\mathbf{G} * \boldsymbol{J} - \theta(-\boldsymbol{E}^i)] \tag{10}$$

and using (4) to get

$$\tilde{\boldsymbol{F}} = \mathcal{F}[\hat{\theta}(\mathbf{G} * (\theta \boldsymbol{J}))] \tag{11}$$

which, of course, is the definition of $\tilde{\boldsymbol{F}}$. We can now use (9) to derive the nth approximation $\tilde{\boldsymbol{F}}^{(n)}$ of $\tilde{\boldsymbol{F}}$ from the nth approximation of $\boldsymbol{J}$, i.e., $\boldsymbol{J}^{(n)}$. The relationship is written as

$$\tilde{\boldsymbol{F}}^{(n)} = \mathcal{F}[\mathcal{F}^{-1}[\tilde{\mathbf{G}}\tilde{\boldsymbol{J}}^{(n)}] - \theta(\mathcal{F}^{-1}[\tilde{\mathbf{G}}\tilde{\boldsymbol{J}}^{(n)}])]. \tag{12}$$

The desired iterating relation $\tilde{\boldsymbol{J}}^{(n+1)}$ and $\tilde{\boldsymbol{J}}^{(n)}$ may now be written. Using (8) and (12),

$$\tilde{\boldsymbol{J}}^{(n+1)} = \tilde{\mathbf{G}}^{-1}[-\tilde{\boldsymbol{E}}_t + \mathcal{F}[\mathcal{F}^{-1}[\tilde{\mathbf{G}}\tilde{\boldsymbol{J}}^{(n)}] - \theta(\mathcal{F}^{-1}[\tilde{\mathbf{G}}\tilde{\boldsymbol{J}}^{(n)}])]]. \tag{13}$$

2.2. Procedure for applying the method

The step-by-step procedure for constructing the solution of the transformed surface current $\tilde{\boldsymbol{J}}$ will now be given.

(1) Begin with an estimate of $\tilde{\boldsymbol{J}}^{(0)}$, which is the Fourier transform of the induced surface current, or equivalently, the scattered *far field* within a known multiplicative factor. That the far scattered field is directly related to the Fourier transform of the induced current is well-known in electromagnetics and has been derived in several standard texts (see for instance Eq. (2.23b) of [14]). Typically, the initial approximation for $\tilde{\boldsymbol{J}}$, viz., $\tilde{\boldsymbol{J}}^{(0)}$, can be obtained as follows:

(a) Estimate $\tilde{\boldsymbol{F}}$, the Fourier transform of the scattered field, $\boldsymbol{F}$, outside the scatterer, using GTD or other asymptotic solutions.[1]

(b) Subtract $\tilde{\boldsymbol{E}}_1$, the Fourier transform of the tangential component of the incident electric field truncated to the surface of the scatterer.

(c) Multiply the result of Step (b) by $\tilde{\mathbf{G}}^{-1}$. Note that $\tilde{\mathbf{G}}^{-1}$ is known and the operation is algebraic.

(d) Take the inverse Fourier transform of the result of Step (c) and truncate it to the surface of the scatterer to obtain $\tilde{\boldsymbol{J}}^{(0)}$, the initial approximation for $\tilde{\boldsymbol{J}}$. The Fourier transform is typically done numerically using the Fast Fourier Transform (FFT).

(2) Multiply $\tilde{\boldsymbol{J}}^{(0)}$ by $\tilde{\mathbf{G}}$, the known transform of the Green's Dyadic. Note this involves algebraic multiplication and not the usual time-consuming convolution operation.

(3) Take the inverse Fourier transform of the product $\tilde{\mathbf{G}}\tilde{\boldsymbol{J}}^{(0)}$ using both *visible and invisible ranges.*

(4) Apply the truncation operator θ to $\mathcal{F}^{-1}[\tilde{\mathbf{G}}\tilde{\boldsymbol{J}}^{(0)}]$, which gives the approximation to the tangential component of the scattered electric field $\boldsymbol{E}_t^s$ on the surface S. The accuracy of the solution can be conveniently checked at this point by verifying the satisfaction of the boundary condition by the tangential component of $\boldsymbol{E}^s$, viz., $\{\boldsymbol{E}_t^s = -\boldsymbol{E}_t^i\}$ on S. As mentioned in the introduction, this is an important feature of the method.

(5) Subtract $\theta(\mathcal{F}^{-1}[\tilde{\mathbf{G}}\tilde{\boldsymbol{J}}^{(0)}])$ from the total $\mathcal{F}^{-1}[\tilde{\mathbf{G}}\tilde{\boldsymbol{J}}^{(0)}]$ already evaluated.

(6) Take the Fourier transform of the difference obtained in Step 5.

[1] Note that GTD (Keller's) solutions may either have singularities or may be in error near shadow and reflection boundaries or at caustics, and the Uniform Theory of Diffraction (UTD) [15] and the Uniform Asymptotic Theory (UAT) [15] that are employed to repair GTD break down at caustics. The Spectral Theory of Diffraction (STD), on the other hand, is uniform for all observation angles. The criterion for choosing any of these asymptotic forms of solution is convenience of computation for desired accuracy. For a comparative evaluation of the accuracy of the GTD, UTD, UAT, and STD, the reader is referred to [15].

(7) Subtract $\hat{\boldsymbol{E}}_1$, the Fourier transform of the tangential component of the incident electric field truncated on the surface, from the result in Step 6.

(8) Multiply the result obtained in Step 7 by $\hat{\mathbf{G}}^{-1}$. Note that $\hat{\mathbf{G}}^{-1}$ is also known and the operation is again algebraic as in Step 2. The result thus obtained is $\hat{\boldsymbol{J}}^{(1)}$, which is the first iteration of the scattered far field.

(9) Take the inverse Fourier transform of $\hat{\boldsymbol{J}}^{(1)}$ obtained in Step 8 and evaluate it on S to get the desired induced surface current on the scatterer. In other words, perform the operation $\theta(\mathcal{F}^{-1}[\hat{\boldsymbol{J}}^{(1)}])$. For an exact solution, this operation is redundant, since $\boldsymbol{J} = \theta\boldsymbol{J}$, and hence, $\theta[\mathcal{F}^{-1}[\mathcal{F}[\theta\boldsymbol{J}]]) = \theta\theta\boldsymbol{J} = \boldsymbol{J}$. However, the Fourier inversion of an nth approximate solution $\hat{\boldsymbol{J}}^{(n)}$ will not give rise to a current distribution that is nonzero except on S. This step provides a test for the accuracy and for the convergence of the approximate solution by comparing the approximate $\hat{\boldsymbol{J}}^{(0)}$ with $\mathcal{F}[\theta(\mathcal{F}^{-1}[\hat{\boldsymbol{J}}^{(1)}])]$.

(10) Take $\mathcal{F}[\theta(\mathcal{F}^{-1}[\hat{\boldsymbol{J}}^{(1)}])]$ to derive an *improved* approximation for $\hat{\boldsymbol{J}}^{(1)}$.

(11) Repeat as necessary using, for instance, the *improved* $\hat{\boldsymbol{J}}^{(1)}$ from Step 10 in the iteration Equation (13) to generate the next higher-order approximation $\hat{\boldsymbol{J}}^{(2)}$.

Before closing this section, we should point out that Galerkin's method applied in the transformed domain also provides an alternate, and in some cases the more desirable, approach for deriving the solution to the transformed integral equation. $\hat{\boldsymbol{J}}^{(0)}$, $\hat{\boldsymbol{J}}^{(1)}$, etc., as well as other suitable functions may be employed as a basis set for this purpose. An example of the use of the Galerkin procedure in the spectral domain approach may be found in [11].

In the following section, we show in some detail, the application of the iteration procedure just described to a two-dimensional scattering problem, viz., the diffraction by a finite screen or a strip.

3. Diffraction by a finite screen (strip)

In the last section, we presented a general iteration method for obtaining solution of the integral equation in the transform domain with the GTD or other high-frequency solution as the zero-order approximation. This iteration method not only allows us to improve on the GTD or similar solutions but also provides a convenient means for testing the satisfaction of the boundary conditions on the surface of the scatterer. Furthermore, the method yields not only the far-field but also the induced surface-current distribution, a feature not readily available in some other high-frequency techniques.

The application of the general procedure outlined in Section 2 is illustrated in this section by using it to solve the two-dimensional problem of a plane-wave diffraction by a finite screen or a strip. This problem was chosen for the following reasons. It is shown that when the angle of incidence is normal or near normal, the GTD solution accurately satisfies the boundary condition $\boldsymbol{E}_{\tan} = 0$ on the strip even when the multiple interaction between the two edges of the strip is neglected. However, it is found that when the angle of incidence is near grazing, the GTD solution is quite unsatisfactory, while the iterated solution generated by the hybrid technique does display the correct behavior.

3.1. Geometry of the strip problem

The geometry of the electromagnetic scattering problem involving a perfectly conducting infinite strip of zero thickness illuminated by a uniform plane wave, whose electric itensity vector is oriented parallel to the edges of the strip, is depicted in Fig. 1. For convenience of analysis, an arbitrary incident wave can always be decomposed into two components with respect to the z-axis, namely, TM_z (E-wave) and TE_z (H-wave). In the following discussion we consider the E-wave case only; the H-wave case can be solved in a similar manner by considering $\boldsymbol{H}^i = \hat{z}H_0^i$.

The incident field is given by

$$E_z^i(\rho, \phi) = \exp\{-ik(x\cos\phi_0 + y\sin\phi_0)\} \tag{14}$$

where the $e^{-i\omega t}$ time dependence is understood.

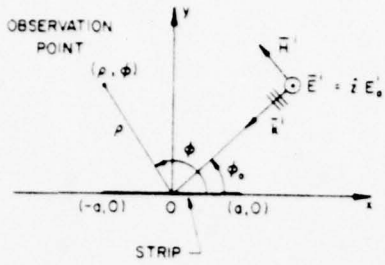

Fig. 1. Diffraction by a strip illuminated by an E-wave.

3.2. Iteration method applied to the strip problem

The integral equation formulation [16] for the problem at hand takes the form

$$-E_z^i(x) = \int_{-a}^{a} J_z(x')G(x-x')\,dx', \quad x \in [-a, a] \tag{15}$$

where $J_z(x')$ is the algebraic sum of the induced surface current densities on the top and the bottom surfaces of the thin strip. The kernel G is the two-dimensional free-space Green's function given by

$$G(x-x') = \tfrac{1}{4}iH_0^{(1)}(k|x-x'|) \tag{16}$$

where $H_0^{(1)}$ is the Hankel function of the first kind of order zero, and $k = 2\pi/\lambda$ is the free-space propagation constant. Note that (15) is the conventional integral equation which equates the integral representation of the tangential component of the scattered E-field radiated by the induced surface current density to the negative of the tangential component of the incident E-field on the surface of the perfectly conducting scatterer as required by the satisfaction of the boundary condition. Hence, (15) is valid on the strip only.

An extended integral equation that is valid for all x can be obtained by including the scattered fields outside the strip as well. If the scattered field on the interval $(-\infty, -a)$ is designated by $F_1(x)$ and the scattered field on the interval (a, ∞) is designated by $F_2(x)$, then the extended form of (15) becomes:

$$\int_{-a}^{a} J_z(x')G(x-x')\,dx' = \theta(-E_z^i(x)) + F_1(x) + F_2(x) \tag{17}$$

where θ is defined in (2).

Since the Fourier transform of the induced surface current density can be related to the far field, (17) is Fourier transformed to give

$$\tilde{J}_z(\alpha)\tilde{G}(\alpha) = [\theta(-E_z^i)]^{\sim} + \tilde{F}_1(\alpha) + \tilde{F}_2(\alpha) \tag{18}$$

where $\tilde{}$ indicates the Fourier transform pair defined in (5) which simplifies in the present one-dimensional problem to

$$\tilde{F}(\alpha) = \int_{-\infty}^{\infty} F(x)\,e^{-i\alpha x}\,dx \tag{19a}$$

and

$$F(x) = \frac{1}{2\pi}\int_{-\infty}^{\infty} \tilde{F}(\alpha)\,e^{i\alpha x}\,d\alpha. \tag{19b}$$

The Fourier transform of the two-dimensional Green's function in (18) takes the form

$$\tilde{G}(\alpha) = \frac{i}{2\sqrt{k^2-\alpha^2}}. \tag{20}$$

Note that (18) is an algebraic equation in the spectral domain in contrast to the convolution form of the integral equation (17) in the spatial domain. The reason for working in the spectral domain will become clear when the method of solution for (18) is developed. Following the procedure discussed in Section 2 and in terms of the notations introduced in the present problem, we proceed as follows.

(1) Obtain $\tilde{J}_z^{(0)}(\alpha)$, the initial approximation of the Fourier transform of the induced surface current density, or equivalently, the scattered *far field* within a known multiplicative factor, as follows:

(1.1) Find the expressions for the first estimate of $\tilde{F}_1^{(0)}(\alpha) + \tilde{F}_2^{(0)}(\alpha)$. Note that GTD may be used to get closed-form expressions for $\tilde{F}_1^{(0)}(\alpha)$ and $\tilde{F}_2^{(0)}(\alpha)$ since these can be

obtained from the GTD solutions to the two half-plane problems as shown in Fig. 2. The expressions for $\tilde{F}_1^{(0)}$ and $\tilde{F}_2^{(0)}$ as obtained from GTD read

$$\tilde{F}_1^{(0)}(\alpha) = \tfrac{1}{2}i[e^{i(ka\cos\phi_0}\sqrt{8k}\sin\tfrac{1}{2}\phi_0] \times \frac{e^{i\alpha a}}{(\alpha + k\cos\phi_0)\sqrt{\alpha + k}} - \frac{i\,e^{ia(\alpha + k\cos\phi_0)}}{(\alpha + k\cos\phi_0} \tag{21a}$$

and

$$\tilde{F}_2^{(0)}(\alpha) = -\tfrac{1}{2}i[e^{-i(ka\cos\phi_0}\sqrt{8k}\cos\tfrac{1}{2}\phi_0] \times \frac{e^{-i\alpha a}}{(\alpha + k\cos\phi_0)\sqrt{k - \alpha}} + \frac{i\,e^{-ia(\alpha + k\cos\phi_0)}}{(\alpha + k\cos\phi_0)}. \tag{21b}$$

Note that these expressions are free of singularities for all α.

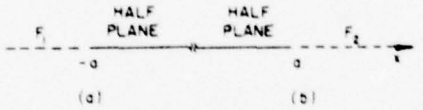

Fig. 2. Transform of $F_1(x)$ can be approximated by the GTD solution to the half-plane problem (a) shown on the left-hand side; transform of $F_2(x)$ can be approximated by the GTD solution to the half-plane problem (b) shown on the right-hand side.

(1.2) Solve for the initial approximation of $\tilde{J}_z(\alpha)$, $\tilde{J}_z^{(0)}(\alpha)$, by numerically carrying out the operations shown below:

$$\tilde{J}_z^{(0)}(\alpha) = \mathscr{F}\left[\theta\left(\mathscr{F}^{-1}\left[\frac{[\theta(-E^i)]^{\sim} + \tilde{F}_1^{(0)}(\alpha) + \tilde{F}_2^{(0)}(\alpha)}{\tilde{G}(\alpha)}\right]\right)\right].$$

(2) Use (13) to further improve the solution as necessary.

The check for satisfaction of the integral equation can be applied very simply by computing $\tilde{J}(\alpha)\tilde{G}(\alpha)$, taking its inverse Fourier transform, and verifying how well it approaches $-E^i$ on the surface of the scatterer.

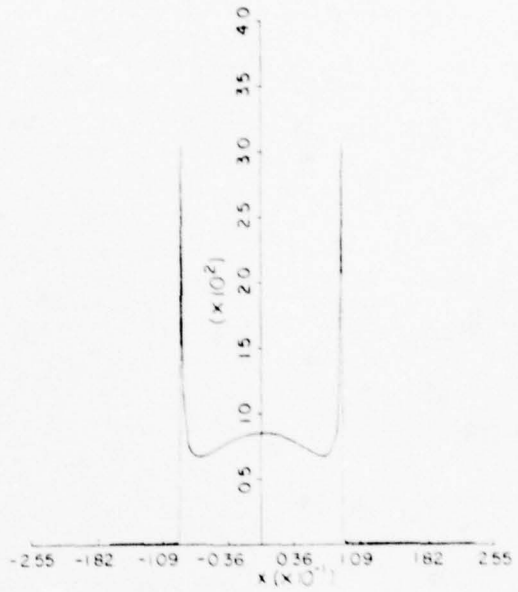

Fig. 3. Magnitude of the induced surface current density distribution normalized to $(\tfrac{1}{2}\lambda Z_0)^{-1}$ on the strip of $ka = 4$ (1.273λ wide), $\phi_0 = 90°$.

3.3. Numerical results and discussions

Normal incidence

Fig. 3 shows the calculated induced surface current density distribution on the strip with $ka = 4$ (1.3λ wide) for normal incidence. Note that the current density becomes large at the edges, as it should for E-wave incidence, although no specific condition was enforced at the edges, nor any special care exercised. Note also that the approximate current is confined essentially on the surface of the strip and extends very little outside of this surface. Thus, the solution in this case is very close to the true solution and this is easily verified by truncating the current density, computing the scattered field it radiates on the strip, and verifying that the scattered field is indeed very nearly equal to $-E^i$.

Fig. 4 depicts the result for $ka = 40$, i.e. a 13λ strip. Note that the peak in the center is no longer present and the current there approaches that given by the physical optics approximation. There

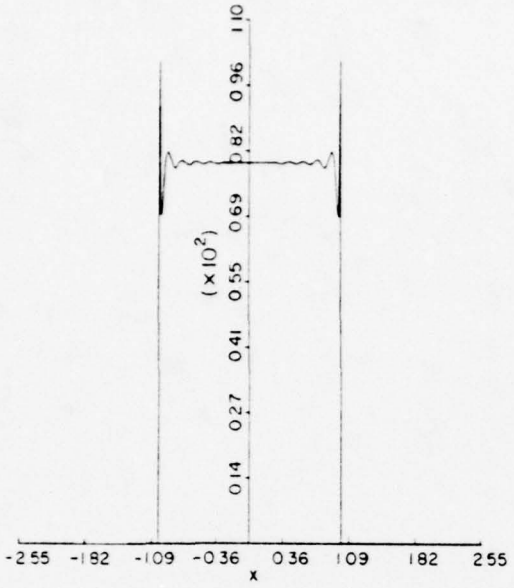

Fig. 4. Magnitude of the induced surface current density distribution normalized to $(ikZ_0)^{-1}$ on the strip of $ka = 40$. (12.73λ wide), $\phi_0 = 90°$.

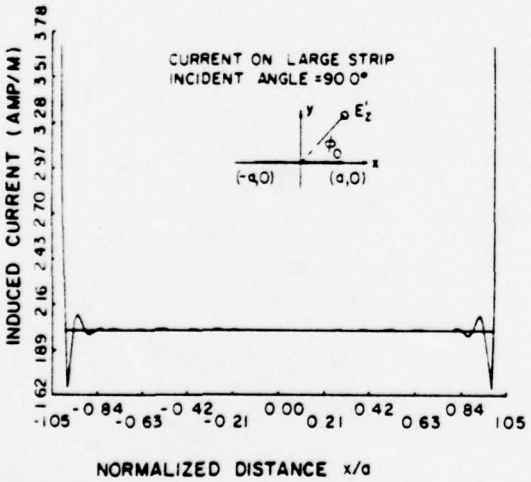

Fig. 5. Moment method (applied in the spectral domain) solution of the magnitude of the induced surface current density distribution normalized to $1/Z_0$ on the strip of $ka = 50$. (15.92λ wide), $\phi_0 = 90°$.

are now more oscillations, however, and the current density has a sharp dip before rising to infinity at the edges.

Fig. 5 displays the moment method applied in the spectral domain solution [18] and the comparison with the one obtained here is quite favorable.

Fig. 6 exhibits the satisfaction of the boundary condition after one iteration. As mentioned before, such a test is not available in the conventional GTD approach.

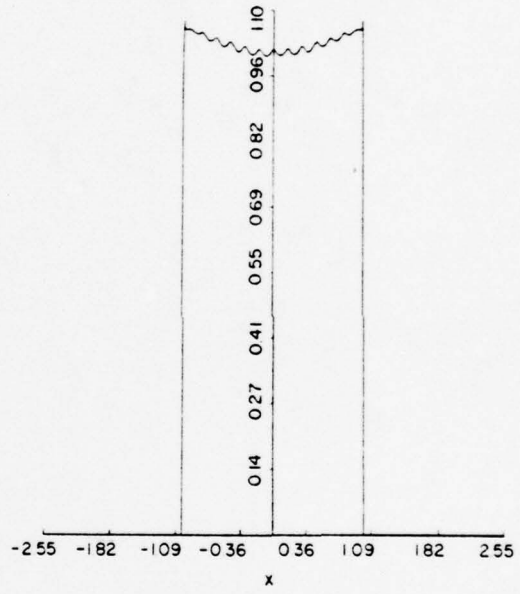

Fig. 6. Magnitude of the scattered E-field evaluated on the strip of $ka = 40$, $\phi_0 = 90°$ (one iteration).

Near grazing incidence

Let us next turn to the interesting case of a near grazing incidence where the zero-order current density has a long tail extending beyond the edge of the strip (see Fig. 7). This result is to be expected since the two half-plane GTD solutions used in the zero-order approximation represent a poor approximation for the induced current for shallow incidence angles. If this tail is truncated, the

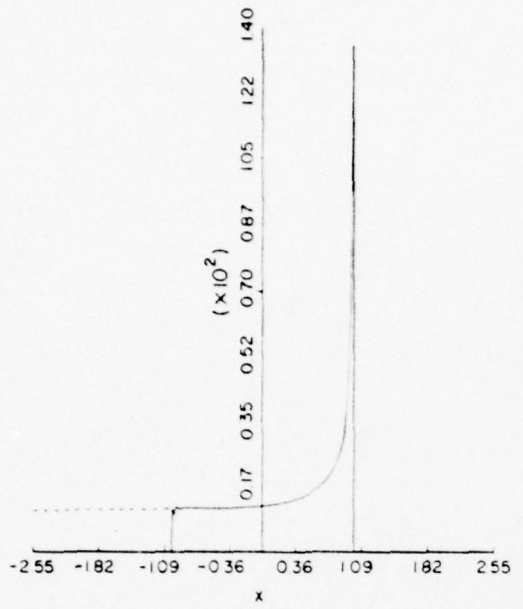

Fig. 7. Magnitude of the induced surface current density distribution normalized to $(ikZ_0)^{-1}$ on the strip of $ka = 40$, $\phi_0 = 10°$ (no iteration).

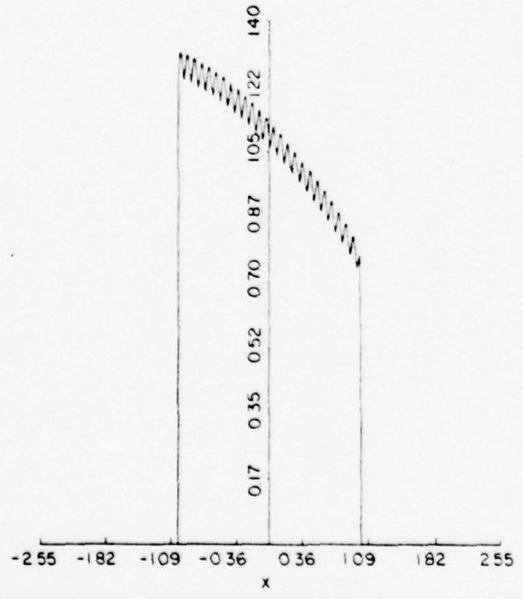

Fig. 8. Magnitude of the scattered E-field evaluated on the strip of $ka = 40$, $\phi_0 = 10°$ (no iteration).

remaining portion of the current density on the strip produces a scattered field on the surface of the strip which is significantly different from $-E^i$, where $|E^i| = 1$, as may be seen from Fig. 8.

Fig. 9 shows the effect of one iteration on the zero-order GTD solution shown in Fig. 7. Note that the current density is significantly altered in the neighborhood of the shadowed edge demonstrating the fact that even with a relatively poor initial guess, the convergence is quite rapid in this case.

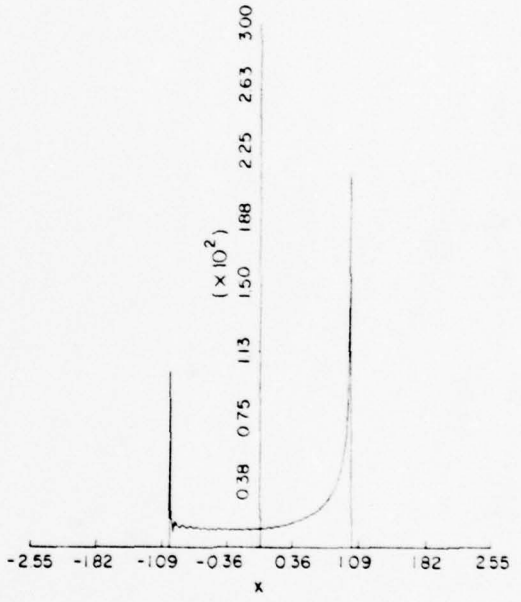

Fig. 9. Magnitude of the induced surface current density distribution normalized to $(ikZ_0)^{-1}$ and truncated on the strip of $ka = 40$, $\phi_0 = 10°$ (one iteration).

To see that this is indeed an improved solution, the truncated portion of it is used to calculate the scattered field. It is observed that the satisfaction of the boundary condition has been improved as shown in Fig. 10.

To verify the convergence of the solution numerically, one more iteration is performed and the result is depicted in Fig. 11. Note that the shape of the surface current density does not change

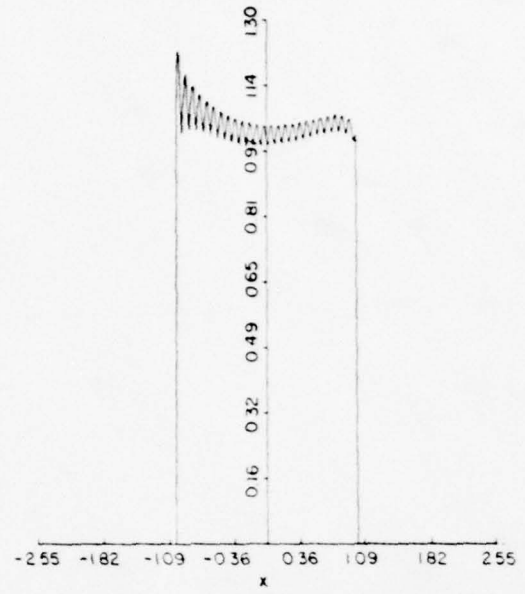

Fig. 10. Magnitude of the scattered E-field evaluated on the strip of $ka = 40$, $\phi_0 = 10°$ (one iteration).

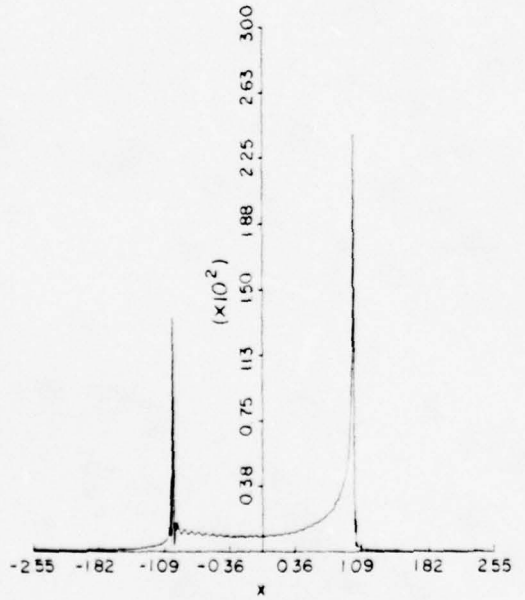

Fig. 11. Magnitude of the induced surface current density distribution normalized to $(ikZ_0)^{-1}$ on the strip of $ka = 40$, $\phi_0 = 10°$ (two iterations).

much which indicates a settling down of the solution has occurred. Also, note that the tail extending outside of the strip has been reduced to an insignificant quantity, which, when truncated, will produce little effect on the scattered field on the surface of the strip.

To further validate the solution, the moment method solution [18] of the same problem with slightly different parameters is shown in Fig. 12 for a comparison. Again, the agreement is good. However, in terms of computational efficiency, the present method is far superior to the moment-method solution for the accuracy realized.

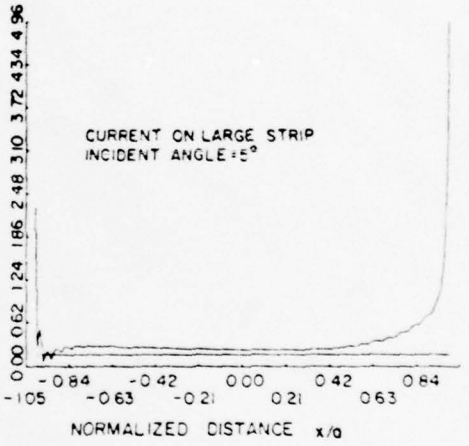

Fig. 12. Moment method (applied in the spectral domain) solution of the magnitude of the induced surface current density distribution normalized to $1/Z_0$ on the strip of $ka = 50$, $\phi_0 = 5°$.

3.4. Summary

Before closing this section, it is worthwhile to recapitulate the main points of the approach discussed. The finite screen (strip) problem has been solved by a combination of the integral-equation and asymptotic high-frequency techniques. Formulation of the integral equation in the Fourier transform domain allows one to conveniently obtain the zero-order approximation to the transformed unknown surface current density from the solution of two half-plane problems.

Higher-order solutions have been obtained via the iteration steps outlined above and the numerical convergence has been demonstrated. The iteration process generates the proper edge singularities even when they are not present in the original approximation, e.g., physical optics. However, additional iterations are necessary in that case. Validity of the solution has been substantiated by numerically verifying the satisfaction of the boundary condition to within a close tolerance.

4. Concluding remarks

In addition to the finite screen problem discussed here, the spectral domain approach has been found useful for other electromagnetic scattering and radiation problems of considerable interest [10, 11, 19, 20]. It has been applied to the problems of electromagnetic scattering by rectangular [19] and cylindrical rods [11], a finite plate [10], a cylindrical shell [20], etc. The spectral domain procedure for testing the accuracy of high-frequency solutions also has been applied to a number of problems of practical interest. One such example is the canonical problem of a corner in a thin plate for which an asymptotic solution was recently derived by Albertsen [21], using a multiple Wiener–Hopf procedure. Testing his solution for the satisfaction of the boundary condition that the tangential electric field be zero on the plate, one finds that the solution satisfies the boundary condition only approximately and contains some extraneous infinities that must be removed. Even so, the solution in its original form represents a good starting point for deriving iterated solutions for the quarter-plane problem. Both the surface current and the far-fields can be improved via the spectral-domain approach.

As another example, we quote the problem of constructing the Green's function for a magnetic dipole radiating in the presence of a smooth curved surface, e.g., a cylinder or a cone. The conventional GTD solution derived from applying Watson transformation to the modal series solution for the cylinder breaks down when the point of observation is close to the axial direction of the cylinder. This is because the effective wave number for propagation along the axis approaches zero, whereas the asymptotic solution requires that the wave number times the radius of the cylinder be large. Several different asymptotic solutions based on the modification of Fock's solution for the sphere problem have recently been presented for the axial region by a number of authors. The spectral domain approach has been found useful not only for testing the relative accuracy of these solutions, but for iteratively improving them as well [13].

References

[1] M. Kline and I. Kay, *Electromagnetic Theory and Geometrical Optics*, New York, John Wiley (1964).

[2] A.J. Poggio and E.K. Miller, "Integral equation solutions of three-dimensional scattering problems", in: *Computer Techniques for Electromagnetics*, R. Mittra, Ed., Pergamon Press, New York (1973).

[3] J.B. Keller, "Geometrical theory of diffraction", *J. Opt. Soc. Am. 52* (1962) 116–130.

[4] R.G. Kouyoumjian, "The geometrical theory of diffraction and its application", in: *Topics in Applied Physics*, Vol. 3, R. Mittra, Ed., Springer, New York (1976) 165–215.

[5] G.A. Deschamps, "Ray techniques in electromagnetics", *Proc. IEEE 60* (1972) 1022–1035.

[6] G.L. James, *Geometrical Theory of Diffraction for Electromagnetic Waves*, Peter Peregrinus, Ltd., London (1976).

[7] H. Bach, "Engineering applications of the geometrical Theory of diffraction", in: *Modern Topics in Electromagnetics and Antennas*, E.J. Maanders and R. Mittra, Eds., Peter Peregrinus Ltd., London (1977).

[8] R. Mittra, Y. Rahmat-Samii and W.L. Ko, "Spectral theory of diffraction", *Appl. Phys. 10* (1976) 1–13.

[9] Y. Rahmat-Samii and R. Mittra, "A spectral domain interpretation of high frequency diffraction phenomena", *IEEE Trans. Ant. and Prop.* AP-25 (5) (1977) 676–687.

[10] W.L. Ko and R. Mittra, "A new approach based on a combination of integral equation and asymptotic techniques for solving electromagnetic scattering problems", *IEEE Trans. Ant. and Prop. AP-25* (2) (1977) 187–197.

[11] R. Mittra and W.L. Ko, "An approach to high-frequency scattering from smooth convex surfaces", *IEEE Trans. Ant. and Prop. AP-25* (6) (1977) 781–788.

[12] M. Tew and R. Mittra, "Accuracy tests for asymptotic solutions to radiation from a cylinder", University of Illinois at Urbana-Champaign, EM Lab Tech. Rept. No. 77-22, Oct. 1977; *see* "Accuracy tests for high frequency asymptotic solutions", by R. Mittra and M. Tew, *IEEE Trans. Ant. and Prop.*, to appear.

[13] M. Tew and R. Mittra, "Reciprocity test for asymptotic solutions", National Radio Science Meeting, Boulder, Colorado, Jan. 1978; *see* "An integral E-field accuracy test for asymptotic solutions", by R. Mittra and M. Tew, to appear.

[14] R.E. Collin and F.J. Zucker, *Antenna Theory*, McGraw-Hill, New York (1969).

[15] Y. Rahmat-Samii and R. Mittra, "Spectral analysis of high-frequency diffraction of an arbitrary incident field by a half plane—comparison with four asymptotic techniques", *Radio Science 13* (1) (1978) 31–48.

[16] A.W. Maue, "Formulation of general diffraction problems through an integral equation", *Zeitschrift für Physik 126* (1949) 601–618.

[17] R. Mittra and S.W. Lee, *Analytical Techniques in the Theory of Guided Waves*, Macmillan, New York (1971) 81.

[18] R. Mittra and T.S. Li, "A spectral domain approach to the numerical solution of electromagnetic scattering problems", *AEU 29* (1975) 217–222.

[19] W.L. Ko and R. Mittra, "A new look at the scattering of a plane wave by a rectangular cylinder", *AEU* (1977) 494–500.

[20] W.L. Ko and R. Mittra, "High frequency scattering from smooth surfaces with edges—A spectral domain Approach", presented at the National Radio Science Meeting at the University of Colorado; Boulder, Colorado, Nov. 1978.

[21] N.C. Albertsen, "A diffraction coefficient for the vertex of a quarter-plane", The Technical Univeristy of Denmark; Lyngby, Denmark, Applied Mathematical Physics Laboratory Report (1976).

Special reprint
from
AEÜ ARCHIV FÜR ELEKTRONIK UND ÜBERTRAGUNGSTECHNIK
ELECTRONICS AND COMMUNICATION

Band 33 (1979), pp. 149–156

Penetration of an EM Wave into a Cylindrical Cavity and the Current Induced on a Wire inside

by Edward K. Yung *, Shung-Wu Lee *, and Raj Mittra *

This paper addresses the problem of computing the current induced in a thin wire located inside a cylindrical cavity with a circumferential slot when the cavity is illuminated by an incident plane wave. The calculation is carried out in two steps. First, the problem of penetration of the incident field into the cavity is solved by the method of moments under the assumption that the presence of the wire inside the cavity creates little or no perturbation of the interior field. Next, the induced current on the wire is calculated by the following two methods: (i) use of a simple analytical formula derived from the application of the Wiener-Hopf techniques to the finite wire problem; (ii) numerical solution of an integral equation. Extensive numerical results for the induced current are presented. It is found that the current is sensitive to the cylinder radius, the cavity height, the frequency of excitation, and the wire location, but is relatively less sensitive to the variation in the slot length. In addition, the induced current on a wire inside the cavity can be much larger than its counterpart is free space illuminated by the same incident plane wave at frequencies where the cavity is near resonance.

Einkopplung einer EM-Welle in einen zylindrischen Resonator und induzierter Strom auf einem Draht im Inneren

Der Strom wird berechnet, der in einem dünnen Draht innerhalb eines zylindrischen Hohlraumresonators durch einen Umfangsschlitz induziert wird, wenn eine ebene Welle einfällt, und zwar in zwei Schritten: Zuerst wird mit der Momentenmethode und der Annahme, daß der Draht im Resonator das innere Feld nicht oder nur wenig stört, berechnet, wie das einfallende Feld in den Resonator eindringt. Dann wird der im Draht induzierte Strom mit den folgenden beiden Verfahren ermittelt: 1. Durch Anwendung der Wiener-Hopf-Methode auf das Problem des endlichen Drahtes wird eine einfache analytische Formel abgeleitet. 2. Eine Integralgleichung wird numerisch gelöst. Aus den umfangreichen numerischen Ergebnissen ergibt sich, daß der induzierte Strom von Zylinderradius, Resonatorhöhe, Lage des Drahtes und der Frequenz stärker abhängt und weniger von der Schlitzlänge. Außerdem kann der von der gleichen ebenen Welle im Draht induzierte Strom innerhalb des Resonators bei seinen Resonanzfrequenzen viel größer sein als im gleichen Draht ohne Resonator.

1. Introduction

The penetration of an electromagnetic wave through an aperture into a cylindrical structure is of current interest because of its application to EMP, to EMC, and to biological studies. As early as 1949, Sommerfeld [1] studied the problem of an infinitely long circular cylinder with a longitudinal slot, illuminated by a normally incident plane wave. Using a Fourier analysis approach, Sommerfeld reduced the problem to a system of infinitely many linear equations, but declared resignedly, "We can do practically nothing with the problem." Silver and Saunders [2] used the saddle-point integration method for the inversion of Fourier transforms and extracted the far field of Sommerfeld's problem. Hitherto, a number of extensions along this line of work have been reported [3], [4]. With the advent of high-speed digital computers, Sommerfeld's penetration problem can now be readily solved by numerical means [5], [6]. The 3-dimensional version of Sommerfeld's problem was recently carried out by Safavi-Naini, Lee and Mittra [7], [8].

In the present paper, an extension of the penetration problem of Safavi-Naini et al. is investigated, in which a thin wire is added inside the cavity and the problem is to determine the current induced on the wire. The wire is oriented parallel to the longitudinal direction of the cylindrical cavity. If the slot in the cavity wall is also longitudinal, there is little induced current on the wire. Hence we concentrate on the more interesting case, namely, the slot which is circumferential on the cylindrical cavity wall. The composite geometry of the present problem is sketched in Fig. 1.

Due to the thinness of the wire, it appears reasonable to assume that the presence of the wire does not perturb the field generated inside the cavity. Thus, the problem under consideration can be solved in two steps:

(A) Determine the field $\hat{E}$ inside the cavity as if the wire were absent.

(B) Using $\hat{E}$ as an incident field, determine the induced current $I(z)$ as if the wire were situated in the free space.

We emphasize that the above two-step approach is an approximation. The exact degree of approxi-

* Dr. E. K. Yung, Dr. S.-W. Lee, Prof. Dr. R. Mittra, Electromagnetics Laboratory, Department of Electrical Engineering, University of Illinois, Urbana, Ill. 61801, USA.

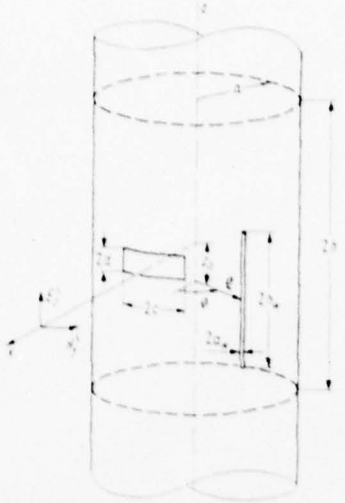

Fig. 1. An infinitely long cylinder with a cavity and a wire inside, illuminated by an incident plane wave through a circumferential slot on the cavity wall.

mation can be determined by solving the coupled cavity and wire problem in its entirety, but is beyond the scope of this paper.

The plan for the present paper is as follows: In Section 2, we consider the first part (Part A) of the problem, in which the wire is removed from the cavity and the penetration of an incident plane wave into the cavity is solved by the moment method [9]. In Section 3, we study the current induced on the wire inside the cavity when it is illuminated by the field $\vec{E}$ computed in Part A. Since $\vec{E}$ is given in terms of a doubly infinite series of eigenfunctions of the cavity, it can be interpreted as a spectrum of plane waves. As a result, the induced current $I(z)$ can be determined by superimposing the currents due to each component of the plane wave spectrum. The latter problem is determined by the following two methods:

1. The moment method based on an integral equation formulation [10], and
2. the simple approximation formula recently developed by Chang, Lee, and Rispin [11], [12].

It should be noted that both of the above methods apply only if the incident plane wave is homogeneous. In the present problem, however, the field $\vec{E}$ inside the cavity consists of both homogeneous and inhomogeneous plane wave components. Hence, the above two methods have to be extended via analytical continuation to cover the case of an incident inhomogeneous plane wave. Numerical results are given in Section 4.

2. Field in the Cavity

In this section, the field $\vec{E}$ excited in the cavity with the wire absent is derived. The geometry of the problem under consideration in this section is illustrated in Fig. 1, with the wire removed. The conducting circular cylinder is infinitely long and is of radius a. A cylindrical cavity is formed inside the cylinder by two conducting plates located at $z = \pm h$. The cavity is coupled to exterior excitations through a circumferential slot on its cylindrical wall. The rectangular slot is of dimension $2c \times 2d$ and centered at $(x = a,\ y = 0,\ z = 0)$. The width of the slot is assumed to be small in terms of wavelength, i.e.,

$$2kd \ll 1. \tag{1}$$

The structure is illuminated by a normally incident plane wave of unit magnitude described by

$$\vec{E}^i = \hat{z}\, e^{jkx}, \quad \vec{H}^i = \hat{y}\, \frac{1}{\eta}\, e^{jkx} \tag{2}$$

where the time harmonic factor $e^{+j\omega t}$ has been suppressed and $\eta = \sqrt{\mu/\varepsilon} = 120\,\pi$ is the intrinsic impedance of the free space.

The symmetry of the configuration, together with the plane wave excitation given in eq. (2), dictate that the tangential electric field across the aperture be an even function of ϕ. Furthermore, the narrowness of the slot enables us to assume that the aperture field is approximately constant in z and is z-directed. Thus, the tangential electric field across the aperture $\vec{E}_a = E_a\,\hat{z}$ can be represented by a Fourier-cosine series:

$$E_a = \sum_{\mu=0}^{\infty} E_\mu \cos \Gamma_\mu \phi; \quad |\phi| \leq \phi_0, \quad |z| \leq d. \tag{3}$$

In accordance with the boundary condition that E_a vanishes at $\phi = \pm\phi_0$ ($\phi_0 = c/a$), Γ_μ are found to be

$$\Gamma_\mu = \frac{(2\mu + 1)\,\pi}{2\phi_0}; \quad \mu = 0, 1, 2, \ldots. \tag{4}$$

Due to the assumed direction of the aperture electric vector (or the equivalent magnetic current), it can be shown that a field TM with respect to z is sufficient to represent the total field inside the cavity. Such a field can be generated via a z-directed magnetic vector potential $\vec{A} = A_z\,\hat{z}$. The relation between A_z and the magnetic field is

$$\vec{H} = \frac{1}{\mu}\, \nabla \times \vec{A}. \tag{5}$$

Inside the cavity, A_z is a linear combination of all possible elementary wave functions that are solutions to the scalar Helmholtz equation [13]. It assumes the form

$$A_z(\varrho, \phi, z) = \sum_{m,n=0}^{\infty} \sum A_{mn} J_m(\gamma_n \varrho) \cos m\phi \cos \varkappa_n z \tag{6}$$

where $$\gamma_n = \begin{cases} \sqrt{k^2 - \varkappa_n^2} & \text{for } k^2 \geq \varkappa_n^2, \\ -j\sqrt{\varkappa_n^2 - k^2} & \text{for } k^2 < \varkappa_n^2, \end{cases} \tag{7}$$

and $$\varkappa_n = n\,\pi/h, \quad n = 0, 1, 2, \ldots. \tag{8}$$

The constants A_{mn} are unknowns, and J_m are the mth order Bessel functions of the first kind. Note that with the choices of the eigenvalues $\varkappa_n$ in eq. (8), the boundary conditions that E_ϱ and E_ϕ be zero at $z = \pm h$ are automatically satisfied.

The constants A_{mn} in eq. (6) are unknown quantities, and by enforcing the conditions that E_z be zero on the cylindrical wall and equal to E_a on the aperture, they can be evaluated in terms of E_μ, the expansion coefficients of E_a given in eq. (3). First, we evaluate E_z (referring to eq. (5)) at $\varrho = a$ to obtain

$$\frac{1}{\mathrm{j}\omega\mu\varepsilon}\sum_{m,n=0}^{\infty}\gamma_n^2 A_{mn} \mathrm{J}_m(\gamma_n a)\cos m\phi\cos\alpha_n z = \Omega(\phi,z)\sum_{\mu=0}^{\infty}E_\mu\cos\Gamma_\mu\phi;\quad |\phi|\leqq\pi,\ |z|\leqq h \tag{9}$$

where Ω is the characteristic function of the aperture:

$$\Omega(\phi,z)=\begin{cases}1 & \text{for}\quad |\phi|\leqq\phi_0,\quad |z|\leqq d,\\ 0 & \text{otherwise.}\end{cases} \tag{10}$$

We recognize that eq. (9) is a standard Fourier-Bessel series with unresolved coefficients A_{mn}. Hence, A_{mn} are determined by standard procedures with the results

$$A_{mn}=\frac{\mathrm{j}4\omega\mu\varepsilon\cos m\phi_0\sin\alpha_n d}{\varepsilon_m\varepsilon_n\pi\alpha_n\gamma_n^2 h\mathrm{J}_m(\gamma_n a)}\sum_{\mu=0}^{\infty}E_\mu\frac{(-1)^\mu\Gamma_\mu}{\Gamma_\mu^2-m^2}, \tag{11}$$
$$m,n=0,1,2,\ldots$$

in which ε_m is the Neumann number, defined by

$$\varepsilon_m=\begin{cases}2 & \text{for}\quad m=0\\ 1 & \text{for}\quad m\neq 0.\end{cases}$$

In the region exterior to the cylindrical structure, the symmetry of the configuration again leads to a TM field with respect to z. Thus, the exterior field is also determined via a z-directed magnetic vector potential $\bar{A}=\Psi\hat{z}$. For reasons which will be obvious later, Ψ is partitioned into three wave functions: $\Psi=\Psi^{\mathrm{i}}+\Psi^{\mathrm{r}}+\Psi^{\mathrm{s}}$. The first of these Ψ^{i} represents the incident plane wave; it is independent of a and is given by

$$\Psi^{\mathrm{i}}=\frac{\mathrm{j}2}{\omega}\sum_{m=0}^{\infty}\frac{\mathrm{j}^m}{\varepsilon_m}\mathrm{J}_m(k\varrho)\cos m\phi. \tag{12}$$

The field components of Ψ^{i} are given in eq. (2). The second wave function Ψ^{r} represents the reflected wave when the aperture is closed by a perfect conductor; it assumes the form

$$\Psi^{\mathrm{r}}=\frac{\mathrm{j}2}{\omega}\sum_{m=0}^{\infty}\frac{\mathrm{j}^m}{\varepsilon_m}\left\{-\frac{\mathrm{J}_m(ka)}{\mathrm{H}_m^{(2)}(ka)}\right\}\mathrm{H}_m^{(2)}(k\varrho)\cos m\phi \tag{13}$$

where $\mathrm{H}_m^{(2)}$ are the mth order Hankel functions of the second kind. The third wave function Ψ^{s} corresponds to the field produced by the equivalent magnetic current. In contrast to both Ψ^{i} and Ψ^{r}, Ψ^{s} depends on a and is represented by a continuous spectrum of cylindrical waves:

$$\Psi^{\mathrm{s}}=\sum_{m=0}^{\infty}\cos m\phi\int_{-\infty}^{\infty}F_m(\alpha)\mathrm{H}_m^{(2)}(\gamma\varrho)\mathrm{e}^{\mathrm{j}\alpha z}\mathrm{d}\alpha, \tag{14}$$

where F_m are unknown functions, and

$$\gamma=\begin{cases}\sqrt{k^2-\alpha^2} & \text{for}\quad k^2\geqq\alpha^2\\ -\mathrm{j}\sqrt{\alpha^2-k^2} & \text{for}\quad k^2<\alpha^2.\end{cases} \tag{15}$$

To determine F_m, we first evaluate E_z^+ at $\varrho=a$ to obtain

$$\frac{1}{\mathrm{j}\omega\mu\varepsilon}\sum_{m=0}^{\infty}\cos m\phi\int_{-\infty}^{\infty}\gamma^2F_m(\alpha)\mathrm{H}_m^{(2)}(\gamma a)\mathrm{e}^{\mathrm{j}\alpha z}\mathrm{d}\alpha = \Omega(\phi,z)\sum_{\mu=0}^{\infty}E_\mu\cos\Gamma_\mu\phi;\quad |\phi|\leqq\pi,\ |z|\leqq\infty. \tag{16}$$

Then, we multiply both sides of the equation above by $\cos n\phi$, $n=0,1,2,\ldots$, and after that, integrate the equation over the entire domain of interest. By invoking the orthogonal properties of $\cos n\phi$, F_m are determined in terms of E_μ:

$$F_m(\alpha)=\frac{\mathrm{j}2\omega\mu\varepsilon\cos m\phi_0\sin\alpha d}{\varepsilon_m\pi^2\alpha\gamma^2\mathrm{H}_m^{(2)}(\gamma a)}\sum_{\mu=0}^{\infty}E_\mu\frac{(-1)^\mu\Gamma_\mu}{\Gamma_\mu^2-m^2};\quad m=0,1,2,\ldots. \tag{17}$$

With A_{mn} and F_m defined by eqs. (11) and (17), the requirement that the tangential electric field be continuous across the aperture is automatically satisfied. However, these definitions, of themselves, do not ensure the continuity of the tangential magnetic field across the aperture. To enforce the continuity of the magnetic field, we proceed as follows: In the region exterior to the cylinder, the three partial magnetic fields H_ϕ^{i}, H_ϕ^{r}, and H_ϕ^{s} (H_ϱ^+ is immaterial) corresponding respectively to the three wave functions defined in eqs. (12) through (14) are

$$H_\phi^{\mathrm{i}}=\frac{2k}{\mathrm{j}\omega\mu}\sum_{m=0}^{\infty}\frac{\mathrm{j}^m}{\varepsilon_m}\mathrm{J}_m'(k\varrho)\cos m\phi,$$
$$H_\phi^{\mathrm{r}}=\frac{2k}{\mathrm{j}\omega\mu}\sum_{m=0}^{\infty}\frac{\mathrm{j}^m}{\varepsilon_m}\left[-\frac{\mathrm{J}_m(ka)}{\mathrm{H}_m^{(2)}(ka)}\right]\mathrm{H}_m^{(2)\prime}(k\varrho)\cos m\phi, \tag{18}$$
$$H_\phi^{\mathrm{s}}=\frac{-1}{\mu}\sum_{m=0}^{\infty}\cos m\phi\int_{-\infty}^{\infty}\gamma F_m(\alpha)\mathrm{H}_m^{(2)\prime}(\gamma\varrho)\mathrm{e}^{\mathrm{j}\alpha z}\mathrm{d}\alpha.$$

Inside the cavity H_ϕ is given by

$$H_\phi=\frac{-1}{\mu}\sum_{m,n=0}^{\infty}\gamma_n A_{mn}\mathrm{J}_m'(\gamma_n\varrho)\cos m\phi\cos\alpha_n z. \tag{19}$$

Hence, the desired continuity of the tangential magnetic field across the aperture now reads

$$\frac{2k}{\mathrm{j}\omega\mu}\sum_{m=0}^{\infty}\frac{\mathrm{j}^m}{\varepsilon_m}\left[\mathrm{J}_m'(ka)-\frac{\mathrm{J}_m(ka)}{\mathrm{H}_m^{(2)}(ka)}\mathrm{H}_m^{(2)\prime}(ka)\right]\cos m\phi - \frac{1}{\mu}\sum_{m=0}^{\infty}\cos m\phi\int_{-\infty}^{\infty}\gamma F_m(\alpha)\mathrm{H}_m^{(2)\prime}(\gamma a)\mathrm{e}^{\mathrm{j}\alpha z}\mathrm{d}\alpha = -\frac{1}{\mu}\sum_{m,n=0}^{\infty}\gamma_n A_{mn}\mathrm{J}_m'(\gamma_n a)\cos m\phi\cos\alpha_n z; \tag{20}$$
$$|\phi|\leqq\phi_0,\quad |z|\leqq d.$$

The above equation can be simplified by recognizing that the term in the bracket on the LHS is the Wronskian of Bessel functions:

$$\mathrm{J}_m'(ka)-\frac{\mathrm{J}_m(ka)}{\mathrm{H}_m^{(2)}(ka)}\mathrm{H}_m^{(2)\prime}(ka)=\frac{\mathrm{j}2}{\pi ka\mathrm{H}_m^{(2)}(ka)}.$$

By substituting the above result into eq. (20), it becomes

$$\sum_{m=0}^{\infty}\cos m\phi\int_{-\infty}^{\infty}\gamma F_m(\mathfrak{x})\,H_m^{(2)\prime}(\gamma a)\,e^{j\mathfrak{x}z}\,d\mathfrak{x}-$$
$$-\sum_{m,n=0}^{\infty}\sum\cos m\phi\,\gamma_n A_{mn}J_m'(\gamma_n a)\cos\mathfrak{x}_n z= \tag{21}$$
$$=\frac{4}{\pi\omega a}\sum_{m=0}^{\infty}\frac{j^m\cos m\phi}{\varepsilon_m H_m^{(2)}(ka)};$$
$$|\phi|\le\phi_0,\quad |z|\le d.$$

Applying the method of Galerkin [9], the preceding equation can be solved numerically. We multiply both sides of the equation above by $\cos\nu\phi$, $\nu=0,1,2,\ldots$, and integrate the resultant equation over the aperture region, leading to

$$\sum_{m=0}^{\infty}g_{m\nu}\int_{-\infty}^{\infty}\frac{\sin\mathfrak{x}d}{\mathfrak{x}}\gamma F_m(\mathfrak{x})\,H_m^{(2)\prime}(\gamma a)\,d\mathfrak{x}-$$
$$-\sum_{m,n=0}^{\infty}\sum g_{m\nu}\frac{\sin\mathfrak{x}_n d}{\mathfrak{x}_n}\gamma_n A_{mn}J_m'(\gamma_n a)= \tag{22}$$
$$=\frac{4d}{\pi\omega a}\sum_{m=0}^{\infty}\frac{j^m}{\varepsilon_m}\frac{g_{m\nu}}{H_m^{(2)\prime}(ka)};\quad \nu=0,1,2,\ldots,$$

where $g_{m\nu}$ stands for

$$g_{m\nu}=\frac{\sin(m-\nu)\phi_0}{m-\nu}+\frac{\sin(m+\nu)\phi_0}{m+\nu}. \tag{23}$$

Then, we replace A_{mn} and F_m in eq. (23) by their definitions in eqs. (11) and (17). After some algebraic manipulations, we arrive at

$$\sum_{\mu=0}^{\infty}E_\mu(A_{\mu\nu}^{(1)}+A_{\mu\nu}^{(2)})=D_\nu;\quad \nu=0,1,2,\ldots \tag{24}$$

where

$$A_{\mu\nu}^{(1)}=\frac{(-1)^\mu\Gamma_\mu}{\pi}\sum_{m=0}^{\infty}\frac{g_{m\nu}\cos m\phi_0}{\varepsilon_m(\Gamma_\mu^2-m^2)}\cdot$$
$$\cdot\int_0^{\infty}\frac{\sin^2\mathfrak{x}_n d\,H_m^{(2)\prime}(\gamma a)}{\mathfrak{x}^2\gamma H_m^{(2)}(\gamma a)}\,d\mathfrak{x},$$

$$A_{\mu\nu}^{(2)}=-\frac{(-1)^\mu\Gamma_\mu}{h}\sum_{m=0}^{\infty}\frac{g_{m\nu}\cos m\phi_0}{\varepsilon_m(\Gamma_\mu^2-m^2)}\cdot$$
$$\cdot\sum_{n=0}^{\infty}\frac{\sin^2\mathfrak{x}_n d\,J_m'(\gamma_n a)}{\mathfrak{x}_n^2\gamma_n J_m(\gamma_n a)},$$

and $$D_\nu=\frac{-jd}{k^2a}\sum_{m=0}^{\infty}\frac{j^m g_{m\nu}}{\varepsilon_m H_m^{(2)}(ka)}.$$

Eq. (25) is the system of infinitely many linear equations that we intended to derive. In general, this system of equations cannot be solved. However, if the series in eq. (3) is truncated at a finite number N, the system becomes a system of $N\times N$ algebraic equations, in which the unknowns E_μ, $\mu=0,1,2,\ldots,N$, can be determined by solving the equations simultaneously by standard procedures such as the method of Gaussian elimination. After E_μ are determined, it is a matter of direct substitution of E_μ into eqs. (5), (6) and (11) to obtain the field inside the cavity. For example, the z-component of the electric field E_z is given by

$$E_z=\frac{4}{\pi h}\sum_{\mu=0}^{\infty}E_\mu(-1)^\mu\Gamma_\mu\cdot \tag{25}$$
$$\cdot\sum_{n=0}^{\infty}\frac{\sin\mathfrak{x}_n d\cos\mathfrak{x}_n z}{\varepsilon_n\mathfrak{x}_n}\sum_{m=0}^{\infty}\frac{\cos m\phi\cos m\phi_0 J_m(\gamma_n\varrho)}{\varepsilon_m(\Gamma_\mu^2-m^2)J_m(\gamma_n a)};$$
$$\varrho\le a,\quad |\phi|\le\pi,\quad |z|\le h.$$

This completes our derivation for the field inside the cavity due to the incidence of eq. (2) in the absence of the wire.

3. Current Induced on a Wire in the Cavity

In this section, the current induced on the wire inside the cavity when it is illuminated by the field $\hat{E}$ is derived. We attack the problem by assuming that the presence of the wire does not perturb the field generated inside the cavity. This enables us to use $\hat{E}$ as an incident field and to determine the induced current $I(z)$ as if the wire were situated in the free space.

With reference to eq. (26), we note that the electric field tangential to the wire E_z is given in terms of a doubly infinite series of eigenfunctions of the cavity. The series can be interpreted as a spectrum of plane waves. Explicitly, E_z is rewritten as

$$E_z=\sum_{n=-\infty}^{\infty}f_n(\varrho,\phi)\exp(jk\cos\theta_n z); \tag{26}$$
$$\varrho\le a,\quad |\phi|\le\pi,\quad |z|\le h,$$

where $$\theta_n=\cos^{-1}(n\pi/kh), \tag{27}$$

$$f_n=\frac{2}{\pi h}\sum_{\mu=0}^{\infty}E_\mu\frac{(-1)^\mu\Gamma_\mu\sin\mathfrak{x}_n d}{\mathfrak{x}_n}\cdot$$
$$\cdot\sum_{m=0}^{\infty}\frac{\cos m\phi\cos m\phi_0 J_m(\gamma_n\varrho)}{\varepsilon_m(\Gamma_\mu^2-m^2)J_m(\gamma_n a)}. \tag{28}$$

We interpret each component of the field in eq. (26) as a plane wave in free space propagating in the direction θ_n with respect to the z-axis.

In this report, two methods are used to compute the current induced on the wire due to each component of the plane wave spectrum described in eq. (26). The first of these methods is based on an integral equation formulation:

$$\left(\frac{\partial^2}{\partial z^2}+k^2\right)\int_{z_0-h_w}^{z_0+h_w}I_n^{(1)}(z')\,K(z,z')\,dz'= \tag{29}$$
$$=-j4\pi\omega\varepsilon f_n\exp(jk\cos\theta_n z).$$

The above thin wire scattering problem has been thoroughly studied in recent years, and a number of efficient programs to compute the unknown current $I_n^{(1)}$ have been developed. The program developed by Butler [10], which is based on solving eq. (29) by the method of moments, is adopted here. Applying the principle of superposition, the induced current I is given by

$$I(z)=\sum_{n=-\infty}^{\infty}f_n(\varrho,\phi)\,I_n^{(1)}(z), \tag{30}$$

where ϱ is evaluated at the location of the wire.

As is well-known, using moment methods to compute the current on a wire is extremely time-

comsuming when the wire is of the order of several wavelengths. An alternative method that is suitable for long wires is to use the simple approximation formula developed recently by Chang, Lee and Rispin [11], [12]. The techniques used to derive this simple formula are briefly described below:

1. Using a Wiener-Hopf method, the reflection coefficient from the end of a semi-infinite wire illuminated by a plane wave of unit amplitude is determined.
2. By considering the multiple bounces of the current waves, the current induced on a wire of finite length can be expressed in terms of two Neumann series involving the just mentioned reflection coefficient. The series are then summed up into a closed form to give the desired approximation formula.

The induced current due to each component of the plane-wave spectrum is denoted by $I_n^{(2)}$ and is given by

$$I_n^{(2)}(z) = \left[C(\pi-\theta_n)\frac{R(\pi, h_w - z')}{R(\pi, 2h_w)} + \right.$$
$$\left. + \Delta(\pi-\theta_n, h_w - z')\, V(\theta_n, h_w)\right] U(h_w - z') +$$
$$+ \left[C(\theta_n)\frac{R(\pi, h_w + z')}{R(\pi, 2h_w)} + \right. \quad (31)$$
$$\left. + \Delta(\theta_n, h_w + z')\, V(\pi-\theta_n, h_w)\right] U(h_w + z') +$$
$$+ V(\theta_n, z'),$$

where $z' = z - z_0$. In the above formula, V represents the current induced on an infinitely long cylinder by a unit plane wave:

$$V(\theta, z) = -\frac{\mathrm{j}4\pi}{\eta}\frac{\exp(-\mathrm{j}k\cos\theta_n z')}{\sin\theta_n W}, \quad (32)$$

in which W stands for

$$W = -\mathrm{j}\pi \mathrm{J}_0(k a_w \sin\theta_n)\,\mathrm{H}_0^{(2)}(k a_w \sin\theta_n), \quad (33)$$

where J_0 and $\mathrm{H}_0^{(2)}$ are, respectively, the zeroth-order Bessel function of the first kind and the Hankel function of the second kind, and a_w is the radius of the cylinder. The universal function U in the simple formula represents the current on an infinitely long center-fed antenna generated by a unit voltage impulse. For a thin-wire antenna and for a sufficiently large kz, U can be accurately approximated by

$$U(z) = \frac{2\pi}{\eta}\frac{\exp(-\mathrm{j}k|z'|)}{\ln(2k|z'|) - \mathrm{j}\pi/2 - 2\ln(k a_w) - \gamma}, \quad (34)$$

where $\gamma = 0.57712\ldots$ is the Euler's constant. The reflection coefficient R in eq. (31) is defined by

$$R(\theta, z) = \quad (35)$$
$$= -\frac{\eta}{\pi}\left[\ln\left(k a_w \sin\frac{\theta_n}{2}\right) + \gamma + \mathrm{j}\frac{\pi}{2} + \frac{\mathrm{e}^{\mathrm{j}v_0}}{2}E_1(\mathrm{j}v_0)\right],$$

where $v_0 = k z'(1 - \cos\theta_n)$,

and E_1 is the exponential integral. Finally, Δ and C are, respectively, shorthand notations for

$$\Delta = R(\theta_n, 2h_w) - R(\theta_n, h_w + z'), \quad (36)$$

$$C = \frac{R(\pi-\theta_n, 2h_w)\, V(\theta_n, h_w)\, R(\pi, 2h_w)\, U(2h_w) - }{1 - [R(\pi, 2h_w)\cdot}$$
$$\frac{- R(\theta_n, 2h_w)\, V(\pi-\theta_n, h_w)}{\cdot\, U(2h_w)]^2}. \quad (37)$$

Again, the total induced current is obtained by superimposing all $I_n^{(2)}$. As is illustrated in Fig. 2,

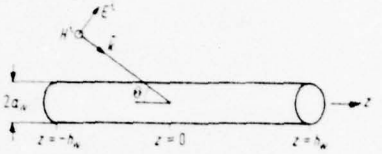

Fig. 2. A finite length cylinder illuminated by an incident plane wave at an oblique angle.

the electric field of the incident plane wave is in the θ-direction and has an amplitude $f_n/\sin\theta_n$. Therefore, I is related to $I_n^{(2)}$ by

$$I(z) = \sum_{n=-\infty}^{\infty} f_n(\varrho, \phi)\frac{I_n^{(2)}(z)}{\sin\theta_n}, \quad (38)$$

where ϱ is evaluated at the location of the wire.

A careful scrutiny of the techniques in deriving both $I_n^{(1)}$ and $I_n^{(2)}$ reveals that the two methods apply only if the incident plane wave is homogeneous, i.e., $\cos^2\theta_n \leqq 1$ or real incident angle θ_n. In the present problem, however, the field $\vec{E}$ inside the cavity consists of both homogeneous and inhomogeneous components. Hence, both methods have to be extended by analytical continuation to cover the case of an incident inhomogeneous plane wave.

Let us first consider $I_n^{(1)}$ which is obtained by solving eq. (29). Note that eq. (29) is developed by equating the axial component of the electric field on the wire and that of the incident field. The tangential component of the incident electric field is $f_n \exp(+\mathrm{j}k\cos\theta_n z)$ which remains valid even in the case when $\cos^2\theta_n > 1$. Thus no modification is necessary here, although allowances in the actual computer programming must be made to accommodate the rapidly oscillating nature of $\exp(+\mathrm{j}k\cos\theta_n z)$ when $\cos\theta_n$ is large.

Next, we have to extend the formula of $I_n^{(2)}$ in eq. (31). In the case of an inhomogeneous plane wave, $\sin\theta_n$ is pure imaginary, and may be calculated from

$$\sin\theta_n = \pm\mathrm{j}\,|\sqrt{\cos^2\theta_n - 1}\,|\,; \quad \cos^2\theta_n > 1. \quad (39)$$

The question is then: "Which sign in eq. (39) should be used in the calculation?" Consider an inhomogeneous plane wave propagating in the x, z plane:

$$E_y = \exp[-\mathrm{j}k(x\sin\theta_n + z\cos\theta_n)]; \quad (40)$$
$$\cos^2\theta_n > 1.$$

In order to satisfy the radiation condition, the field must decay (instead of grow) exponentially

as $x \to +\infty$. This imposes a condition on $\sin\theta_n$, viz.,

$$\mathrm{Im}(\sin\theta_n) < 0\,. \tag{41}$$

Thus, the lower sign (minus sign) in eq. (39) must be used in the calculation of $I_n^{(2)}$ from eqs. (32), (33), (35), and (38). Furthermore, W in eq. (33) becomes

$$W = 2\,\mathrm{I}_0(k a_w)\sqrt{\cos^2\theta_n - 1}\;\mathrm{K}_0(k a_w)\sqrt{\cos^2\theta_n - 1}\,, \tag{42}$$

where I_0 and K_0 are, respectively, the zeroth order modified Bessel functions.

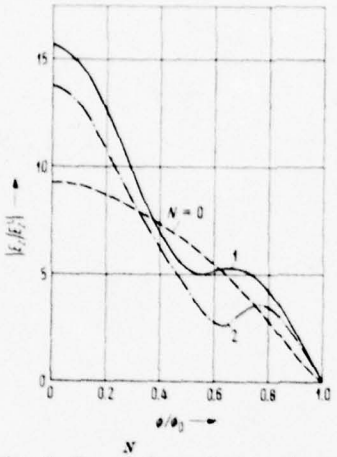

Fig. 3. $E_z = \sum_{n=0}^{N} E_n \cos\Gamma_n\phi$ in the aperture as a function of ϕ with N as a parameter. The geometrical parameters are: $a = 0.3\,\lambda$, $c = 0.3\,\lambda$, $d = 0.015\,\lambda$, $h = 0.6\,\lambda$.

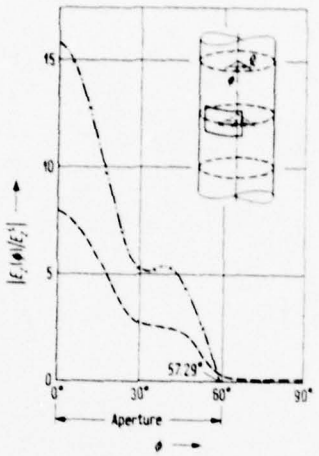

Fig. 4. E_z inside the cavity as a function of ϕ with ϱ/a as a parameter. The geometrical parameters are: $a = 0.3\,\lambda$, $c = 0.3\,\lambda$, $d = 0.015\,\lambda$, $h = 0.6\,\lambda$, $\phi_0 = 1$:

— · — $\sum_{n=0}^{1} E_n \cos\Gamma_n\phi$,

× $\varrho/a = 1.0$ (eq. (25)),

– – – – $\varrho/a = 0.95$ (eq. (25)).

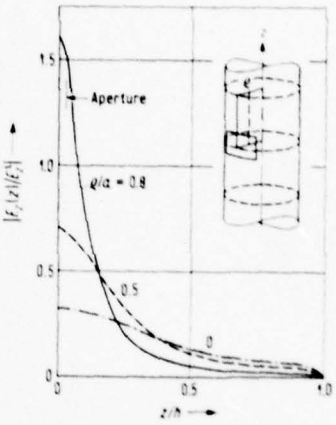

Fig. 5. E_z inside the cavity as a function of z with ϱ/a as a parameter. The geometrical parameters are: $a = 0.3\,\lambda$, $c = 0.3\,\lambda$, $d = 0.015\,\lambda$, $h = 0.6\,\lambda$, $\phi = 0$.

4. Numerical Results and Discussion

In determining the field inside the cavity with the wire absent, the series representation of the aperture field in eq. (3) is truncated at $n = N$ (the series contains $N+1$ terms). We must first establish the convergence of the aperture field with respect to N. The aperture fields as calculated with $N = 0$, 1, and 2 are shown in Fig. 3. We notice that the aperture fields as computed by $N = 1$ and that by $N = 2$ agree reasonably at the main lobe but not so well at the side lobe. For many practical cases, the three-term expansion $N = 2$ is generally sufficiently accurate for computing the aperture field.

An indication of the accuracy of the field $\hat{E}$ inside the cavity is how well $\hat{E}$ satisfies the boundary condition on the cavity wall (including the aperture). In Fig. 4, E_z as computed from eq. (26) is plotted as a function of ϕ. In the aperture defined by $|\phi| \leq 57.29°$, the calculated E_z agrees extremely well with the two-term expansion of the aperture field calculated from eq. (3). It drops to less than 0.01% of the aperture field on the wall where E_z should be ideally zero. Also shown in Fig. 4 is E_z at points just behind the aperture, $\varrho/a = 0.995$. The variations of E_z with respect to z at $\varrho/a = 0$, 0.5 and 0.8 are sketched in Fig. 5. As a function of decreasing (ϱ/a), E_z decreases rapidly from its value in the aperture, while it increases at an even faster rate from zero on the cavity wall toward the center of the cavity. These features are illustrated in Fig. 6 where E_z is plotted as a function of ϱ at $z = 0$ and $z/h = 0.3$.

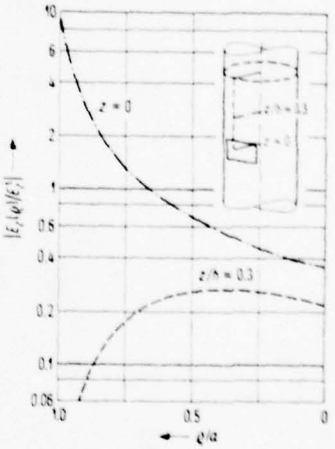

Fig. 6. E_z inside the cavity as a function of ϱ with z/h as a parameter. The geometrical parameters are: $a = 0.3\,\lambda$, $c = 0.3\,\lambda$, $d = 0.015\,\lambda$, $h = 0.6\,\lambda$.

Part B of the problem is to compute the current induced on the wire inside the cavity. As mentioned in previous sections, the simple formula developed by Chang, Lee and Rispin [8] must be extended to compute the current on a finite wire due to an incident inhomogeneous plane wave. Since the method of moments does not require any modification for handling the case of an inhomogeneous incident wave, it provides us a verification of the extended simple formula. The comparison of the

induced currents on a wire in *free space* due to a plane wave of unit strength as computed by both methods is illustrated in Fig. 7, and we notice that the results are in reasonable agreement. Now, we may apply this extended formula to compute the induced current on a wire inside the cavity. In Fig. 8, the current as calculated by the simple formula is compared with that obtained by the method of moments. Again, the agreement between the two results is acceptable. It should be noted that the current inside the cavity is normalized with respect to the center current on a wire of the same length in free space. Since the convergence of the moment method must be established on a case-by-case basis, the simple formula is used hereafter to compute the induced current even in the case where the wire is as short as 0.4 wavelength.

Although we have already established that the three-term expansion is usually adequate to represent the aperture electric field, it is still appropriate here to examine the convergence of the current induced on a wire inside the cavity with

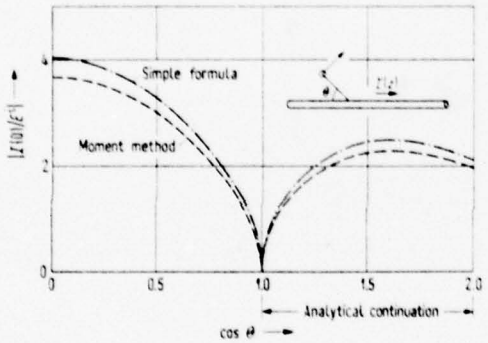

Fig. 7. Comparison of the simple formula and the moment method for the determination of the current induced at the center of a cylinder in free space as a function of the angle of incidence θ (real and imaginary); $a_w = 0.001\ \lambda$, $h_w = 0.25\ \lambda$.

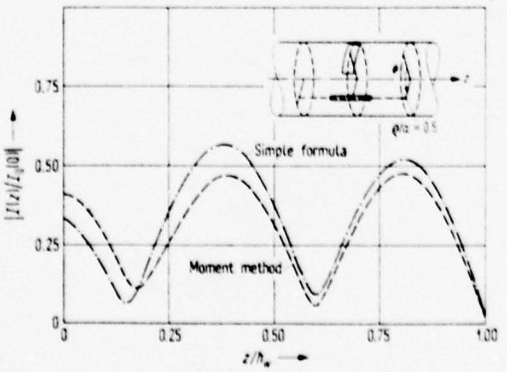

Fig. 8. Comparison of the simple formula and the moment method for the determination of the induced current distribution on a wire inside the cavity. The geometrical parameters are: $a = 0.3\ \lambda$, $\theta = 0.3\ \lambda$, $d = 0.015\ \lambda$, $h = 0.6\ \lambda$, $a_w = 0.001\ \lambda$, $h_w = 1.2\ \lambda$, $\varrho/a = 0.5$, $\phi = 0$, $z_0 = 0$.

varying numbers of expansions. In Fig. 9, the induced currents as calculated with $N = 0$, 1, and 2 are sketched. We see that, as far as the induced current is concerned, the two-term expansion ($N = 1$) is sufficient.

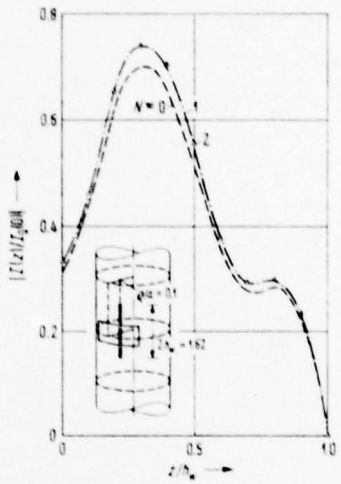

Fig. 9. Induced current on a wire inside the cavity as a function of z with N as a parameter. The geometrical parameters are: $a = 1.0\ \lambda$, $c = 0.6\ \lambda$, $d = 0.015\ \lambda$, $h = 2.2\ \lambda$;

$$E_a = \sum_{n=0}^{N} A_n \cos \Gamma_n \phi.$$

Inside a given cavity, *it is expected that* the induced current on a given wire with its position fixed would increase with the enlargement of the length of the slot $2c$. The induced current at the center of the wire does increase with c when c is relatively small as compared with the radius of the cavity a. The center current acquires its peak value when c/a is about 0.9 and begins to decrease thereafter. These characteristics are demonstrated in Fig. 10.

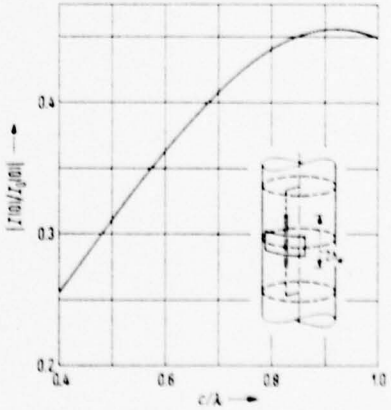

Fig. 10. Induced current at the center of the wire inside the cavity as a function of slot length $2c$. The geometrical parameters are: $a = 1$, $d = 0.015$, $h = 2.2$, freq. $= 0.3$, $a_w = 0.001\ \lambda$, $h_w = 0.2\ \lambda$, $\varrho/a = 0.1$, $\phi = 0$, $z_0 = 0$.

In Fig. 11, we show the center current on the wire as a function of a, $0.25 \leq a/\lambda \leq 0.8$, with the other dimensions fixed. We observe that there are three peaks. The first of these peaks corresponds to the resonance at which $J_0(\gamma_0 a) = 0$. The second and third peaks correspond respectively to $J_1(\gamma_0 a) = 0$ and $J_0(\gamma_1 a) = 0$. It should be noted that the resonances would occur more often beyond the range of Fig. 12, and numerical solutions for large a would not be reliable.

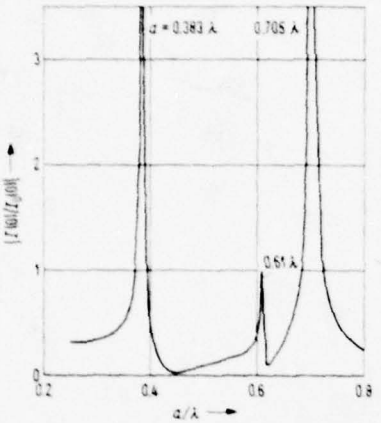

Fig. 11. Induced current at the center of the wire inside the cavity as a function of cylinder radius a. The geometrical parameters are: $c = 0.3\ \lambda$, $d = 0.015\ \lambda$, $h = 0.6\ \lambda$, $h_w = 0.2\ \lambda$, $\varrho/a = 0.1$.

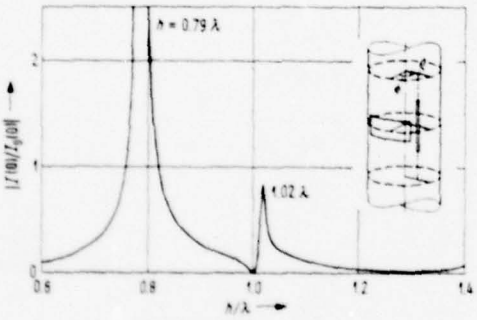

Fig. 12. Induced current at the center of the wire inside the cavity as a function of cavity length $2h$. The geometrical parameters are: $a = 0.5\ \lambda$, $c = 0.3\ \lambda$, $d = 0.015\ \lambda$, $a_w = 0.001\ \lambda$, $h_w = 0.2\ \lambda$, $\varrho/a = 0.1$.

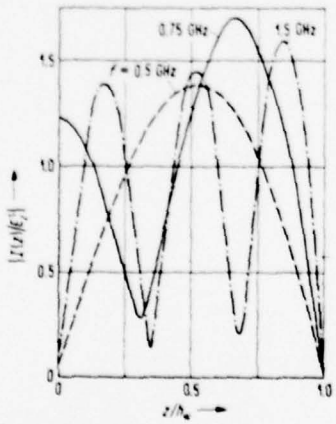

Fig. 13. Current distribution induced on a wire inside the cavity with frequency as a parameter. The geometrical parameters are: $a = 0.35$ m, $c = 0.25$ m, $d = 0.005$ m, $h = 0.82$ m, $a_w = 0.001$ m, $h_w = 0.3$ m.

The center current on a wire as a function of the length of the cavity $2h$ with other dimensions fixed is plotted in Fig. 12. Two peaks are observed in Fig. 12. The first peak is related to the resonance corresponding to $J_0(\gamma_1 a) = 0$, but we are unable to analyze the nature of the smaller peak at $h = 1.02\ \lambda$.

Finally, we examine the variation of the induced current with respect to the frequency of the incident plane wave. The induced currents at representative frequencies are sketched in Fig. 13, which reflects the alteration of the electrical length of the wire.

This report was supported by contract No. N000 14-75-C-0293.

(Received November 11th, 1978.)

References

[1] Sommerfeld, A., Partial differential equations in physics. Academic Press, New York 1949, pp. 29, 159.

[2] Silver, S. and Saunders, W. T., The external field produced by a slot in an infinite circular cylinder. J. appl. Phys. **21** [1950], 153–158.

[3] Barakat, R. and Levin, E., Diffraction of a plane EM wave by a perfectly conducting cylindrical lamina. J. Opt. Soc. Amer. **54** [1964], 1089–1094.

[4] Wallenberg, R. F., Radiation from aperture in conducting cylinders of arbitrary cross section. Transact. IEEE AP-**17** [1974], 56–62.

[5] Bailin, L. L. and Spellmire, R. J., Convergent representations for the radiation fields from slots in large circular cylinders. Transact. IRE AP-**5** [1957], 374–383.

[6] Safavi-Naini, S., Diffraction of electromagnetic waves by a slotted circular cylinder. M. S. Thesis, University of Illinois, Urbana, 1976.

[7] Safavi-Naini, S., Lee, S. W., and Mittra, R., Transmission of an EM wave through the aperture of a cylindrical cavity. Electromagnetic Lab. Tech. Rep. No. 76-1, University of Illinois, Urbana, 1976.

[8] Safavi-Naini, S., Lee, S. W., and Mittra, R., Transmission of EM wave through the aperture of a cylindrical cavity. Transact. IEEE EMC-**19** [1977], 74–81.

[9] Harrington, R. F., Field computation by moment methods. Macmillan, New York 1968, pp. 7, 178.

[10] Butler, C. M., Evaluation of potential integral at singularity of exact kernel in thin-wire calculations. Transact. IEEE AP-**23** [1975], 293–294.

[11] Chang, D. C., Lee, S. W., and Rispin, L., Simple expressions for current on a thin cylindrical receiving antenna. Sci. Rep. No. 20, University of Colorado, Dec. 1976.

[12] Chang, D. C., Lee, S. W., and Rispin, L., Simple formula for current on a cylindrical receiving antenna. Transact. IEEE AP-**26** [1978], 683–690.

[13] Harrington, R. F., Time-harmonic electromagnetic fields. McGraw-Hill Book Co., New York 1962, p. 200.

Accuracy Test for High-Frequency Asymptotic Solutions

R. MITTRA, FELLOW, IEEE, AND M. TEW

Abstract—Asymptotic solutions, or solutions whose accuracy increases as some parameters increase, have seen increasing use in recent years. For example, the problem of a magnetic dipole radiating on an infinite circular cylinder has had three different asymptotic solutions proposed. Unfortunately, it is difficult to assess the accuracy of these asymptotic solutions, or even to determine their relative accuracy. An accuracy test based on the satisfaction of the *E*-field boundary condition on the cylinder surface is proposed. The test is performed by relating the spectral domain representation of the surface *H*-field (given by the asymptotic solution) to that of the *E*-field and then inverse transforming to obtain the surface *E*-field. In some cases analytic and numerical techniques are combined to aid in evaluation of the spectral content of the surface *H*-field. The proposed test is applied to two of the published solutions and to a third solution generated to bridge the differences between them. Three-dimensional plots of the resulting surface *E*-field are presented. It was found that the proposed test is most sensitive to the source-region behavior of the solution and relatively insensitive to the large path length behavior.

INTRODUCTION

THE PROBLEM of determining the induced surface currents on an infinite circular cylinder excited by a slot radiator has received increased attention in recent years. One reason for this interest is the usefulness of the induced currents in calculating various electrical parameters. In a conformal slot array, for instance, knowledge of the currents allows calculation of both the mutual impedance between two slots and the far-field pattern. The work reported here is concerned with a test which attempts to evaluate the accuracy of existing solutions for the infinite cylinder problem.

An exact modal solution to the cylinder problem does exist [1], [2]. However, for large radii, the solution (whose form is an infinite series with each term containing an infinite integral) converges so slowly as to make its use impractical. For large kR (k is the wavenumber and R is the radius), three asymptotic solutions have been published [3]–[7]. Two of the solutions [3]–[6] are derived from manipulation of the modal solution and are asymptotically correct for large path lengths. One of these solutions [3], [4], which is used in the testing program developed in this paper, will hereafter be referred to as Asymptotic Solution 1 or AS-1. Another solution which is also tested herein is based on a modification of the work of V. A. Fock addressing the problem of radiation on a sphere. This solution is asymptotic in both the sense of large path length and large radius and will hereafter be referred to as Asymptotic Solution 2 or AS-2. In contrast to the AS-1 solution, the AS-2 solution has the feature that it exhibits the appropriate asymptotic behavior of the surface current, both in the vicinity of the source and at large distances away from it. This property of the AS-2 solution will be shown to have a profound effect on the results of the boundary condition test to be described below.

Manuscript received March 22, 1978; revised August 12, 1978. This work was supported in part by the Joint Services Electronics Program (U.S. Army, U.S. Navy, and U.S. Air Force) under Contract DAAG-29-78-C-0016, and in part by the Army Research Office under contract DAAG-29-77G-0111.

The authors are with the Electromagnetics Laboratory, Department of Electrical Engineering, University of Illinois, Urbana, IL 61801.

0018-926X/79/0100-0062$00.75

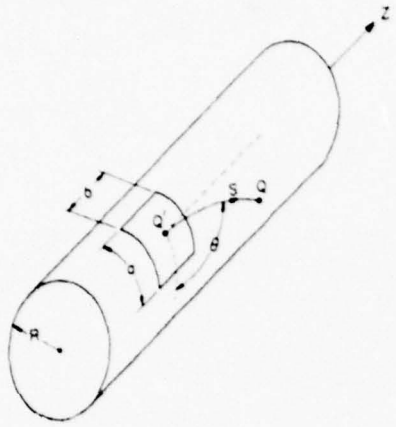

(a)

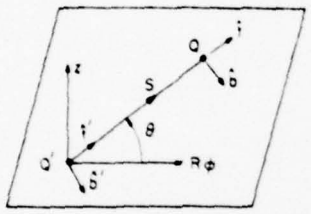

(b)

Fig. 1. Geometry of cylinder problem. (a) Infinite cylinder with slot. (b) Developed cylinder.

Because all of the asymptotic solutions for the cylinder are approximate, a test which could determine the relative accuracy of the solution is highly desirable. This paper proposes such a test based on satisfaction of the E-field boundary condition. The test is applied to the AS-1 solution, a modified version of the AS-1 solution, and to the AS-2 solution. When possible, an exact analytic solution was also tested.

THE PROBLEM

The problem addressed consists of an infinite perfectly conducting cylinder of radius R, as shown in Fig. 1(a). A standard ρ, ϕ, z cylindrical coordinate system is imposed on the cylinder so that the z-axis coincides with the cylinder axis. The coordinate system is set up so that $\rho = R$, $\phi = 0$, $z = 0$ defines the center of the slot (or coincides with an elemental magnetic dipole radiator). As shown, s is the path length on the cylinder surface, and θ is measured from the ϕ-axis to the surface path.

The cylinder is a developable surface, and a geodesic path on the cylinder surface becomes a straight line on the infinite strip that makes up a developed cylinder. Fig. 1(b) shows the developed cylinder and introduces the local $\hat{n}'$, $\hat{b}'$, $\hat{t}'$ and $\hat{n}$, $\hat{b}$, $\hat{t}$ coordinate systems, where $\hat{n}'$, $\hat{n}$ are the outward normal to the surface, and $\hat{t}'$, $\hat{t}$ are tangent to the surface path at the source and observation points, respectively ($\hat{b}' = \hat{t}' \times \hat{n}'$, $\hat{b} = \hat{t} \times \hat{n}$). On the developed cylinder $\hat{t}'$ is parallel to $\hat{t}$, $\hat{n}'$ is parallel to $\hat{n}$, and $\hat{b}'$ is parallel to $\hat{b}$; however, this is not the case for the undeveloped cylinder. Each of the asymptotic solutions tested determines the surface H-field components at the observation point Q in terms of the field parallel to the surface ray H_t, and the field perpendicular to both the surface ray and the surface normal H_b. Thus each solution tested is of the form

$$\bar{H}(Q) = \bar{M} \cdot (\hat{b}'\hat{b}H_b + \hat{t}'\hat{t}H_t), \tag{1}$$

where $\bar{M}$ is the magnetic dipole moment. For all results reported here, $\bar{M} = \hat{\phi}$, i.e., a circumferentially oriented source was used.

SOLUTIONS TESTED

The results of tests on three asymptotic solutions are included: the AS-1 solution, the AS-2 solution, and a modified version of the AS-1 solution.

The AS-1 solution is given by

$$H_b(Q) \sim v(\xi)G(s)$$

$$H_t(Q) \sim (2j/ks)u(\xi)G(s)$$

$$G(s) = \frac{k^2}{2\pi\eta}\frac{e^{-jks}}{ks} \qquad \eta = \frac{\sqrt{\mu_0}}{\sqrt{\epsilon_0}} \approx 377\,\Omega$$

$$\xi = \left(\frac{k}{2R_t^2}\right)^{1/3} s, \tag{2}$$

where η is the impedance of free space, and u and v are Fock functions. ξ is a normalized distance parameter, with R_t being the radius of curvature along the surface ray path (radius of curvature in the direction of $\hat{t}$). For the cylinder case under consideration $R_t = R/\cos^2\theta$. Note that $\xi \to 0$ whenever $R \to \infty$ or $\theta \to \pi/2$. For the case when $\xi \to 0$ the AS-1 solution reduces to

$$H_b(Q) \sim G(s)$$

$$H_t(Q) \sim (2j/ks)G(s), \tag{3}$$

and the form of H_b identically recovers the $(ks)^{-1}$ term from the exact solution of a magnetic dipole radiating on an infinite flat-ground plane.

The AS-2 solution is found by

$$H_b(Q) \sim [(1-j/ks)v(\xi) - (1/ks)^2 u(\xi) + j(\sqrt{2}kR_t)^{-2/3} \cdot v'(\xi) + j(\sqrt{2}kR_t)^{-2/3}(R_t/R_b)u'(\xi)]\,G(s)$$

$$H_t(Q) \sim (j/ks)[v(\xi) + (1-2j/ks)u(\xi) + j(\sqrt{2}kR_t)^{-2/3} \cdot u'(\xi)]\,G(s), \tag{4}$$

where v and u are Fock functions, and v' and u' are their derivatives, respectively. ξ and $G(s)$ were defined above, and R_b is the radius of curvature transverse to the surface ray (radius of curvature in the direction of $\hat{b}$). Two features of the AS-2 solution stand out. As $kR \to \infty$ the solution reduces to

$$H_b(Q) \sim [1 - j/ks - (1/ks)^2]\,G(s)$$

$$H_t(Q) \sim (2j/ks)[1 - j/ks]\,G(s), \tag{5}$$

which identically recovers the exact solution for a magnetic dipole radiating on an infinite flat plane (this is in contrast to the AS-1 solution which recovered only the $1/s$ term of H_b and the $1/s^2$ term of H_t). As $\theta \to \pi/2$ the AS-2 solution may be put in the following form:

$$H_b(Q) \sim [H_b(Q)]_{\text{planar}} + (A/kR)e^{-jks}/\sqrt{ks}, \tag{6}$$

where A is a constant. The surface ray along the cylinder axis thus exhibits less attenuation than a corresponding ray on a flat plane. (This type of asymptotic behavior, as $\theta \to \pi/2$, is also exhibited by another solution [5]–[6].

Thus two distinct differences exist between the AS-1 and AS-2 solutions in the limiting cases of $kR \to \infty$ and $\theta \to \pi/2$. One concerns the higher order terms ($1/s^2$, $1/s^3$) of the solution and may be thought of as a localized source-region effect. The other difference lies in the attenuation of a ray propagating along the cylinder axis ($\theta = \pi/2$), where the AS-1 solution decays as $1/s$, and the AS-2 solution decays as $1/\sqrt{s}$. This effect, then, is hardly significant near the source, where the $1/s^2$ and $1/s^3$ terms dominate, but it determines the field behavior far away from the source.

In an attempt to separate the above two effects, a third solution has been constructed, which is a modified AS-1 solution and will be denoted AS-3. The AS-3 solution is given by

$$H_b(Q) \sim [u(\xi) - j/ks - (1/ks)^2]\, G(s)$$

$$H_t(Q) \sim (2j/ks)[u(\xi) - j/ks]\, G(s). \tag{7}$$

As is apparent, the AS-1 solution has been modified by the addition of the higher order terms present in the exact solution of the planar problem. The AS-3 solution will recover the exact planar solution when $kR \to \infty$, just as the AS-2 solution does. However, along $\theta = \pi/2$ the AS-3 solution decays as $1/s$, while the AS-2 solution decays as $1/\sqrt{s}$.

The rationale behind creation of the AS-3 solution is contained in the following argument. The AS-1 and AS-2 solutions are quite different—not only in the construction of the solution, but also in the behavior under limiting cases. Both the source region behavior and the "asymptotic" behavior (for large ks along $\theta = \pi/2$) are significantly different. Even if a test revealed differences between the AS-2 and AS-1 solutions, it might still be difficult to determine anything about the local accuracy of the solution, i.e., it might be difficult to determine the "cause" of the difference in test results. Creation of the AS-3 solution is designed to alleviate this problem. Also, since AS-1 and AS-3 have the same behavior as $\theta \to \pi/2$, comparison of their test results may reveal the role of the source region in satisfaction of the test. Similarly, AS-3 and AS-2 have the same behavior in the source region (as $kR \to \infty$), so comparison of their test results may reveal the role of the $1/\sqrt{s}$ term.

In review, we have three asymptotic solutions to test—two have been published, and the third has been created to somewhat bridge the differences between the first two. The test proposed will investigate how well the E-field boundary condition on the cylinder surface is satisfied.

E-FIELD TEST

The tangential E-field must be zero everywhere on the surface of a perfect conductor. The exact solution for a circumferential slot radiating on a perfectly conducting circular cylinder thus would have $E_\phi = 0$ everywhere on the cylinder and $E_z = 0$ everywhere except in the extent of the slot. The E-field test checks to see how well the asymptotic solutions satisfy this condition.

The most direct and attractive method of determining the surface E-field would be to compute the normal derivative of the H-field. Unfortunately, the asymptotic solutions are valid only for points on the cylinder surface, so that such a direct computation is unfeasible. Accordingly, an indirect procedure must be used. An indirect evaluation of the surface E-field is conducted in the following manner: each of the asymptotic solutions predicts the H-field on the cylinder surface. Through the use of Maxwell's equations the surface H-field may be related to the surface E-field and the boundary condition checked. Use of the spectrum of the H-field instead of the direct surface field makes analysis straightforward as well as allowing the use of a fast-Fourier transform (FFT) algorithm for efficient numerical calculation.

The test proceeds as follows.

1) A cylindrical transform is defined as

$$\tilde{H}_{\substack{z\\ \phi}}(n, k_z) = 1/2\pi \int_0^{2\pi} d\phi \int_{-\infty}^{\infty} dz\, H_{\substack{z\\ \phi}}(\phi, z) e^{jn\phi} e^{jk_z z}. \tag{8}$$

2) Electric and magnetic vector potentials are expanded with unknown coefficients

$$\begin{matrix} A_z \\ F_z \end{matrix} = \frac{1}{2\pi} \sum_{n=-\infty}^{\infty} e^{jn\phi} \int_{-\infty}^{\infty} \begin{matrix} f_n(k_z) \\ g_n(k_z) \end{matrix} H_n^{(2)}(\rho\sqrt{k^2 - k_z^2}) \cdot e^{jk_z z}\, dz. \tag{9}$$

Observe that n and k_z are "transform variables", k is the wavenumber, and $H_n^{(2)}$ is the nth order Hankel function of the second kind, representing an outward-traveling cylindrical wave. For future notation, the complex variable γ will be used to replace the radical in the argument of the Hankel function $\gamma = \sqrt{k^2 - k_z^2}$.

3) Through the use of

$$\bar{H} = \nabla \times \bar{A} - j\omega\epsilon_0 \bar{F} + 1/j\omega\mu_0 \nabla\nabla \cdot \bar{F} \tag{10}$$

one may determine the unknown coefficients f_n and g_n in terms of the transform of the surface H-field as

$$f_n(k_z) = \frac{-1}{\gamma H_n'^{(2)}(\gamma R)} \left[\tilde{H}_\phi(n, k_z) + \frac{nk_z}{\gamma^2 R} \tilde{H}_z(n, k_z) \right]$$

$$g_n(k_z) = \frac{j\omega\mu_0}{\gamma^2 H_n^{(2)}(\gamma R)} \tilde{H}_z(n, k_z), \tag{11}$$

where $H_n'^{(2)}$ is the derivative of the $H_n^{(2)}$ Hankel function.

4) Applying

$$\bar{E} = -\nabla \times \bar{F} - j\omega\mu_0 \bar{A} + 1/j\omega\epsilon_0 \nabla\nabla \cdot \bar{A} \tag{12}$$

permits computation of the surface E-field, accomplishing the desired test.

The above procedure can be condensed into two steps of actual computation by combining (9)–(12). While the resulting expressions appear to be complex, this two-step procedure is significant because it essentially involves only a two-dimensional Fourier transform, modification and combination of the transformed fields, and then inverse Fourier transformation and summation of the Fourier coefficients. The analysis is computationally efficient because the FFT can be used to evaluate all integrals involved.

Practically speaking, the greatest difficulty in the above procedure comes in accurately determining the spectrum of the surface H_ϕ-field. Both the AS-3 and AS-2 solutions have $1/s^2$

and $1/s^3$ singularities, while the AS-1 solution has a $1/s$ singularity. The "peakiness" of these H_ϕ-fields means that special care must be taken in using the FFT to determine the spectrum.

The first attempt to overcome this problem involved raising the magnetic dipole slightly above the cylinder surface so that the field was no longer singular but had a finite peak. After this step had been implemented, a convergence check of the FFT integral showed that the FFT was able to handle the $1/s$ peak correctly with reasonable sampling rates, but the $1/s^2$ and $1/s^3$ peaks yielded erroneous results. Further measures were necessary to achieve a reliable test of the AS-3 and AS-2 solutions (for a reasonable computer size).

The key to achieving a reliable check of the AS-2 and AS-3 solutions lies in recognizing that the singular form of the source region is that of a planar case, and that the singularity has an analytic transform. Specifically, the planar singularity can be expressed as

$$H_\phi|_s = \frac{1}{2\pi\eta jk}\left(\frac{\partial^2}{\partial^2(R\phi)^2} + k^2\right)\frac{e^{-jks}}{s}$$

$$H_z|_s = \frac{1}{2\pi\eta jk}\,\frac{\partial^2}{\partial(R\phi)\partial z}\,\frac{e^{-jks}}{s}, \tag{13}$$

where s is the path length given by $s = \sqrt{\Delta^2 + (R\phi)^2 + z^2}$, and Δ is the height of the dipole above the cylinder. Because the singularities may be expressed as derivatives, their analytic transform is obtainable and is of the form

$$\bar{H}_z|_s = \frac{Q}{2\pi\eta jk}\left(\frac{-nk_z}{R}\right)\frac{1}{4\pi jR}\,\frac{e^{-j\Delta\sqrt{k^2-(n/R)^2-k_z^2}}}{\sqrt{k^2-(n/R)^2-k_z^2}}$$

$$\bar{H}_\phi|_s = \frac{Q}{2\pi\eta jk}\left(-\frac{n^2}{R^2} + k^2\right)\frac{1}{4\pi jR}\,\frac{e^{-j\Delta\sqrt{k^2-(n/R)^2-k_z^2}}}{\sqrt{k^2-(n/R)^2-k_z^2}}, \tag{14}$$

where Q is a constant.

The total field on the cylinder can then be expressed as

$$\bar{H}(Q) = \bar{H}_{\text{planar}}(Q) + \bar{H}_{\text{difference}}(Q), \tag{15}$$

where $\bar{H}(Q)$ is the total field as predicted by an asymptotic solution, and $\bar{H}_{\text{planar}}(Q)$ is the field that would exist on a flat infinite ground plane. (This division may be thought of as taking the planar field, "wrapping" it around the cylinder, and subtracting it from $\bar{H}(Q)$.) The transform of the surface fields is given by

$$\tilde{\bar{H}}(n, k_z) = \tilde{\bar{H}}_{\text{planar}}(n, k_z) + \tilde{\bar{H}}_{\text{difference}}(n, k_z) \tag{16}$$

and $\tilde{\bar{H}}_{\text{planar}}(n, k_z)$ is given analytically in (14). $\tilde{\bar{H}}_{\text{difference}}(Q)$ is at most on the order of $1/\sqrt{s}$, so that evaluation of $\tilde{\bar{H}}_{\text{difference}}(n, k_z)$ can be reliably obtained from application of the FFT. Any test which involves breaking the fields up into planar and difference fields will be termed a *hybrid* computation, because it combines analytic and numerical techniques. The only difference between a "hybrid computation" and a "direct computation" is in the method of obtaining the spectrum. After the spectrum is found both tests proceed identically. Fig. 2 compares the phase of $\tilde{H}_\phi$ for a fixed value of k_z, when the transform was derived from hybrid and direct computations. Comparison with the phase of the modal transform reveals the increased accuracy of the hybrid method.

To utilize the E-field test the three asymptotic solutions are

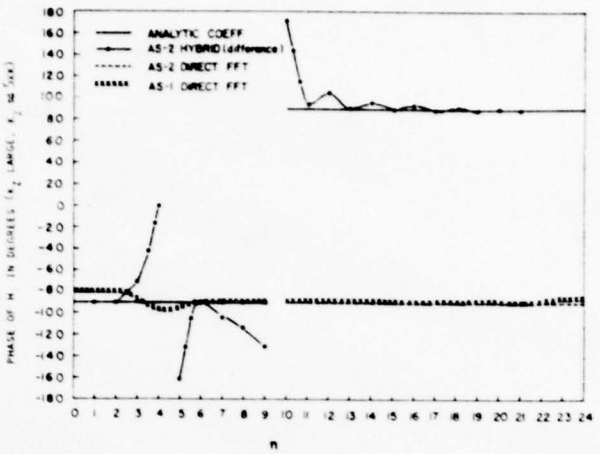

Fig. 2. Effect of hybrid computation of phase of $H\phi$ transform.

compared to an exact modal solution [2]. The procedure used in deriving the exact modal solution is essentially the same as that used to perform the E-field test. The difference lies in the fact that while the test begins with the asymptotic H-field, the modal solution begins with the known E-field (known for an elemental source). In a manner similar to the test, the H-spectrum may be found from the known E-fields and can be expressed in terms of the E-spectrum. This provides analytic H_z and H_ϕ spectrums that can be compared to those resulting from the asymptotic solutions. After the H-spectrum is obtained from the E-field it may be tested just like any other spectrum. This "check", which begins with a surface E-field, finds the H-spectrum, and then returns to the surface E-field, is also valuable in assuring that the FFT sampling of the spectrum is sufficient.

During actual application of the test, the source used was a slot radiator instead of an elemental dipole. This was necessary because the surface E-field of the slot is finite, although discontinuous, while the surface E-field from the elemental source is singular. Sampling the E-spectrum sufficiently well to represent the singular surface field would make the computer requirements prohibitively large, while the more regular slot is readily handled.

Representation of the slot spectrum was achieved by first determining the H-field spectrum due to an elemental dipole source (the direct asymptotic solutions or, for the analytic case, $\bar{E}_{\text{surface}} = \hat{z}(\delta(\rho - R)\,\delta(\phi)\,\delta(z))$. The H-spectrum was then multiplied by the transform of the slot distribution, which was equivalent to convolving the elemental source with a distribution in the space domain. For a finite slot as shown in Fig. 1(a) the transforms used were of the form $[\sin(k_z b/2)]/(k_z b/2)$ to represent a uniform E_z-field, and of the form $\cos(\alpha n)/[\pi^2/4 - (\alpha n)^2]$, $\alpha = \arcsin(a/2R)$ to represent a half-period cosine spreading in ϕ.

The totality of the E-field check has now been determined. The components of the spectrum of the H-field that result from an elemental source are determined. For the asymptotic solutions the spectrum is determined either by direct application of the FFT or by use of the hybrid technique; for the exact case the H-spectrum may be found analytically. Regardless of its source, the H-spectrum is then multiplied by the transform of the assumed slot distribution, accomplishing the convolution that is necessary to represent the slot distribution.

The E-field spectrum is then found from modification and combination of the H-field spectrum components. Finally, inverse Fourier transformation and summation of the Fourier coefficients gives the surface E-field. The next section compares the surface E-fields given by the three asymptotic solutions and compares them to the analytic solution.

RESULTS OF THE E-FIELD TEST

All results presented here are for the following configuration:

- cylinder radius $R = 1.517\ \lambda$,
- slot width $b = 0.3068\ \lambda$,
- slot length $a = 0.6858\ \lambda$,
- extent of z sampling $= 12.5\ \lambda$,
- number of samples in $z = 128$,
- extent of ϕ sampling $= 2\pi$ rad,
- number of Fourier coefficients in $\phi = 64$.

This set of parameters results in a sampling of the spectrum out to $k_z \approx 5 \bullet k$.

The figures that follow are three-dimensional views of the surface E_ϕ-field that results from carrying out the test. These three-dimensional plots are more valuable in representing shape and form than in revealing magnitude values. The surface E-field is calculated after multiplication by the spectrum of the assumed slot distribution, so E_ϕ should be zero everywhere. Since all of the magnitudes are symmetric in z, only half of the total surface is presented in each plot.

The test was first applied to the analytic H-spectrum. This was the standard to which all the other solutions were compared. The analytic solution resulted in E_ϕ that was essentially zero (a totally flat curve) and an E_z that was well contained. The fact that E_z went to zero in a smooth curve in the z-direction instead of a discontinuous curve was due to the numerical calculation. This curve revealed that the error introduced by performing finite sums and integrals was negligible.

The test was next applied directly to the AS-2 solution. The resulting E_z-field was considerably more spread than in the analytic case. The E_ϕ-field, instead of being zero, showed two sharp peaks near the source and a rippled character away from the source.

The effect of using a hybrid computation on the AS-2 solution can be seen in Fig. 3. The beneficial effects of using the hybrid computation were easily seen in the E-fields. The form of E_z was much closer to the analytic shape than when the direct FFT was used, and the peaks of E_ϕ were removed entirely. E_ϕ still retained some of its rippled character, but overall the error was greatly reduced.

Since the previous tests revealed the desirability of using the hybrid computation when possible, the results of testing the AS-3 solution by direct FFT are not shown. Applying the hybrid method to the AS-3 solution generated forms that were practically indistinguishable from those that resulted from applying the hybrid method to the AS-2 solution.

Because the AS-1 solution only has a singularity (peak) on the order of $1/s$, it is not necessary to resort to a hybrid computation to obtain a reliable check. Fig. 4 presents the resulting surface E_ϕ-field. As can be seen, the E_ϕ-field has significant nonzero content. The extent of the corresponding E_z-field was much broader than that of the modal solution.

While the three-dimensional plots are good for determining the overall trend and elucidating the general shape of curves, it is often difficult to use them to get specific information

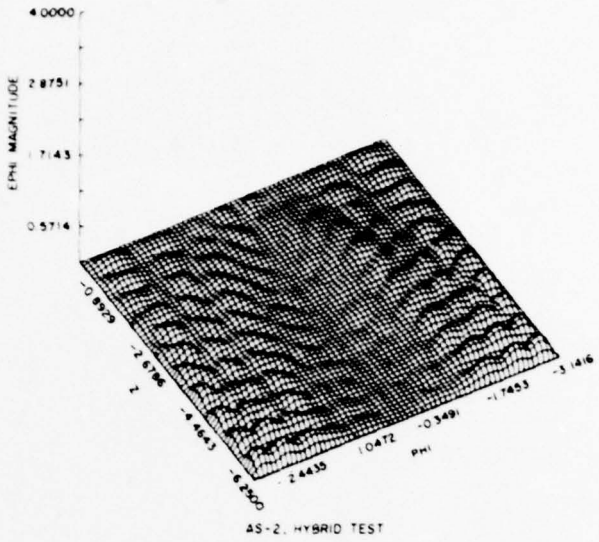

Fig. 3. Surface E_ϕ-field from hybrid test of AS-2 solution.

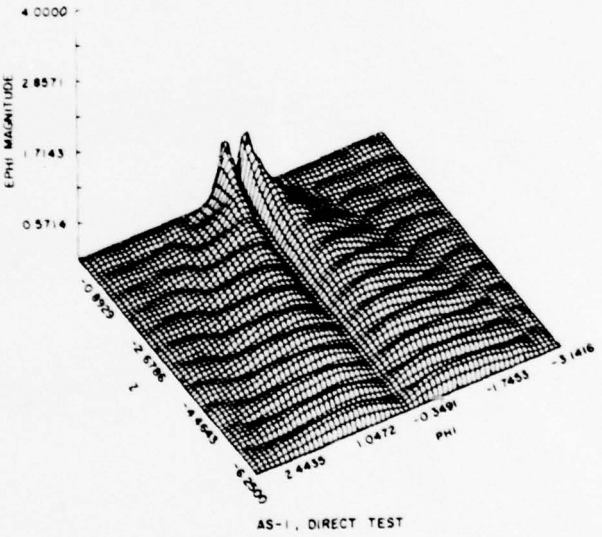

Fig. 4. Surface E_ϕ-field from direct test of AS-1 solution.

about a single point or constant coordinate cut. The point of interest may, for example, be hidden behind a peak which obscures it from view. Accordingly, Fig. 5 is a graph of the resultant E_z-field along the $\phi = 0$ cut, i.e., through the slot and along the cylinder axis. There are several features of interest here.

1) The analytic solution predicts well the expected discontinuity in E_z.

2) The AS-2 and AS-3 solutions checked with the hybrid computation are indistinguishable from one another. Their E_z-field is slightly more spread than that of the analytic solution.

3) The AS-1 solution with a direct test does attain the desired shape curve, however, it has significant E_z content over a much larger region than either the AS-2 or AS-3 solutions (where E_z should be zero).

4) The direct computation applied to the AS-2 solution yields a sharp peak at the edge of the slot. The large field

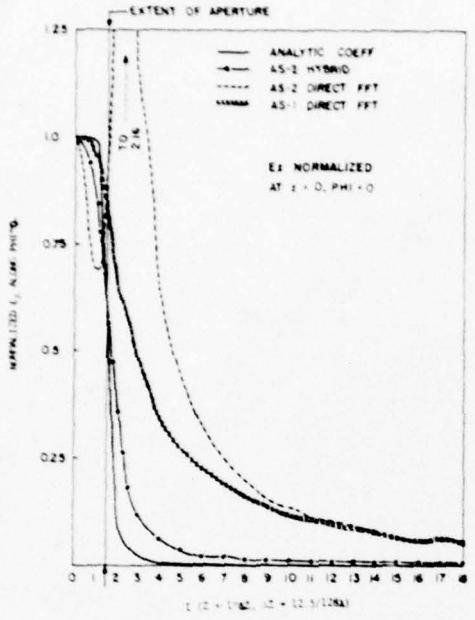

Fig. 5. Surface E_2-field along $\phi = 0°$ cut.

values extend outside the slot region where the field should go to zero.

The three dimensional plots concealed the local behavior at the edge of the slot resulting from a direct computation of the AS-2 solution. This $\phi = 0$ cut, however, shows dramatically the improvement when a hybrid computation is used.

DISCUSSION OF E-FIELD TEST

In the beginning it was hoped that the E-field test would provide a means of reliably judging the accuracy of the asymptotic solutions.

The resulting E-field after performance of the test does provide a good qualitative measure of how well the asymptotic solution satisfies the E-field boundary condition. Indeed, application of the test to the transform of the exact modal solution did result in fields that satisfied the boundary condition quite well. In addition, application of the test to approximate asymptotic solutions showed that they did not test as well as the exact solution. In this respect, the E-field test does provide a good "global test" of a proposed solution, i.e., if the solution is accurate everywhere, the solution will show good results from the test.

On the other hand, when comparing the relative accuracy of approximate solutions, the source-region behavior appears to be more critical for satisfaction of the test than the large path length behavior—asymptotic solutions that contain higher order terms ($1/s^2$, $1/s^3$) in the source region H-field do satisfy the E-field test better than solutions that contain only terms on the order of $1/s$. The large path length behavior did not appreciably affect the test results. If the source region behavior was the same (for a limiting case), then a solution that decayed as $1/s$ tested essentially the same as a solution that decayed as $1/\sqrt{s}$. In fact, the surface E-fields that resulted were indistinguishable when graphed, though there were *slight* numerical differences. In general, it seemed that the energy contained in the long path length region was so small compared to the source region energy that its effect of the results was negligible. This is not surprising in view of the nature of the E-field test, i.e., based on an integral of the surface H-fields.

Emphasis of the source region is not necessarily detrimental to the E-field test, for it is likely that the source region will heavily influence the computation of values of physical parameters of interest, such as the mutual impedance between two slots on a curved surface. Wire antennas provide a good analogy, for the source region behavior dominates calculation of the self- and mutual-impedance and the current behavior at the end plays less of a role. An E-field boundary condition check of a wire antenna would be little influenced by the current far away from the source but would be source region sensitive. It is not surprising then, that the E-field check reveals little about the local character of solution but instead provides more of a global test. The point should be made, however, that a large path length solution for the antenna current would probably be of very limited use since both the impedance behavior and the radiation pattern derived from this type of asymptotic solution would be grossly in error. The E-field test proposed in this paper is able to distinguish between a solution which has a better overall behavior on the entire surface and an alternate solution which is only good in local isolated regions but has large errors in other regions where the current is significant.

Some numerical difficulties were encountered during execution of the test. The high-order source-region terms made it quite difficult for the FFT to accurately compute the integral involved. Since use of the FFT requires equally spaced sampling over the interval, a sampling sufficient to accurately evaluate the peak resulted in matrix sizes too large for some computers (CDC CYBER 74, for example). For solutions whose source-region behavior went to a planar-type singularity in the limit, however, analytic evaluation of the planar spectrum allowed completion of the test. A solution which contains higher order source-region terms but does not go to planar-type behavior in the limit will be quite difficult to test by this method unless it has an analytical transform (or unless the investigator has an extraordinarily large computer). However, such a behavior would not be expected to be physically meaningful anyhow.

The second solution [5]–[6] is a good example of this, for it contains the $1/s^2$ source region term, but not the $1/s^3$ term. This solution could be tested by modifying its source-region behavior by the addition of the $1/s^3$ term and performing a hybrid computation. This has not been done since comparison of the AS-3 and AS-2 tests indicate that solutions with the same limiting source-region behavior will yield virtually identical E-field tests.

To sum up, it appears that the E-field test can provide a measure of the accuracy of a proposed asymptotic solution. An FFT is employed so that the evaluation of the integrals involved may be efficiently performed, but some care must still be taken in the computation. The test reveals that solutions which have planar-type source-region behavior in the limit satisfy the E-field boundary condition better than those that only have terms on the order of $1/s$. The test is, however, relatively insensitive to the large path-length behavior of a solution.

REFERENCES

[1] L. L. Bailin, "The radiation field produced by a slot in a large circular cylinder," *IRE Trans. Antennas Propagat.*, vol. AP-3, no. 3, pp. 128–137, July 1955.

[2] R. F. Harrington, *Time-Harmonic Electromagnetic Fields*. New York: McGraw-Hill, 1961.

[3] Y. Hwang and R. G. Kouyoumjian, "The mutual coupling between slots on an arbitrary convex cylinder," ElectroScience Lab., Dep. Elec. Eng., Ohio State Univ., Semi-Annu. Rep. 2902-21, prepared under Grant NGL 36-003-138, 1975.

[4] P. H. Pathak, "Analysis of a conformal receiving array of slots in a perfectly conducting circular cylinder by the geometrical theory of diffraction," ElectroScience Lab., Dep. Elec. Eng., Ohio State Univ., Tech. Rep. ESL 3735-2, prepared under Contract N00140-74-C-6017, 1975.

[5] Z. W. Chang, L. B. Felsen, A. Hessel, and J. Shmoys, "Surface ray method in the analysis of conformal arrays," *Digest 1976 AP-S Int. Symp.*, Univ. Massachusetts, Amherst, MA, Oct. 1976, pp. 366-369.

[6] Z. W. Chang, L. B. Felsen, and A. Hessel, "Surface ray methods for mutual coupling in conformal arrays on cylinder and conical surface," Polytechnic Inst. New York, Final Rep., prepared under Contract N00123-76-C-0236, Sept. 1975-Feb. 1976.

[7] S. W. Lee and S. Safavi-Naini, "Asymptotic solution of surface field due to a magnetic dipole on a cylinder," Electromagnetics Lab., Dep. Elect. Eng., Univ. Illinois at Urbana-Champaign, Tech. Rep. No. 76-11, supported by Contract N00019-76-M-0622, 1976.

D

Radio Science, Volume 14, Number 2, pages 217–237, March–April 1979

Source radiation in the presence of smooth convex bodies

R. Mittra and S. Safavi-Naini

Electrical Engineering Department, University of Illinois at Urbana-Champaign, Urbana, Illinois 61801

(Received July 21, 1978.)

The problem of radiation from sources in the presence of smooth, convex, impenetrable objects is considered, and a brief survey of various high frequency techniques is presented. A generalization of the geometrical theory of diffraction, and two new techniques based on the spectral domain approach and an asymptotic evaluation of the radiation integral for the surface current, also are discussed. Some numerical results derived from the spectral domain formulas are presented and a comparison with available theoretical and experimental data is included.

1. INTRODUCTION

The problems of radiation from sources in the presence of impenetrable smooth convex objects and the diffraction of a plane wave by such objects are of great practical interest in the design of antennas on structures, e.g., conformal arrays. Unfortunately, the exact analytical solutions to these problems, based on the methods of "separation of variables" or "function-theoretic" procedures (Wiener-Hopf technique, residue calculus, etc.), exist only for a very limited number of scattering geometries. Furthermore, the exact solutions are typically highly complex in nature; hence, the process of extracting numerical results from them can be very time-consuming and is by no means trivial. This situation has motivated many researchers to explore approaches to the problems of radiation and scattering from smooth convex structures.

In the low and resonant frequency ranges, several reliable numerical procedures, e.g., the moment method, are available for solving the radiation and scattering problems. However, in the high frequency domain, numerical techniques based on matrix methods become unwieldy if not impractical, prompting one to employ asymptotic techniques suitable for large k ($= 2\pi/\lambda$), where λ is the wavelength of the illuminating wave.

In this work, we begin by presenting, in section 2, a survey of various high frequency asymptotic techniques for the problem stated above. The survey is necessarily brief, and covers only the highlights of a number of important approaches to the problem at hand, namely, Fock's theory, the geometrical theory of diffraction (GTD), and the direct integral equation approach. The reader interested in further details may choose to consult the works of *Bowman et al.* [1969], *Uslenghi* [1972], and *Kouyoumjian* [1965].

In section 3, we consider the generalization of GTD and present some new approaches to the curved surface radiation and scattering problems. Some numerical results based on one of these new approaches are presented in section 3, and a comparison with other available methods is included.

2. SURVEY OF AVAILABLE HIGH FREQUENCY ASYMPTOTIC TECHNIQUES

2.1. *Watson transformation.* One of the first successful attempts to derive an asymptotic expansion for the far-field generated by a point source located in the proximity of a conducting surface was made by *Watson* [1918]. His method, essentially, consisted of two steps: (a) transforming the original infinite series solution into a contour integral (by Cauchy's residue theorem); (b) deforming the contour of integration so as to capture a set of complex poles of the integrand. The original integral is then expressed in terms of an infinite series which converges very rapidly, provided the observation point is in the shadow region. The first few terms of this series were later interpreted as "creeping waves." The method was first applied to a sphere and circular cylinder, and later to some other geometries as well. The mathematical rigor of the method was the subject of further investigations

0048-6604/79/0304-0217$01.00

by other researchers [*Pflumm*, 1960; *Fischer*, 1966; *Cohen*, 1965]. Although the Watson transformation can only be applied to a few simple geometries, e.g., the sphere, cylinder, cone, spheroid, etc., it is still regarded as one of the cornerstones of the more general high frequency techniques because of its mathematical rigor. The Watson transformation is especially powerful in the shadow region of the geometric optics field. In the lit region, the above-mentioned contour integral is evaluated using the "stationary phase" method and yields the reflected field from the surface. In this region, the most significant contribution to the total scattered field typically comes from the surface current induced on the smooth convex part of the object; the so-called "physical optics" approximation can be applied [*Crispin and Maffett*, 1965; *Siegel*, 1958; *Siegel et al.*, 1959] to derive the reflected field. The physical optics method is based upon approximating the induced surface current in the lit region of the object by the current that would be induced on the local tangent plane, and by assuming that the surface current is zero in the shadow region. The far field is constructed by substituting the above estimate for the induced surface current in the integral representation of the scattered field, and evaluating the same in an asymptotic sense. The dominant term of the asymptotic expansion of this integral can be shown to be identical to the first term of the Luneberg-Kline expansion of the geometrical optics far field [*Luneberg*, 1944; *Kline and Kay*, 1965]. However, the higher-order terms derived from the physical optics approach do not provide us with correct results in the shadow or transition regions where the diffracted field contributes the most.

In the next section, we discuss Fock's theory, which can fill the gap between the physical optics in the lit region and the "creeping wave" representation in the shadow region.

2.2. *Fock's theory*. The region between the lit and the shadow part on a surface is called the "penumbra region." The angular width of this region is approximately given by $(\lambda r_0^2/\pi)^{1/3}$ where λ is the wavelength of the illumination and r_0 is the radius of curvature of the surface of the object in this region in the incident plane (Figure 1). Fock's theory invokes the principle of the *local* character of the field in the penumbra region [*Fock*, 1946*a*] and is based on the conjecture that all bodies with a smoothly varying curvature have the same current

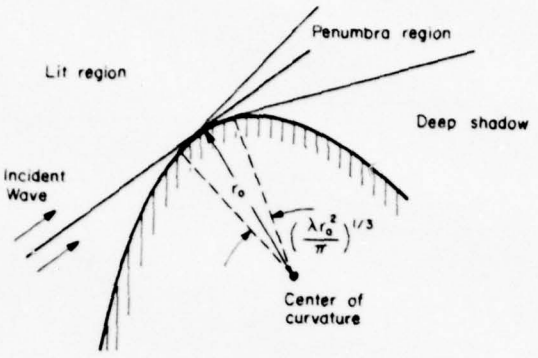

Fig. 1. Section of the body in the plane of incidence.

distribution in the penumbra region, provided that the curvature and the incident wave are the same near the point under consideration. This principle allows one to locally replace the surface of the object by a portion of a paraboloid of revolution. A unique feature of the expressions for Fock currents is that they provide a convenient transformation of the geometric optics currents in the lit region into the creeping wave currents in the shadow region. Fock himself deduced the pertinent formulas for the surface currents by treating a convex body problem [*Fock*, 1946*a*] described below.

Consider a convex body and a plane wave incident in the direction of the x axis. If the equation of the surface is

$$f(x,y,z) = 0 \tag{1}$$

then the curve representing the boundary of geometrical shadow is given by

$$f(\bar{r}) = 0, \quad \frac{\partial f}{\partial x} = 0 \tag{2}$$

Consider a point O on the boundary of the shadow region where we set up a rectangular coordinate system as shown in Figure 2 ($\hat{z}$: normal to the surface; $\hat{x}$: in the direction of propagation; and $\hat{y}$: the tangent to the boundary of shadow). In the vicinity of this point, the surface of the body could be locally replaced by a paraboloid of revolution which is expressed by the equation.

$$z + (1/2)(ax^2 + 2bxy + cy^2) = 0 \tag{3}$$

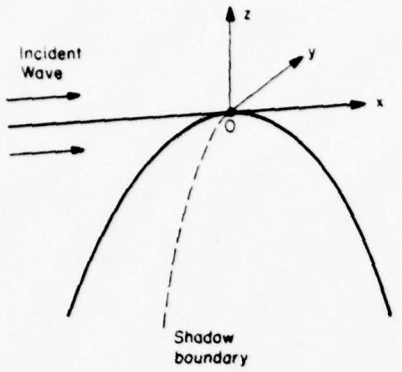

Fig. 2. Plane wave incident upon a smooth convex body.

Each of the field components satisfies the Helmholtz equation

$$(\nabla^2 + k^2)\Psi = 0 \tag{4}$$

The fact that the incident wave travels along the x axis suggests that Ψ be written in the form

$$\Psi = \tilde{\Psi} e^{-jkx} \tag{5}$$

where an $\exp(j\omega t)$ time dependence has been assumed. Substituting (5) in (4) gives

$$\nabla^2\tilde{\Psi} - 2jk(\partial/\partial x)\tilde{\Psi} = 0 \tag{6}$$

At this point, two basic assumptions are introduced in Fock's theory, namely, (i) $\tilde{\Psi}$'s are relatively slowly varying functions of coordinates, (ii) $\tilde{\Psi}$ varies more rapidly in the z direction than in x and y, i.e.,

$$\frac{\partial\tilde{\Psi}}{\partial z} = O\left(\frac{k}{m}\tilde{\Psi}\right), \quad \frac{\partial\tilde{\Psi}}{\partial x} = O\left(\frac{k}{m'}\tilde{\Psi}\right),$$

$$\frac{\partial\tilde{\Psi}}{\partial y} = O\left(\frac{k}{m'}\tilde{\Psi}\right) \tag{7}$$

Based upon (7), we can write (6) as

$$\partial^2\tilde{\Psi}/\partial z^2 - 2jk\,\partial\tilde{\Psi}/\partial x = 0 \tag{8}$$

and consequently $m' = m^2$ (m is very large), where the terms of relative order $1/m^2$ have been omitted.

Inserting these estimates and assumptions into the Maxwell's equation, we can find some simple expressions for all the field components in terms of H_y and H_z. If we write H_y as

$$H_y = H_y^0 e^{-jkx}\tilde{\Psi} \tag{9}$$

where H_y^0 is the magnitude of the incident wave at infinity, then Ψ must satisfy

$$\partial^2\tilde{\Psi}/\partial z^2 - 2jk\,\partial\tilde{\Psi}/\partial x = 0 \tag{10}$$

with boundary condition

$$\partial\tilde{\Psi}/\partial z - jk(ax + by + 1/\sqrt{\eta})\tilde{\Psi} = 0 \tag{11}$$

on the surface of the body. Equation (11) is the simplified version of the Leontovich boundary condition where

$$\eta = \varepsilon - j\sigma/\omega$$

The final solution for H_y on the surface of the body, which satisfies the boundary condition and the condition at infinity, may be written in the form

$$H_y = H_y^{ex}\,G(\xi,q) \tag{12}$$

where

H_y^{ex} = external field
$G(\xi,q) = e^{-(j/3)\xi^3}V_1(\xi,q)$
$V_1(\xi,q)$ = Fock function defined in the appendix A
$\xi = m(ax + by)$ = reduced distance from the shadow boundary $= l/d$
$m = (kr_0/2)^{1/3}$, m^{-1} is the angular width of penumbra region
d = the width of penumbra region $= (2r_0^2/k)^{1/3}$
l = distance between the observation point and the shadow bounary along the incident ray (Figure 3).
$q = -jm/\sqrt{\eta} = -(j/\sqrt{\eta})\sqrt[3]{k/2a}$ ($= 0$ for conducting body)

The other tangential component of the magnetic field H_x on the surface of the body can be obtained in a similar manner:

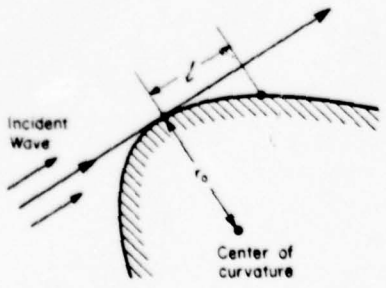

Fig. 3. Geometric meaning of the quantity l in (12).

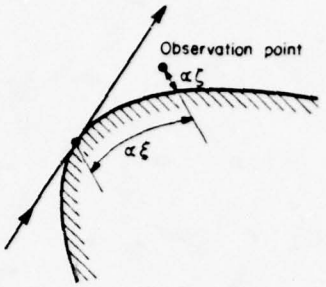

Fig. 4. Coordinates of observation point in terms of ξ and ζ.

$$H_z = H_z^{ex}\,[-(j/m)\,e^{-(j/3)\xi^3/3} f(\xi)] \tag{13}$$

where $f(\xi)$ is another Fock function defined in appendix A. Fock's formulas not only give the surface value of the field, but also can be utilized to find the field in the proximity of the object. For a plane wave incidence, the first order, i.e., $O(1/m)$ terms for the scattered field within a certain layer around the object, can be written as

$$H_x = 0, \quad H_y = H_y^0 e^{-jkx}\bar{\Psi}(\xi,\zeta), \quad H_z = H_z^0 e^{-jkx}\bar{\Phi}(\xi,\eta) \tag{14}$$

$$E_x = (j/m)H_y^0 e^{-jkx}\partial\bar{\Psi}/\partial\zeta, \quad E_y = H_z, \quad E_z = -H_y$$

where

$$\zeta = 2am^2[z + (1/2)(ax^2 + 2bxy + cy^2)]$$

= reduced height from the surface of the body (see Figure 4).

$$\bar{\Psi} = -je^{j\xi\zeta - j/3\,\xi^3)} \int_c e^{-j\xi t}\left[w_1(t-\zeta) - \frac{w_1'(t) - qw_1(t)}{w_2'(t) - qw_2(t)} \cdot w_2(t-\zeta)\right] dt$$

$$\bar{\Phi} = \frac{-je^{j\xi\zeta - (j/3)\xi^3}}{2\sqrt{\pi}} \int_c e^{-\beta t}\left[w_1(t-\zeta) - \frac{w_1(t)}{w_2(t)} \cdot w_2(t-\zeta)\right] dt \tag{15}$$

The path of integration for $\bar{\Phi}$ and $\bar{\Psi}$ is shown in Figure 5.

Fock's expressions for the field components in the penumbra region ($\xi \approx 0$) can be extended to

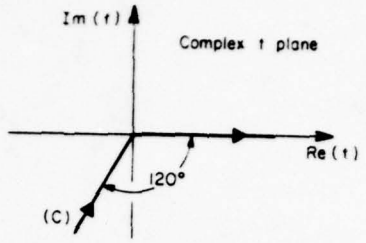

Fig. 5. Path of integration for (15) in the complex t-plane.

the shadow region by introducing some modifications in the definition of parameter ξ. *Goodrich* [1959] has generalized the argument used by Fock in the penumbra region to anywhere in the shadow region by introducing a new set of variables, ξ and ζ, for the incremental distances along the path leading into the shadow region. In this generalization, the parameter ξ as defined in (12) is replaced by

$$\xi = \int_0^s \left(\frac{kR(s)}{2}\right)^{1/3} \frac{ds}{R(s)} \tag{16}$$

where s is the arc length along the geodesics which originate from the shadow boundary and go into the shadow region along the surface, and $R(s)$ is the radius of curvature of the surface along the geodesics. For the case of a circular cylinder of radius a (Figure 6), the expression of ξ simplifies to

$$\xi = (ka/2)^{1/3}\,\theta = s/d \tag{17}$$

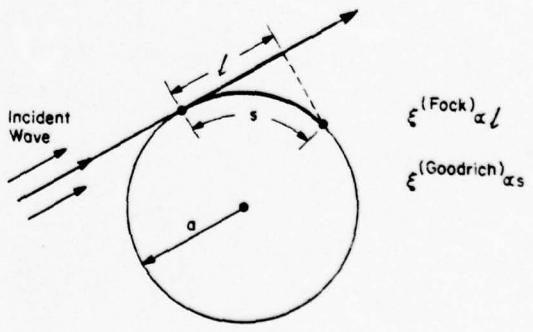

Fig. 6. Comparison between the various definitions of parameter ξ for the case of a circular cylinder.

Fock also treated the case where the point source was very close to the surface of the body. He analyzed the radiation of electric dipoles near a spherical model of the earth [*Fock*, 1945] and derived the formulas for the scattered fields in terms of functions (attenuation functions) similar to $\tilde{\Phi}$ and $\tilde{\Psi}$, which are valid both in the shadow and transition regions [*Logan and Yee*, 1962]. Fock's assumptions were later proven in a more systematic and mathematically rigorous manner by *Cullen* [1958] and *Hong* [1967] by using a direct integral equation approach. This method is described in the next section.

2.3. *Direct integral equation approaches.* This method, which is closely related to Fock's theory, can be illustrated by analyzing the diffraction of a plane electromagnetic wave by an arbitrary conducting body (large compared with λ). *Cullen* [1958] obtained a first-order asymptotic solution to the integral equation for the induced surface current

$$\vec{J}(\vec{r}) = 2\hat{n}(\vec{r}) \times \vec{H}^{\text{inc}}(\vec{r}) - (1/2\pi)\hat{n}(\vec{r}) \times \int_S \int \mathrm{d}s' \, \frac{1 + jkR}{R^3} \{\vec{J}(\vec{r}') \times \hat{R} e^{-jkR}\} \tag{18}$$

where $\hat{n}(\vec{r})$ is the outward unit normal to the surface at $\vec{r}$, $\vec{H}^{\text{inc}}(\vec{r})$ is the incident magnetic field on the surface (S) of the body, and $R = \vec{r} - \vec{r}'$ ($\vec{r}'$ is a variable point on the surface).

Fock used this integral equation to deduce the important principle of local character of the field in the penumbra region. Cullen derived a first-order asymptotic solution to (18) which agreed with Fock's results given in (12) and (13). Cullen's method consists of transforming the two-dimensional integral equation (18), in the penumbra region, to a one-dimensional, Volterra-type equation. This is accomplished by applying the stationary phase technique to the original integral while integrating with respect to one of the variables. The resulting one-dimensional Volterra equation is then solved in Cullen's method by the Fourier transform technique. A similar procedure was used by *Hong* [1967] to analyze, asymptotically, the diffraction of electromagnetic and acoustic plane waves by smooth convex bodies. We will now proceed to explain Hong's method in a little more detail by referring back, once again, to the integral equation (18). The surface is parameterized by the geodesic coordinate system (σ,v) such that the shadow boundary for the incident plane wave traveling along the tangent $\hat{\sigma}(0,v)$ to the $v = 0$ curve is the $\sigma = 0$ curve. The quantities $\hat{\sigma}(\sigma,v)$, $\hat{b}(\sigma,v)$ and $\hat{n}(\sigma,v)$ form a right-hand local orthonormal basis ($\hat{n} = \hat{\sigma} \times \hat{b}$) as shown in Figure 7.

Since the incident field has a phase factor $\exp[-jk\hat{\sigma}(0,0) \cdot \vec{r}(\sigma,0)]$, we write the surface current in the form

$$\vec{J}(\vec{r}) = [I_\sigma(\vec{r})\,\hat{\sigma}(\vec{r}) + I_b(\vec{r})\,\hat{b}(\vec{r})]\, e^{-jk\sigma} \tag{19}$$

where σ is the arc length along the geodesic. Substituting (19) back into (18) and restricting the resulting equation to the points on the geodesic $v = 0$, we obtain two coupled two-dimensional integral equations for $I_\sigma(\sigma,0)$ and $I_b(\sigma,0)$. It can be shown that these integrals have saddle points at $v = 0$ (for the v integration). Applying the "steepest descent path" method to v integration, and keeping the terms up to the order $1/M_0^2$, where $M_0 = [k\rho_\sigma(\sigma,0)]^{1/3}$, we obtain the following decoupled one-dimensional, Volterra-type integral equations for $I_b(\xi,0)$ and $I_\sigma(\xi,0)$

$$I_\sigma(\xi,0) = 2I_\sigma^{\text{inc}}(\xi,0) - \int_{-\infty}^{\xi} \mathrm{d}\tau\, I_\sigma(\xi,0)\, K_\sigma(\xi - \tau) + O(M_0^{-3})$$

$$I_b(\xi,0) = 2I_b^{\text{inc}}(\xi,0) - \int_{-\infty}^{\xi} \mathrm{d}\tau\, I_b(\xi,0)\, K_b(\xi - \tau) + O(M_0^{-3}) \tag{20}$$

$\rho_\sigma(\sigma,v)$ is the radius of curvature of the surface

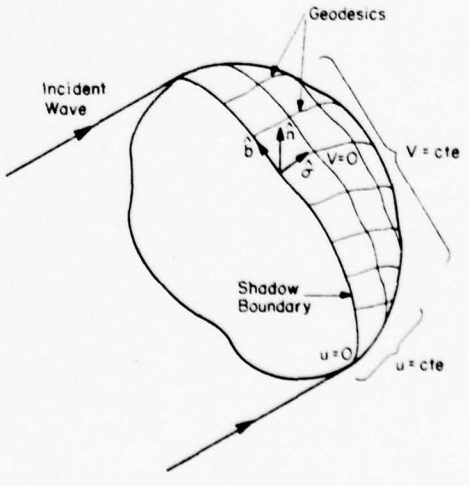

Fig. 7. Geodetic coordinate system on a smooth convex body.

along geodesics (v = constant curves) at point (σ, v).

Solving (20) by Fourier transforms, we obtain the expression for the induced currents in the penumbra and shadow regions, and the first-order solutions are found to be the same as those of Fock and GTD [*Levy and Keller*, 1959]. One of the important conclusions drawn from Hong's solution is that the leading term in the asymptotic expansion, which is the same for the acoustic and electromagnetic problems, is independent of curvature in the direction transverse to the geodesic, provided the divergence factor is suppressed. However, we should bear in mind that Hong's method was designed for the case of axial incidence on symmetric objects, and in this case, the geodesics are torsionless. The above conclusion does not seem to be valid in the cases where the rays have nonzero torsion [*Lee and Safavi-Naini*, 1976, 1978]. In Hong's expressions for the surface current, the transverse curvature has only a second-order effect. It was also shown that up to the terms of order $(k\rho_\sigma)^{-2/3}$ in the asymptotic expansion, the tangential and binormal components of the creeping waves are not coupled.

Both Fock's theory and the direct integral equation approach give the induced surface current, or the scattered field in the neighborhood of the surface of the scatterer, due to an incident plane wave. These expressions can also be used to derive the radiated field via the use of the reciprocity theorem.

The methods which have been discussed thus far are mathematically rigorous. However, they are limited in the scope of their application to geometries satisfying some special smoothness and symmetry criteria. Geometrical theory of diffraction, which we discuss in the next section, has a broader scope, although it does lack the mathematical rigor of approaches described until now.

2.4. *Geometrical theory of diffraction (GTD).* Geometrical theory of diffraction (GTD), developed by J. B. Keller [*Levy and Keller*, 1959; *Keller*, 1956, 1957; *Kouyoumjian*, 1975; *Pathak and Kouyoumjian*, 1972], is a generalization of geometrical optics. It is based upon the assumption that fields propagate along rays. Keller's major contribution was to introduce the new kinds of rays called the "diffracted rays," which, together with the geometrical optics rays, constitute the total field. In our problem, namely, a source radiating in the proximity of the smooth object, the diffracted rays travel along the curves on the surface of the scatterer. By applying Fermat's principle to these surface rays, we conclude that the above-mentioned curves should be geodesics on the surface of the body. In the GTD procedure, one assigns a value to the field along each of these surface rays. The total field at any point in the space is the sum of the fields due to various rays (incident, reflected, and diffracted) passing through that point. An important advantage of the GTD approach is that it can be applied to both scalar (acoustic) and vector (electromagnetic) problems and to smooth convex objects of an arbitrary shape.

Consider the problem of determining the radiated field of a scalar point source located on the surface of a smooth convex opaque body. If the observation point is in the shadow region, the ray paths originating at Q and reaching P (observation point) are comprised of two sections. One of these sections follows the straight line path P_1P, while the other travels along a geodesic on the surface (Figure 8). Let us consider the propagation of the field along each section separately.

(a) *Rays in free space:* Behavior of the fields along these rays can be determined by obtaining a high frequency asymptotic solution to Maxwell's equation in a source-free homogeneous isotropic medium. We begin with the Luneburg-Kline asymptotic expansion of the electric field [*Luneberg*, 1944; *Kline and Kay*, 1965]:

$$\vec{E}(\vec{r}) \sim k' e^{-jk_0 S(\vec{r})} \sum_{m=0}^{\infty} (jk)^{-m} \vec{e}_m(\vec{r}) \tag{21}$$

and insert it into Maxwell's equations. This results in the following equations governing the propagation of electromagnetic fields along the rays.

$$[\nabla S(\vec{r})]^2 = 1 \quad \text{(Eikonal equation)} \tag{22}$$

$$2(\nabla S \cdot \nabla)\vec{e}_m + (\nabla^2 S)\vec{e}_m = -\nabla^2 \vec{e}_{m-1}$$

$$\text{(Transport equation)} \tag{23}$$

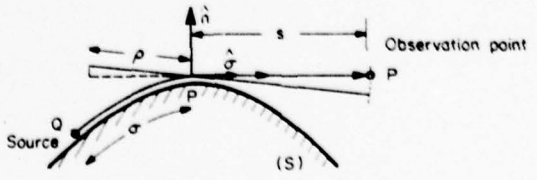

Fig. 8. Diffraction by a smooth convex body when the observation point is in the shadow region of the source Q.

$$\nabla S \cdot \vec{e}_m = -\nabla \cdot \vec{e}_{m-1} \quad \text{(Gauss's Law)} \tag{24}$$

$$\vec{e}_{-1} = 0, \quad m = 0, 1, 2, \ldots$$

The zeroth-order solution to the above system of equations, which turns out to be in agreement with what one would obtain by geometric optics, may be written as

$$\vec{E}(\sigma) \sim \vec{E}_0(0) e^{-jk_0 S(0)} \left[\frac{\rho_1 \rho_2}{(\rho_1 + \sigma)(\rho_2 + \sigma)} \right]^{1/2} e^{-jk_0 \sigma} \tag{25}$$

where σ is the distance traveled along the ray from the reference point O($\sigma = 0$) on the ray path (Figure 9). ρ_1 and ρ_2 are the principal radii of curvature of the wavefront at $\sigma = 0$. It is apparent that the expression fails when $\sigma = -\sigma_1$ or $\sigma = -\rho_2$, i.e., at the caustic lines (Figure 9). In the cases where it is convenient to choose the point of diffraction on the surface of a body as the reference point O, the formula (25) should be modified as follows:

$$\vec{E}(\sigma) \sim \vec{\delta}_0 [\rho / \sigma(\rho + \sigma)]^{1/2} e^{-jk\sigma} \tag{26}$$

In these cases, the point of diffraction itself is a caustic, and ρ is the distance between this point and the second caustic.

(b) *Surface rays:* These rays follow the surface S along the geodesics into the shadow region, and shed energy tangentially as they propagate. In order to study the behavior of the field along with these rays, we introduce a special ray-fixed coordinate system, $\hat{\sigma}$, $\hat{n}$, $\hat{b}$, with $\hat{\sigma}$: unit vector tangent to the ray; $\hat{n}$: outward unit normal to the surface; and $\hat{b} = \hat{t} \times \hat{n}$ or binormal direction; a vector field can be decomposed into its components along these unit vectors as

$$\vec{E} = E_\sigma \hat{\sigma} + E_n \hat{n} + E_b \hat{b} \tag{27}$$

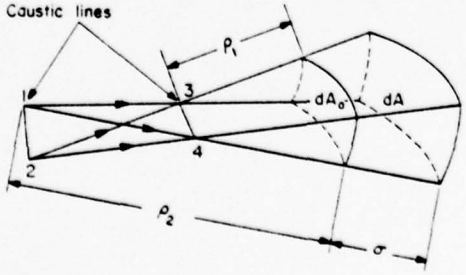

Fig. 9. Diverging pencil of rays in free space.

At this point, several important assumptions are introduced in the GTD approach [*Levy and Keller*, 1959]: (i) $\vec{E}$ and $\vec{H}$ are orthogonal to each other and to the ray. (ii) Variation of the phase of the field along the ray is the same for both fields. (iii) E_n and E_b propagate independently, and $E_\sigma = 0$. (iv) E_b satisfies the scalar wave equation $(\nabla^2 + k^2)\, u = 0$ with the boundary condition $u = 0$ on the surface S, while E_n satisfies the same equation with the boundary condition $\partial u / \partial n = 0$.

The next step in the GTD approach is to conjecture, on the basis of the solution to some canonical problems, that the surface field propagating along each ray is comprised of an infinite set of "modes." Along a ray-fixed path, GTD assigns a complex value to each component of the field associated with the individual modes. The propagation of this modal field is described by the equation

$$a(\sigma) = A(\sigma) e^{-j\Phi_0 - k\sigma)} \tag{28}$$

where σ is the distance between an arbitrary point along the ray and the source Q and Φ_0 is the phase of the field at the source point. Next, invoking the principle of conservation of energy between two adjacent rays, and using the fact that the surface rays shed energy tangentially, we can arrive at the following expression for $a(\sigma)$:

$$a(\sigma) = K \left(\frac{d\Psi_1}{\rho d\Psi_2} \right)^{1/2} \exp\left[-jk\sigma - \int_0^{\sigma} \alpha(\sigma')\, d\sigma' \right] \tag{29}$$

where $\alpha(\sigma)$ is the "attenuation constant," K is proportional to the strength of the source, and $d\Psi_1$, $d\Psi_2$ and ρ are shown in Figure 10. The quantity $[d\Psi_1/(\rho d\Psi_2)]^{1/2}$ indicates the "spreading of the surface ray tube" as it travels along the surface. Equations (26) and (29) describe the laws of propagation for the rays which originate from the source point Q, are diffracted at P_1, and reach the observa-

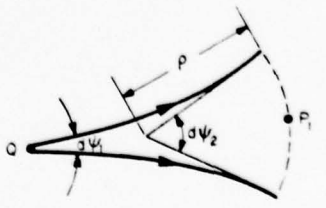

Fig. 10. Divergence of surface rays.

tion point P. To complete the solution, we need to determine the actual values of the fields from these equations. These require the knowledge of $\hat{\delta}_0$ and K, which, in turn, are related to the initial values of the rays QP_1 and P_1P as well as the attenuation constant $\alpha(\sigma)$. The initial value of the field at Q is related to the strength of the source by $L(Q)$, the so-called "launching coefficient," while the initial value of the field at P_1 is related to the actual field on the surface at P_1 through the "diffraction coefficient" $D(P_1)$. If we now sum up the contributions of all the modes, we obtain the final solution [*Kouyoumjian*, 1975; *Pathak and Kouyoumjian*, 1972] for the field radiated in the shadow region by an infinitesimal magnetic dipole of strength $\tilde{M}$ located on a smooth convex conducting body:

$$\tilde{E}^d(P) = \tilde{M} \cdot [\hat{b}(Q)\hat{n}(Q_1)F + \hat{\sigma}(Q)\hat{b}(P_1)G] \cdot [\rho/s(\rho + s)]^{1/2} e^{-jks} \tag{30a}$$

where

$$F = \frac{-jke^{-jk\sigma}}{4\pi}\left(\frac{d\Psi_1}{\rho d\Psi_2}\right)^{1/2} \sum_{p=1}^{\infty} L_p^h(Q) D_p^h(P_1) \cdot \exp\left[-\int_0^{\sigma} \alpha_p^h(\sigma')d\sigma'\right] \tag{30b}$$

and the expression for G is obtained by replacing the superscript h by s in (30b), where h and s stand for hard and soft boundary conditions, namely, $u = 0$ and $\partial u/\partial n = 0$, respectively. The quantities $L_p^{h,s}$, $D_p^{h,s}$, and $\alpha_p^{h,s}$, appearing in (30b), in general depend upon the local geometry and the electromagnetic characteristic of the surface, frequency k, and the mode of propagation. They are determined by studying the asymptotic expansions of the exact solutions of some special canonical problems. Keller and Levy [*Levy and Keller*, 1959; *Keller and Levy*, 1959] have derived the first few terms of the asymptotic expansions for D and α by considering the canonical problems of scalar diffraction by a circular cylinder, sphere, elliptical and parabolic cylinder. A study of the above-mentioned asymptotic expansions and the works of *Franz and Klante* [1959] and *Voltmer* [1970], who have also investigated the same problem, as well as a comparison with the results of the direct integral equation approach, reveals the following characteristics of the solution: (i) the first-order terms in the asymptotic expansion of D and α are independent of whether the problem under consideration is scalar or vector; (ii) the first-order approximations of D and α are dependent only on ρ_σ, the radius of curvature of the surface along the ray; (iii) the second-order terms are functions not only of ρ_σ, but also of $d\rho_\sigma/d\sigma$, $d^2\rho_\sigma/d\sigma^2$, and $\rho_{\sigma\sigma}$ (the radius of the curvature of the surface transverse to the ray). Finally, the higher-order terms are different for scalar and vector problems.

The leading terms in the asymptotic expansion of "diffraction coefficient" D, "attentuation constant" α, and "launching coefficient" L are presented below.

"Soft" polarization:

$$[D_p^s]^2 = \frac{\pi^{1/2} 2^{-5/6} \rho_\sigma^{1/3} e^{-j\pi/12}}{k^{1/6}[Ai'(-r_p)]^2} \tag{31}$$

$$\alpha_p^s = [(r_p e^{j\pi/6})/\rho_\sigma](k\rho_\sigma/2)^{1/3} \tag{32}$$

$$L_p^s = e^{-j\pi/12}(2\pi k)^{1/2}(2/k\rho_\sigma)^{2/3} Ai'(-r_p) D_p^s \tag{33}$$

"Hard" polarization:

$$[D_p^h]^2 = \frac{\pi^{1/2} 2^{-5/6} \rho_\sigma^{1/3} e^{-j\pi/12}}{k^{1/6} r_p' [Ai(-r_p')]^2} \tag{34}$$

$$\alpha_p^h = [(r_p' e^{j\pi/6})/\rho_\sigma](k\rho_\sigma/2)^{1/3} \tag{35}$$

$$L_p^h = e^{j\pi/12}(2\pi k)^{1/2}(2/k\rho_\sigma)^{1/3} Ai(-r_p') D_p^h \tag{36a}$$

where $Ai(x)$ is the Airy function:

$$Ai(x) = \frac{1}{\pi}\int_0^{\infty} \cos\left(\frac{t^3}{3} + xt\right) dt \quad (x \text{ real}) \tag{36b}$$

and $Ai(-r_p) = 0$, $Ai'(-r_p') = 0$, (Ai' is the derivative of Ai with respect to its argument). Higher-order terms in the expansion of D, α, and L have been given by *Kouyoumjian* [1975] and *Pathak and Kouyoumjian* [1974] and in some of the other works on GTD mentioned earlier.

The expression (30) is convenient to use in the shadow region. However, in the shadow part of the transition region, since the exponential decay of the terms in (30) is weak, the convergence of the series representation is very slow. Furthermore, the series diverges in the lit part of the transition region. Consequently, in these regions, it is more reasonable to use an integral representation for the surface ray field, which, in our case, can be expressed in terms of Fock functions [*Kouyoumjian*, 1975].

Attempts have been made to establish the mathematical validity of GTD and to minimize its "nondeductive parts" (parts which are based upon physical intuition or the study of the asymptotic solution of some simple problem geometrical concepts of different kinds of rays, diffraction coefficients, attenuation constants, etc.). *Kravtsov* [1964] and *Ludwig* [1966] have analyzed the field near the caustic surface (smooth envelope of a family of rays), and have developed a "uniform asymptotic solution" in the sense that it is finite at the caustic and reduces to geometrical optics away from the caustic.

3. GENERALIZATION OF GTD AND INVESTIGATION OF ALTERNATE METHODS

3.1. *Generalization of GTD to arbitrary surfaces.* Keller's generalization of GTD for the analysis of the field diffracted from a smooth convex object is closely related to what is known as the "boundary layer technique" in the theory of differential equations [*Buchal and Keller*, 1960]. On the other hand, the "uniform asymptotic theory" is analogous to the method used by *Langer* [1960] and *Olver* [1956] to find the asymptotic solutions of the second-order differential equations near their "turning points," which are counterparts of the transition regions in our case [*Zauderer*, 1970].

The second procedure is based upon the generalization of the geometrical optical interpretation of the circular cylinder problem. The solution obtained by this method involves some functions with unknown phase and amplitude, similar to Bessel and Hankel functions. Since the surface of a smooth object is actually the caustic surface of diffracted rays, the above-mentioned formulation is applicable in this case, too. *Lewis et al.* [1967] have modified this solution to make it satisfy the boundary condition on a convex body. Using ray formalism, they have obtained an asymptotic solution in a complicated form which they call "creeping wave;" it satisfies the boundary condition on and is uniformly valid near and away from the surface. It should be mentioned that the method has been developed primarily for scalar diffraction problems.

Creeping waves that travel on the surface of the body generate other kinds of diffracted rays in the presence of any irregularities in the geometric or electromagnetic characteristics of the surface. The effects of discontinuity in the surface curvature, its higher-order derivatives, or the surface impedance have been studied by many authors [*Weston*, 1962; *Keller and Kaminetzky*, 1972; *Thompson*, 1962; *Christiansen*, 1966]. An exhaustive study of various diffraction mechanisms and corresponding diffraction coefficients, as well as constants associated with the propagation of creeping waves, has been carried out by *Albertsen* [1974].

At this point, let us examine the most important features of the GTD and its various modifications. GTD formulation is essentially scalar in nature and is heuristic in some parts. Thus, when GTD is applied to a vector problem, it is not surprising that the coupling between various components of the fields are neglected, and each one of them is treated as an uncoupled scalar wave. The other assumptions in GTD are concerned with the directions of these field components and the kind of boundary conditions they satisfy (see section 2.4). As mentioned earlier, nondeductive parts of GTD are based on asymptotic expansions of known solutions to some selected "canonical" problems. Quite often these canonical problems are not general enough to describe fully and accurately the local behavior of the field for an arbitrary structure. Finally, most of the canonical problems investigated are two-dimensional in nature. The only exception to this is the sphere. However, insofar as the geometric properties of the surface are concerned, the sphere is a very special case since its radius of curvature is the same in all directions and, consequently, the surface rays are torsionless. Finally, GTD fails when the observation point is located in the transition regions, shadow boundaries or in the neighborhood of a caustic. In each of these regions, one needs to modify carefully the GTD formulas and often such a modification is not simple. Nevertheless, in spite of these difficulties, GTD is recognized to be a powerful high frequency technique for computing the leading terms of the asymptotic solution. Two of the principal attributes of GTD are its simplicity and wide scope of application.

3.2. *Spectral domain approach.* We now examine an approach different from GTD which uses the spectrum of the induced current, or the expression for the radiated field, as a starting point. In order to gain a better insight into the curved-surface radiation and scattering problem and to verify the basic assumptions of GTD, it is worthwhile to consider such alternative approaches, particularly if they apply to canonical problems which are more

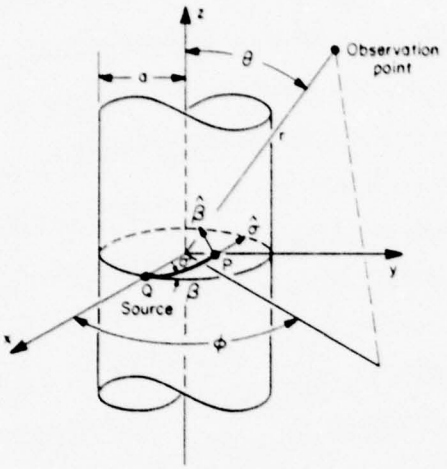

Fig. 11. Geometry of the cylinder problem.

general in nature than those employed to derive the GTD results. An example of such a study would be to consider the case of surface ray propagation with nonzero torsion, a situation that occurs when a magnetic dipole source radiates from a location on the surface of a circular cylinder.

The geometry of the problem is shown in Figure 11. The radius of the cylinder is a and the source, which is an infinitesimal magnetic dipole with density $\bar{M}$, is located at the point Q described by the spherical polar coordinates ($r = a$, $\theta = 90°$, $\phi = 0°$). Each point P on the surface of the cylinder is defined by a "geodetical polar coordinate" system (σ,β), where σ is the arc length of the geodesic connecting Q to P and β is the angle between $\hat{\phi}$ (at point Q) and geodesic QP. The local orthonormal basis vectors $(\hat{\sigma},\hat{\beta})$ are also associated with these two parameters. The observation point in the far field is specified by its spherical polar coordinates (r,θ,ϕ). The radiated field at an arbitrary point can be expressed in terms of two potentials, Φ and Ψ, which, in cylindrical coordinates, can be written as:

$$\Phi = \frac{1}{2\pi}\sum_{n=-\infty}^{\infty} e^{-jn\phi}\int_{-\infty}^{\infty} f_n(k_z)\, H_n^{(2)}(k_t\rho)\, e^{-jk_z z}\, dk_z \tag{37}$$

$$\Psi = \frac{1}{2\pi}\sum_{n=-\infty}^{\infty} e^{-jn\phi}\int_{-\infty}^{\infty} g_n(k_z)\, H_n^{(2)}(k_t\rho)\, e^{-jk_z z}\, dk_z \tag{38}$$

For the problem under consideration, we can express the spectral weight coefficients as

$$f_n(k_z) = \frac{-j\omega\varepsilon M_\phi}{2\pi k_t^2 H_n^{(2)\prime}(k_t a)\, a} \tag{39}$$

$$g_n(k_z) = \frac{1}{k_t H_n^{(2)\prime}(k_t a)\, a}\left[\frac{M_z}{2\pi} - \frac{nk_z M_\phi}{2\pi k_t^2 a}\right] \tag{40}$$

where

$$k_t = \begin{cases} (k^2 - k_z^2)^{1/2}, & k > k_z \\ -j(k_z^2 - k^2)^{1/2}, & k < k_z \end{cases} \tag{41}$$

In order to derive an asymptotic expansion of (37) and (38), we proceed as follows. As a first step, we apply Watson's transformation to the infinite summation with respect to n and employ appropriate asymptotic formulas for Hankel functions with large order and argument to derive the following expressions for (37) and (38) under the conditions that ka is large and ϕ small compared to π:

$$\Phi \sim \frac{\omega\varepsilon M_\phi}{(2\pi)^2 a}\left(\frac{2\pi}{\rho}\right)^{1/2} e^{j\pi/4}\int_{-\infty}^{\infty} dk_z e^{-j\Omega}\frac{m^2}{k_t^{5/2}} f_0(\xi_1) \tag{42}$$

$$\Psi \sim \frac{jM_\phi}{(2\pi)^2 a}\left(\frac{2\pi}{\rho}\right)^{1/2}\frac{e^{j\pi/4}}{2}\int_{-\infty}^{\infty} dk_z e^{-j\Omega}\frac{k_z}{k_t^{5/2}}$$
$$[jmg_1(\xi_1) + 2m^3 g_0(\xi_1)] - j\frac{M_z}{(2\pi)^2}\left(\frac{2\pi}{\rho}\right)^{1/2}\frac{e^{j\pi/4}}{2}$$
$$\int_{-\infty}^{\infty} dk_z \frac{e^{-j\Omega}}{k_t^{1/2}} g_0(\xi_1) \tag{43}$$

where

$\Omega = k_z z + k_t[\rho + a(\phi - \pi/2)]$

$m = (k_t a/2)^{1/3}$

$\xi_1 = m(\phi - \pi/2)$

f_0, g_0, g_1 = Fock's functions defined in appendix A

M_ϕ and M_z = components of $\bar{M}$, $(\bar{M}\cdot\hat{n} = 0)$

Next, applying the saddle-point technique to (42) and (43) and keeping only the first-order terms, the far field can be written in terms of its components along the normal and tangent to the surface at the "stationary point" P_1 as

$$E_{\alpha_2} = (\bar{M}\cdot\hat{\beta}_1)\left(\frac{jke^{-j\pi/4}}{4\pi}\right) g_0(\xi_{1s})\frac{e^{-jkR}}{R} - \frac{(\bar{M}\cdot\hat{\phi}_1)(\hat{\phi}_1\cdot\hat{\beta}_1)}{4\pi a} e^{-j\pi/4}\left(\frac{k\rho_s}{2}\right)^{1/3} g_1(\xi_{1s})\frac{e^{-jkR}}{R} \tag{44}$$

$$E_{\beta_2} = \frac{(\bar{M}\cdot\hat{\phi}_1)(\hat{\phi}_1\cdot\hat{\sigma}_1)}{2\pi a}\left(\frac{k\rho_s}{2}\right)^{2/3} e^{-j\pi/4} f_0(\xi_{1s})\frac{e^{-jkR}}{R} \tag{45}$$

where

P_1 = the stationary point of Ω which turns out to be the same as the point of diffraction predicted by GTD.
$\xi_{1s} = (ka/2)^{1/3}(\phi - \pi/2)\sin^{1/3}\theta$
ρ_s = radius of curvature of geodesic QP_1
σ = arc length QP_1
R = the distance between the point of diffraction P_1 and the observation point
$n_2 = \hat{\sigma}_2 \times \hat{\beta}_2$, normal to the surface at P_1

The details of the derivations of (44) and (45) are given in appendix B.

Figure 12 illustrates the geometric meaning of some of the parameters appearing in (44) and (45), for the observation point located in the shadow region. In this case, ξ_{1s}, which is identical to ξ given in (16), is the reduced distance traveled by the surface ray before leaving the surface tangentially.

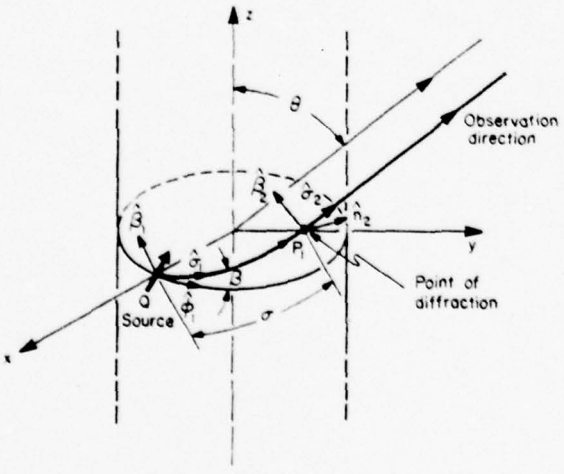

Fig. 12. Diffraction of rays by a cylindrical body.

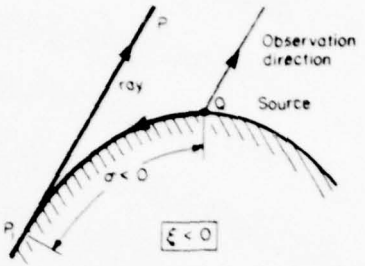

Fig. 13. Diffraction of "pseudo-rays."

In the lit region, the geometric interpretations of σ and ξ are shown in Figure 13. The rays, like QP_1P, that do not obey the generalized Fermat's principle are called "pseudo-rays" [*Kouyoumjian*, 1975]. The ray QP_1P appears to travel along the surface up to the point P_1 and then leaves the surface at P_1 tangentially in the opposite direction, to reach the observation point P. It should be noted that formulas (44) and (45) give us the contribution of the ray which travels along the shortest path on the surface and, thus, suffers the least attenuation. It is not difficult to see that, in general, there are infinitely many rays which contribute to the total field at any observation point. However, their contributions are very small compared to that of QP_1 and their phases and amplitudes can be determined in a similar manner (appendix B). Several other remarks on the formulas given in (44) and (45) are in order:

(a) Numerical results indicate that good agreement between (44), (45), and the exact modal solution is obtained for $ka > 10$.

(b) The zeroth-order terms in the asymptotic expansion of the normal component of the field E are identical to those given by GTD; however, the $k^{-1/3}$ terms derived from the two approaches are *different*.

(c) The tangential component of the field, E_β, given by (45), also is different from the corresponding expression based on GTD by a multiplicative polarization factor. Specifically,

$$E_\beta \text{ in (45)} = \left[\frac{(\bar{M}\cdot\hat{\phi}_1)}{(\cos\beta)(\bar{M}\cdot\hat{\sigma}_1)}\right] \quad \text{(GTD)} \tag{46}$$

Consequently, our results agree with GTD only for the circumferential ray, i.e., for $\beta = 0$. In addition, for an axial magnetic dipole ($\bar{M}\cdot\hat{\phi}_1 = 0$), GTD

gives a nonzero value for the field in the $\hat{\beta}_2$ direction; our solution predicts that this field is identically zero, a result which is in complete agreement with the exact solution for the problem.

Yet another important distinguishing feature of the spectral domain formulas from the corresponding areas based on GTD is worth noting. As mentioned earlier, GTD neglects the effect of torsion on the diffraction of surface rays propagating along smooth objects. In contrast, the spectral domain formulas (44) and (45) indeed exhibit the effect of the torsions of rays. The explicit manifestation of the torsion effect can be seen very clearly if we write these formulas in the following form:

$$E_{\alpha_2} = E_{\alpha_2}^{\mathrm{GTD}} + \left[(\tilde{M} \cdot \hat{\alpha}_1)\left(\frac{\tau\rho_\alpha}{2}\right) - (\tilde{M} \cdot \hat{\beta}_1)\frac{(\tau\rho_\alpha)^2}{2} \right] \cdot \frac{ke^{-jks}}{4\pi}\left(\frac{k\rho_\alpha}{2}\right)^{-2/3} g_1(\xi_{1s})\frac{e^{-jkR}}{R}$$

$$E_{\beta_2} = E_{\beta_2}^{\mathrm{GTD}} - (\tau\rho_\alpha)(\tilde{M} \cdot \hat{\beta}_1)\frac{ke^{-jks}}{4\pi}\left(\frac{k\rho_\alpha}{2}\right)^{-1/3} \cdot f_0(\xi_{1s})\frac{e^{-jkR}}{R}$$

where τ is the torsion of the surface ray. In the above expression the effect of the torsion of the surface rays has been isolated and explicitly expressed as additional correcting terms to the GTD solution for torsionless rays. We observe that these additional terms are proportional to τ and are absent when the ray is torsionless ($\tau = 0$), as would be expected.

In contrast to GTD, formulas (44) and (45) are valid irrespective of the location of the observation point, be it in the lit, shadow, or transition regions. Although not valid in the paraxial region ($\beta \approx 90°$), they can be generalized to work along this direction also.

Finally, let us consider the possibility of the generalization of (44) and (45) to other convex surfaces of more general nature. By "more general" surfaces we mean those surfaces which are not substantially different from cylinders, some examples being cylinders with noncircular (elliptical, hyperbolic, and parabolic) cross sections and conical surfaces with small apex angles. The key step in a systematic approach to generalizing (44) and (45) is to use the generalized definition of ξ given in (16).

Figure 14 exhibits some initial results of the generalization of these formulas to the case of a cone. In these graphs, the Hughes results have been reproduced from *Bargeliotes et al.* [1975]. It is evident that results obtained from the present approach agree quite well with the series solution which is rather tedious and time-consuming. We also observe from Figure 14 (right) that there is a noticeable discrepancy between the analytical solution and the experiment. Thus, within the range of experimental error, our results agree quite well with those published in the literature.

3.3. *Approach based on an asymptotic evaluation of the radiation integral of the surface current.* As a final topic, we consider an approach based on the asymptotic evaluation of the radiation integral expressed in terms of the induced surface current which is itself derived in an asymptotic manner for surfaces with large radius of curvature.

It was shown in section 2 that Fock's theory can provide us with an expression for the scattered field in the neighborhood of a smooth convex body illuminated by a plane wave. Using this solution in conjunction with the reciprocity principle, we can find the far field radiated by a point source located on the surface of the body. By generalizing the definition of ξ in Fock's theory, we can also write the final result in a GTD format and represent it as a surface ray. The total field at a point on the surface is obtained by adding all the possible rays which reach the observation point P. Various techniques can be used to determine the field propagation along these rays. For instance, when the source is located on the surface and the surface is a conical one, the field at each point can be decomposed into two parts:

$$F = F_1 + F_2 \tag{47}$$

where F_1 is the geometrical optics field when the observation point is directly illuminated by the source, and is the creeping-wave contribution derivable via an extension of Fock's theory when the point is in the shadow region. The other term, F_2, is the so-called tip contribution, and can be obtained by physical optics or GTD. *Goodrich et al.* [1959] have applied this procedure to find the radiation pattern of slot arrays on cones.

The approximate induced surface current distribution can be obtained by Fock's theory, GTD [*Fock*, 1945, 1946*a*,*b*; *Kouyoumjian*, 1975] or some other appropriate high frequency technique. The

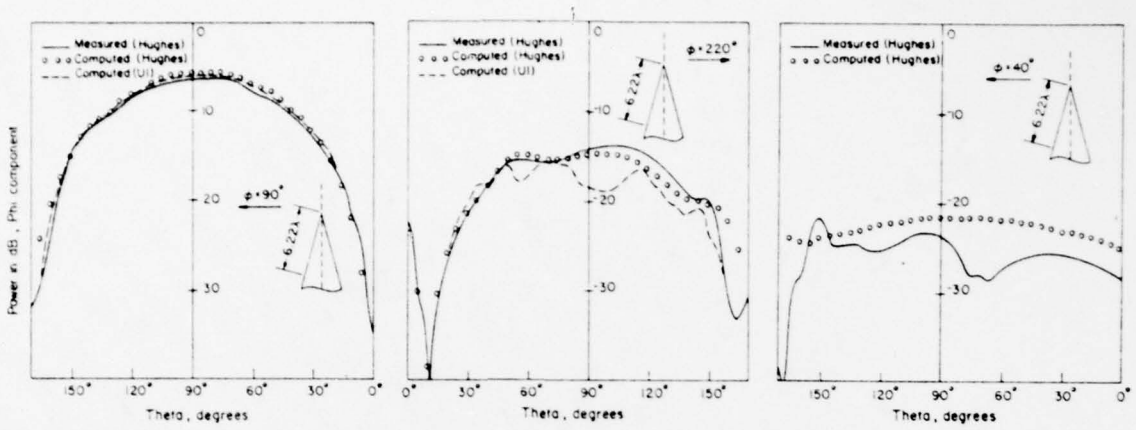

Fig. 14. Comparison between spectral domain results (UI), modal approach (Hughes), and experimental measurements (Hughes). The UI results are derived from a generalized version of (44) and (45) for a cone. The Hughes results have been reproduced from *Bargeliotes et al.* [1975] and are based on a modal series of 13 terms. All results are for $\lambda/2$ radial slot on a cone of half-angle 10°. (Left) $\phi = 90°$ cut. (Middle) $\phi = 220°$ cut. (Right) $\phi = 40°$ cut illustrating the discrepancy between theoretical (Hughes) and experimental (Hughes) presumably attributable to experimental error.

induced surface current due to a magnetic dipole on a perfectly conducting circular cylinder and cone has been calculated by *Chang et al.* [1976], and *Chan et al.* [1977] whose procedure is based upon an asymptotic expansion of the exact modal solution to the above-mentioned problems. Lee *et al.* [*Lee and Mittra*, 1977; *Lee and Safavi-Naini*, 1978] have treated the same problem by a method based on Fock's asymptotic solution of the problem of a sphere [*Fock*, 1949]. These expressions for the current distribution can be used in the radiation integral representation of the far field.

The numerical evaluation of this integral is a formidable task, especially when the frequency is very high. Thus, it is highly desirable to have an analytical and explicit formula for the far field expressed in terms of the surface current. We now discuss an approach for accomplishing this task and examine the problem of deriving an asymptotic expansion of the far field radiated due to a point source located on the surface of a smooth, conducting, and convex body of an arbitrary shape.

Consider an arbitrary smooth convex surface S shown in Figure 15. Let a magnetic dipole source be located at a point Q on S. We parameterize the surface S introducing a "geodetical polar coordinate" system with the pole located at Q such that an arbitrary point P_1 on the surface is defined by a pair of numbers (σ,β), where σ is the arc length of the geodesic QP_1 and β is the angle between QP_1 and some reference direction at Q. Unit vectors along the constant parameter curves $\hat{\sigma}$ and $\hat{\beta}$ are locally orthogonal. The unit normal to the surface, $\hat{n}$, is given by $\hat{n} = \hat{\sigma} \times \hat{\beta}$. An element of length in this coordinate system may be written as

$$ds^2 = d\sigma^2 + G\, d\beta^2 \tag{48}$$

The radiation integral for the scattered far field can be written as

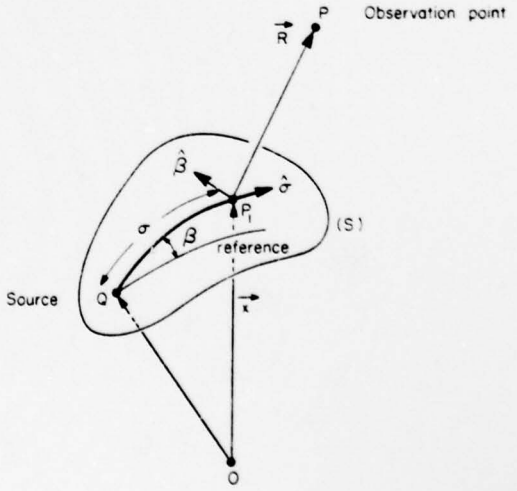

Fig. 15. Source radiation in the presence of a smooth convex surface, parameterized by geodetical polar coordinate system.

$$\bar{E} = \frac{-j\omega\mu}{4\pi} \int_S \int \bar{J}(1 - \hat{R}\hat{R}) \frac{\exp(-jkR)}{R} \, dS \tag{49}$$

where R is the distance between any point on the surface and the observation point. In the geodetical polar coordinate system, we can rewrite a scalar component of (49), say M, in terms of a double integral of the following general form

$$M = \int_0 \int F(\sigma,\beta;P) \frac{\exp\{-jk(R+\sigma)\}}{R} \sqrt{G} \, d\sigma \, d\beta \tag{50}$$

where we have assumed the following form for the surface current:

$$\bar{J}(P_s) = \bar{f}(P_s) \exp(-jk_1\sigma) = J_\sigma \hat{\sigma} + J_\beta \hat{\beta}$$
$$k_1 = k - jk_2; \quad k = 2\pi/\lambda, \quad k_2 > 0, \quad k_2 \ll k \tag{51}$$

where $\bar{f}(P_s)$ is a relatively slowly varying function when k, the free-space wave number, is large. This assumption is based upon a close scrutiny of different asymptotic formulas given for the induced surface current.

When the observation point P is located in the shadow region, the main contribution to (50) comes from a small neighborhood of the stationary point of the integrand, and the stationary phase method for multiple integrals [*Chako*, 1965; *Jones and Kline*, 1958] is applicable. The asymptotic expansion of (49) has been derived up to the order of $k^{-5/3}$. The details of calculation can be found in appendix C. The final result is

$$\bar{E} = (-k^2/8\pi^2) [\bar{U}_0 + \bar{U}_1 + O(k^{-11/6})] \tag{52}$$

where

$$U_0 = \hat{\beta} J_\beta \frac{D_0}{k^{1/6}} \left[\frac{\rho_g}{R(R+\rho_g)} \right]^{1/2} e^{-jkR} \tag{53}$$

$$U_1 = \{[AJ_\beta + (\partial/\partial\sigma)(J_\sigma e^{-Ajk\sigma})e^{-Ajk\sigma}]\hat{\beta} + (BJ_\beta + CJ_\sigma)\hat{n}\}$$
$$\cdot (D_1/k^{7/6}) [\rho_g/(R+\rho_g)R]^{1/2} e^{-jkR} \tag{54}$$

$$D_0 = e^{-j\pi/4} 6^{1/6} \Gamma(1/2)\Gamma(1/3) \rho_\sigma^{2/3} \tag{55}$$

$$D_1 = (-je^{-j\pi/4}/3) 6^{7/6} \Gamma(2/3)\Gamma(1/2) \rho_\sigma^{4/3} \tag{56}$$

A, B, and C are dependent upon geometric properties of the surface at the stationary point which turns out to be exactly the same as the "point of diffraction" of surface rays. The quantities A, B, and C are given by

$$A = \frac{1}{2G} \frac{\partial}{\partial\sigma} G - \frac{\rho_\sigma}{2} \frac{\partial}{\partial\sigma} \left(\frac{1}{\rho_\sigma} \right) + \frac{\rho_g}{2G} \left[\frac{L^{\beta\beta}}{\rho_\sigma} + (L^{\beta\sigma})^2 - (1/2) \frac{\partial^2 G}{\partial\sigma^2} \right] + O\left(\frac{1}{R} \right) \tag{57}$$

$$B = L^{\beta\sigma}/G^{1/2}, \quad C = -1/\rho_\sigma \tag{58}$$

where

ρ_σ = radius of curvature of the geodesic
ρ_g = geodetic radius of curvature
$L^{\beta\beta}$, $L^{\beta\sigma}$ = coefficients of the second fundamental form of the surface (S)

A geometric interpretation of these parameters has been illustrated in Figure 16. It is evident from this figure that $[\rho_g/R(R+\rho_g)]^{1/2}$ is simply the divergence factor of the rays leaving the surface tangentially at the point of diffraction. In using formula (56), we should bear in mind that the various terms in U_0 and U_1 are not of the same order. For example, in the deep shadow, J_σ is exponentially larger than J_β.

The formulas given in (56) have been tested and compared with other available solutions. An important conclusion derived from this comparison is that although the method of radiation integral is based on less restrictive assumptions, it is perhaps not as useful as the spectral domain approach because the stationary point of the phase of the integrand in (50) is of the second order and, hence, the asymptotic expansion of this integral con-

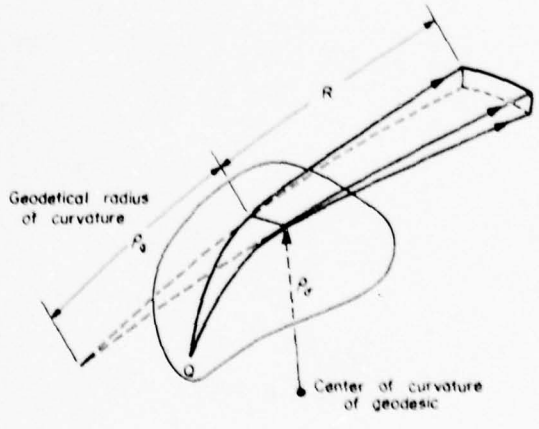

Fig. 16. Diffraction of rays by a smooth convex body and geometric meaning of quantities ρ_g, ρ_σ, and R.

verges rather slowly except when $k\rho_s$ is very large ($\approx$40 or more).

APPENDIX A: FOCK FUNCTIONS

In studies of radio wave propagation around the earth by Van der Pol, Bremmer, Pryce, Fock, and others, and also the later studies of diffraction of electromagnetic waves by certain bodies of revolution [*Nicholson*, 1910; *van der Pol*, 1919, 1937; *Pryce*, 1953; *Fock*, 1946*a,b,c*; *Wait and Conda*, 1959; *Wait*, 1959; *Belkina*, 1949; *Goriainov*, 1958; *Fock et al.*, 1957; *Rice*, 1954], a class of universal functions was introduced which can be used to predict the amplitude and the phase of the reflected or diffracted field by smooth convex surfaces [*Logan and Yee*, 1962]. An exhaustive treatment of these functions which, in general, are defined as Fourier integrals having combinations of Airy integrals in their integrands, has been carried out by *Logan* [1959] (see also *Bowman et al.* [1969] and *Logan and Yee* [1962]).

Since the first extensive application of these functions to diffraction theory was done by Fock, many authors named them after him. Here we list only the most important formulas and expressions for these functions without going through the details of their derivations. We have followed Logan's set of notations for these functions [*Logan*, 1959]. However, since his time dependence factor, $\exp(-i\omega t)$, is different from the one we have used throughout this paper, namely $\exp(+j\omega t)$, our expressions, listed below, are conjugates of what have been presented by Logan.

We start with general definitions. Fock's most general form of the "Van der Pol–Bremmer diffraction formula" is

$$V(x,y_1,y_2,q) = \exp(j\pi/4)\left(\frac{x}{\pi}\right)^{1/2}\int_{-\infty}^{\infty} e^{-jvt} w_2(t-y_>)\cdot\left[v(t-y_<) - \frac{v'(t)-qv(t)}{w_2'(t)-qw_2(t)} w_2(t-y_<)\right]dt \quad \text{(A1)}$$

where $w_1(t)$, $w_2(t)$, $u(t)$, and $v(t)$ are Fock-type Airy functions, defined as

$$u(t) = \sqrt{\pi}\, Bi(t), \quad v(t) = \sqrt{\pi}\, Ai(t),$$

$$w_1(t) = u(t) + jv(t), \quad w_2(t) = w_1(t)^*$$

We note that w_1 and w_2 can also be defined as in section 2. $y_>$ and $y_<$ are the larger and smaller of the two numbers y_1 and y_2. $V(x,y_1,y_2,q)$ is proportional to the attenuation suffered by an electromagnetic wave generated by a source located at reduced height y_1 above the surface of a smooth convex body, when it reaches the observation point located at reduced height y_2 above the same surface. x is the reduced distance between the source and the observation point along the surface, and q is dependent upon the impedance of the surface. Let us consider some useful limiting cases.

When $y_1 = y_2 = 0$, then $V(x,0,0,q)$ is denoted by V_0, where

$$V_0(x,q) = \frac{e^{j\pi/4}}{2}\left(\frac{x}{\pi}\right)^{1/2}\int_{-\infty}^{\infty}\frac{e^{-jvt} w_2(t)}{w_2'(t)-qw_2(t)}dt \quad \text{(A2)}$$

We also have

$$v(x) = V_0(x,0) = \frac{e^{j\pi/4}}{2}\left(\frac{x}{\pi}\right)^{1/2}\int_{-\infty}^{\infty}\frac{e^{-jvt} w_2(t)}{w_2'(t)}dt \quad \text{(A3)}$$

$$u(x) = \lim_{q\to\infty}[-2jxq^2 V_0(x,q)] = \frac{e^{j3\pi/4}}{\sqrt{\pi}}x^{3/2}\int_{-\infty}^{\infty}\frac{e^{-jvt} w_2'(t)}{w_2(t)} \quad \text{(A4)}$$

When $y_1 = 0$ and $y_2 \to \infty$, then $V \to V_1(x,q)$:

$$V_1(x,q) = \frac{1}{\sqrt{\pi}}\int_{-\infty}^{\infty}\frac{e^{-jvt}}{w_2'(t)-qw_2(t)}dt \quad \text{(A5)}$$

and also

$$g(x) = V_1(x,0) = \frac{1}{\sqrt{\pi}}\int_{-\infty}^{\infty}\frac{e^{-jvt}}{w_2'(t)}dt \quad \text{(A6)}$$

$$f(x) = \lim_{q\to\infty}(-qV_1(x,q)) = \frac{1}{\sqrt{\pi}}\int_{-\infty}^{\infty}\frac{e^{-jvt}}{w_2(t)}dt \quad \text{(A7)}$$

Based on (A6) and (A7), a class of functions can be defined:

$$f^{(n)}(x) = \frac{(-j)^n}{\sqrt{\pi}}\int_\Gamma \frac{t^n\cdot e^{-jvt}}{w_2(t)}dt = \frac{d^n f(x)}{dx^n} \quad \text{(A8)}$$

$$g^{(n)}(x) = \frac{(-j)^n}{\sqrt{\pi}}\int_\Gamma \frac{t^n e^{-jvt}}{w_2'(t)}dt = \frac{d^n g(x)}{dx^n} \quad \text{(A9)}$$

where Γ is any path in the complex t plane which comes from $-\infty$ in a sector defined by $-\pi \le$

$\arg(t) < -\pi/3$ and goes to $+\infty$ in the sector $-\pi/3 < \arg(t) < \pi/3$. In what follows, we will give the suitable formulas for $f(x)$ and $g(x)$ in different ranges. Tabulated values and graphs of these functions can be found in the work of *Belkina* [1949], *Fock* [1946*a*,*b*,*c*], and *Logan* [1959].

When x is very large and negative, the following asymptotic expansions for $f(x)$ and $g(x)$ can be used [*Logan*, 1959]:

$$f(x) \sim -2jxe^{-x^3/3}\left\{1 + \frac{j}{4x^3} + \frac{1}{2x^6} - \frac{j175}{64x^9} - \frac{395}{16x^{12}} + \frac{j318175}{1024x^{15}} + \cdots\right\} \tag{A10}$$

$$g(x) \sim 2e^{-x^3/3}\left\{1 - \frac{j}{4x^3} - \frac{1}{x^6} + \frac{j469}{64x^9} + \frac{5005}{64x^{12}} - \frac{j1122121}{1024x^{15}} - \cdots\right\} \tag{A11}$$

The above formulas are valid and accurate for $x \ll -1$. For moderate values of x, namely, $-1 \le x \le 1$, it is difficult to find an appropriate expression. Although there are some analytical techniques such as the stationary phase method or the Poisson summation formula which may be used to evaluate $f^{(n)}$ and $g^{(n)}$ for these values, another possible way which is probably easier and more efficient is to interpolate the tabulated values of these functions in this range.

In the vicinity of zero ($|x| \approx 0$), the Taylor expansion can be used to calculate f and g. The coefficients are given by

$$f^{(n)}(0) = e^{-j(5n\pi/6 - \pi/3)}\sqrt{\pi}\left(\frac{3\pi}{2}\right)^{(2/3)n - (1/4)}\sum_{m=0}^{\infty} A_m(n)\left(\frac{2}{3\pi}\right)^{2m}\tau\left(2m - \frac{4n-1}{6}, \frac{3}{4}\right) \tag{A12}$$

$$g^{(n)}(0) = e^{-j5n\pi/6}\sqrt{\pi}\left(\frac{3\pi}{2}\right)^{(2/3)n - (1/4)}\sum_{m=0}^{\infty} B_m(n)\left(\frac{2}{3\pi}\right)^{2m}\tau\left(2m - \frac{4n-3}{6}, \frac{1}{4}\right) \tag{A13}$$

where $\tau(\lambda,\mu)$ is the generalized tau function:

$$\tau(\lambda,\mu) = \sum_{n=0}^{\infty}\frac{(-1)^n}{(n+\mu)^\lambda}, \quad \lambda > 1 \tag{A14}$$

$$A_0(n) = 1, \quad A_1(n) = (5/48)(n-1)$$

$$A_2(n) = 5(5n^2 - 143n + 26385/16)/(2^9 \cdot 3^2)$$

$$B_0(n) = 1, \quad B_1(n) = -7(n - 3/2)/48$$

$$B_2(n) = (49n^2 + 364n + 39849/16)/(2^9 \cdot 3^2)$$

When x is large, and positive, residue series can be used to compute $f_x^{(n)}$ and $g_x^{(n)}$:

$$f^{(n)}(x) = e^{j(2n+3)\pi/6}\sum_{p=1}^{\infty}\frac{(r_p)^n \exp(r_p x e^{-j5\pi/6})}{Ai'(-r_p)} \tag{A15}$$

$$g^{(n)}(x) = e^{j(n+3)\pi/6}\sum_{p=1}^{\infty}\frac{(r_p')^{n-1}\exp(r_p' x e^{-j5\pi/6})}{Ai(-r_p')} \tag{A16}$$

where $Ai(-r_p) = 0$ and $Ai'(-r_p') = 0$ for $p = 1,2,3,\ldots$.

APPENDIX B: DERIVATION OF (44) AND (45)

Here, we consider only the derivation of the asymptotic expansion of Φ for a circumferential magnetic dipole. In this case, Φ may be written as:

$$\Phi = \frac{j\omega\varepsilon M_\phi}{(2\pi)^2}\int_{-\infty}^{\infty} dk_z \frac{e^{-jk_z z}\, S(k_t)}{k_t^2} \tag{B1}$$

where

$$S(k_t) = \sum_{n=-\infty}^{\infty} e^{-jn\phi}\frac{H_n^{(2)}(k_t\rho)}{H_n^{(2)}(k_t a)} \tag{B2}$$

Applying the Watson transformation to (B2),

$$S(k_t) = \frac{j}{2}\int_{C+D}\frac{H_\nu^{(2)}(k_t\rho)}{H_\nu^{(2)}(k_t a)}\frac{e^{-j\nu(\phi-\pi)}}{\sin\nu\pi}\,d\nu \tag{B3}$$

where C and D are shown in Figure 17. Or,

$$S(k_t) = j\int_{-\infty-j\delta}^{\infty-j\delta}\frac{\cos[\nu(\pi-\phi)]\, H_\nu^{(2)}(k_t\rho)}{\sin(\nu\pi)\, H_\nu^{(2)}(k_t a)}\,d\nu \tag{B4}$$

Substituting the expansion

$$\frac{\cos\nu(\pi-\phi)}{\sin\nu\pi} = j\sum_{i=1}^{2}\sum_{l=0}^{\infty} e^{-j\nu(\phi_i + 2\pi l)} \tag{B5}$$

where $\phi_1 = \phi$ and $\phi_2 = 2\pi - \phi$, in (B4), the result will be:

$$S(k_t) = \sum_{i=1}^{2}\sum_{l=0}^{\infty}\int_{-\infty-j\delta}^{\infty-j\delta}\frac{H_\nu^{(2)}(k_t\rho)}{H_\nu^{(2)}(k_t a)} e^{-j\nu(\phi_i + 2\pi l)}\,d\nu \tag{B6}$$

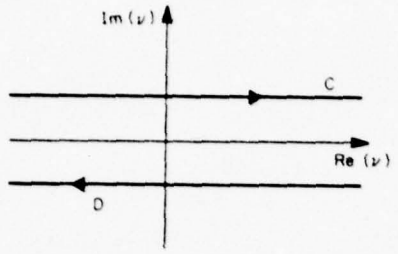

Fig. 17. Paths C and D in Watson transformation.

Each term of the above expansion is associated with a "creeping wave" travelling in a counter-clockwise ($i = 1$) or clockwise ($i = 2$) direction around the cylinder. Following the ray concept, each creeping wave appears to be travelling along a specific surface ray. Now, as $\rho \to \infty$ (far zone) for each fixed ν, we have [*Abramowitz and Stegun*, 1970]:

$$H_\nu^{(2)}(k_t\rho) \sim \left(\frac{2}{\pi k_t \rho}\right)^{1/2} e^{-j(k_t\rho - \nu\pi/2 - \pi/4)} \tag{B7}$$

On the other hand, it can be shown that the significant contribution to $S(k_t)$ comes from a small neighborhood of $k_t a$. In this neighborhood, where $k_t a$ and ν are large and close to each other ($|k_t a - \nu| \leq |\nu|^{1/3}$), the Hankel asymptotic expansion (B7) is no longer valid. In this case, it is necessary to expand Bessel functions in terms of Fock-type Airy functions, $w_1(t)$ and $w_2(t)$, and their derivatives [*Logan*, 1959]:

$$H_\nu^{(2)}(x) \sim (j/m\sqrt{\pi})\{w_2(t) - (1/60m^2)[4tw_2(t) + t^2 w_2'(t)] + \ldots\} \tag{B8}$$

$$H_\nu^{(2)'}(x) \sim (-j/m^2\sqrt{\pi})\{w_2'(t) + (1/60m^2)[4tw_2'(t) + (6 - t^3)w_2(t)] + \ldots\} \tag{B9}$$

where

$$m = \left(\frac{x}{2}\right)^{1/3}, \quad t = \frac{\nu - x}{m} \quad (m \text{ is very large})$$

Inserting (B7) and the first-order terms of (B8) and (B9) into (B6) and (B1), we obtain

$$\Phi \sim [\omega\varepsilon M_\phi/(2\pi)^2]\,(2\pi/\rho)\,e^{j\pi/4} \cdot \sum_{l=1}^{2}\sum_{l=0}^{\infty}\int_{-\infty}^{\infty} dk_t\, e^{-j\Omega_{il}} f_0(\xi_{il})\,\frac{m^2}{k_t^{5/2}} \tag{B10}$$

where

$$m = (k_t a/2)^{1/3}$$

$$\Omega_{il} = k_z z + k_t[\rho + a(\phi_i + 2\pi l - \pi/2)]$$

$$\xi_{il} = m(\phi_i + 2\pi l - \pi/2)$$

Introducing a new integration variable α:

$$k_z = k\sin\alpha \tag{B11}$$

$$k_t = k\cos\alpha \tag{B12}$$

and

$$\beta_{il} = \tan^{-1}\{z/[\rho + a(\phi_i + 2\pi l - \pi/2)]\} \tag{B13}$$

we have:

$$\Omega_{il} = kR_{il}\cos(\beta_{il} - \alpha) \tag{B14}$$

where

$$R_{il} = \{z^2 + [\rho + a(\phi_i + 2\pi l - \pi/2)]\}^{1/2}$$

Now (B10) takes the following form:

$$\Phi \sim \frac{\omega\varepsilon M_\phi}{(2\pi)^2}\left(\frac{2\pi}{\rho}\right)^{1/2}\frac{m_0^2}{k^{3/2}}\,e^{j\pi/4} \cdot \sum_{i=1}^{2}\sum_{l=0}^{\infty}\int_\gamma d\alpha\, e^{-jkR_{il}\cos(\alpha-\beta_{il})}\cos^{-5/6}\alpha \quad f_0(\xi_{il}) \tag{B15}$$

γ is the path of integration in the complex α plane, which is shown in Figure 18.

Now we deform the path of integration into the steepest descent path, SDP, passing through the saddle point of the phase of the integrand. Performing the saddle-point integration, we can derive the

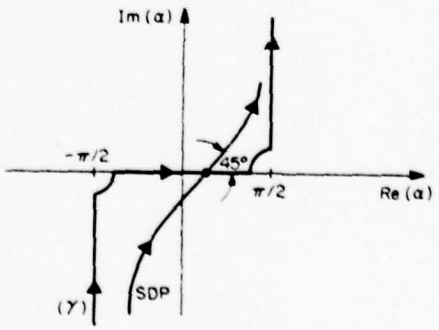

Fig. 18. Steepest descent path (SDP) for integral (B15).

asymptotic expansion of (B15) for large kR_{il}. The first-order term is

$$\Phi \sim \frac{\omega\varepsilon M_0}{2\pi k^2} e^{j\pi/2} \left(\frac{ka}{2}\right)^{1/3} \sum_{i=1}^{2} \sum_{l=0}^{\infty} (\cos\beta_{il})^{-4/3} \cdot \frac{e^{-jkR_{ils}}}{R_{ils}} f_0(\xi_{ils}) \tag{B16}$$

where R_{ils} and ξ_{ils} are the values of these parameters at the stationary point specified by $\alpha = \beta_{il}$. Equation (B16) is the creeping-wave representation of the far field. If the cylinder is large ($ka \gg 1$) and $|\phi|$ is not very close to π, then only the first term ($i = 0$, $l = 1$) has the most important contribution to the total infinite sum, and the other terms are not significant. Neglecting the other terms, we obtain the result given in (44) and (45). It should be emphasized that (44) and (45) are not valid when $|\beta|$ is close to $\pi/2$ (paraxial region) because, in this case, $k_t a$ is very small, and (B7), (B8), and (B9) no longer apply.

The other formulas can be derived in a similar manner.

APPENDIX C: ASYMPTOTIC EVALUATION OF RADIATION INTEGRAL

Consider the following double integral:

$$U(k) = \int_D \int g(x,y)\, e^{jk\Phi(x,y)}\, dx dy \tag{C1}$$

where $g(x,y)$ is rather slowly varying, and $\Phi(x,y)$ has a stationary point (x_s,y_s) inside domain D. The objective is to derive an asymptotic expansion for (C1) when k is large.

Suppose g and Φ have the following forms around (x_s,y_s):

$$g(x,y) = (x - x_s)^{\lambda_0 - 1} (y - y_s)^{\mu_0 - 1} g_1(x,y), \quad \lambda_0, \mu_0 > 1$$

$$\Phi(x,y) = \Phi(x_s,y_s) + a_{\delta,0}(x - x_s)^{\delta}[1 + P(x,y)] + b_{0,\tau}(y - y_s)^{\tau}[1 + Q(x,y)] \tag{C2}$$

Chako [1965] has derived the following asymptotic series for U:

$$U(k) \sim B_0 \sum_{p,q=0}^{\infty} A_{pq}(\alpha_1 + \alpha_2)(\beta_1 + \beta_2) \cdot \Gamma\left(\frac{\lambda_0 + p}{\delta}\right) \Gamma\left(\frac{\mu_0 + q}{\tau}\right) \frac{1}{(ka_{\delta,0})^{p/\delta}} \frac{1}{(kb_{0,\tau})^{q/\tau}} \tag{C3}$$

where

$$B_0 = \frac{1}{(ka_{\delta,0})^{\lambda_0/\delta}} \frac{1}{(kb_{0,\tau})^{\mu_0/\tau}} \frac{1}{(\delta\tau)} e^{jk\Phi(x_s,y_s)}$$

$$\alpha_1 = \exp\left[j\pi(\lambda_0 + p)/(2\delta)\right]$$

$$\alpha_2 = \exp\left\{\left[j\pi/(2\delta)\right]\left[(\lambda_0 + p)(2\delta + e^{j\pi\delta}) - 2\delta\right]\right\}$$

$$\beta_1 = \exp\left[j\pi(\mu_0 + q)/(2\tau)\right]$$

$$\beta_2 = \exp\left\{\left[j\pi/(2\tau)\right]\left[(\mu_0 + q)(2\tau + e^{j\pi\tau}) - 2\tau\right]\right\}$$

$$g_1(x,y) = \sum_{k,l=0}^{\infty} g_{kl}(x - x_s)^k (y - y_s)^l$$

$$P(x,y) = \sum_{m+n\geq 1} a_{mn}(x - x_s)^m (y - y_s)^n$$

$$Q(x,y) = \sum_{m+n\geq 1} b_{mn}(x - x_s)^m (y - y_s)^n$$

$$A_{00} = g_{00}$$

$$A_{10} = g_{10} - g_{00}\left[(\lambda_0 + 1)\, a_{10}/\delta + b_{10}/\tau\right]$$

$$A_{01} = g_{01} - g_{00}\left[a_{01}/\delta + (\mu_0 + 1)\, b_{01}/\tau\right]$$

In order to apply this procedure to the integrals of the type (50) for which

$$\phi(x,y) = -\Omega(\sigma,\beta) = -(R + \sigma) \tag{C4}$$

$$g(x,y) = F(\sigma,\beta,P)\sqrt{G}/R \tag{C5}$$

When F is one of the components of $\bar{J}(1 - \hat{R}\hat{R})$, one should first determine the stationary point of Ω, wherein its first-order derivatives vanish. The second step is to compute the various-order derivatives of Ω, J, $\hat{R}$, ..., at this point, and then insert them into (C3). We give just the main formulas needed for these derivations.

Suppose the surface of the body, $\bar{r}(\sigma,\beta)$, is parameterized by a geodetical polar coordinate system. As discussed previously, in this system, σ is the arc length of the surface geodesic connecting the pole Q to $\bar{r}(\sigma,\beta)$, and β is the angle between the geodesic and some fixed reference geodesic at Q (Figure 15).

The element of length in this system is given by

$$ds^2 = d\sigma^2 + G(\sigma,\beta)\, d\beta^2 \tag{C6}$$

Let us denote $d\bar{r}(u)/du$ by $\bar{r}_u$; then we have the following set of relations

$$\hat{x}_{\alpha\beta} = \frac{-\partial G/\partial\sigma}{2}\,\hat{X}_\sigma + \frac{\partial G/\partial\rho}{2G}\,\hat{x}_\beta + L^{\beta\beta}\,\hat{x}_3 \tag{C7}$$

$$\hat{x}_{\beta\sigma} = \hat{x}_{\sigma\beta} = [(\partial G/\partial\sigma)/2G]\,\hat{x}_\beta + L^{\beta\sigma}\,\hat{x}_3 \tag{C8}$$

$$\hat{x}_{\sigma\sigma} = -\hat{x}_3/\rho_\sigma \tag{C9}$$

where $\hat{x}_\sigma = \hat{\sigma}$ and $\hat{x}_\beta/\sqrt{G} = \hat{\beta}$ are unit vectors along β = const. and σ = const. curves, and

$$\hat{x}_3 = \hat{n} = (\hat{x}_\sigma \times \hat{x}_\beta)/\sqrt{G} \tag{C10}$$

is the outward unit normal to the surface. Another quantity of interest is the "geodetical curvature" κ_g given by

$$\kappa_g = (\partial G/\partial\sigma)/2G \tag{C11}$$

Using the above relations, we can derive the following expressions which hold true at the stationary point:

$$\partial\Omega/\partial\sigma = 1 - \hat{R}\cdot\hat{X}_\sigma = 0 \tag{C12}$$

$$\partial\Omega/\partial\beta = -\hat{R}\cdot\hat{x}_\beta = 0 \tag{C13}$$

$$\frac{\partial^2\Omega}{\partial\sigma^2} = 0, \quad \frac{\partial^2\Omega}{\partial\sigma\partial\beta} = 0, \quad \frac{\partial^2\Omega}{\partial\beta^2} = G\left(\frac{1}{R} + \frac{1}{\rho_g}\right) \tag{C14}$$

where $\rho_g = 1/\kappa_g$, and

$$\frac{\partial^3\Omega}{\partial\sigma^3} = \frac{1}{\rho_\sigma^2}, \quad \frac{\partial^3\Omega}{\partial\sigma^2\partial\beta} = -L^{\beta\sigma}/\rho_\sigma \tag{C15}$$

$$\frac{\partial^3\Omega}{\partial\beta^2\partial\sigma} = \frac{G}{R^2} + \frac{\partial G/\partial\sigma}{R} + \frac{\partial^2 G/\partial\sigma^2}{2} - \frac{L^{\beta\beta}}{\rho_\sigma} \tag{C16}$$

$$\frac{\partial^3\Omega}{\partial\beta^3} = \frac{3\partial G/\partial\beta}{2R} + \frac{\partial G}{\partial\beta}\frac{\partial G}{\partial\sigma}\frac{1}{4G} + L^{\beta\sigma}\,L^{\beta\beta} + \frac{1}{2}\frac{\partial^2 G}{\partial\sigma\partial\beta} \tag{C17}$$

where ρ_σ is the radius of curvature of the geodesic.

Equations (C12) and (C13) determine the location of the stationary point. At this point $\hat{R} = \hat{x}_\sigma$, which, if we introduce the ray concept, tells us that the surface rays leave the surface at the "point of diffraction" tangentially. Equation (C14) indicates that the stationary point is of second order, so that we need higher-order derivatives of the phase. $L^{\sigma\sigma}$, $L^{\beta\sigma}$, and $L^{\beta\beta}$ are coefficients of the second fundamental form of the surface evaluated at the stationary point. They are defined as

$$L^{\sigma\sigma} = \hat{x}_{\sigma\sigma}\cdot\hat{x}_3, \quad L^{\sigma\beta} = \hat{x}_{\sigma\beta}\cdot\hat{x}_3, \quad L^{\beta\beta} = \hat{x}_{\beta\beta}\cdot\hat{x}_3$$

Using the relationships given above, one can find the expansion coefficients g_{kl}, a_{mn}, b_{mn}, and A_{pq} in (C3). Zeroth- and first-order terms in (C3) give us formulas (52).

A few remarks should be made concerning the expansion presented in (C3). First of all, (C3) is a doubly infinite series; therefore, for each fixed power of k^{-1} a finite number of terms should be summed up. The coefficients of various terms in these finite sums, namely A_{pq}'s, become very complicated when p and q are greater than 0 or 1. Another difficulty with this series is that when the stationary point of the phase is of an order higher than 1, the difference between the order of the successive terms (when they are ordered according to the descending power of k) becomes very small, and consequently the infinite series converges very slowly. For instance, in our problem where $\delta = 3$ and $\tau = 2$ (stationary point is of second order), sometimes the difference between the orders of successive terms is $k^{-1/6}$, which indicates the weak convergence (in an asymptotic sense) of the expansion in the cases where the frequency is not very large.

Acknowledgments. The work reported in this paper was supported in part by the US Office of Naval Research under grant N000-19-78-C-0064, and in part by the National Science Foundation grant NSF-ENG 76-08305. The authors are also indebted to their colleagues S. W. Lee and Y. Rahmat-Samii for helpful discussions and encouragement. It also gives the authors great pleasure to acknowledge the inspiration they have received from the pioneering works of H. Bremmer on a wide variety of topics related to the propagation of electromagnetics waves. These include the development of asymptotic techniques, radiation of sources near spherical earth, the application of transform methods, and many more fundamental contributions in theoretical electromagnetics which Bremmer has made during the last forty years.

REFERENCES

Abramowitz, M., and I. A. Stegun (1970), *Handbook of Mathematical Functions*, p. 364, Dover, New York.

Albertsen, N. C. (1974), Diffraction of creeping waves, *Tech. Rep.*, Technical University of Denmark, Lyngby, Denmark.

Bargeliotes, P. C., A. T. Villeneuve, and W. H. Kummer (1975), *Pattern Synthesis of Conformal Arrays*, 79 pp., Radar Microwave Laboratory, Aerospace Groups, Hughes Aircraft Company, Culver City, California.

Belkina, M. G. (1949), *Tables to Calculate the Electromagnetic Field in the Shadow Region for Various Soils*, Soviet Radio Press, Moscow (translated by M. D. Friedman, ASTIA Document No. AD110298, 1956).

Bowman, J. J., T. B. A. Senior, and P. L. E. Uslenghi (1969), *Electromagnetic and Acoustic Scattering by Simple Shapes*, 728 pp., North-Holland, Amsterdam.

Buchal, R. N., and J. B. Keller (1960), Boundary layer problems in diffraction theory, *Commun. Pure Appl. Math.*, *13*, 85–114.

Chako, N. (1965), Asymptotic expansion of double and multiple integrals occurring in diffraction theory, *J. Inst. Math. Appl.*, *1*, 372–422.

Chan, K. K., L. B. Felsen, A. Hessel, and J. Shmoys (1977), Creeping waves on a perfectly conducting cone, *IEEE Trans. Antennas Propagat.*, *AP-25*, 661–671.

Chang, Z. W., L. B. Felsen, and A. Hessel (1976), Surface ray methods for mutual coupling in conformal arrays on cylindrical surfaces, *Fin. Rep.*, 81 pp., Department of Electrical Engineering and Electrophysics Polytechnic Institute of New York, Farmingdale, New York.

Christiansen, N. C. (1966), Diffraction of creeping waves, paper presented at URSI Spring Meeting, Washington, DC.

Cohen, D. C. (1965) New eigenfunction expansions and alternative representations for the reduced wave equations, *J. Math. Mech.*, *14*, 403–412.

Crispin, J. W., Jr., and A. L. Maffett (1965), Radar cross-section estimation for simple shapes, *Proc. IEEE*, *53*, 833–843.

Cullen, J. A. (1958), Surface current induced by short-wavelength radiation, *Phys. Rev. A*, *9*, 1863–1867.

Fischer, E. (1966), On the Watson transformation, *Commun. Pure Appl. Math.*, *19*, 287–297.

Fock, V. A. (1945), Diffraction of radio waves around the earth's surface, *J. Phys. USSR*, *9*, 225–266.

Fock, V. A. (1946*a*), The distribution of currents induced by a plane wave on the surface of a conductor, *J. Phys. USSR*, *10*, 130–136.

Fock, V. A. (1946*b*), The field of a plane wave near the surface of a conducting body, *J. Phys. USSR*, *10*, 399–409.

Fock, V. A. (1946*c*), *Tables of the Airy Function*, Moscow.

Fock, V. A. (1949), The field from a vertical and a horizontal dipole raised above the earth's surface, *Zh. Eksp. Teor. Fiz.*, *19*, 916–926. (English translation in *Electromagnetic Diffraction and Propagation Problems*, pp. 235–253, Pergamon, New York, 1965.)

Fock, V. A., L. A. Vainshtein, and M. G. Belkina (1957), *Diffraction of Electromagnetic Waves by Certain Bodies of Revolution*, Soviet Radio Press, Moscow.

Franz, W., and K. Klante (1959), Diffraction by surfaces of variable curvature, *IRE Trans. Antennas Propagat.*, *AP-7*, S68–S70.

Goodrich, R. F. (1959), Fock theory—An appraisal and exposition, *IRE Trans. Antennas Propagat.*, *AP-7*, S28–S36.

Goodrich, R. F., R. E. Kleinman, A. L. Maffett, C. E. Schonsted, K. M. Siegel, M. G. Chernin, H. E. Shank, and R. E. Plummers (1959), Radiation from slot arrays and cones, *IRE Trans. Antennas Propagat.*, *AP-7*, 213–222.

Goriainov, A. S. (1958), An asymptotic solution of the problem of diffraction of a plane wave by a conducting cylinder, *Radio Eng. Electron. Phys.*, *3*(5), 23–39.

Hong, S. (1967), Asymptotic theory of electromagnetic and acoustic diffraction by smooth convex surfaces of variable curvature, *J. Math. Phys.*, *8*, 1223–1232.

Jones, D. S., and M. Kline (1958), Asymptotic expansion of multiple integrals and the method of stationary phase, *J. Math. Phys.*, *37*, 7–28.

Keller, J. B. (1956), Diffraction by a convex cylinder, *IRE Trans. Antennas Propagat.*, *AP-4*, 312–321.

Keller, J. B. (1957), Diffraction by an aperture, I and II, *J. Appl. Phys.*, *28*, 426–444, 570–579.

Keller, J. B., and B. R. Levy (1959), Decay exponents and diffraction coefficients for surface waves on surfaces of nonconstant curvature, *IRE Trans. Antennas Propagat.*, *AP-7*, S68–S70.

Keller, J. B., and L. Kaminetzky (1972), Diffraction coefficients for higher order edges and vertices, *SIAM J. Appl. Math.*, *22*, 109–134.

Kline, M., and I. Kay (1965), *Electromagnetic Theory and Geometrical Optics*, Interscience, New York.

Kouyoumjian, R. G. (1965), Asymptotic high-frequency methods, *Proc. IEEE*, *53*, 864–876.

Kouyoumjian, R. G. (1975), The GTD and its application, chap. 6 of *Numerical and Asymptotic Techniques in Electromagnetics*, edited by R. Mittra, Springer, New York.

Kravtsov, Yu. A. (1964), A modification of the geometrical optics method (in Russian), *Radiofizika*, *7*, 664–673.

Langer, R. E. (1960), Turning point in linear asymptotic theory, *Res. Rep. No. 127*, University of Wisconsin, Madison, Wisconsin.

Lee, S. W., and R. Mittra (1977), Mutual admittance between slots on a cylinder or cone, *Tech. Rep.*, Electromagnetics Laboratory, University of Illinois at Urbana-Champaign, Urbana, Illinois.

Lee, S. W., and S. Safavi-Naini (1976), Asymptotic solution of surface field due to a magnetic dipole on a cylinder, *Tech. Rep. 76-11*, Electromagnetics Laboratory, University of Illinois at Urbana-Champaign, Urbana, Illinois.

Lee, S. W., and S. Safavi-Naini (1978), Approximate asymptotic solution of surface field due to a magnetic dipole on a cylinder, *IEEE Trans. Antennas Propagat.*, *AP-26*, 593–598.

Levy, B. R., and J. B. Keller (1959), Diffraction by a smooth object, *Commun. Pure Appl. Math.*, *12*, 159–209.

Lewis, R. M., N. Bleistein, and D. Ludwig (1967), Uniform asymptotic theory of creeping waves, *Commun. Pure Appl. Math.*, *20*, 295–328.

Logan, N. A. (1959), General research on diffraction theory, Vols. 1 and 2, *Tech. Reps. LMSD-288087 and LMSD-288088*, ASTIA Nos. AD241228 and AD243182, Lockheed Missiles and Space Division, Sunnyvale, California.

Logan, N. A., and K. S. Yee (1962), A mathematical model for diffraction by convex surfaces, in *Electromagnetic Waves*, edited by R. E. Langer, pp. 139–180, University of Wisconsin Press, Madison, Wisconsin.

Ludwig, D. (1966), Uniform asymptotic expansions at a caustic, *Commun. Pure Appl. Math.*, *19*, 215–250.

Luneberg, R. K. (1944), *Mathematical Theory of Optics*, Brown University, Providence, Rhode Island.

Nicholson, J. W. (1910), On the bending of electric waves around the earth, *Phil. Mag.*, *18*, 757–760.

Olver, F. W. J. (1956), Asymptotic solution of linear differential equation of second order in a domain containing one transition point, *Phil. Trans. Roy. Soc. London, Ser. A*, *249*, 65–97.

Pathak, P. H., and R. G. Kouyoumjian (1972), The radiation from apertures in curved surfaces, *Rep. 3001-2*, Electroscience Laboratory, Department of Electrical Engineering, Ohio State University, Columbus, Ohio.

Pathak, P. H., and R. G. Kouyoumjian (1974), An analysis of the radiation from apertures in curved surfaces, *Proc. IEEE*, *62*, 1438–1447.

Pflumm, E. (1960), Expansion Problems Arising from the Watson Transformation, *Res. Rep. BR-35*, New York University, New York.

Pryce, M. H. L. (1953), The diffraction of radiowave by the curvature of the earth, *Advan. Phys.*, *2*, 67–95.

Rice, S. O. (1954), Diffraction of plane radio waves by a parabolic cylinder—Calculation of shadows behind the hills, *Bell Syst. Tech. J.*, *33*, 417–504.

Siegel, K. M. (1958), Far-field scattering from bodies of revolution, *Appl. Sci. Res.*, *B7*, 293–328.

Siegel, K. M., R. F. Goodrich, and V. H. Weston (1959), Comments on far field scattering from bodies of revolution, *Appl. Sci. Res.*, *B8*, 8–12.

Thompson, J. R. (1962), Radio propagation over a sectionally cylindrical surface, *Proc. Roy. Soc., Ser. A*, *267*, 183–196.

Uslenghi, P. L. E. (1972), *Lectures on High-Frequency Scattering Methods*, Sorrento, Italy, Sept. 5–8, Air Force Office of Scientific Research, Air Force Systems Command, USAF. (Author's present address: University of Illinois at Chicago Circle, Chicago, Illinois.)

van der Pol, B. (1919), On the propagation of electromagnetic waves around the earth, *Phil. Mag.*, *38*, 365–380.

van der Pol, B. (1937), Diffraction of electromagnetic waves from an electrical point source around a finitely conducting sphere with applications to radio-telegraphy and the theory of the rainbow, 1 and 2, *Phil. Mag.*, *24*, 141–176 and 825–864.

Voltmer, D. R. (1970), Diffraction by doubly curved convex surfaces, Ph.D. dissertation, Ohio State University, Columbus, Ohio.

Wait, J. R. (1959) *Electromagnetic Radiation from Cylindrical Structures*, Pergamon, New York.

Wait, J. R., and A. M. Conda (1959), Diffraction of electromagnetic waves by smooth obstacles for grazing angles, *J. Res. Nat. Bur. Stand. Sect. D*, *63D*, 181–197.

Watson, G. N. (1918), The diffraction of electric waves by the earth, *Proc. Roy. Soc., Ser. A*, *A95*, 83–99.

Weston, V. H. (1962), The effect of a discontinuity in curvature in high frequency, *IRE Trans. Antennas Propagat.*, *AP-10*, 775–780.

Zauderer, E. (1970), Uniform asymptotic solutions of the reduced wave equation, *J. Math. Anal. Appl.*, *30*, 157–171.

ACCURACY TESTS AND ITERATIVE PROCEDURES FOR HIGH FREQUENCY ASYMPTOTIC SOLUTIONS - A SPECTRAL DOMAIN APPROACH

Raj Mittra and Mark Tew
University of Illinois, Urbana, Illinois

ABSTRACT

In this paper we describe three procedures for evaluating the accuracy of high frequency asymptotic solutions. Two of the tests are based on the spectral domain approach while the third can be implemented either in the space domain or in the spectral domain. A method for improving the solution via an iterative procedure is also presented.

INTRODUCTION

High frequency asymptotic solutions of the wave equation play a very important role in electromagnetics and acoustics. For low frequencies, the integral equation formulation combined with the method of moments provides a convenient approach for solving radiation and scattering problems. However, because the matrix size required to handle such problems becomes too large above the resonance region, one is forced to seek alternate means, such as ray-optical techniques, for deriving asymptotic solutions in the high frequency range. Unlike moment method solutions which are numerically vigorous, asymptotic solutions are approximations, and as such, pose problems in evaluating their accuracy. The problem of assessing the accuracy of asymptotic solutions has come under investigation only in recent years [1] - [4]. Presented here are three procedures for evaluating the accuracy of an asymptotic solution by examining its effect on satisfaction of boundary conditions. In addition, two of the proposed tests lend themselves for use as an iterative equation, offering the possibility of systematic improvement of a proposed solution.

ACCURACY TESTS FOR ASYMPTOTIC SURFACE FIELDS

Two of the accuracy tests to be discussed deal with the problem of a magnetic dipole radiating in the presence of an infinitely long, perfectly conducting, circular cylinder. This problem has received increased attention in recent years because of the insights it provides into the performance of slot antennas on curved surfaces. Knowledge of the induced currents, for example, allows the engineer to calculate mutual coupling between slot antennas in a conformal array or to accurately compute far-field patterns from a single slot or slot array. The exact modal solution to this problem [5] - [6], which is in the form of an infinite series of infinite integrals, converges so slowly as to make its use impractical for numerical calculation. Various approximate solutions, more suitable for numerical computation, have been proposed [7] - [11]. Two of the solutions, [7] - [9], are derived from manipulation of the modal solution. These solutions are denoted as Asymptotic Solution - 1 (AS-1) [7] - [8], and Asymptotic Solution - 2 (AS-2) [9], based on their chronological order of publication. The third approximate solution [10] - [11] is based on a modification of the work of V. A. Fock, which addresses the problem of radiation on a sphere and is denoted Asymptotic Solution - 3, or AS-3.

The next section describes in detail the three published solutions and gives the appropriate formulae.

Proposed Solutions to Cylinder Problem

Figure 1a presents the geometry of the problem. An infinitely long, perfectly conducting, circular cylinder of radius R is located with the cylinder axis coinciding with the z-axis of a standard ρ, ϕ, z cylindrical coordinate system. An infinitesimal, phi-directed, magnetic dipole is located on the cylinder surface at Q' given by the coordinates $\rho = R$, $\phi = 0$, $z = 0$. The H-field on the cylinder surface is observed at a point Q located at $\rho = R$, $\phi = \phi_T$, $z = z_T$. The proposed solutions are ray-type solutions, and the surface fields are dependent on the geodesic path between Q and Q' defined by the surface path length, s, and ray angle, θ, measured from the ϕ-axis to the surface ray.

The cylinder is a developable surface and a geodesic path on the cylinder surface becomes a straight line on the infinite strip that makes up a developed cylinder. Figure 1b shows the developed cylinder and introduces the local $\hat{n}'$, $\hat{b}'$, $\hat{t}'$ and $\hat{n}$, $\hat{b}$, $\hat{t}$ coordinate systems, where $\hat{n}'$, $\hat{n}$ are the outward normal to the surface, and $\hat{t}'$, $\hat{t}$ are tangent to the surface path at the source and observation points respectively ($\hat{b}' = \hat{t}' \times \hat{n}'$, $\hat{b} = \hat{t} \times \hat{n}$). Both the AS-1 and AS-3 solutions give the surface field in terms of fields parallel to $\hat{b}$ and $\hat{t}$ as

$$\bar{H}(Q) = \bar{M} \cdot (\hat{b}'\hat{b}H_b + \hat{t}'\hat{t}H_t) \qquad (1)$$

where $\bar{M}$ is the magnetic dipole moment. In this section a circumferentially oriented dipole is treated, i.e., $\bar{M} = \hat{\phi}$. For this case, conventional H_z and H_ϕ fields can be found from H_b and H_t using the relationships

$$H_\phi = \cos^2\theta\, H_t + \sin^2\theta\, H_b \qquad (2a)$$

$$H_z = \sin\theta\cos\theta(H_t - H_b) \quad . \qquad (2b)$$

Each of the proposed solutions gives the surface H-fields in terms of a combination of "Fock functions," $u(\xi)$, $v(\xi)$, and $v_1(\xi)$ and their derivatives $u'(\xi)$, $v'(\xi)$, and $v_1'(\xi)$, respectively. ξ is a normalized distance parameter given by $\xi = \left(\frac{k}{2R_t^2}\right)^{1/3} s$ where k is the wavenumber, R_t is the radius of curvature in the direction of t given by $R_t = R/\cos^2\theta$ and s is the path length, $s = \sqrt{(R\phi)^2 + z^2}$. The radius of curvature in the direction of $\hat{b}$ is also employed and is given by $R_b = R/\sin^2\theta$. The AS-1 solution as tested gives the surface fields as

$$H_b(Q) \sim v(\xi)G(s) \qquad (3a)$$

$$H_t(Q) \sim \left(\frac{2i}{ks}\right)u(\xi)G(s) \quad , \qquad (3b)$$

where H_t of (3b) differs from the H_t given in [7]-[8] by a factor of 2 (this is done so that as $k \to \infty$ the H_t of (3b) recovers identically the $(ks)^{-2}$ term of the known exact solution). The AS-3 solution is given by

$$H_\phi(Q) \sim [v(\xi)[\sin^2\theta + \frac{j}{ks}(1 - 3\sin^2\theta)] + (\frac{j}{ks})\sec^2\theta[u(\xi) - \sin^2\theta v_1(\xi)]\,G(s) \quad (4a)$$

$$H_z(Q) \sim -\sin\theta\cos\theta\, v(\xi)[1 - \frac{3j}{ks}]G(s) \quad (4b)$$

for the case of a circumferentially oriented dipole. The AS-3 solution gives the surface fields as

$$H_b(Q) \sim \{(1 - \frac{j}{ks})v(\xi) - (\frac{1}{ks})^2 u(\xi) + j(\sqrt{2}\,kR_t)^{-2/3}[v'(\xi) + (R_t/R_b)u'(\xi)]\}G(s) \quad (5a)$$

$$H_t(Q) \sim (\frac{j}{ks})\{v(\xi) + (1 - \frac{2j}{ks})u(\xi) + j(\sqrt{2}\,kR_t)^{-2/3}u'(\xi)\}G(s)\ . \quad (5b)$$

In Equations (3)-(5), $G(s) = k^2/(2\pi j\eta)\cdot e^{-jks}/ks$, where η is the wave impedance of free space.

In addition to the three published solutions, a fourth solution has been constructed, which is a modified AS-1 solution and is denoted AS-4. The AS-4 solution is given by

$$H_b(Q) \sim [v(\xi) - j/ks - (1/ks)^2]G(s) \quad (6a)$$

$$H_t(Q) \sim (2j/ks)[u(\xi) - j/ks]G(s)\ . \quad (6b)$$

As θ goes to ninety degrees (a ray propagating down the cylinder axis), H_b becomes identical to H_ϕ and the solutions reduce to

$$H_\phi(Q) \sim G(s) \text{ for AS-1} \quad (7a)$$

$$H_\phi(Q) \sim [1 - \frac{j}{ks} + (\frac{\pi}{2})^{1/2}e^{-j\pi/4}\frac{(ks)^{1/2}}{kR}]G(s) \text{ for AS-2} \quad (7b)$$

$$H_\phi(Q) \quad [1 - \frac{j}{ks} - (\frac{1}{ks})^2 + \frac{3}{4}(\frac{\pi}{2})^{1/2}e^{-j\pi/4}\frac{(ks)^{1/2}}{kR}]G(s) \text{ for AS-3}\ . \quad (7c)$$

and $$H_\phi(Q) = [1 - \frac{j}{ks} - (\frac{1}{ks})^2]G(s) \text{ for AS-4}\ . \quad (7d)$$

The four solutions presented here embody some important differences. For example, as $kR \to \infty$, both the AS-3 and AS-4 solutions recover the exact solution to the problem of a magnetic dipole radiating over a ground plane. The AS-1 solution recovers the ks^{-1} terms; while the AS-2 solution recovers both the $(ks)^{-1}$ and $(ks)^{-2}$ terms, missing only the $(ks)^{-3}$ term. Since these differences involve terms that have significant contribution only for very short path lengths ($s < 1\lambda$), these differences are referred to as "source-region" differences.

Long-path length differences are most apparent along theta equal to ninety degrees. Here, for large s, both the AS-2 and AS-3 solutions vary asymptotically as $(ks)^{-1/2}$, while the AS-1 and AS-4 solutions show a free-space-like attenuation of $(ks)^{-1}$.

The accuracy tests presented are closely examined to determine if they can discriminate between the various solutions. An accuracy test which relies on the entire solution being correct is termed a global test. That is, a global test is not associated with any particular region of the proposed solution, but tests the entire solution. A test which is associated with a region or a point is termed a local test. A local test, then, would be able to discriminate between the AS-2 and AS-3 solutions even though their source region forms are identical, because of the differences in the long path length behavior.

THE E-FIELD TEST

In implementing an accuracy test, the best approach is usually to compare the approximate solution to the exact solution. As stated before, computational difficulties with the exact solution preclude that option in this case. If the exact solution is unavailable for comparison, then an accuracy test can be formulated by determining how well the approximate solution satisfies boundary conditions for the problem - in this case, the electric field boundary condition at the perfectly conducting surface.

The most direct and attractive method of determining the surface E-field would be to compute the normal derivative of the H-field. Unfortunately, the asymptotic solutions are valid only for points on the cylinder surface, so that such a direct computation is unfeasible. Accordingly, an indirect procedure must be used. An indirect evaluation of the surface E-field is conducted in the following manner: Each of the asymptotic solutions predicts the H-field on the cylinder surface. Through the use of Maxwell's equations, the surface H-field can be related to the surface E-field and the boundary condition checked. Use of the spectrum of the H-field instead of the direct surface field makes analysis straightforward and allows use of a Fast-Fourier Transform (FFT) algorithm for efficient numerical calculation.

The test proceeds as follows:

1. A cylindrical transform is defined

$$\tilde{H}_{\substack{z\\ \phi}}(n,k_z) = 1/2\pi \int_0^{2\pi} d\phi \int_{-\infty}^{\infty} dz\, H_{\substack{z\\ \phi}}(\phi,z) e^{-jn\phi}\, e^{-jk_z z} \quad . \tag{8}$$

2. Electric and magnetic vector potentials are expanded with unknown coefficients

$$\left.\begin{matrix} A_z \\ F_z \end{matrix}\right\} = \frac{1}{2\pi} \sum_{n=-\infty}^{\infty} e^{jn\phi} \int_{-\infty}^{\infty} \begin{matrix} f_n(k_z) \\ g_n(k_z) \end{matrix} H_n^{(2)}(\rho\sqrt{k^2-k_z^2})\, e^{jk_z z}\, dz \quad . \tag{9}$$

Observe that n and k_z are "transform variables," k is the wavenumber, and $H_n^{(2)}$ is the n^{th} order Hankel function of the second kind, representing an outward-traveling cylindrical wave. For future notation, the complex variable γ is used to replace the radical in the argument of the Hankel function, $\gamma = \sqrt{k^2-k_z^2}$.

3. Through the use of

$$\bar{H} = \nabla\times\bar{A} - j\omega\varepsilon_o\bar{F} + 1/j\omega u_o \quad \nabla\nabla\cdot\bar{F} \tag{10}$$

one may determine the unknown coefficients f_n and g_n in terms of the transform of the surface H-field as

$$f_n(k_z) = \frac{-1}{\gamma H_n'^{(2)}(\gamma R)} \left[\tilde{H}_\phi(n,k_z) + \frac{nk_z}{\gamma^2 R} \tilde{H}_z(n,k_z)\right]$$

$$g_n(k_z) = \frac{j\omega\mu_o}{\gamma^2 H_n^{(2)}(\gamma R)} \tilde{H}_z(n,k_z) \qquad (11)$$

where $H_n'^{(2)}$ is the derivative of the $H_n^{(2)}$ Hankel function.

4. Applying

$$\bar{E} = -\nabla x\bar{F} - j\omega\mu_o\bar{A} + 1/j\omega\varepsilon_o \nabla\nabla\cdot\bar{A} \qquad (12)$$

permits computation of the surface E-field, accomplishing the desired test.

The above procedure can be condensed into two steps of actual computation by combining Equations (9), (10), (11), and (12). While the resulting expressions appear to be complex, this two-step procedure is significant because it essentially involves only a two-dimensional Fourier transform, modification and combination of the transformed fields, and then inverse Fourier transformation and summation of Fourier coefficients. The analysis is computationally efficient because the FFT can be used to evaluate all the integrals involved.

Practically speaking, the greatest difficulty in the above procedure comes in accurately determining the spectrum of the surface H_ϕ field. Both the AS-3 and AS-4 solutions have $1/s^2$ and $1/s^3$ singularities, while the AS-1 solution has a $1/s$ singularity. The "peakiness" of these H_ϕ fields means that special care must be taken in using the FFT to determine the spectrum.

One attempt to overcome this problem involved raising the magnetic dipole slightly above the cylinder surface so that the field was no longer singular, but had a finite peak. After this step had been implemented, a convergence check of the FFT integral showed that the FFT was able to handle the $1/s$ peak correctly with reasonable sampling rates, but the $1/s^2$ and $1/s^3$ peaks yielded erroneous results. Further measures were necessary to achieve a reliable test of the AS-3 and AS-4 solutions (for a reasonable computer size).

The key to achieving a reliable check of the AS-3 and AS-4 solutions lies in recognizing that the singular form of the source region is that of a planar case, and that the singularity has an analytic transform. Specifically, the planar singularity can be expressed as

$$H_\phi|_s = \frac{1}{2\pi njk}\left(\frac{\partial^2}{\partial^2(R\phi)^2} + k^2\right)\frac{e^{-jks}}{s}$$

$$H_z|_s = \frac{1}{2\pi njk}\left(\frac{\partial^2}{\partial(R\phi)\partial z}\frac{e^{-jks}}{s}\right) \qquad (13)$$

where s is the path length given by $s = \sqrt{\Delta^2+(R\phi)^2+z^2}$, and Δ is the height of the dipole above the cylinder. Because the singularities can be expressed as derivatives, their analytic transform is obtainable and is of the form

$$\tilde{H}_z|_s = \frac{Q}{2\pi njk}\left(\frac{-nk_z}{R}\right)\frac{1}{4\pi jR}\frac{e^{-j\Delta\sqrt{k^2-(n/R)^2-k_z^2}}}{\sqrt{k^2-(n/R)^2-k_z^2}} \qquad (14a)$$

$$\tilde{H}_\phi\Big|_s = \frac{Q}{2\pi njk}\left(-\frac{n^2}{R^2}+k^2\right)\frac{1}{4\pi jR}\,\frac{e^{-j\Delta\sqrt{k^2-(n/R)^2-k_z^2}}}{\sqrt{k^2-(n/R)^2-k_z^2}} \tag{14b}$$

where Q is a constant.

The total field on the cylinder can then be expressed as

$$\bar{H}(Q) = \bar{H}_{PLANAR}(Q) + \bar{H}_{DIFFERENCE}(Q) \tag{15}$$

where $\bar{H}(Q)$ is the total field as predicted by an asymptotic solution, and $\bar{H}_{PLANAR}(Q)$ is the field that would exist on a flat, infinite ground plane. (This division may be thought of as taking the planar field, "wrapping" it around the cylinder, and subtracting it from $\bar{H}(Q)$). The transform of the surface fields is given by

$$\tilde{\bar{H}}(n,k_z) = \tilde{\bar{H}}_{PLANAR}(n,k_z) + \tilde{\bar{H}}_{DIFFERENCE}(n,k_z) \tag{16}$$

and $\tilde{\bar{H}}_{PLANAR}(n,k_z)$ is given analytically in Equation (14). $\bar{H}_{DIFFERENCE}(Q)$ is at most on the order of $1/\sqrt{s}$, so that evaluation of $\tilde{\bar{H}}_{DIFFERENCE}(n,k_z)$ can be reliably obtained from application of the FFT. Any test which involves breaking the fields up into planar and difference fields will be termed a hybrid computation, because it combines analytic and numerical techniques. The only difference between a "hybrid computation" and a "direct computation" is in the method of obtaining the spectrum. After the spectrum is found, both tests proceed identically. Figure 2 compares the phase of $\tilde{H}_\phi$ for a fixed value of k_z, when the transform was derived from hybrid and direct computations. Comparison with the phase of the modal transform reveals the increased accuracy of the hybrid method.

To utilize the E-Field Test the three asymptotic solutions are compared to an exact modal solution [6]. The procedure used in deriving the exact modal solution is essentially the same as that used to perform the E-Field Test. The difference lies in the fact that while the test begins with the asymptotic H-field, the modal solution begins with the known E-field (known for an elemental source). In a manner similar to the test, the H-spectrum can be found from the known E-fields and be expressed in terms of the E-spectrum. This provides analytic H_z and H_ϕ spectrums that can be compared to those resulting from the asymptotic solutions. After the H-spectrum is obtained from the E-field, it can be tested just like any other spectrum. This "check" that begins with a surface E-field, finds the H-spectrum and then returns to the surface E-field is also valuable inassuring that the FFT sampling of the spectrum is sufficient.

During actual application of the test, the source used was a slot radiator instead of an elemental dipole. This was necessary because the surface E-field of the slot is finite, although discontinuous, while the surface E-field from the elemental source is singular. Sampling the E-spectrum sufficiently well to represent the singular surface field would make the computer requirements prohibitively large, while the more regular slot is readily handled.

Representation of the slot spectrum was achieved by first determining the H-field spectrum due to an elemental dipole source (the direct asymptotic solutions or, for the analytic case, $\bar{E}_{SURFACE} = \hat{z}(\delta(\rho-R)\delta(\phi)\delta(z))$. The H-spectrum was then multiplied by the transform of the slot distribution, which is equivalent to convolving the elemental source with a distribution in the space domain. For a finite slot as shown in Fig. 1a, the transforms used were of the form

$[\sin(k_z b/2)]/(k_z b/2)$ to represent a uniform E_z field, and of the form $\cos(\alpha n)/[\pi^2/4 - (\alpha n)^2]$, $\alpha = \arcsin(a/2R)$ to represent a half-period cosine spreading in ϕ.

The totality of the E-field check has now been determined. The components of the spectrum of the H-field that result from an elemental source are determined. For the asymptotic solutions the spectrum is determined either by direct application of the FFT or by use of the hybrid technique; for the exact case, the H-spectrum may be found analytically. Regardless of its source, the H-spectrum is then multiplied by the transform of the assumed slot distribution; thus, the convolution that is necessary to represent the slot distribution is accomplished. The E-field spectrum is then found from modification and combination of the H-field spectrum components. Finally, inverse Fourier transformation and summation of the Fourier coefficients give the surface E-field.

Results of the E-Field Test

Figures 3 and 4 give representative results after the E-Field Test has been implemented. The test was first applied to the analytic H-spectrum. This was the standard to which all other solutions were compared. The analytic solution resulted in an E_ϕ that was essentially zero (a totally flat curve) and an E_z that was well-contained. The fact that E_z went to zero in a smooth curve in the z-direction instead of a discontinuous curve was due to the numerical calculation, and revealed that the error introduced by performing finite sums and integrals was negligible. Figure 3 shows the surface electric fields that resulted from testing the AS-1 solution. Because the AS-1 solution only has a singularity (peak) on the order of 1/s, it was not necessary to resort to a hybrid computation to obtain a reliable check. As can be seen, the E_ϕ field has significant non-zero content and the extent of the corresponding E_z field is much broader than that of the modal solution.

Figure 4 shows the effects of testing the AS-3 solution using the hybrid method. The hybrid method was used because of the higher-order source region terms present in the AS-3 solution. The resultant surface E_ϕ field is very small and displays a rippled character.

The fields that resulted from testing the AS-4 solution using the hybrid technique were essentially identical to those of Fig. 4, although there were slight numerical differences.

DISCUSSION OF E-FIELD TEST

The E-Field Test represents an example of global test. That is, the test is applied once, and the results determine if the field everywhere is correct. If the approximation does accurately predict the surface magnetic fields, then the corresponding electric fields will re-create those obtained by testing the analytic H-transform, within the constraints of numerical accuracy. When results do not duplicate those of the analytic standard, then one can only say that some error is present. Specifying what the error is, or in what region it occurs, is very difficult, perhaps impossible, from observing the results of a single test. However, by comparing the results from tests of different approximate solutions, some insight can be gained.

The results presented here provide a good example of what can be learned from comparing test results of different solutions. Figures 3 and 4 reveal that the E-Field Test is sensitive to the source region behavior of the proposed solution

and relatively insensitive to the large-path length behavior. The surface E_ϕ fields of Fig. 3, corresponding to the AS-1 solution, are quite different from those of Fig. 4 resulting from the AS-4 solution, despite the fact that their large-path length behaviors are identical. The approximate solutions of Figs. 3 and 4 differ only in the $(ks)^{-2}$ and $(ks)^{-3}$ source region terms. This point is reinforced by the fact that Fig. 4 represents results from a test of either the AS-3 and AS-4 solutions. As $kR \to \infty$, the source regions of the AS-3 and AS-4 solutions both go to a planar-type singularity. Along theta equal to ninety degrees, however, the AS-3 shows attenuation as $(ks)^{-1/2}$ for large path lengths, while the AS-4 solution shows attentuation as $(ks)^{-1}$. The E-Field Test was unable to discern between the AS-3 and AS-4 solutions, despite the significant differences in large path length behavior.

In summary, the resulting E-field after performance of the test does provide a good qualitative measure of how well the asymptotic solution satisfies the E-field boundary condition. Indeed, application of the test to the transform of the exact modal solution did result in fields that satisfied the boundary condition quite well. In addition, application of the test to approximate asymptotic solutions showed that they did not test as well as the exact solution. In this respect, the E-Field Test does provide a good "global test" of a proposed solution, i.e., if the solution is accurate everywhere, the solution will show good results from the test.

On the other hand, when comparing the relative accuracy of approximate solutions, the source region behavior appears to be more critical for satisfaction of the test than the large path length behavior -- asymptotic solutions that contain higher-order terms ($1/s^2$, $1/s^3$) in the source region H-field do satisfy the E-Field Test better than solutions that contain only terms on the order of $1/s$. The large-path length behavior did not appreciably affect the test results.

Emphasis of the source region is not necessarily detrimental to the E-Field Test, for it is likely that the source region will heavily influence the computation of values of physical parameters of interest, such as the mutual impedance between two slots on a curved surface. Wire antennas provide a good analogy, for the source region behavior dominates calculation of the self- and mutual-impedance, and the current behavior at the end plays less of a role. An E-field boundary condition check of a wire antenna would not be influenced very much by the current far away from the source, but be source region sensitive. It is not surprising, then, that the E-field check reveals little about the local character of the solution, but instead provides more of a global test. The point should be made, however, that a large path length solution for the antenna current would probably be of very limited use, since both the impedance behavior and the radiation pattern derived from this type of asymptotic solution would be grossly in error. The E-Field Test proposed in this paper is able to distinguish between a solution which has a better overall behavior on the entire surface and an alternate solution which is only good in local isolated regions, but has large errors in other regions where the current is significant.

Some numerical difficulties were encountered during execution of the test. The high-order source-region terms made it quite difficult for the FFT to accurately compute the integral involved. Since use of the FFT requires equally spaced sampling over the interval, a sampling sufficient to accurately evaluate the peak resulted in matrix sizes too large for some computers (CDC CYBER 74, for example). For solutions whose source-region behavior went to a planar-type singularity in the limit, however, analytic evaluation of the planar spectrum allowed completion of the test. A solution which contains higher-order source region terms but does not go to planar type behavior in the limit is quite difficult to test by this

method unless it has an analytical transform (or unless the investigator has an extraordinarily large computer). However, such a behavior would not be expected to be physically meaningful anyhow.

The AS-2 solution is a good example of this, for it contains the $1/s^2$ source region term, but not the $1/s^3$ term. This solution could be tested by modifying its source-region behavior by the addition of the $1/s^3$ term and performing a hybrid computation. This was not done, since comparison of the AS-3 and AS-4 tests indicates that solutions with the same limiting source region behavior yield virtually identical E-Field Tests.

To sum up, it appears that the E-Field Test can provide a measure of the accuracy of a proposed asymptotic solution. An FFT is employed so that the evaluation of the integrals involved may be efficiently performed, but some care must still be taken in the computation. The test reveals that solutions which have planar-type, source-region behavior in the limit satisfy the E-field boundary condition better than those that only have terms on the order of 1/s. The test is, however, relatively insensitive to the large path-length behavior of a solution.

INTEGRAL E-FIELD TEST

Introduction

The E-Field Test just described was qualitative in nature and highly dependent on the source region accuracy of the proposed solution. The E-Field Test was global in nature and unable to discriminate between solutions which had similar characteristics in the source regions, but varied in their long-path-length behavior. The "Integral E-Field Test" described here is an attempt to achieve a "local" test. This test is also based on satisfaction of the electric field boundary condition at the perfectly conducting surface.

The Integral E-Field Test is quantitative in nature, is straightforward in application, and displays a mixed local/global nature. Under some circumstances, the test lends itself to application as an iterative equation for point-by-point improvement of a proposed solution.

Inspiration for the Integral E-Field Test came from the observation that Lorentz Reciprocity allows the use of test dipoles that can be located at the tester's discretion. A new equation results from each new location of the test dipole (or dipoles), which opens the possibility of achieving a "local" test. It is seen that the Integral E-Field Test displays a mixed local/global character, in general, but that along theta equal to ninety degrees the source region of a proposed solution can be essentially excluded from contributing to the accuracy test, yielding a very strong local or point-test character. Under those circumstances the Integral E-Field Accuracy Test also lends itself to formulation as an iterative equation, allowing point-by-point improvement of a proposed solution.

Formulation of the Integral E-Field Test

The Integral E-Field Test may be formulated using Green's Identities, Generalized Lorentz Reciprocity, or from first principles using Maxwell's Equations and Gauss' Law. The defining equation for the Integral E-Field Test is given by:

$$-\iint_S (\bar{E}^A \times \bar{H}^B - \bar{E}^B \times \bar{H}^A) \cdot d\bar{a} = \iiint_V (\bar{H}^B \cdot \bar{M}^A - \bar{H}^A \cdot \bar{M}^B) dv \qquad (17)$$

where fields and sources from two different environments, A and B, are related in a single equation. In order to achieve an accuracy test, Environment A will denote

the environment of the approximate solution, that is, an infinitely long, perfectly conducting circular cylinder in free space. An infinitesimal phi-directed magnetic dipole, $\overline{M}^A$, radiates in the presence of the cylinder (Fig. 1a). Environment B is made up entirely of free space. A magnetic dipole source (or sources), $\overline{M}^B$, is placed in Environment B, giving rise to electric and magnetic fields $\overline{E}^B$ and $\overline{H}^B$ (Fig. 5). The fields in Environment A are termed "asymptotic fields" because they are given by the approximate asymptotic solution. The fields in Environment B are termed "test fields" because they are employed to evaluate the accuracy of a proposed solution. The volume V is defined as being enclosed by surface S, which is made up of concentric circular cylinders, S_c and S_∞. Cylinder S_c has radius $R + \delta$, where δ is vanishingly small, and S_∞ has infinite radius. In Environment A, S_c and S_∞ are placed so that their axes coincide with the axis of the perfectly conducting cylinder; while in Environment B, S can be placed anywhere as long as it does not intersect any of the sources, $\overline{M}^B$. Since the sources in both Environments A and B are of finite extent, the fields $\overline{E}^A$, $\overline{H}^A$, $\overline{E}^B$, and $\overline{H}^B$ obey the radiation condition - with the result that the surface integral over S_∞ is zero. Equation 17 can then be rewritten as

$$\int_{S_c}\int \overline{E}^A\times\overline{H}^B\cdot d\overline{a} = \int_{S_c}\int \overline{E}^B\times\overline{H}^A\cdot d\overline{a} - \iiint_V(\overline{H}^B\cdot\overline{M}^A - \overline{H}^A\cdot\overline{M}^B)dV \quad . \tag{18}$$

The accuracy test is accomplished by arguing that the exact solution to a dipole radiating in the presence of, but not on, the perfectly conducting cylinder would satisfy the boundary condition that the tangential electric field is zero everywhere on the perfectly conducting cylinder surface. Taking δ to be vanishingly small, the surface S_c almost coincides with the conducting surface so that the magnitude of the left-hand side of Equation 18 can be made as small as desired, approaching zero in the limit as δ goes to zero. The amount that the right-hand side of Equation 18 differs from zero is termed the "error," ε, and is used as a basis for comparing proposed solutions to the problem embodied in Environment A,

$$\varepsilon = \int_{\substack{S_c \\ \delta\to 0}}\int \overline{E}^B \times \overline{H}^A\cdot d\overline{a} - \iiint_V(\overline{H}^B\cdot\overline{M}^A - \overline{H}^A\cdot\overline{M}^B)dv \quad . \tag{19}$$

If delta-function type sources are used for both Environments A and B (and they are implied by the proposed solutions of Environment A), then the volume integral of Equation 19 reduces to a sampling operation and becomes

$$\varepsilon = \int_{\substack{S_c \\ \delta\to 0}}\int \overline{E}^B \times \overline{H}^A\cdot d\overline{a} - H^B(M^A) + H^A(M^B) \tag{20}$$

where the symbol $H^i(M^j)$ denotes the operation $\overline{H}^i(x_j, y_j, z_j)\cdot\hat{M}^j$ in which the fields of Environment i are sampled at the position of the sources in Environment j, and the dot product is taken with the unit vector parallel to the "j" source. Now, if ε is sufficiently small, Equation 20 can be cast into the form of an iterative equation

$$H^{A(1)}(M^B) = H^B(M^A) - \int_{\substack{S_c \\ \delta\to 0}}\int \overline{E}^B \times \overline{H}^{A(0)}\cdot d\overline{a} = H^{A(0)}(M^B) - \varepsilon \quad . \tag{21}$$

Thus, the field at a point (the location of source M^B) can be updated by modifying the proposed approximate solution by the error term associated with that point.

Observe that the exact solution would satisfy $\varepsilon = 0$ in Equation 20, so that using Equation 21 to iterate would not change the field value.

In review, the formulation of the Integral E-Field Accuracy Test has been accomplished through the use of well-known properties of electromagnetic fields. The resulting equation is straightforward, involves known quantities, and, in general, consists only of sampling operations and numerical integration. In some cases, the test can lend itself to point-by-point improvement of a proposed solution. Local or point-test character is embodied in two ways: 1) By the explicit sampling operation of the surface magnetic field, and 2) by the fact that the near field of the test dipole tends to emphasize the local magnetic fields in the integral of Equation 20. The test, in general, cannot be entirely local, however, for the integral of Equation 20 covers the entire surface of the cylinder. In particular, unless the test electric fields can be constructed to be nearly zero in the region around the asymptotic source, then the large magnetic fields in the asymptotic source region will certainly contribute to the integral and thus affect the test results. Thus, one would expect the Integral E-Field Test to have a mixed local/global character.

It is proper at this point to note that while the development of the Integral E-Field Test has been carried out in the space domain, spectral domain calculations are an alternative when using the test. Specifically, Parseval's Theorem can be used to change the space integral of Equation 20 to an integral in the transform domain. Performing the integration in the transform domain is particularly valuable if a proposed solution is to be tested at a large number of points, for in that case, "moving" the test dipole around can be accomplished by adding the proper phase shift terms to the integrand of Equation 20. It is the authors' experience that use of transform domain integration results in a considerable gain in computational efficiency over spatial integration. To justify use of the spectral domain, though, the asymptotic solution must be tested at enough points to recover the expense of obtaining the spectral domain representation of the proposed solution.

Practical Considerations for the Integral E-Field Accuracy Test

While Equation 19, which defines the test, appears to lend itself to direct evaluation, several practical aspects of the evaluation must be considered. First, an important step in formulating Equation 19 was that the tangential E-field vanish for a source radiating in the presence of the cylinder, while the published solutions are for the case of a dipole radiating on the cylinder surface. To perform the test, the proposed solutions were extended to the case of a dipole radiating a distance Δ away from the cylinder by modifying the path length s used in determining the surface field. The modified path length s' used in Equations 3-7 was computed from $s' = \sqrt{s^2 + \Delta^2}$, where s is the surface path length. In addition to satisfying the assumption made in formulating the test, raising the dipole allows numerical calculation of the integral in Equation 20, since the H^A fields have a finite peak and are not singular (source region H^A fields are singular for a dipole located on the surface).

Location of the test dipole(s) with respect to the surface coinciding with the perfectly conducting cylinder (this surface is denoted S_c^B) greatly influences the test results. A test dipole placed so that it sampled the surface magnetic field of the approximate solution would seem to lend a local character to the test. However, a test dipole so located would introduce singular E^B fields, which makes numerical integration more difficult. Accordingly, the test dipole is, in general,

located a Δ distance away from the surface corresponding to the cylinder surface. The E^B fields on the surface of integration are calculated exactly, but the H^A field at M^B is approximated by the H^A field at the point on S_c^B closest to the location of M^B. In other words, if the sampling operation $H^A(M^B)$ required finding $H^A(R + \Delta, \phi_t, Z_t)$, this would be approximated by $H^A(R, \phi_t, Z_t)$. The error introduced by this approximation was checked by applying the test to a problem with a known solution, that of a magnetic dipole radiating over an infinite ground plane. For Δ equal to one sixteenth of a wavelength, the error introduced by this assumption was negligible compared to ε's computed in the cylinder test.

Observe that the user has complete freedom to place one or several test dipoles in Environment B. For example, two test dipoles could be used, located at $(R + \Delta, \phi_{TST}, Z_{TST})$ and $(R + \Delta, \phi_{TST}, -Z_{TST})$. This would have the effect of creating a plane of zero E^B fields that coincide with the H^A source region. Evaluation of the integral of Equation 20 shows that this would decrease the contribution of the source region H_Z^A fields (due to zero E_ϕ^B) and emphasize the source region H_ϕ^A field. As this illustrates, use of multiple-dipole test configurations generally involves a trade-off of some kind, so that the simple single test dipole located Δ away from S_c^B has been chosen as the "standard" test.

Results of the Integral E-Field Test

Representative results of the Integral E-Field Test are presented in Figs. 6-13. These represent application of the test to the AS-1, AS-2 and AS-3 solutions along theta equal to ninety degrees and along theta equal to zero degrees. A single test dipole was used for Figs. 6-8 and 11-13. For tests along $\theta = \pi/2$, along the cylinder axis, a two-test-dipole configuration was also used with phi-directed test dipoles located at $(R + \Delta, 0, Z_{TST})$ and $(R - \Delta, 0, Z_{TST})$. The test equation under these conditions becomes

$$\varepsilon = \int_{\substack{S_c \\ \delta \to 0}} \int (E_Z^B H_\phi^A - E_\phi^B H_Z^A) da - H_\phi^B(M^A) + H_\phi^A(M^B) \qquad (22)$$

The figures present the H_ϕ field to be tested, error results, and H_ϕ after application of the iterative equation. Several factors combine to increase confidence in the test results along $\theta = 90°$. First, the magnitude of the error term is relatively small with respect to the magnitude of $H^{A(0)}(M^B)$, so that the criterion for successful iteration is close to being met. Second, for both single- and dual-dipole tests, the asymptotic source-region field contributes very little to the integral that makes up the error term. For the single dipole, this is easily seen from the fact that for $Z_{TST} >> \Delta$ along $\theta = 90°$, the E^B field evaluated at (R,0,0) will be primarily ϕ-directed with a very small E_Z or E_ϕ component. At the same time, the test field E^B directly underneath the test dipole will have a very large E_z component, emphasizing the local H_ϕ field. For two dipoles located at $(R \pm \Delta, 0, Z_{TST})$, the plane of zero tangential electric fields is tangent to the cylinder at $\phi = 0$, thus reducing the asymptotic source region contribution. Local H_ϕ field emphasis does not occur with the two-dipole test, however, since the plane of zero tangential E-fields extends through $Z = Z_{TST}$. Thus, for $Z_{TST} >> \Delta$ along

$\theta = 90°$, the Integral E-Field Test should have a very strong local character and be almost unaffected by the source-region accuracy of the proposed solution.

Single-dipole tests along angles other than $\theta = 90°$ will introduce an asymptotic source region contribution to the integral of Equation 20, with the amount of contribution dependent on the path length and θ-angle. The local E-fields in the vicinity of the test dipole remain large, so that it is expected that the test will display a mixed local/global character. The results of Figs. 11, 12, and 13 reflect this; for while the zeroth-order magnitudes are relatively close, there is a large variance in the associated errors. If the test were truly local, the associated errors should also be relatively close. Examination of Figs. 11 and 13 reveals that along $\theta = 0°$ the iterative equation is divergent instead of convergent. Close examination of the results of the evaluation of the integral of Equation 20 reveals that the contribution from the vicinity of the source dominated the contribution from the rest of the surface, including the region around the test dipole. The integral of Equation 20, in turn, is the highest contributor to the error, ε. Thus, for $\theta = 0°$, the Integral E-Field Test retains local character only in the sampling operation. The large source-region contribution drives the error term up so that its magnitude is not small compared to $H^{A(0)}(M^B)$ and the iterative equation diverges.

One may be tempted to employ two dipoles located at $(x_t^{(1)} = R\cos\phi_t, y_t^{(1)} = R\sin\phi_t, Z_t)$ and at $(x_t^{(2)} = 2R - x_t^{(1)}, y_t^{(2)} = y_t^{(1)}, Z_t)$ to obtain asymptotic source-region cancellation. This introduces the problem of determining the scattered field at the location of the second dipole. Unfortunately, if surface equivalent currents are used to find the scattered field at the test dipole, then it can be shown that the test is identical to a single-dipole test. That is, the use of surface equivalent currents to find $H^A(M^B)$ always leads to the result that $\varepsilon = 0$, for <u>any</u> proposed solution <u>when</u> M^B is entirely located external to S_c^B. (Observe that for $\theta = 90°$, the second dipole lies outside of v, and this problem is not encountered.) Use of other approximations to find the "scattered field" external to the cylinder would introduce an unknown error, so use of remotely located dipoles was abandoned for angles other than $\theta = 90°$.

Thus, the "Integral E-Field Test" displays, in general, a mixed local/global character which changes according to the location of the test dipole. For $\theta = 90°$ the test has almost entirely a local character, with very little contribution from the asymptotic source region. Under these conditions, the error term is relatively small compared to $H^{A(0)}(M^B)$ and the iterative equation converges. For angles other than $\theta = 90°$ the asymptotic source region begins to contribute to the integral, resulting in a mixed local/global nature. At the same time, errors in the source region tend to increase the magnitude of the error term, so that it is no longer small compared to $H^{A(0)}(M^B)$. In this case, the iterative equation shows less of a tendency to converge and may diverge.

<u>Summary of Integral E-Field Test</u>

Generalized Lorentz Reciprocity has been employed to formulate an accuracy test that can be used to check any proposed solution. The test is straightforward in application and general in nature, that is, not limited to testing only cylindrical geometries. The test is quantitative in nature, and requires only numerical integration for implementation. Either the spectral domain or the spatial domain can be employed for computation of the integral involved. For testing a large number of points, economics tend to favor computation in the spectral domain, while for testing a small number of points spatial domain integration is indicated.

The Integral E-Field Test has local character in that the error computed is associated with a single point, although the entire solution contributes to the computation of the error term. In cases where the error is small compared to the value of the proposed solution, the test lends itself to use as an iterative equation.

When the test is applied to the problem of magnetic dipole radiation in the presence of an infinite, conducting cylinder, it was found that tests along the cylinder axis lend themselves to iteration. Along the axis, solutions that vary as $(ks)^{-1/2}$ test better than solutions that vary as $(ks)^{-1}$ for large path lengths. Tests at points other than on the axis generate error terms that are large with respect to the approximate field value, so that the iterative equation is not convergent. The source regions of each of the proposed solutions were found to contribute significantly to the large error terms for tests of points off the cylinder axis.

OVERVIEW OF E-FIELD AND INTEGRAL E-FIELD TESTS

Two tests based on satisfaction of the E-field boundary condition have been presented. Both have been applied to proposed solutions to the problem of a magnetic dipole radiating in the presence of an infinitely long, perfectly conducting circular cylinder. The E-Field Test is based on relating the spectral domain of the surface magnetic field to that of the surface electric field and then evaluating the surface E-field. The test is effected by observing how well the resultant E-field satisfies the surface boundary condition, and, as such, is a direct test of boundary condition satisfaction. The E-Field Test has a global character in that it can be applied to a proposed solution only once. For the solutions tested so far, the E-Field Test seems most sensitive to the source region of a proposed solution and relatively insensitive to large path length behavior. One cannot say that only the source region is tested, though, because gross errors in a proposed solution might evidence themselves in the E-Field Test.

The Integral E-Field Test can be formulated from Generalized Lorentz Reciprocity and employs "test" dipoles situated in free space. The surface electric field corresponding to the solution being tested is never computed, so that the Integral E-Field Test is, in effect, an indirect boundary condition check. It has local character in that the test results can be associated with the field at a particular point, and the test can be repeated many times at different points for the same proposed solution. Results of the Integral E-Field Test display, in general, a mixed local/global character. For tests on or near the cylinder axis, the local character is very strong; while for tests in the "deep shadow" region, less local character is retained and the asymptotic source region becomes dominant. Under some circumstances, including tests along the cylinder axis, the Integral E-Field Test lends itself to use as a convergent iterative equation. The Integral E-Field Test formulation is quite general, and application is not limited to cylindrical structures.

In summary, the E-Field and Integral E-Field Tests appear to be complementary. One is global and the other has a mixed global/local nature. One test is highly source region sensitive and relatively insensitive to large-path-length behavior. For the other test, the source region can essentially be excluded from contributing to the result. Finally, the possibility of iterative improvement of a proposed solution is offered, if some relatively stringent conditions can be met.

ITERATIVE ACCURACY TEST FOR BOUNDARY CONDITIONS

Both the E-Field Test and the Integral E-Field Test were applied to asymptotic solutions of surface magnetic fields. The asymptotic solutions tested predicted

Solution - 1 (AS-1) [7] - [8], and Asymptotic Solution - 2 (AS-2) [9], based on their chronological order of publication. The third approximate solution [10] - [11] is based on a modification of the work of V. A. Fock, which addresses the problem of radiation on a sphere and is denoted Asymptotic Solution - 3, or AS-3.

both the near field and long-path-length behavior of a magnetic dipole radiator. A more traditional and wide-spread use of asymptotic solutions is to predict the far-field behavior of scattering bodies. For analyzing complex scattering bodies, the engineer today can draw on a range of asymptotic techniques, including different "uniform" solutions. In analyzing a complex body, the investigator is likely to combine contributions from straight and curved edges, and possibly diffracted rays from curved surfaces. A great deal of work is being performed today to generate "diffraction coefficients" for the various diffracting mechanics needed to complete the total solution of the far field. This section presents an iterative method based on spectral domain techniques for solving the far field and induced currents of a scattering body. An important feature of this method is that at each step of the iterative method a boundary condition check is incorporated so that the accuracy of the solution can be evaluated. This boundary condition check at the first iteration also provides a means of evaluating the benefit of a proposed solution. In order to illustrate use of this test, it is applied to check a vertex diffraction coefficient for scalar-wave incidence that has been proposed by Albertsen [12]. Although the application to be illustrated is a scalar problem, the extension to vector electromagnetics problems is straightforward.

The Corner Diffraction Coefficient

The corner diffraction term investigated here gives the field diffracted from the vertex when a scalar plane wave is incident on an infinite, acoustically soft quarter-plane, Fig. 14. Such a problem has been addressed by Kraus and Levine [13], Keller [14], and Radlow [15]. Recently, Albertsen used sequential application of the Weiner-Hopf technique and saddle-point integration to extract a corner diffraction coefficient. Albertsen gives the total scattered field from the quarter-plane as

$$u(x,y,0) = \frac{1}{(2\pi)^2} \int_{-\infty+\mu_i}^{\infty+\mu_i} d\mu \int_{-\infty+\lambda_i}^{\infty+\lambda_i} d\lambda \frac{M^{++}(\mu,\lambda)M^{++}(\mu_0,\lambda)M^{++}(\mu,\lambda_0)M^{++}(\mu_0,\lambda_0)}{\sqrt{k^2-\mu^2-\lambda^2}} \times e^{-ix\mu}\, e^{-iy\lambda}/[(\lambda+\lambda_0)(\mu+\mu_0)] \quad . \tag{23}$$

The scattered field due to the corner only is given by

$$U_c^s(r,\vartheta,\phi) = \left(\frac{e^{i\pi/4}}{8\pi k}\right)^2 \frac{e^{ikr}}{r} D_D(\vartheta_0,\phi_0,\vartheta,\phi) \quad . \tag{24}$$

The corner diffraction coefficient D_D can be determined from

$$D_D(\vartheta_0,\phi_0,\vartheta,\phi) = -4 \frac{M(\vartheta_0,\phi_0,\vartheta,\phi)}{(\mu+\mu_0)(\lambda+\lambda_0)}$$

where

$$M(\vartheta_0,\phi_0,\vartheta,\phi) = M^{++}(\mu,\lambda) \times M^{++}(\mu,\lambda_0) \times M^{++}(\mu_0,\lambda) \times M^{++}(\mu_0,\lambda_0) \tag{26}$$

where

$$\mu = -k \sin\vartheta \cos\phi \quad , \qquad \mu_0 = -k \sin\vartheta_0 \cos\phi_0$$

$$\lambda = -k \sin\vartheta \sin\phi \quad , \qquad \lambda_0 = -k \sin\vartheta_0 \sin\phi_0 \quad .$$

The M^{++} functions are found from

$$M^{++}(\mu,\lambda) = \sqrt{\frac{k}{2}}\sqrt{1-d_1}\; e^{\tau} \tag{27}$$

where H_t of (3b) differs from the H_t given in [7]-[8] by a factor of 2 (this is done so that as $k \to \infty$ the H_t of (3b) recovers identically the $(ks)^{-2}$ term of the known exact solution). The AS-2 solution is given by

where

$$\tau = -\frac{1}{4\pi i}\Big\{ \mathrm{Dilog}(1 - d_1) - \mathrm{Dilog}(1 + d_1)$$

$$+ \mathrm{Dilog}(1 - d_2) - \mathrm{Dilog}(1 + d_2) - i\pi \log(-\zeta_2)$$

$$- (\log(-id_1) - i\tfrac{\pi}{2}) \log(1 + d_1)$$

$$+ (\log(-id_1) + i\tfrac{\pi}{2}) \log(1 - d_1)$$

$$+ (\log(id_2) - i\tfrac{\pi}{2}) \log(1 - d_2)$$

$$- (\log(id_2) + i\tfrac{\pi}{2}) \log(1 + d_2)\Big\} \qquad (28)$$

and

$$d_1 = \zeta_1 K_1,\ d_2 = \zeta_1 K_2$$

$$\left.\begin{matrix}\zeta_1\\ \zeta_2\end{matrix}\right\} = -\frac{1}{k}\left(\lambda \mp i\sqrt{k^2 - \lambda^2}\right)$$

$$\left.\begin{matrix}K_1\\ K_2\end{matrix}\right\} = \frac{1}{k}\left(iu \pm \sqrt{k^2 - u^2}\right)$$

and the Dilog function is defined by $\mathrm{Dilog}(z) = -\int_1^z \frac{\mathrm{Log}\,\xi}{\xi - 1}\,d\xi$. In practice, this corner diffracted field would be added to the edge diffracted field and the geometrical optics field in order to obtain the total field. It is desired, then, that this test assess the contribution of the corner diffraction term to satisfaction of the surface boundary condition (total field equals zero).

Testing Procedure

In order to assess the contribution of corner diffraction to the satisfaction of the boundary condition, a procedure introduced by Ko and Mittra [2] was used. A truncation operator ϑ is employed, which is defined by $\vartheta(A) = \int_A \delta(\vec{r} - \vec{r}_s)dr$, $\vec{r}_s \in S$, where δ is the Dirac delta function and S is the planar scattering surface. The complementary operator $\hat{\vartheta}$ given by $\hat{\vartheta}(A) = A - \vartheta(A)$ is also utilized.

For an acoustically soft scatterer the boundary condition requires that the total field be zero on the scatterer surface. The truncation operators can be used to express the total scattered field in the plane of the scatterer as the sum of a known field [$\vartheta(-U^i)$ to satisfy the boundary condition which requires that the scattered field exactly equal the negative of the incident field on the surface of the scatterer] and a field which exists only outside the surface and is estimated by a proposed solution ($\hat{\vartheta}(F)$), so that

$$U^s = \vartheta(-U^i) + \hat{\vartheta}(F) \qquad . \qquad (29)$$

differences are referred to as "source-region" differences.

Long-path length differences are most apparent along theta equal to ninety degrees. Here, for large s, both the AS-2 and AS-3 solutions vary asymptotically as $(ks)^{-1/2}$, while the AS-1 and AS-4 solutions show a free-space-like attenuation of $(ks)^{-1}$.

A scalar scattering "current," J, is defined by $J = \left(\frac{\partial U(x',y',0^-)}{\partial z} - \frac{\partial U(x',y',0^+)}{\partial z}\right)$, $x',y' \in S$, and the scattered field is given by

$$J * G = U^s, \tag{30}$$

where G is a Green's function operator and * denotes convolution. The Fourier transform of the above equation results in

$$\tilde{J} = \tilde{G}^{-1}[\theta(-U^i) + \hat{\theta}(F)] \tag{31}$$

where $\tilde{}$ denotes the transform domain. Because $\tilde{G}^{-1}$ is known, and F can be estimated from corner and edge diffraction terms, a surface current can be obtained from $J = F^{-1}\{\tilde{J}\}$, where F^{-1} indicates inverse Fourier transformation. The current J is then truncated to the scatterer, $J_t = \theta(J)$, and the associated scattered field determined:

$$U_t = F^{-1}\{\tilde{G} \cdot \tilde{J}_t\} \quad . \tag{32}$$

Note that U_t extends over a wide range and includes fields external to the scatterer, while J_t has been truncated to the scatterer surface. U_t now provides a basis for checking satisfaction of the boundary condition, for U_t can be compared to $(-U^i)$ on the scatterer surface.

This procedure lends itself well to iteration, for the scattered field can be updated by $U^{(j)} = \hat{\theta}(U_t^{(j-1)}) + \theta(-U^i)$, following which the scattering current associated with this field can be found from

$$J^{(j)} = F^{-1}\{\tilde{G}^{-1}\tilde{U}^{(j)}\} \quad . \tag{33}$$

Boundary condition satisfaction for this current can again be checked following truncation of the scattering current and determination of the resulting scattered field.

The iteration-boundary condition check can be carried out by the following procedure:

(1) Obtain a first estimate of the transform of the scattered field in the plane of the scatterer from (7) as

$$U^{(0)} = \theta(-U^i) + \hat{\theta}(F) \tag{34}$$

where the F function is given from edge and/or corner diffraction terms.

Observe that $\theta(-U^i)$ is exact as determined by the surface boundary condition, while $\hat{\theta}(F)$ is approximate, since it has been determined from a proposed asymptotic solution.

(2) Determine the associated scattering current from

$$\tilde{J}^{(0)} = F^{-1}\{\tilde{G}^{-1} \cdot \tilde{U}^{(0)}\} \tag{35}$$

where G is given by $\exp(ikR)/4\pi R$ and R is the distance between the "source" and

one may determine the unknown coefficients f_n and g_n in terms of the transform of the surface H-field as

"observation" points. Note that in this application, R is specialized so that all observation points lie in the plane of the scatterer.

(3) Truncate the current to the scatterer surface

$$J_t^{(0)} = \vartheta(J^{(0)}) \quad . \tag{36}$$

(4) Determine the scattered field in the plane of the scatterer by

$$U_t^{(0)} = F^{-1}\{\tilde{G} \cdot \tilde{J}_t^{(0)}\} \quad . \tag{37}$$

Satisfaction of the boundary condition on the scatterer surface can be checked at this point.

(5) Update the scattered field so that the boundary condition is satisfied.

$$U^{(1)} = \vartheta(-U^i) + \hat{\vartheta}(U_t^{(0)}) \quad . \tag{38}$$

Note that this step is necessary because $\vartheta(U_t^{(0)})$ has been determined from J_t, and will not, in general, satisfy the boundary condition. This step is the parallel to (12), except that the external field estimate has been updated by the iteration procedure, replacing the initial guess.

(6) Continue the iteration by repeating Steps (2) - (5), using $U^{(1)}$ in place of $U^{(0)}$.

Obviously, the iteration can be repeated as many times as desired, or until convergence of the scattering current and scattered field is obtained. The accuracy test is incorporated into Step 4 where the scattered field is obtained at the surface of the scatterer and can easily be examined to determine boundary condition satisfaction. Note that after the boundary condition check has been carried out, in order to continue the iteration, the scattered field on the surface is discarded and replaced by the known, exact scattered field.

Testing the Corner Diffraction Coefficient

In order to test the contribution of corner diffraction to satisfaction of the boundary condition on the surface by the method previously described, it is necessary to find the field exterior to the scatterer ($\hat{\vartheta}F$) associated with corner diffraction. This is accomplished in the following manner. The far field as scattered from the vertex of a quarter-plane is determined on a grid of observation points, which include points described by imaginary angles. This effectively gives the transform of the field in the plane of the scatterer, since the two are related by

$$F\{U^s(x',y',0)\}\Big|_{\substack{\alpha=\sin\vartheta\cos\phi \\ \beta=\sin\vartheta\sin\phi}} = \frac{Q}{\cos\vartheta} U^F \quad , \tag{39}$$

where $U^s(x',y',0)$ is the scattered field in the plane of the scatterer, U^F is the scattered far field, Q is a constant, and ϑ is a standard spherical coordinate observation angle. A Fast-Fourier Transform (FFT) algorithm is used to find the planar scattered field by inverting $F\{U^s(x',y',0)\}$. The complementary operator $\hat{\vartheta}$ is employed to obtain the scattered field exterior to the quarter plane. This

where s is the path length given by $s = \sqrt{\Delta^2 + (R\phi)^2 + z^2}$, and Δ is the height of the dipole above the cylinder. Because the singularities can be expressed as derivatives, their analytic transform is obtainable and is of the form

$$\tilde{H}_z|_s = \frac{Q}{2\pi njk}\left(\frac{-nk_z}{R}\right)\frac{1}{4\pi jR}\frac{e^{-j\Delta\sqrt{k^2-(n/R)^2-k_z^2}}}{\sqrt{k^2-(n/R)^2-k_z^2}} \qquad (14a)$$

is the "F" function desired. Finally, an FFT is again employed to get $\hat{\theta}F^c$, the transform of the F function due to the corner; this term contributes to the transform of the scattered field used in Step (1).

In order to aid in evaluation of the effect of the corner diffraction coefficient on boundary condition satisfaction, two error terms are defined. A global error term ε is defined as $\varepsilon_j = \sqrt{\sum_{n=1}^{N} |[U_j(x_n,y_n) + U^i(x_n,y_n)]|^2/N}$ where x_n and y_n are the positions of the sample points on the scatterer and U_j denotes the scattered field from Equation 37 at the $j^{\underline{th}}$ iteration. A local corner error term Δ_j^α was defined similarly, differing from ε_j only in that (x_n, y_n) was confined to the 0.25λ by 0.25λ region at the $\alpha^{\underline{th}}$ corner. The error terms that resulted from using $\hat{\theta}(F^c) \equiv 0$ (no corner contribution) were compared to those that resulted when a single vertex term was included and to error terms when contributions from all four corners were counted.

The boundary condition test was carried out on a two wavelength by two wavelength plate. The testing procedure was carried through three iterations; Figs. 15 and 16 present the scattered field at each iteration for a normally incident scalar wave. Shown is the scattered field for a constant y value cut through the plate. Figure 15 presents a cut near the edge at $y \simeq 0.1$ wavelength, while Fig. 16 shows a cut near the plate center at $y = 1.0$ wavelength. Figure 17 presents a representative scattering "current" very near the edge at $y \simeq 0.03\lambda$. Because the constant y cuts cannot represent the behavior of the total scattered field, Tables 1 and 2 present results of the "error terms" ε and Δ. Note that both tables include results when only one corner diffraction coefficient was included. The corner error terms of Table 2 are taken at the corner at which a single vertex diffraction coefficient was included.

TABLE 1 Total RMS Error, ε, for Normal Incidence

	ε_1	ε_2	ε_3
	1st Iteration	2nd Iteration	3rd Iteration
No Vertices	.223	.127	.048
One Vertex	.207	.121	.047
Four Vertices	.156	.103	.043

TABLE 2 Local Corner RMS Error, Δ, for Normal Incidence

	Δ_1^1	Δ_2^1	Δ_3^1
	1st Iteration	2nd Iteration	3rd Iteration
No Vertices	.373	.205	.069
One Vertex	.360	.192	.067
Four Vertices	.294	.159	.067

Discussion of Results

The figures and tables indicate that use of vertex diffracted fields does improve boundary condition satisfaction. Of greater interest, however, is the performance of the Iterative Accuracy Test for Boundary Conditions procedure. The authors' experience is that both scattering currents and scattered fields are well converged after three iterations as illustrated in Figs. 15-17.

while the more regular slot is readily handled.

Representation of the slot spectrum was achieved by first determining the H-field spectrum due to an elemental dipole source (the direct asymptotic solutions or, for the analytic case, $\bar{E}_{SURFACE} = \hat{z}(\delta(\rho-R)\delta(\phi)\delta(z))$. The H-spectrum was then multiplied by the transform of the slot distribution, which is equivalent to convolving the elemental source with a distribution in the space domain. For a finite slot as shown in Fig. 1a, the transforms used were of the form

In addition, this procedure seems to be relatively insensitive to the initial approximation; indeed, use of an identically zero scattered field external to the scatterer is an acceptable initial approximation.

For use in electromagnetics problems, then, the Iterative Accuracy Test for Boundary Conditions can serve a dual role. The contribution of a proposed diffraction coefficient to boundary condition satisfaction can be determined by carrying the test through one iteration for two different cases: First using the far field as given by physical optics plus (possibly) other known diffracted fields (such as edge diffraction) and, second, using the far field of the first case plus that added by the proposed diffraction coefficient. Examination of the surface fields indicates the change in boundary condition satisfaction due to the solution under test. Alternatively, the iterative procedure can be used to solve for the far field and scattering currents without resorting to asymptotic techniques. If the body is such that the external scattered field is appreciably different from zero, then asymptotic solutions can be used to formulate the initial guess, with a possible increase in the rate of convergence.

It should be pointed out here that solution for the scattering currents inherent in this method is an important attribute. Given the scattering currents, the engineer is able to compute both far fields and near fields; and the fields so determined are guaranteed to be regular and free of singularities.

SUMMARY

Three different procedures for testing the effect of asymptotic solutions on boundary condition satisfaction have been presented. Two are formulated entirely using spectral domain techniques, while the third retains the option of performing the test entirely in the spatial domain. Two tests are best suited for testing asymptotic solutions to surface fields, while the third can also be employed to test asymptotic solutions that give the scattered far field. One of the tests is particularly well-suited for use as an iterative equation and seems relatively insensitive to the initial approximation. In contrast, the iterative aspects of the Integral E-Field Test are limited to particular cases where certain conditions are met. Two of the tests are global in nature and test the entire solution, while the "Integral E-Field Test" displays both global test and local test characteristics.

With communications, radar, and missile systems moving toward use of higher and higher frequencies, it seems certain that use of asymptotic solutions by engineers will increase. The tests presented here provide a means by which new proposed solutions can be evaluated.

ACKNOWLEDGMENT

The work reported in this paper was supported in part by the Office of Naval Research under Grant N00014-75-C-0293 and, in part, by the Joint Services Electronics Program under Grant DAAB-0772-C-0259

REFERENCES

[1] R. Mittra, Y. Rahmat-Samii and W. L. Ko, Spectral Theory of Diffraction, Appl. Phys. 10, 1, (1976).

[2] W. L. Ko and R. Mittra, A New Approach Based on a Combination of Integral Equation and Asymptotic Techniques for Solving Electromagnetic Scattering Problems, IEEE Trans. Antennas Propagat. AP-25, 187, (1977).

[3] M. Tew and R. Mittra, Accuracy Tests for Asymptotic Solutions to Radiation from a Cylinder, Coordinated Sciences Laboratory Report UILU-Eng 77-2251, University of Illinois at Urbana-Champaign, (1977).

[4] R. Mittra and M. Tew, Accuracy Test for High-Frequency Asymptotic Solutions, IEEE Trans. Antennas Propagat. AP-27, 62, (1979).
[5] L. L. Bailin, The Radiation Field Produced by a Slot in a Large Circular Cylinder, IRE Trans. AP-3, 128, (1955).
[6] R. F. Harrington (1961) Time-Harmonic Electromagnetic Fields, McGraw-Hill, New York.
[7] Y. Hwang and R. G. Kouyoumjian, The Mutual Coupling Between Slots on an Arbitrary Convex Cylinder, ElectroScience Laboratory Semi-Annual Report 2902-21, The Ohio State University, (1975).
[8] P. H. Pathak, Analysis of a Conformal Receiving Array of Slots in a Perfectly-Conducting Circular Cylinder by the Geometrical Theory of Diffraction, ElectroScience Laboratory Technical Report ESL 3735-2, The Ohio State University, (1975).
[9] Z. W. Chang, L. B. Felsen, and A. Hessel, Surface Ray Methods for Mutual Coupling in Conformal Arrays on Cylinder and Conical Surface, Polytechnic Institute of New York Final Report (1976).
[10] S. W. Lee and S. Safavi-Naini, Asymptotic Solution of Surface Field due to a Magnetic Dipole on a Cylinder, Electromagnetics Laboratory Technical Report No. 76-11, University of Illinois at Urbana-Champaign, (1976).
[11] S. W. Lee and S. Safavi-Naini, Approximate Asymptotic Solution of Surface Field due to a Magnetic Dipole on a Cylinder, IEEE Trans. Antennas Propagat. AP-26, 593, (1978)
[12] N. C. Albertsen, Technical University of Denmark, personal communication.
[13] L. Kraus and L. Levine, Diffraction by an Elliptic Cone, Comm. Pure Appl. Math. 14, 49, (1961).
[14] J. B. Keller, Geometrical Theory of Diffraction, J. Opt. Soc. Amer. 52, 116, (1962).
[15] J. Radlow, Note on the Diffraction at a Corner, Archive for Rational Mechanics 19, 62, (1965).

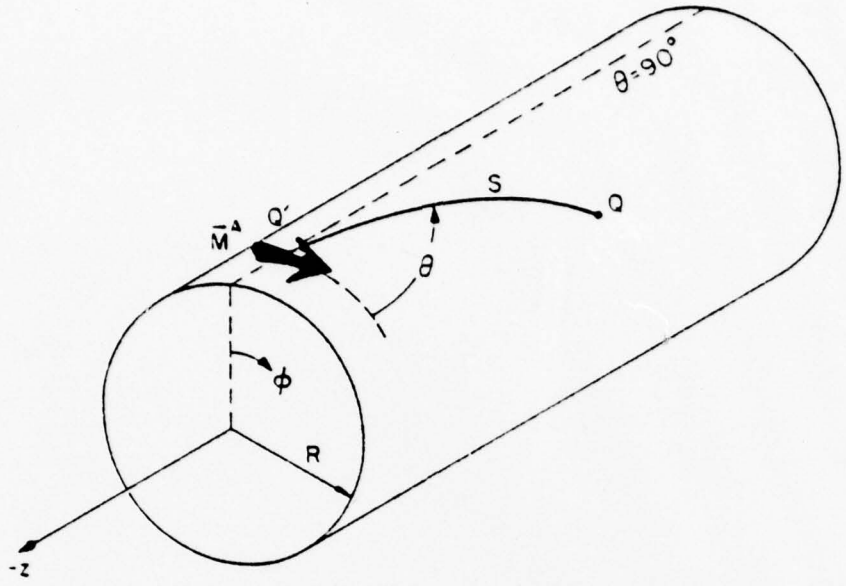

Fig. 1a Geometry of asymptotic solutions: Magnetic dipole in the presence of a perfectly conducting infinite cylinder.

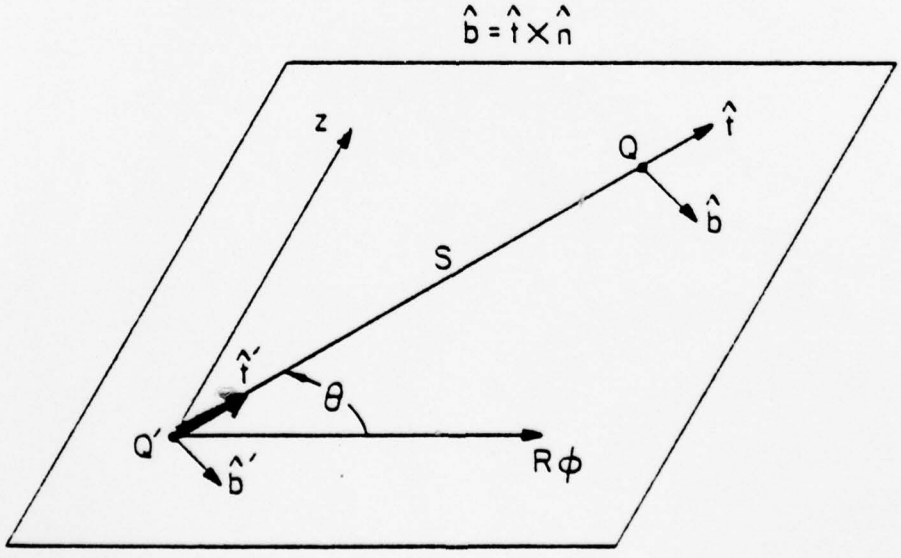

Fig. 1b Geometry of asymptotic solutions: Magnetic dipole in the presence of a perfectly conducting infinite cylinder.

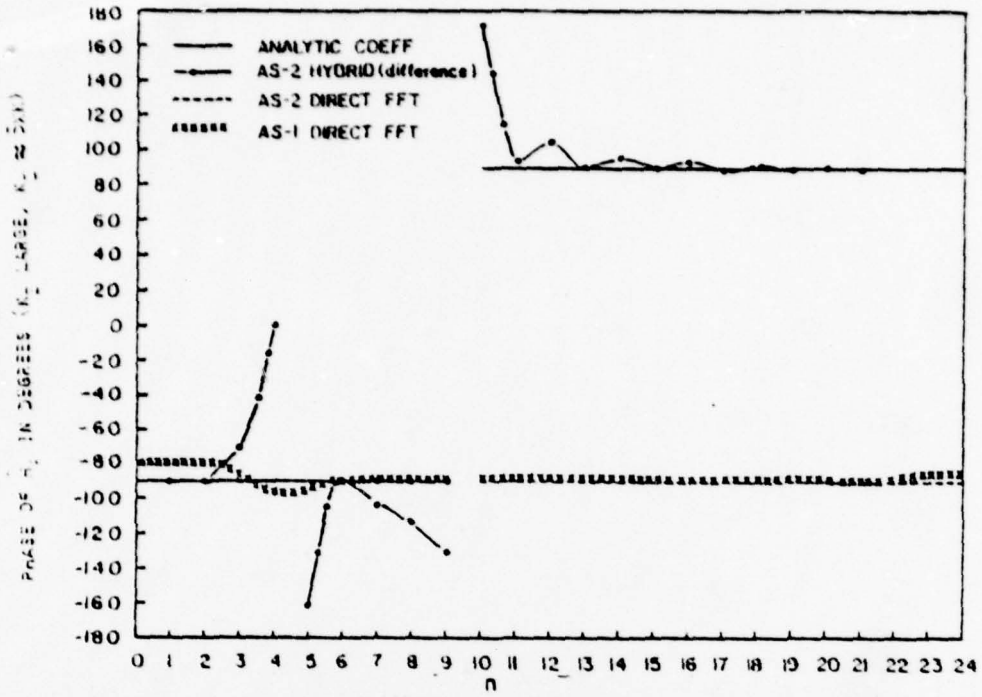

Fig. 2 Effect of hybrid computation on phase of Hϕ transform.

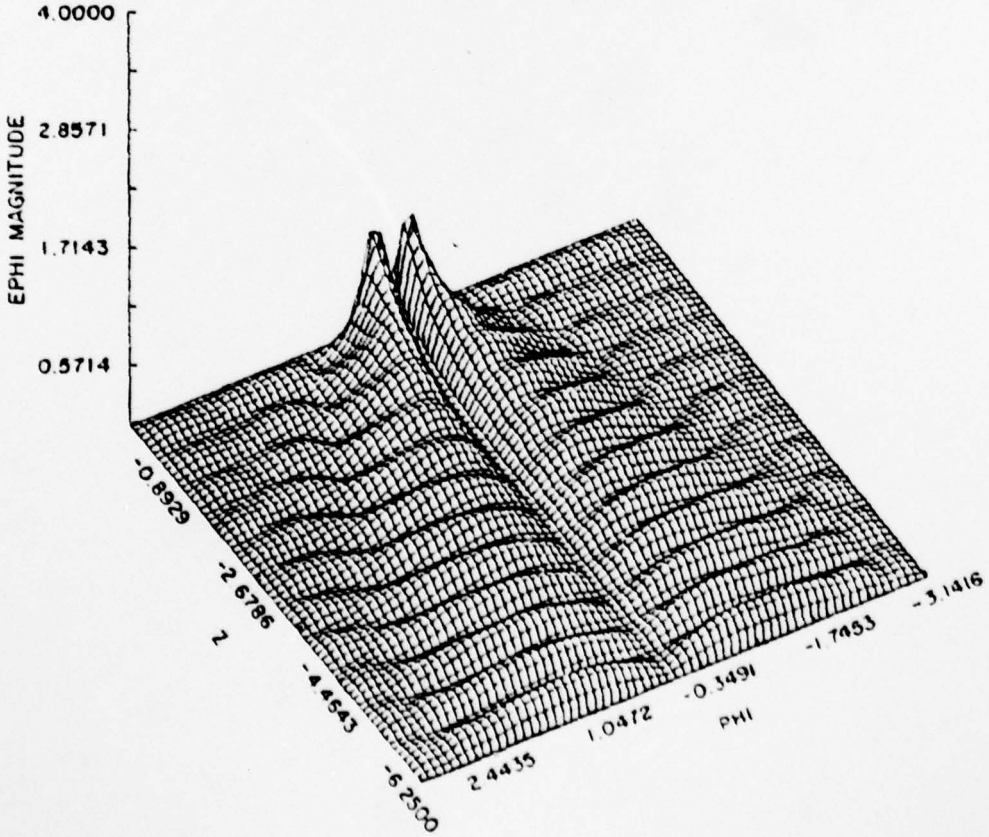

Fig. 3 Surface Eϕ field from direct test of AS-1 solution.

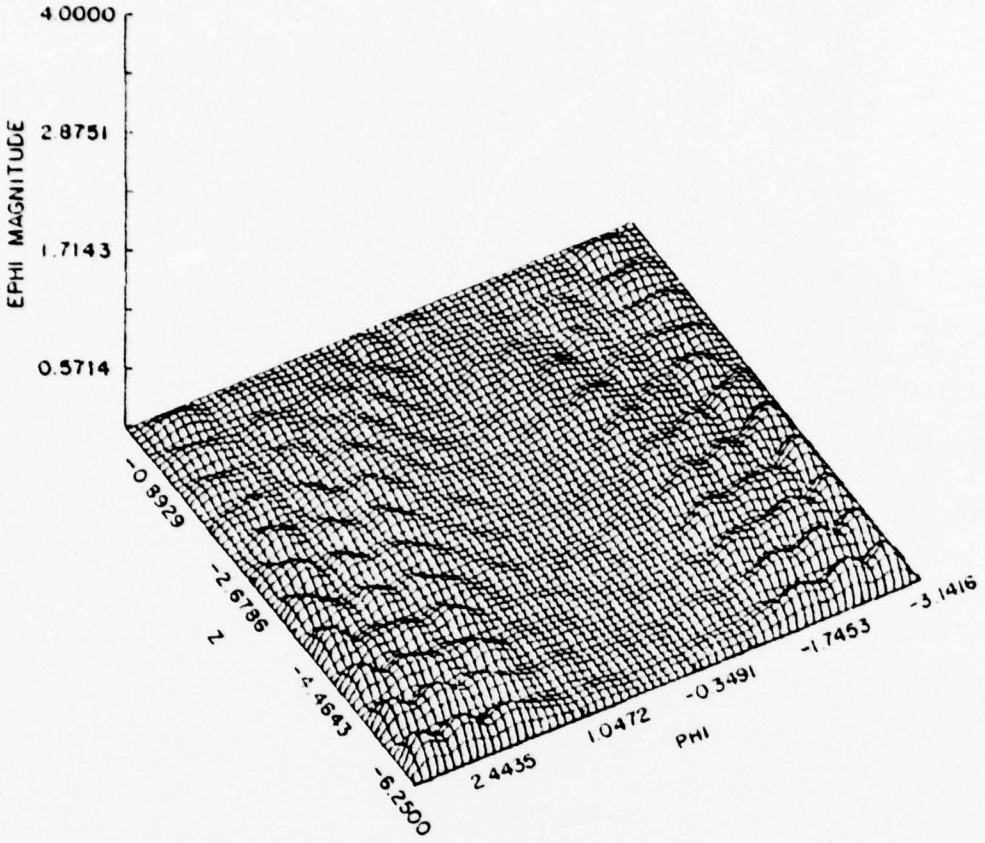

Fig. 4 Surface Eφ field from hybrid test of AS-3 solution.

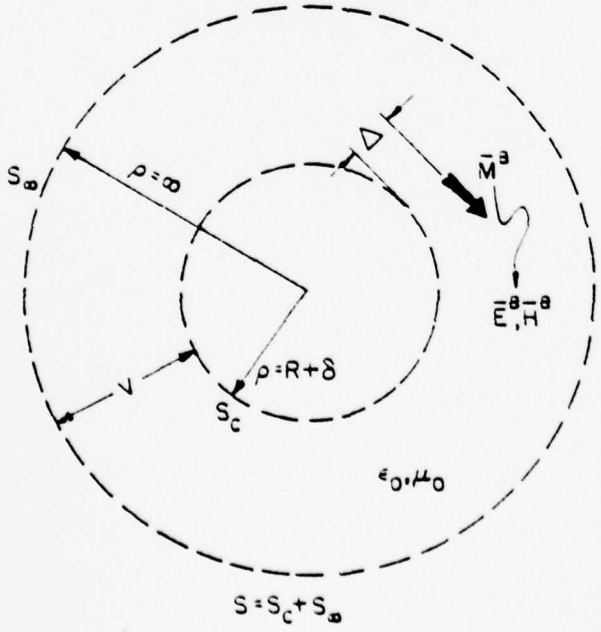

Fig. 5 Free-space test environment: Placement of "reciprocity volume" with respect to test dipole.

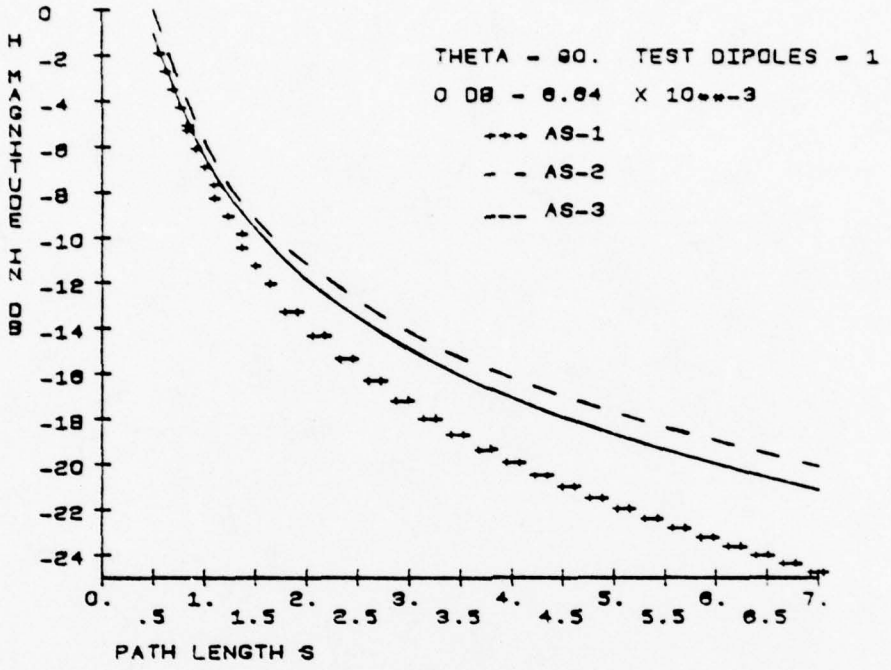

Fig. 6 Magnitude of zeroth-order H_ϕ field along $\theta = 90°$.

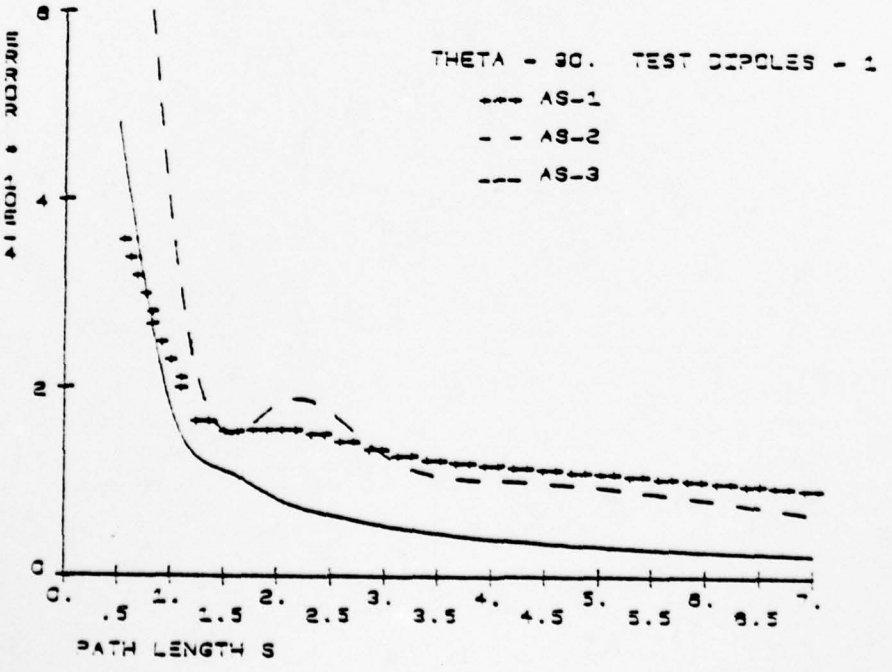

Fig. 7 Results of Integral E-Field Test along $\theta = 90°$: Single test dipole.

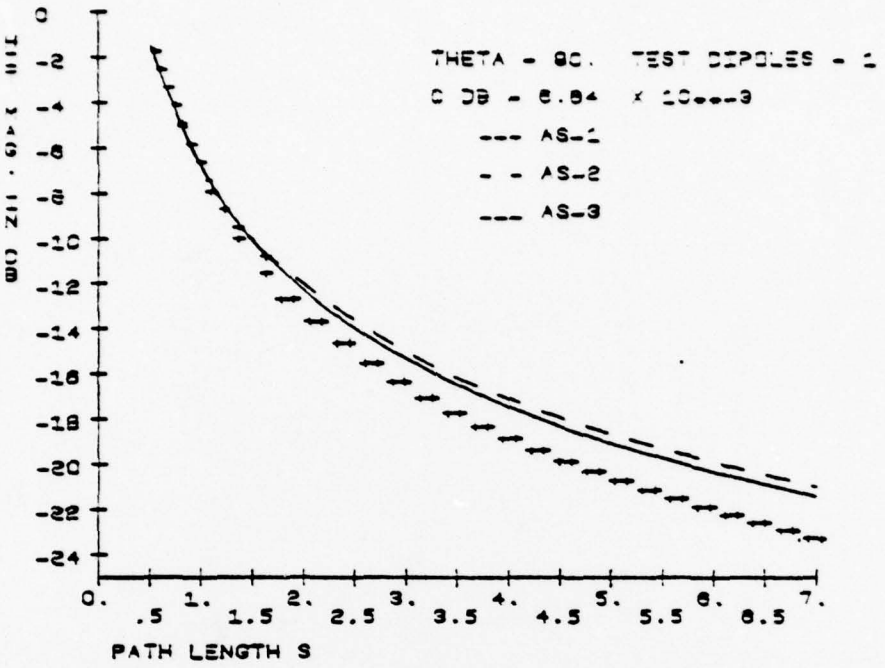

Fig. 8 Iterated magnitudes of H_ϕ field along $\theta = 90°$: Single test dipole.

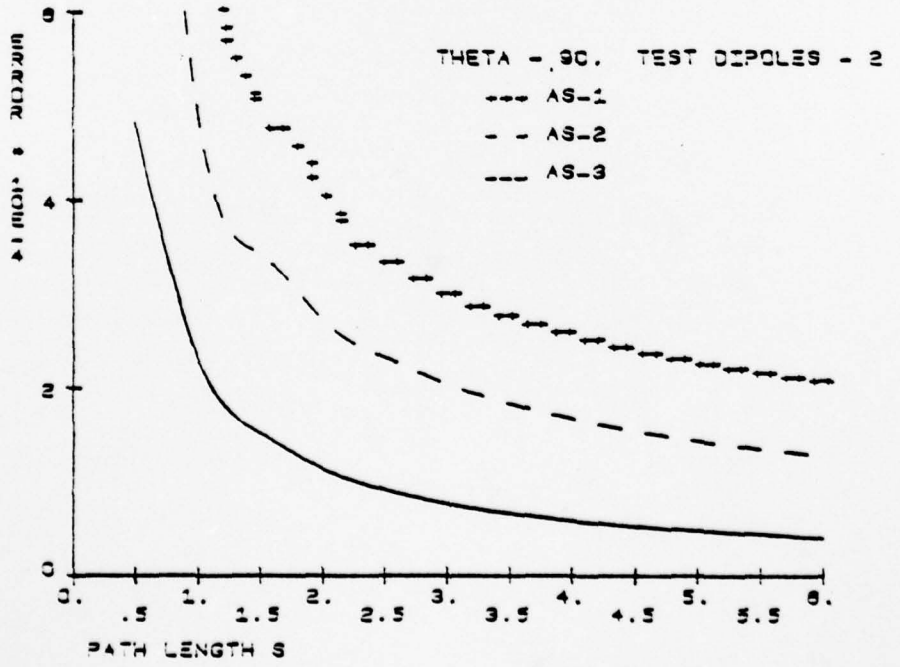

Fig. 9 Results of Integral E-Field Test along $\theta = 90°$: Test dipole and planar image dipole.

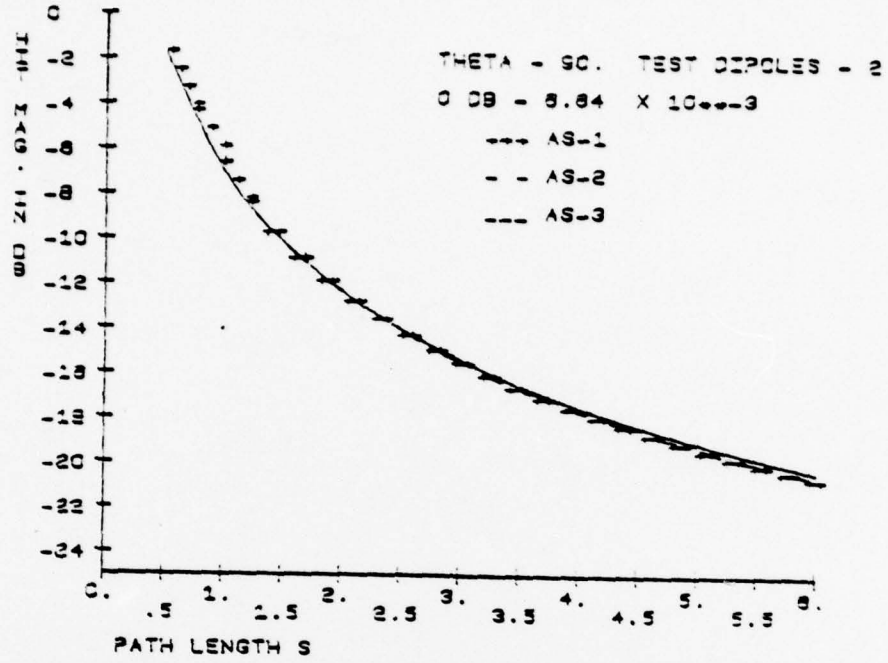

Fig. 10 Iterated magnitudes of H_ϕ field along $\theta = 90°$: Test dipole and planar image dipole.

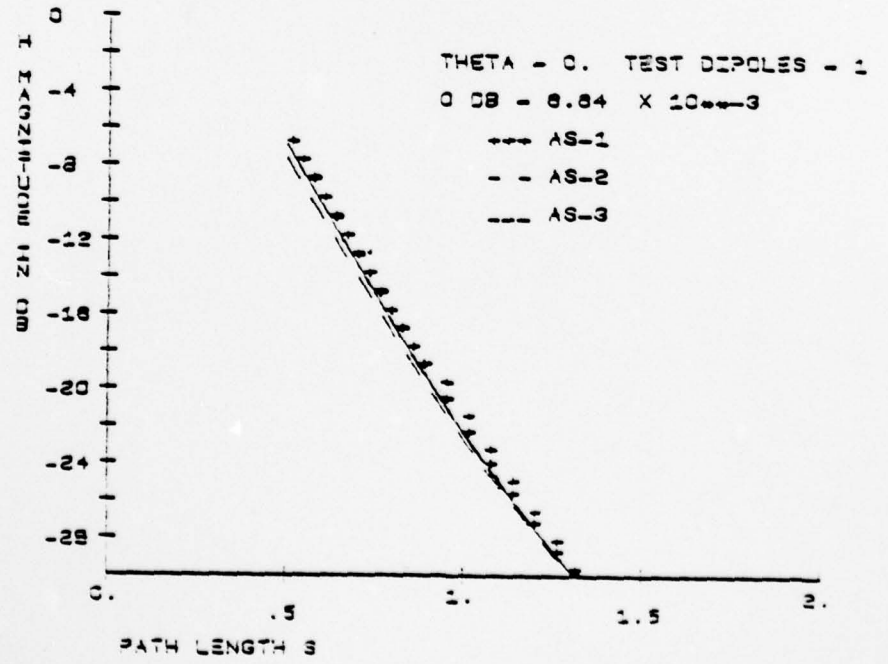

Fig. 11 Magnitude of zeroth-order H_ρ field along $\theta = 0°$.

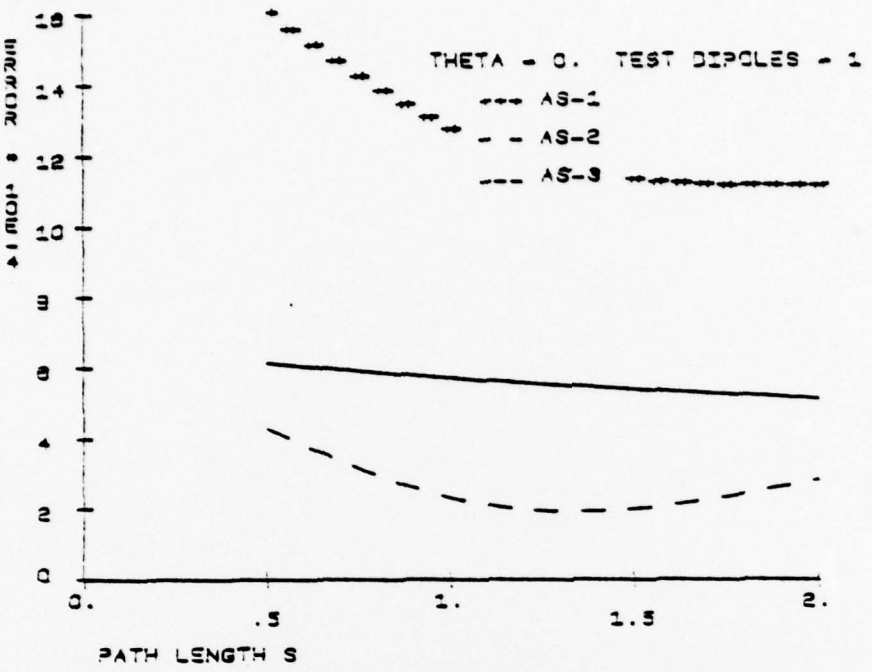

Fig. 12 Results of Integral E-Field Test along $\theta = 0°$.

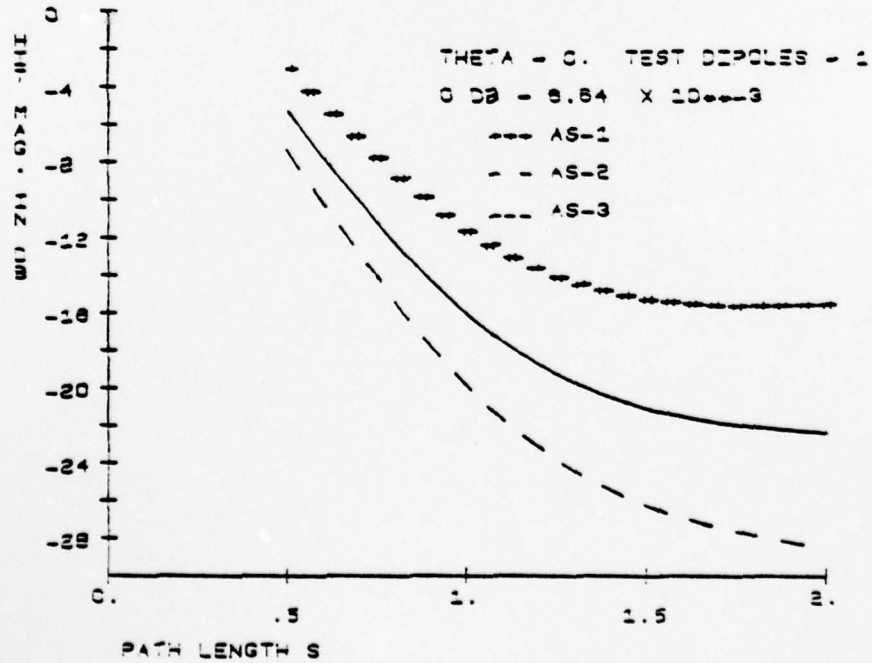

Fig. 13 Iterated magnitudes of H_ρ field along $\theta = 0°$: Single test dipole.

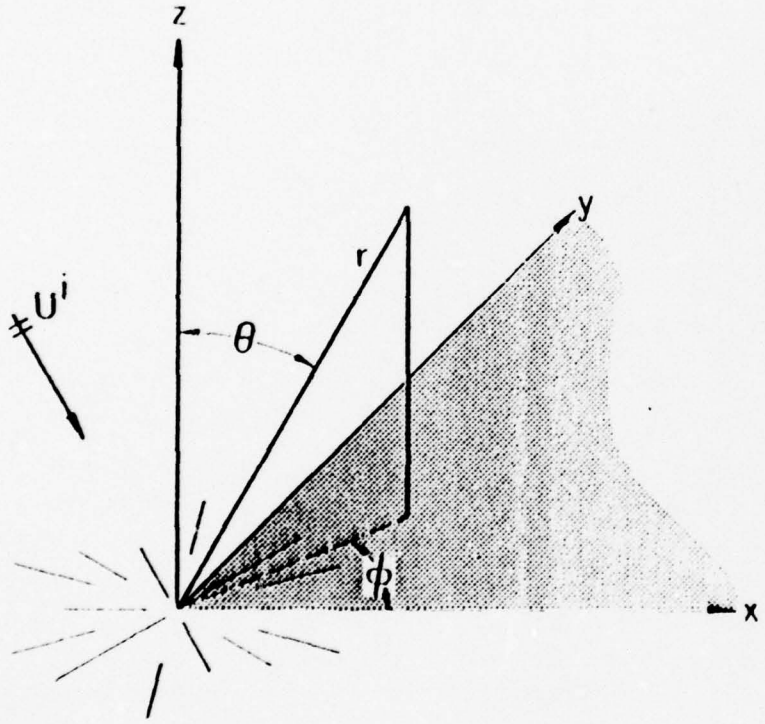

Fig. 14 Scalar wave incident on an acoustically soft quarter-plane.

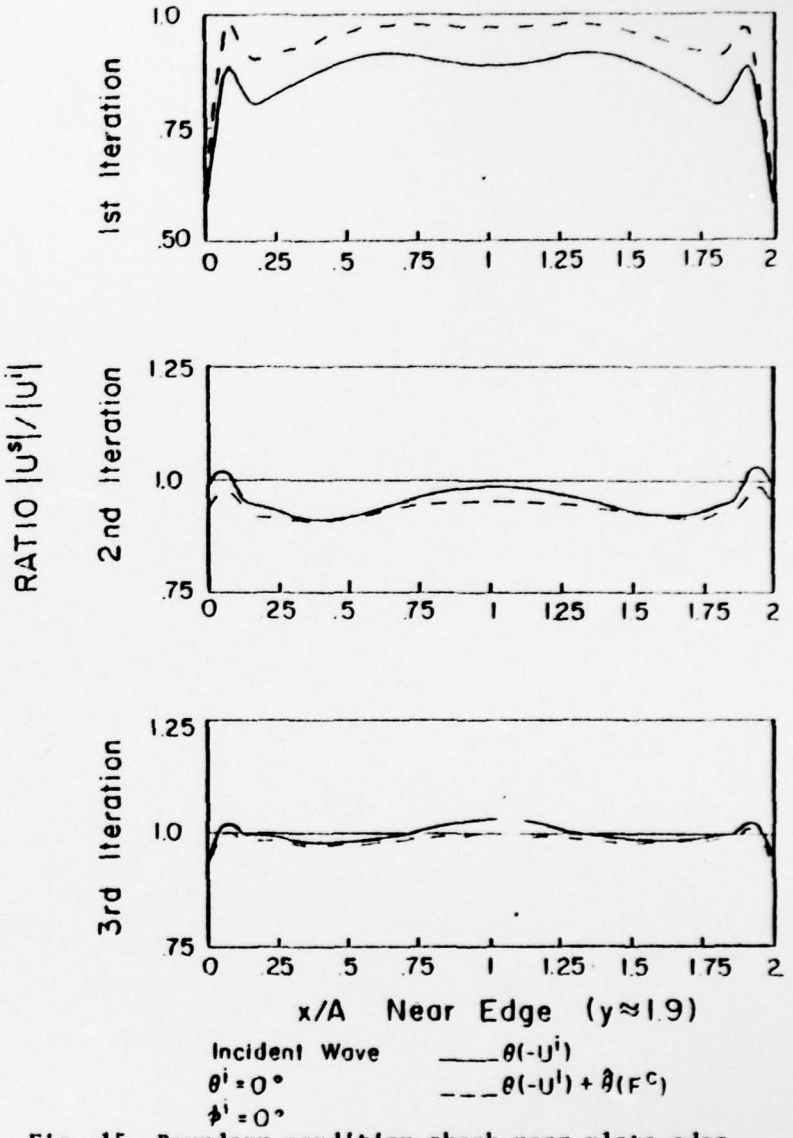

Fig. 15 Boundary condition check near plate edge, normal incidence.

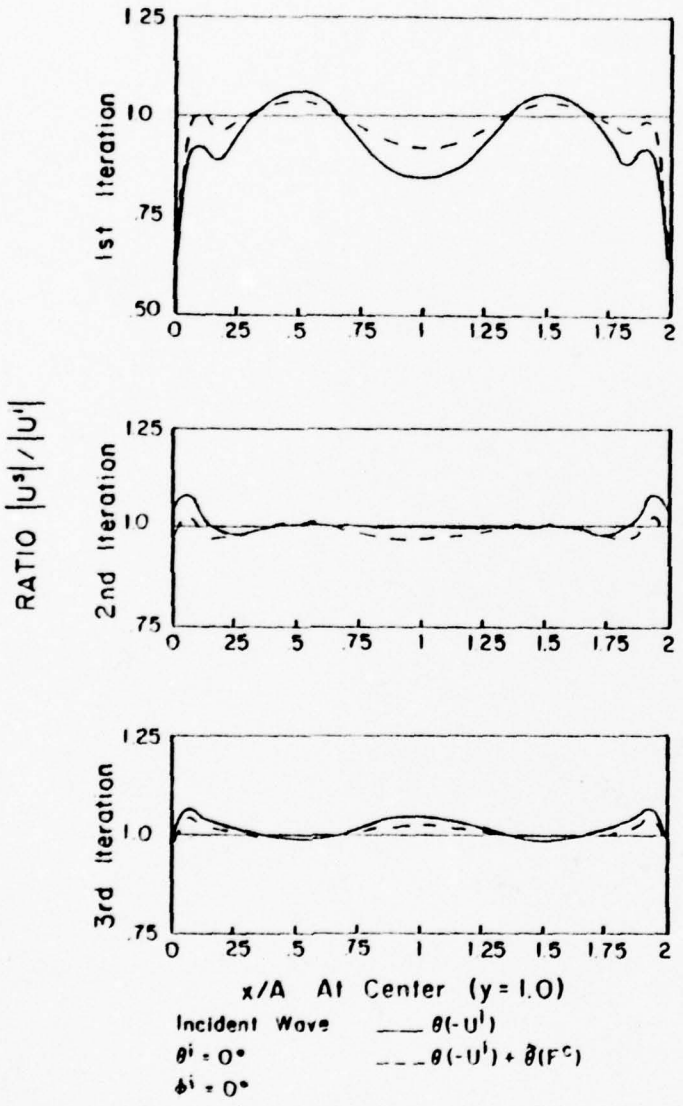

Fig. 16 Boundary condition check at plate center, normal incidence

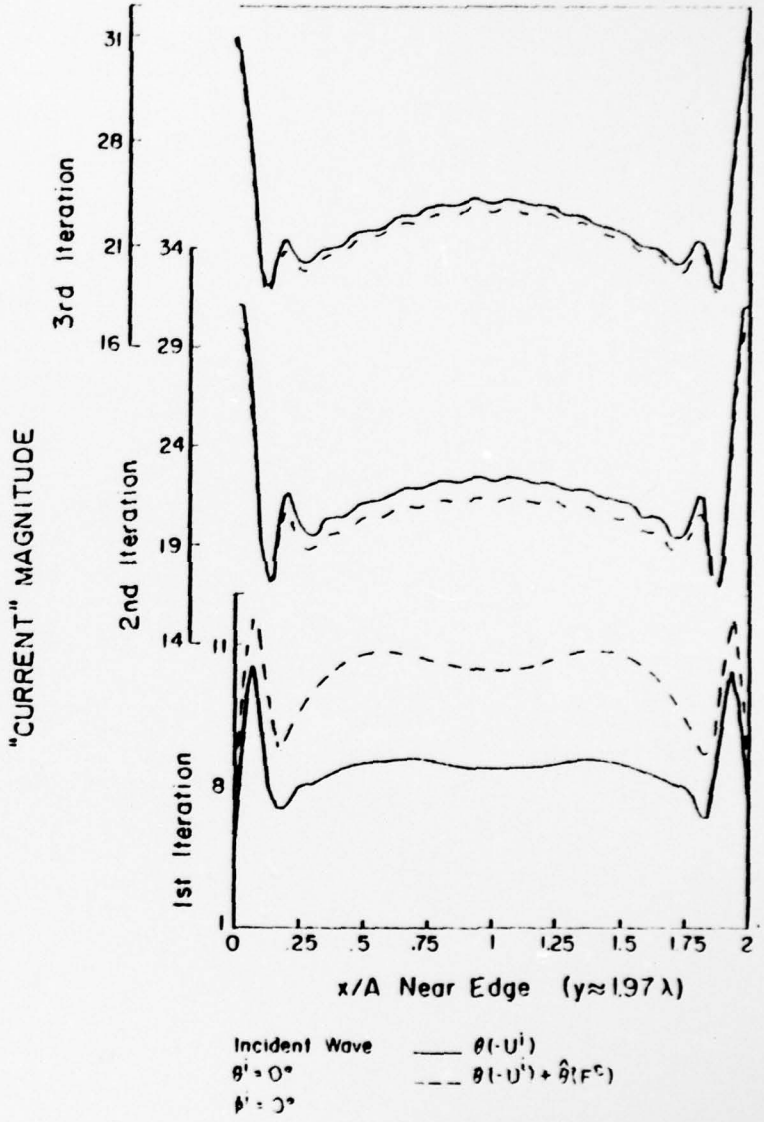

Fig. 17 Scattering currents near plate edge normal incidence.

F

AN INTEGRAL E-FIELD ACCURACY TEST FOR HIGH FREQUENCY ASYMPTOTIC SOLUTIONS

M. Tew and R. Mittra

ABSTRACT

The increasing use of conformal slot arrays has generated considerable interest in the analysis of radiation on cylindrical structures. Since 1974, three different asymptotic solutions to the problem of radiation on an infinite circular cylinder have been published. These solutions, whose accuracy increases as some parameter (such as the wavenumber) increases, have the unfortunate property that it is difficult to estimate their accuracy when finite frequencies are used. Previous attempts by the authors at achieving an accuracy test for evaluating asymptotic solutions resulted in a test that was qualitative in nature and highly dependent on the source region accuracy of the proposed solution. Through the use of Green's Identities, a new test based on satisfaction of the E-Field boundary condition is formulated. The proposed test is quantitative in nature, is straightforward in application and displays a mixed local/global nature. Under some circumstances, the test lends itself to application as an iterative equation for point-by-point improvement of a proposed solution.

Introduction

The problem of magnetic dipole radiating in the presence of a conducting cylinder has received increased attention in recent years because of the insights it provides into the performance of slot antennas on cylindrical structures. Knowledge of the induced currents, for example, allows the engineer to calculate mutual coupling between slot antennas in a conformal array or to accurately compute far-field patterns. Since use of the exact modal solution is impractical for numerical computation of the induced currents, approximate solutions which

are asymptotic in nature are often employed. This paper proposes an accuracy test based on satisfaction of the E-field boundary condition which may be applied to any proposed solution.

The problem addressed consists of an infinitesimal magnetic dipole radiating on an infinitely long, perfectly conducting, circular cylinder. The exact modal solution [1]-[2], which is in the form of an infinite integral, converges so slowly as to make its use impractical for numerical calculation. Various approximate solutions, more suitable for numerical computation, have been proposed [3]-[8]. Two of the solutions, [3]-[6], are derived from manipulation of the modal solution. These solutions are denoted as Asymptotic Solution - 1 (AS-1) [3]-[4], and Asymptotic Solution - 2 (AS-2) [5]-[6], based on their chronological order of publication. The third approximate solution [7]-[8] is based on a modification of the work of V. A. Fock addressing the problem of radiation on a sphere and is denoted Asymptotic Solution - 3, or AS-3.

These approximate solutions are asymptotic in nature, that is, their accuracy increases as some parameter, such as the wavenumber, increases. Unfortunately, the accuracy of these solutions is difficult to determine at finite frequencies. A previous attempt at achieving an accuracy test was based on relating the spectral components of the approximate H-field to the spectral components of the E-field [9]. This test, however, was strongly dependent on the source region accuracy of the proposed solution and was global in nature. That is, the "E-field Accuracy Test" described in [9] had no point-test character, but tested the total solution. This paper proposes an alternative test, the "Integral E-Field Accuracy Test" based on satisfaction of the E-field boundary condition on the cylinder surface. This test may be formulated from either Green's Identities or Generalized Lorentz Reciprocity and displays a mixed global/local character. For some cases, the source region of a proposed solution can be essentially excluded from contributing

to the accuracy test, yielding a very strong local or point-test character. Under those circumstances the "Integral E-Field Accuracy Test" also lends itself to formulation as an iterative equation, allowing point-by-point improvement of a proposed solution. This paper will first review the proposed solutions and follow through with the formulation of the "Integral E-Field Accuracy Test." Results of applying the accuracy test to the proposed solutions as well as a discussion of these results will be presented.

Proposed Solutions

Figure 1a presents the geometry of the problem. An infinitely long, perfectly conducting, circular cylinder of radius R is located with the cylinder axis coinciding with the z-axis of a standard ρ, ϕ, z cylindrical coordinate system. An infinitesimal, phi-directed, magnetic dipole is located on the cylinder surface at Q' given by the coordinates $\rho = R$, $\phi = 0$, $z = 0$. The H-field on the cylinder surface is observed at a point Q located at $\rho = R$, $\phi = \phi_T$, $z = z_T$. The proposed solutions are ray-type solutions, and the surface fields are dependent on the geodesic path between Q and Q' defined by the surface path length, s, and ray angle, θ, measured from the ϕ-axis to the surface ray.

The cylinder is a developable surface and a geodesic path on the cylinder surface becomes a straight line on the infinite strip that makes up a developed cylinder. Figure 1b shows the developed cylinder and introduces the local $\hat{n}'$, $\hat{b}'$, $\hat{t}'$ and $\hat{n}$, $\hat{b}$, $\hat{t}$ coordinate systems, where $\hat{n}'$, $\hat{n}$ are the outward normal to the surface , and t',t are tangent to the surface path at the source and observation points, respectively ($\hat{b}' = \hat{t}' \times \hat{n}'$, $\hat{b} = \hat{t} \times n$). Both the AS-1 and AS-3 solutions give the surface field in terms of fields parallel to $\hat{b}$ and $\hat{t}$ as

$$\bar{H}(Q) = \bar{M} \cdot (\hat{b}'\hat{b}H_b + \hat{t}'\hat{t}H_t) \qquad (1)$$

where $\bar{M}$ is the magnetic dipole moment. In this paper a circumferentially oriented dipole is treated, i.e. $\bar{M} = \hat{\phi}$. For this case, conventional H_z and H_ϕ fields may be found from H_b and H_t from

$$H_\phi = \cos^2\theta\, H_t + \sin^2\theta H_b \tag{2a}$$

$$H_z = \sin\theta\cos\theta(H_t - H_b) \tag{2b}.$$

Each of the proposed solutions gives the surface H-fields in terms of a combination of "Fock functions," $u(\xi)$, $v(\xi)$, and $v_1(\xi)$ and their derivatives $u'(\xi)$, $v'(\xi)$, and $v_1'(\xi)$ respectively. ξ is a normalized distance parameter given by $\xi = (\frac{k}{2R_t^2})^{1/3} s$ where k is the wavenumber, R_t is the radius of curvature in the direction of $\hat{t}$ given by $R_t = R/\cos^2\theta$ and s is the path length, $s = \sqrt{(R\phi)^2 + z^2}$. The radius of curvature in the direction of $\hat{b}$ is also employed and is given by $R_b = R/\sin^2\theta$. The AS-1 solution as tested gives the surface fields as

$$H_b(Q) \sim v(\xi)G(s) \tag{3a}$$

$$H_t(Q) \sim (\frac{2i}{ks})u(\xi)G(s) \tag{3b},$$

where H_t of (3b) differs from the H_t given in [3]-[4] by a factor of 2 (this is done so that as $k \to \infty$ the H_t of (3b) recovers identically the $(ks)^{-2}$ term of the known exact solution). The AS-2 solution is given by

$$H_\phi(Q) \sim \{v(\xi)[\sin^2\theta + \frac{i}{ks}(1 - 3\sin^2\theta)] + (\frac{i}{ks})\sec^2\theta[u(\xi) - \sin^2\theta v_1(\xi)]\}G(s) \tag{4a}$$

$$H_z(Q) \sim -\sin\theta\cos\theta v(\xi)\,[1 - \frac{3i}{ks}]\,G(s) \tag{4b}$$

AD-A077 895 ILLINOIS UNIV AT URBANA-CHAMPAIGN ELECTROMAGNETICS LAB F/G 20/3
INVESTIGATION OF TRANSFORM TECHNIQUES FOR SOLVING ELECTROMAGNET--ETC(U)
DEC 79 R MITTRA , S W LEE , W L KO N00014-75-C-0293
UNCLASSIFIED UIEL-79-13 NL

2 OF 2
AD A077895

END
DATE FILMED
1-80
DDC

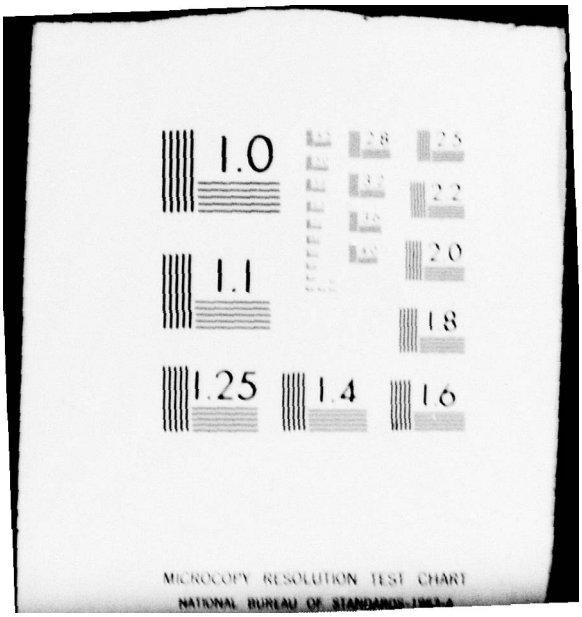
1.0
1.1
1.25
1.4
1.6
2.0
2.2
2.5
MICROCOPY RESOLUTION TEST CHART
NATIONAL BUREAU OF STANDARDS

for the case of a circumferentially oriented dipole. The AS-3 solution gives the surface fields as

$$H_b(Q) \sim \{(1 - \frac{j}{ks})v(\xi) - (\frac{1}{ks})^2 u(\xi) + j(\sqrt{2}\, kRt)^{-2/3}[v'(\xi) + (Rt/Rb)u'(\xi)]\}G(s) \quad (5a)$$

$$H_t(Q) \sim (\frac{j}{ks})\{v(\xi) + (1 - \frac{2j}{ks})u(\xi) + j(\sqrt{2}\, kRt)^{-2/3}u'(\xi)\}G(s) \quad (5b).$$

In Equations (3)-(5), $G(s) = k^2/(2\pi j\eta)\cdot e^{-jks}/ks$, where η is the impedance of free space.

As Θ goes to ninety degrees (a ray propagating down the cylinder axis), H_b becomes identical to H_ϕ and the solutions reduce to

$$H_\phi(Q) \sim (\frac{2j}{ks})G(s) \text{ for AS-1} \quad (6a)$$

$$H_\phi(Q) \sim [1 - \frac{j}{ks} + (\frac{\pi}{2})^{1/2} e^{-j\pi/4} \frac{(ks)^{1/2}}{kR}]G(s) \text{ for AS-2} \quad (6b)$$

and $$H_\phi(Q) \sim [1 - \frac{j}{ks} - (\frac{1}{ks})^2 + \frac{3}{4}(\frac{\pi}{2})^{1/2} e^{-j\pi/4} \frac{(ks)^{1/2}}{kR}]G(s) \text{ for AS-3} \quad (6c).$$

Thus, for Θ equals ninety degrees, both the AS-2 and AS-3 solutions vary asymptotically as $(ks)^{-1/2}$, while the AS-1 solution shows a free-space like attenuation of $(ks)^{-1}$. It will be seen that the proposed accuracy test is particularly well suited for evaluating the solutions along $\Theta = \pi/2$, and thus may aid in determining whether asymptotic behavior as $(ks)^{-1}$ or $(ks)^{-1/2}$ is more correct.

Formulation of the Integral E-Field Test

The Integral E-Field Test may be formulated using Green's Identities, Generalized Lorentz Reciprocity, or from first principles using Maxwell's Equations and Gauss' Law. The defining equation for the Integral E-Field Test is given by:

$$-\iint_S (\bar{E}^A \times \bar{H}^B - \bar{E}^B \times \bar{H}^A) \cdot d\bar{a} = \iiint_V (\bar{H}^B \cdot \bar{M}^A - \bar{H}^A \cdot \bar{M}^B) dv \qquad (7),$$

where fields and sources from two different environments, A and B, are related in a single equation. In order to achieve an accuracy test, Environment A will denote the environment of the approximate solution; that is, an infinitely long, perfectly conducting circular cylinder in free space. An infinitesimal phi-directed magnetic dipole, $\bar{M}^A$, radiates in the presence of the cylinder (Fig 1). Environment B is made up entirely of free space. A magnetic dipole source (or sources), $\bar{M}^B$, will be placed in Environment B, giving rise to electric and magnetic fields $\bar{E}^B$ and $\bar{H}^B$ (Figure 2). The fields in Environment A will be termed "asymptotic fields" because they will be given by the approximate asymptotic solution. The fields in Environment B will be termed "test fields" because they will be employed to evaluate the accuracy of a proposed solution. The volume V is defined as being enclosed by surface S, which is made up of concentric circular cylinders, S_c and S_∞. Cylinder S_c has radius $R + \delta$, where δ is vanishingly small, and S_∞ has infinite radius. In Environment A, S_c and S_∞ will be placed so that their axes coincide with the axis of the perfectly conducting cylinder; while in Environment B, S may be placed anywhere as long as it does not intersect any of the sources, $\bar{M}^B$. Since the sources in both Environments A and B are of finite extent, the fields $\bar{E}^A$, $\bar{H}^A$, $\bar{E}^B$, and $\bar{H}^B$, will obey the radiation condition- with the result that the surface integral over S_∞ is zero. Equation 7 may then be rewritten as

$$\int_{S_c}\int \bar{E}^A \times \bar{H}^B \cdot d\bar{a} = \int_{S_c}\int \bar{E}^B \times \bar{H}^A \cdot d\bar{a} - \iiint_V (\bar{H}^B \cdot \bar{M}^A - \bar{H}^A \cdot \bar{M}^B) dV \qquad (8)$$

The accuracy test is accomplished by arguing that the exact solution to a dipole radiating in the presence of, but not on, the perfectly conducting cylinder would satisfy the boundary condition that the tangential electric

field is zero everywhere on the perfectly conducting cylinder surface. Taking δ to be vanishingly small, the surface S_c almost coincides with the conducting surface so that the magnitude of the left-hand side of Equation 8 can be made as small as is desired, approaching zero in the limit as δ goes to zero. The amount that the right-hand side of Equation 8 differs from zero will be termed the "error", ε, and will be used as a basis for comparing proposed solutions to the problem embodied in Environment A,

$$\varepsilon = \lim_{\delta \to 0} \iint_{S_c} \bar{E}^B \times \bar{H}^A \cdot d\bar{a} - \iiint_v (\bar{H}^B \cdot \bar{M}^A - \bar{H}^A \cdot \bar{M}^B) dv \qquad (9)$$

If delta-function type sources are used for both Environments A and B (and they are implied by the proposed solutions of Environment A), then the volume integral of Equation 9 reduces to a sampling operation and becomes

$$\varepsilon = \lim_{\delta \to 0} \iint_{S_c} \bar{E}^B \times \bar{H}^A \cdot d\bar{a} - H^B(M^A) + H^A(M^B) \qquad (10),$$

where the symbol $H^i(M^j)$ denotes the operation $\bar{H}^i(x_j, y_j, z_j) \cdot \hat{M}^j$ in which the fields of Environment i are sampled at the position of the sources in Environment j, and the dot product is taken with the unit vector parallel to the "j" source. Now, if ε is sufficiently small, Equation 10 may be cast into the form of an iterative equation as

$$H^{A(1)}(M^B) = H^B(M^A) - \lim_{\delta \to 0} \iint_{S_c} \bar{E}^B \times \bar{H}^{A(0)} \cdot d\bar{a} = H^{A(0)}(M^B) - \varepsilon \qquad (11).$$

Thus the field at a point (the location of source M^B) may be updated by modifying the proposed approximate solution by the error term associated with that point. Observe that the exact solution would satisfy $\varepsilon = 0$ in Equation 10, so that using Equation 11 to iterate would not change the field value at all.

In review, the formulation of the Integral E-Field Accuracy Test has been accomplished through the use of well-known properties of electromagnetic fields. The resulting equation is straightforward, involves known quantities, and in general, consists only of sampling operations and numerical integration. In some cases, the test may lend itself to point-by-point improvement of a proposed solution.

Practical Considerations for the Integral E-Field Accuracy Test

While Equation (9), which defines the test, appears to lend itself to direct evaluation, several practical aspects of the evaluation must be considered. First, an important step in formulating Equation 9 was that the tangential E-Field vanishes for a source radiating in the presence of the cylinder, while the published solutions are for the case of a dipole radiating on the cylinder surface. To perform the test, the proposed solutions were extended to the case of a dipole radiating a distance Δ away from the cylinder by modifying the path length, s, used in determining the surface field. The modified path length s' used in Equations (3)-(6) was computed from $s' = \sqrt{s^2 + \Delta^2}$, where s is the surface path length. In addition to satisfying the assumption made in formulating the test, raising the dipole allows numerical calculation of the integral in Equation 9, since the H^A fields have a finite peak and are not singular (source region H^A fields are singular for a dipole located on the surface).

Location of the test dipole(s) with respect to the surface coincident with the perfectly conducting cylinder (this surface will be denoted S_c^B) greatly influences the test results. A test dipole placed so that it sampled the surface magnetic field of the approximate solution would seem to lend a local character to the test. However, a test dipole so located would introduce singular E^B fields, making numerical integration more difficult. Accordingly, the test dipole is, in general, located a Δ distance

away from the surface corresponding to the cylinder surface. The E^B fields on the surface of integration are calcualted exactly, but the H^A field at M^B is approximated by the H^A field at the point on S_c^B closest to the location of M^B. In other words, if the sampling operation $H^A(M^B)$ required finding $H^A(R + \Delta, \phi_t, Z_t)$, this would be approximated by $H^A(R, \phi_t, Z_t)$. The error introduced by this approximation was checked by applying the test to a problem with a known solution, that of a magnetic dipole radiating over an infinite ground plane. For Δ equal to one sixteenth of a wavelength, the error introduced by this assumtion was negligible compared to ε's computed in the cylinder test.

Observe that the user has complete freedom to place one or several test dipoles in Environment B. For example, two test dipoles could be used, located at $(R + \Delta, \phi_{TST}, Z_{TST})$ and $(R + \Delta, \phi_{TST}, -Z_{TST})$. This would have the effect of creating a plane of zero E^B fields that coincide with the H^A source region. Evaluation of the integral of Equation 10 shows that this would decrease the contribution of the source region H_Z^A fields (due to zero E_ϕ^B) and emphasize the source region H_ϕ^A field. As this illustrates, use of multiple-dipole test configurations generally involves a trade-off of some kind, so that the simple single test dipole located Δ away from S_c^B has been chosen as the "standard" test.

Results of the Integral E-Field Test

Results presented in this section are for a case with $R = 1.5174\lambda$ and $\Delta = \lambda/16$, and λ is the wavelength. Fields were sampled through the full 2π radians and from $-2.0\lambda \leq Z \leq Z_{TST} + 2.0\lambda$, where the test dipole was located at $(R + \Delta, \phi_{TST}, Z_{TST})$. A fine numerical integration was performed in the one square wavelength region immediately surrounding

both the "test" and "source" dipoles with sampling rates of 64 points/λ in the z-direction and 78 points/λ in the ϕ-direction. Numerical integration over the rest of the surface was accomplished with a sampling rate of 32 points/λ in the z-direction and 48 points/λ in the ϕ-direction. For cases presented here, a single, phi-directed test dipole located $\lambda/16$ away from S_c^B was used. For tests along $\Theta = \pi/2$, along the cylinder axis, a two-test-dipole configuration was also used with phi-directed test dipoles located at $(R + \Delta, 0, Z_{TST})$ and $(R - \Delta, 0, Z_{TST})$. The test equation under these conditions becomes

$$\varepsilon = \int_{\substack{S_c \\ \delta \to 0}} \int (E_Z^B H_\phi^A - E_\phi^B H_Z^A)\, da - H_\phi^B(M^A) + H_\phi^A(M^B) \qquad (12)$$

Figure 3 shows the fields along the cylinder axis ($\Theta = 90°$) as predicted by each of the three published solutions. Shown are the magnitudes of the zeroth-order H_ϕ fields, unchanged except for the extension of raising the source dipole $\lambda/16$ above the surface. Zero dB reference for all the plots is the magnitude of the AS-2 solution at $z = 0.5\lambda$ along $\Theta = 90°$. Figure 4 presents the "error", ε associated with each of the solutions, while the results of applying Equation 11 are shown in the iterated magnitudes of Figure 5.

Figure 6 presents the errors when the two-test-dipole configuration was used, while Figure 7 shows the iterated magnitudes resulting from a dual dipole test. Figures 8, 9, and 10 present the same information (zeroth-order field magnitude, error, and iterated magnitudes) for a path along $\Theta = 0°$.

Discussion of Results

In figure 4, the error associated with the AS-3 solution is less

the error associated with either the AS-1 or AS-2 solutions for $Z_{TST} > 1\lambda$. The iterated field magnitudes of Figures 5 and 7 show much less dispersion than the zeroth-order magnitudes of Figure 3. The iterated magnitudes are closest to the zeroth-order AS-3 solution. Several factors combine to increase confidence in the test results along $\theta = 90°$. First, the magnitude of the error term is relatively small with respect to the magnitude of $H^{A(0)}(M^B)$, so that the criterion for successful iteration is close to being met. Secondly, for both single and dual dipole tests, the asymptotic source-region field contributes very little to the integral that makes up the error term. For the single dipole, this is easily seen from the fact that for $Z_{TST} >> \Delta$ along $\theta = 90°$, the E^B field evaluated at (R,0,0) will be primarily ϕ-directed with a very small E_z or E_ϕ component. At the same time, the test field E^B directly underneath the test dipole will have a very large E_z component, emphasizing the local H_ϕ field. For two dipoles located at $(R \pm \Delta, 0, Z_{TST})$, the plane of zero tangential electric fields is tangent to the cylinder at $\phi = 0$, reducing the asymptotic source region contribution. Local H_ϕ field emphasis does not occur with the two dipole test, however, since the plane of zero tangential E-fields extends through $Z = Z_{TST}$. Thus, for $Z_{TST} >> \Delta$ along $\theta = 90°$ the Integral E-Field Test should have a very strong local character and be almost unaffected by the source-region accuracy of the proposed solution.

For large Z_{TST} the $(ks)^{-1/2}$ behavior becomes dominant in the AS-2 and AS-3 solutions. The AS-3 solution shows the least error for this range. The iterated values are closest to the zeroth-order AS-3 solution, and deviate most from the zeroth-order AS-1 solution. Because the iterative equation is convergent, and because source-region errors contribute very little to the error term or iterative process for this case, the authors feel that this is a strong indication that asymptotic behavior as $(ks)^{-1/2}$ is more correct than $(ks)^{-1}$ attenuation along $\theta = 90°$.

Single dipole tests along angles other than $\theta = 90°$ will introduce an asymptotic source region contribution to the integral of Equation 10, with the amount of contribution dependent on the path length and Θ-angle. The local E-fields in the vicinity of the test dipole remain large, so that it is expected that the test will display a mixed local/global character. The results of Figures 8, 9, and 10 reflect this, for while the zeroth-order magnitudes are relatively close, there is a large variance in the associated errors. If the test were truly local, the associated errors should also be relatively close. Examination of Figures 8 and 10 reveals that along $\Theta = 0°$ the iterative equation is divergent instead of convergent. Close examination of the results of the integral of Equation 10 reveal that the contribution from the vicinity of the asymptotic source dominated the contribution from the rest of the surface, including the region around the test dipole. The integral of Equation 10, in turn, is the highest contributor to the error, ε. Thus, for $\Theta = 0°$, the Integral E-Field Test retains local character only in the sampling operation. The large source-region contribution drives the error term up so that its magnitude is not small compared to $H^{A(0)}(M^B)$ and the iterative equation diverges.

One may be tempted to employ two dipoles located at $(x_t^{(1)} = R\cos\phi_t, y_t^{(1)} = R\sin\phi_t, Z_t)$ and at $(x_t^{(2)} = 2R - x_t^{(1)}, y_t^{(2)} = y_t^{(1)}, Z_t)$ to obtain asymptotic source region cancellation. This introduces the problem of determining the scattered field at the location of the second dipole. Unfortunately, if surface equivalent currents are used to find the scattered field at the test dipole, then it can be shown that the test is identical to a single dipole test. That is, the use of surface equivalent currents to find $H^A(M^B)$ always leads to the result that $\varepsilon = 0$, for <u>any</u> proposed solut-

ion when M^B is entirely located external to S_c^B. (Observe that for $\Theta = 90°$, the second dipole lies outside of v, and this problem is not encountered). Use of other approximations to find the "scattered field" external to the cylinder would introduce an unknown error, so use of remotely located dipoles was abandoned for angles other than $\Theta = 90°$.

Thus, the "Integral E-Field Test" displays, in general, a mixed local/global character which changes according to the location of the test dipole. For $\Theta = 90°$ the test has almost entirely a local character, with very little contribution from the asymptotic source region. Under these conditions, the error term is relatively small compared to $H^{A(0)}(M^B)$ and the iterative equation converges. For angles other than $= 90°$ the asymptotic source-region begins to contribute to the integral resulting in a mixed local/global nature. At the same time, errors in the source region tend to increase the magnitude of the error term, so that it is no longer small compared to $H^{A(0)}(M^B)$. In this case, the iterative equation shows less of a tendency to converge and may diverge.

Summary

Generalized Lorentz Reciprocity has been employed to formulate an accuracy test that may be used to check any proposed solution. The test is straightforward in application and general in nature, that is, not limited to testing only cylindrical geometries. The test is quantitative in nature, and requires only numerical integration for implementation. The Integral E-Field Test has local character in that the error computed is associated with a single point, although the entire solution contributes to the computation of the error term. In cases where the error is small conmpared to the value of the proposed solution, the test lends itself to use as an iterative equation.

When the test is applied to the problem of magnetic dipole radiation in the presence of an infinite conducting cylinder, it was found that tests along the cylinder axis lend themselves to iteration. Along the axis, solutions that vary as $(ks)^{-1/2}$ test better than solutions that vary as $(ks)^{-1}$ for large path lengths. Tests at points other than on the axis generate error terms that are large with respect to the approximate field value, so that the iterative equation is not convergent. The source regions of each of the proposed solutions were found to contribute significantly to the large error terms for tests of points off the cylinder axis.

References

[1] L. L. Bailin, "The Radiation Field Produced by a Slot in a Large Circular Cylinder," IRE Trans. , vol. AP-3, no 3, pp. 128-237, July, 1955.

[2] R. F. Harrington, Time-Harmonic Electromagnetic Fields. New York: McGraw-Hill Book Company, 1961.

[3] Y. Hwang and R. G. Kouyoumjian, "The mutual coupling between slots on an arbitrary convex cylinder," ElectroScience Laboratory, Department of Electrical Engineering, The Ohio State University, Semi-Annual Report 2902-21, prepared under Grant NGL 36-003-138, 1975.

[4] P. H. Pathak, "Analysis of a conformal receiving array of slots in a perfectly-conducting circular cylinder by the geometrical theory of diffraction," ElectroScience Laboratory, Department of Electrical Engineering, The Ohio State University, Technical Report ESL 3735-2, prepared under Contract N00140-74-C-6017, 1975.

[5] Z. W. Chang, L. B. Felsen, A. Hessel and J. Shmoys, "Surface ray method in the analysis of conformal arrays," Digest of 1976 AP-S International Symposium, held at the University of Massachusetts at Amherst, October 1976, pp. 366-369.

[6] Z. W. Chang, L. B, Felsen, and A. Hessel, "Surface ray methods for mutual coupling in conformal arrays on cylinder and conical surface," Polytechnic Institute of New York, Final Report (September 1975-February 1976), prepared under Contract N00123-76-C-0236, 1976.

[7] S. W. Lee and S. Safavi-Naini, "Asymptotic Solution of Surface Field due to a Magnetic Dipole on a Cylinder," Electromagnetics Laboratory, Department of Electrical Engineering, University of Illinois at Urbana-Champaign, Technical Report No. 76-11, supported by Contract N00019-76-M-0622, 1976.

[8] S. W. Lee and S. Safavi-Naini, "Approximate Asymptotic Solution of Surface Field due to a Magnetic Dipole on a Cylinder," Transactions on Antennas and Propagation, vol. 26, no. 4, July, 1978, pp. 593-598.

[8] R. Mittra and M. Tew, "Accuracy Test for High-Frequency Asymptotic Solutions," Transactions on Antennas and Propagation, vol. 27, no. 1, January, 1979, pp. 62-68.

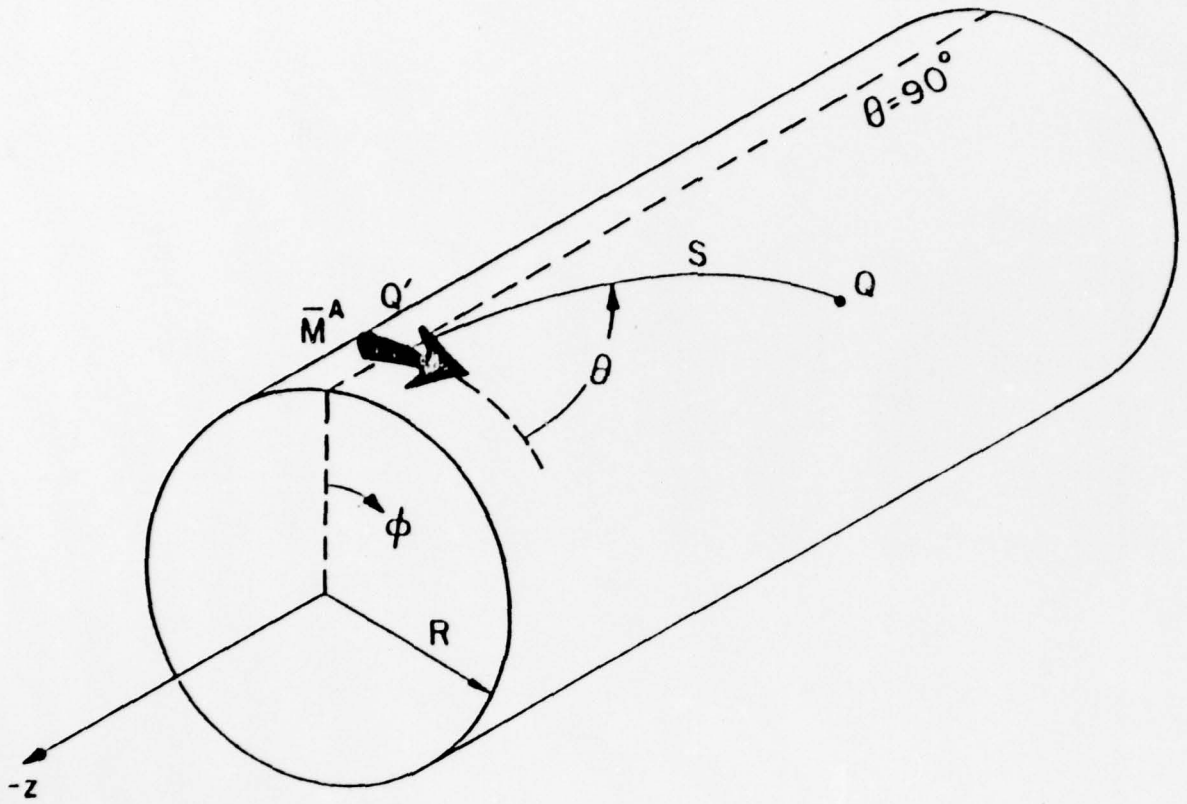

Figure 1a Geometry of asymptotic solutions: Magnetic dipole in the presence of a perfectly conducting infinite cylinder.

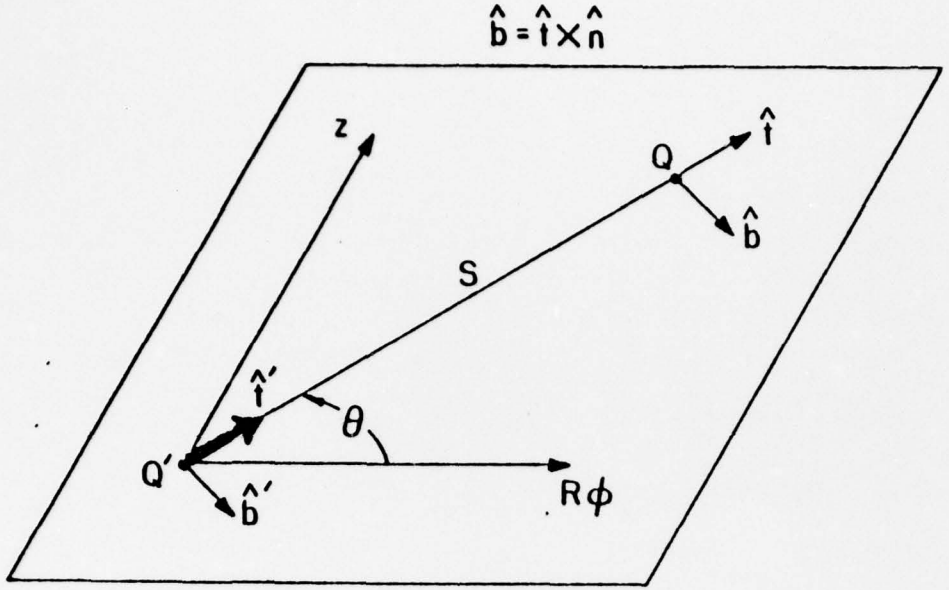

Figure 1b Geometry of asymptotic solutions: Magnetic dipole in the presence of a perfectly conducting infinite cylinder.

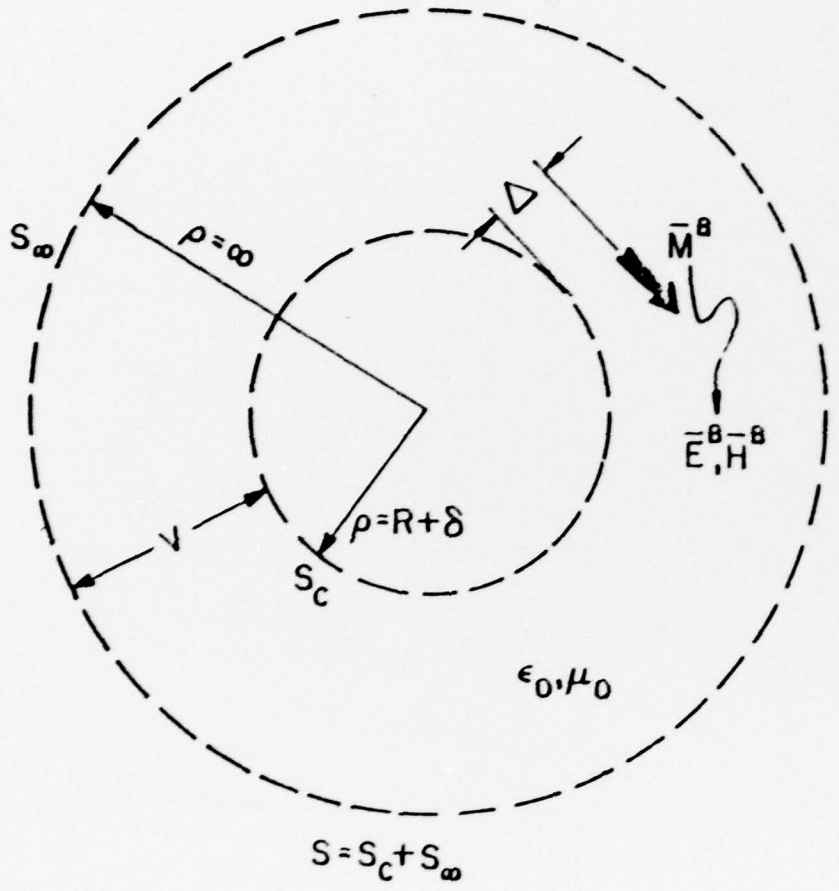

Figure 2 Free-space test environment: Placement of "reciprocity volume" with respect to test dipole.

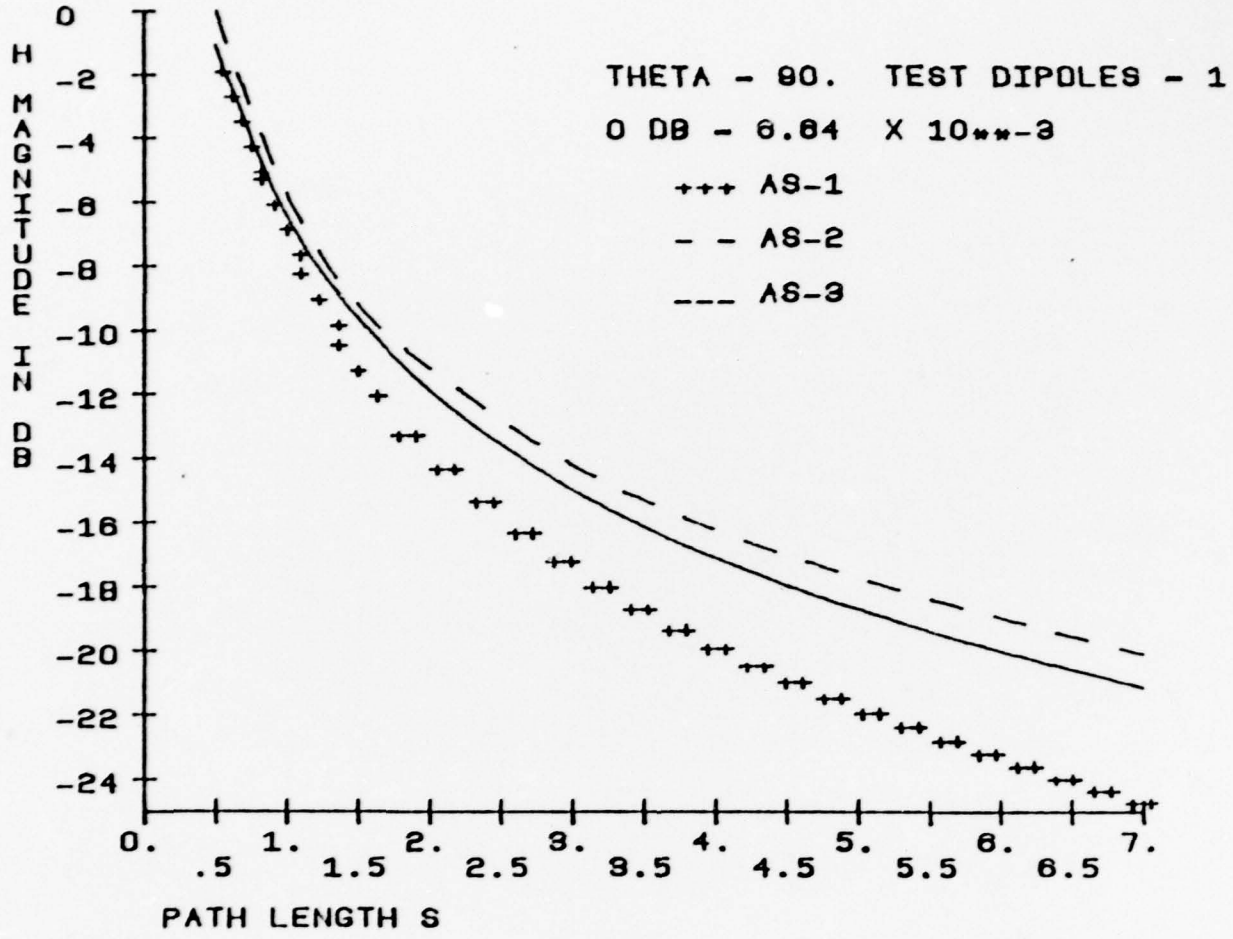

Figure 3 Magnitude of zeroth-order H_ϕ field along $\theta = 90°$.

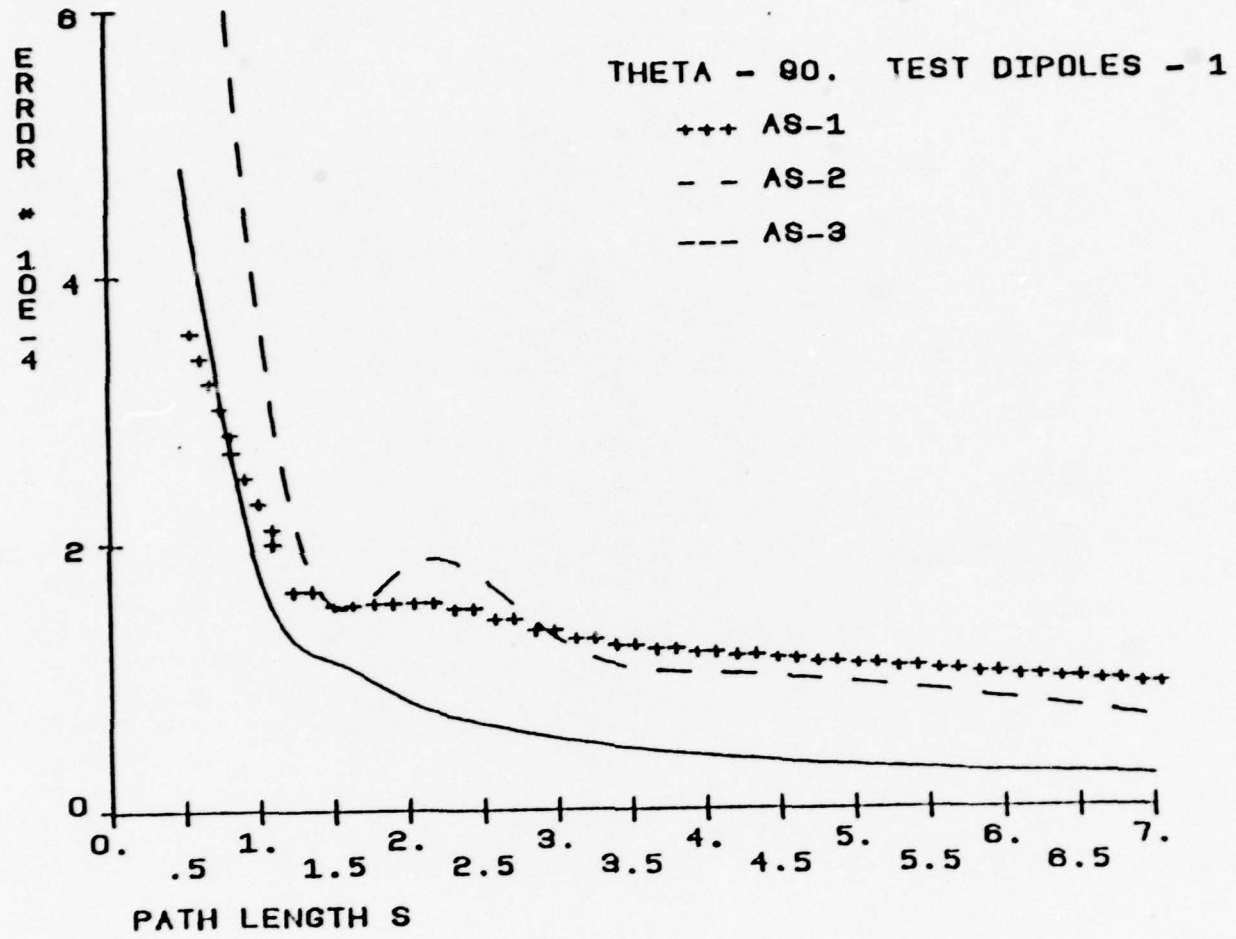

Figure 4 Results of Integral E-Field Test along $\theta = 90°$: Single test dipole.

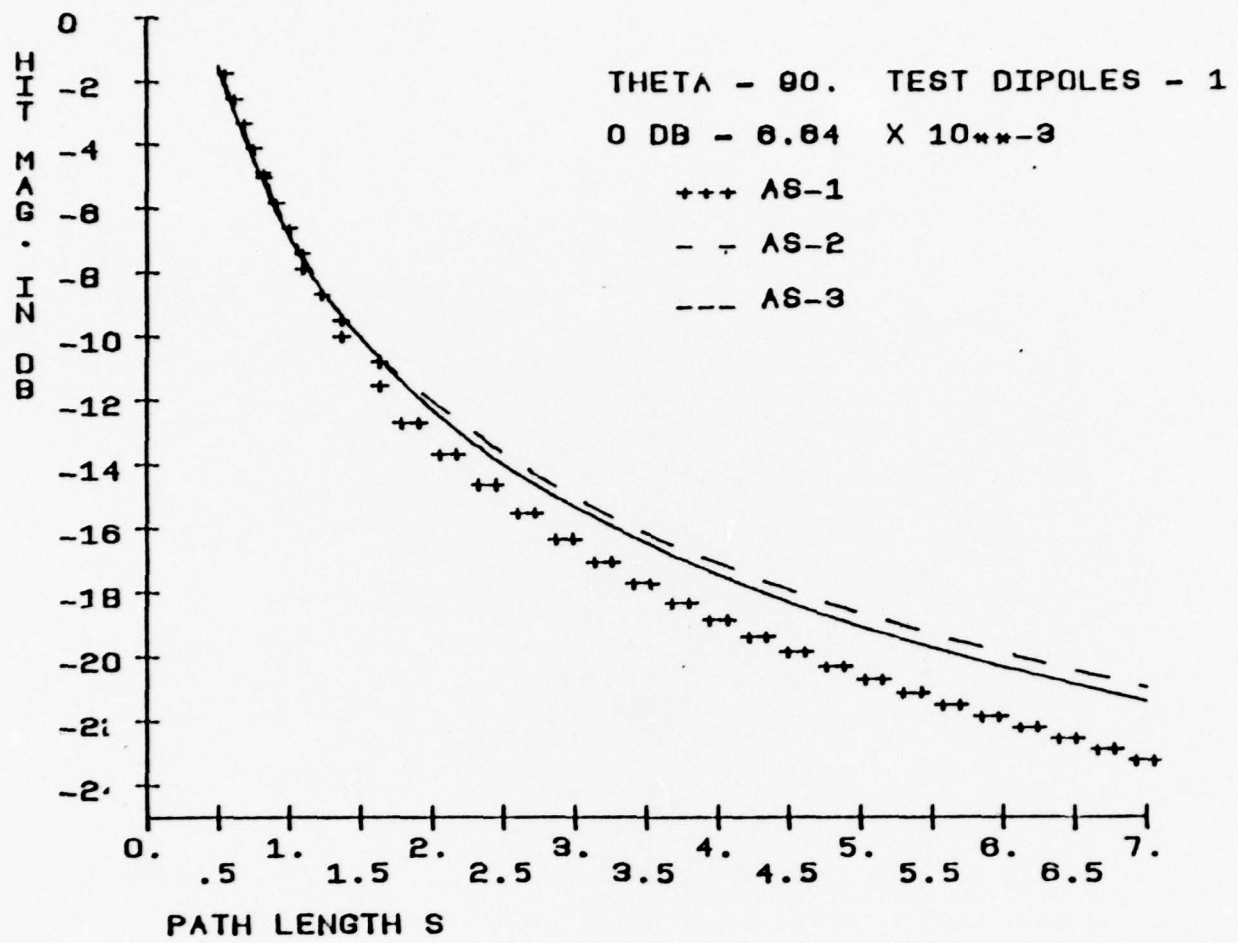

Figure 5 Iterated magnitudes of H_ϕ field along $\theta = 90°$: Simple test dipole.

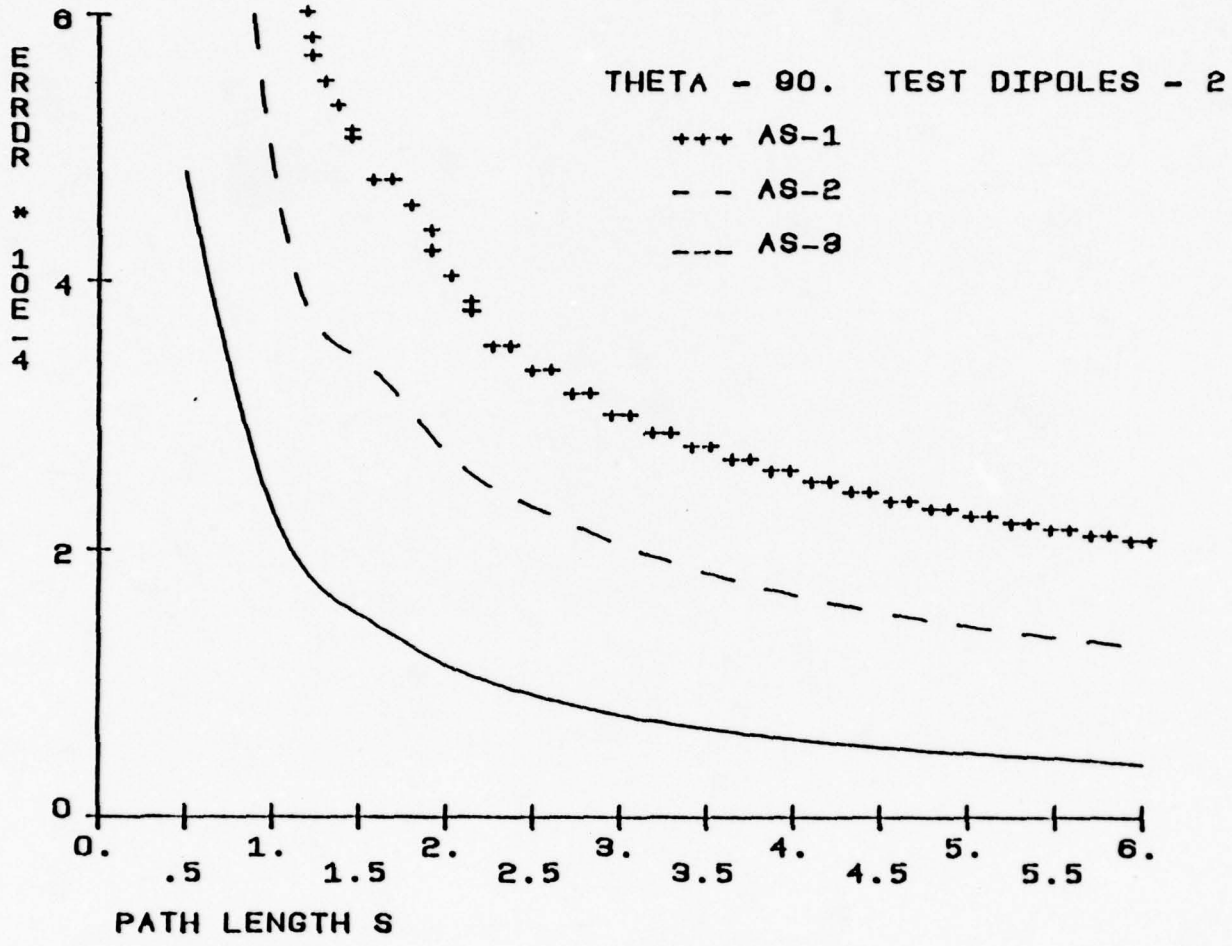

Figure 6 Results of Integral E-Field Test along $\theta = 90°$: Test dipole and planar image dipole.

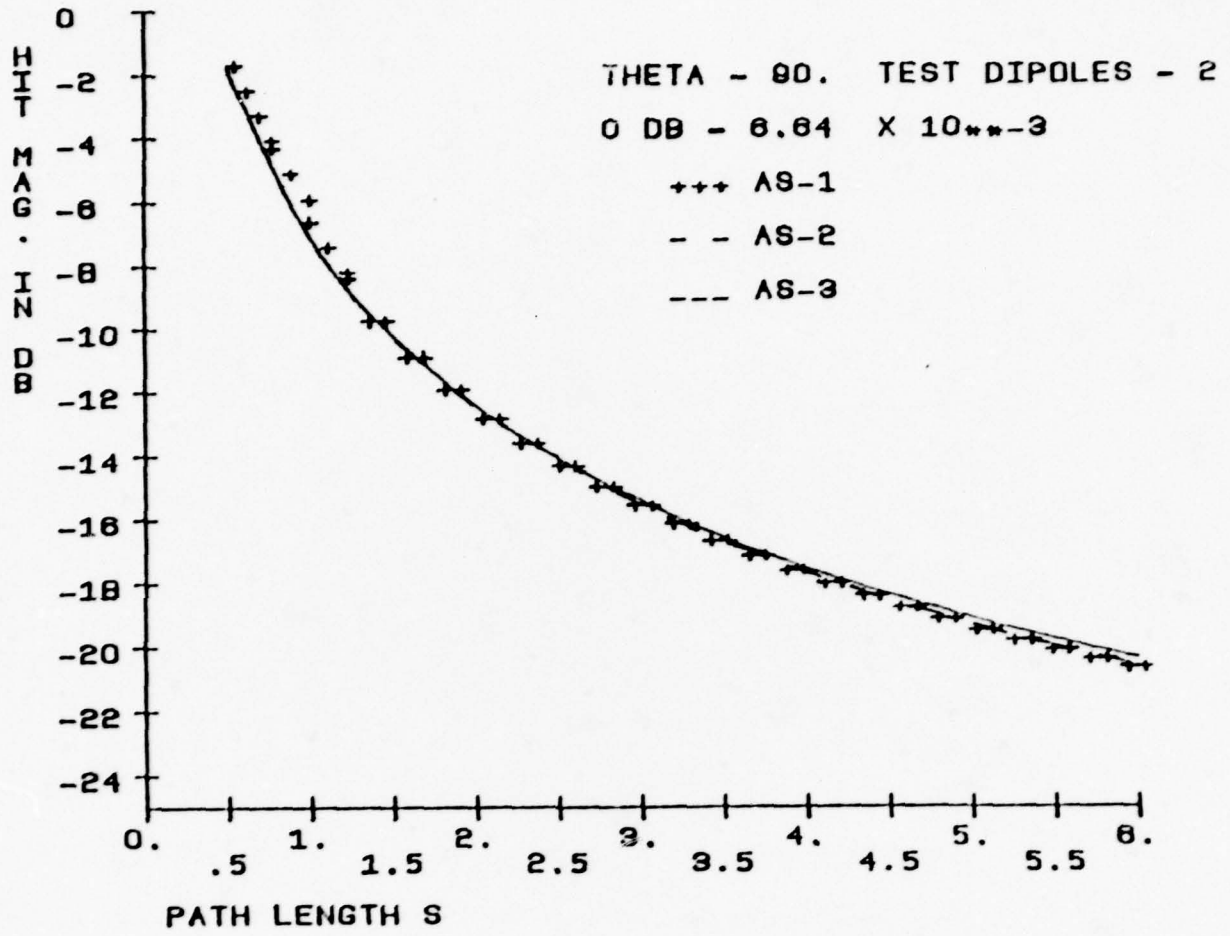

Figure 7 Iterated magnitudes of H field along $\theta = 90°$: Test dipole and planar image dipole.

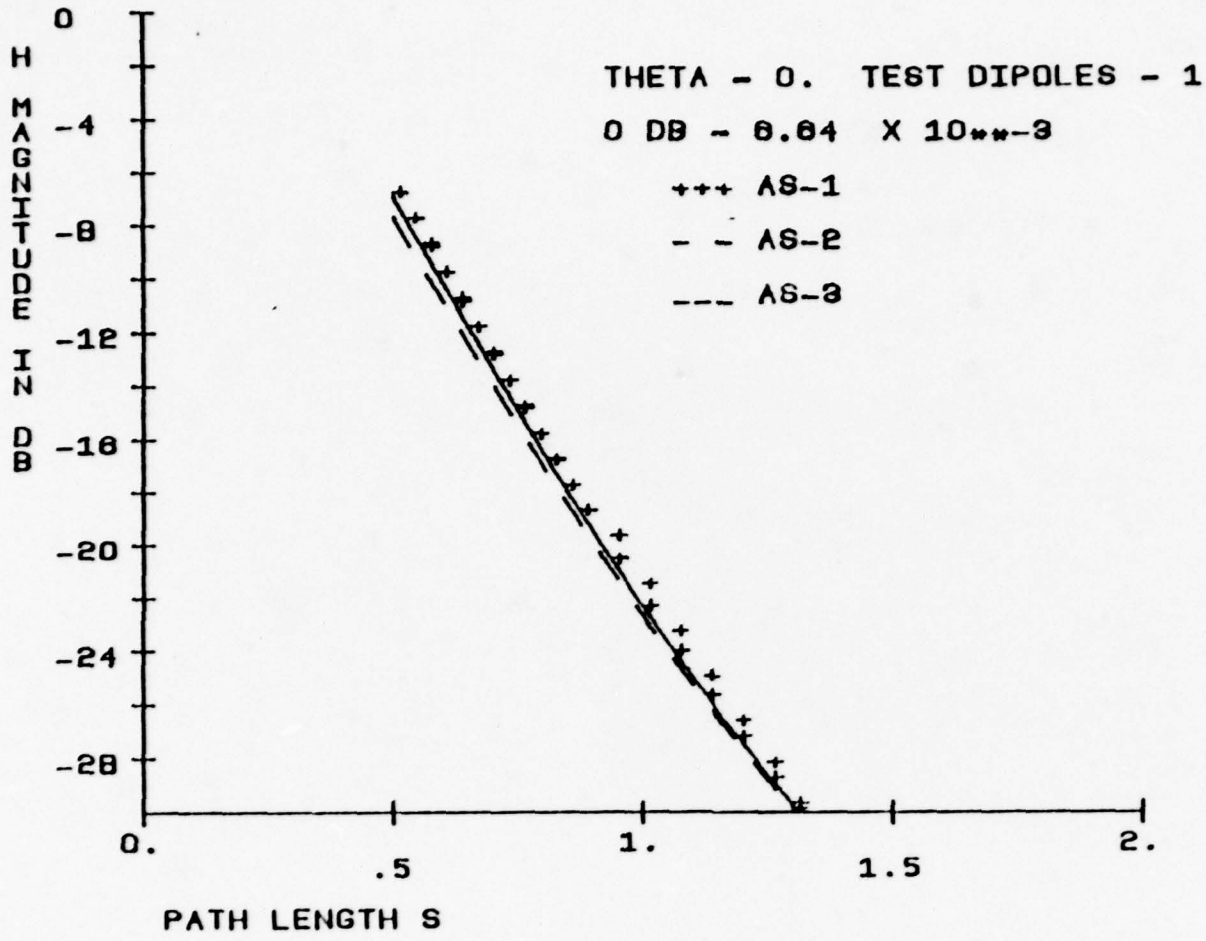

Figure 8 Magnitude of zeroth order H_ϕ field along $\theta = 0°$.

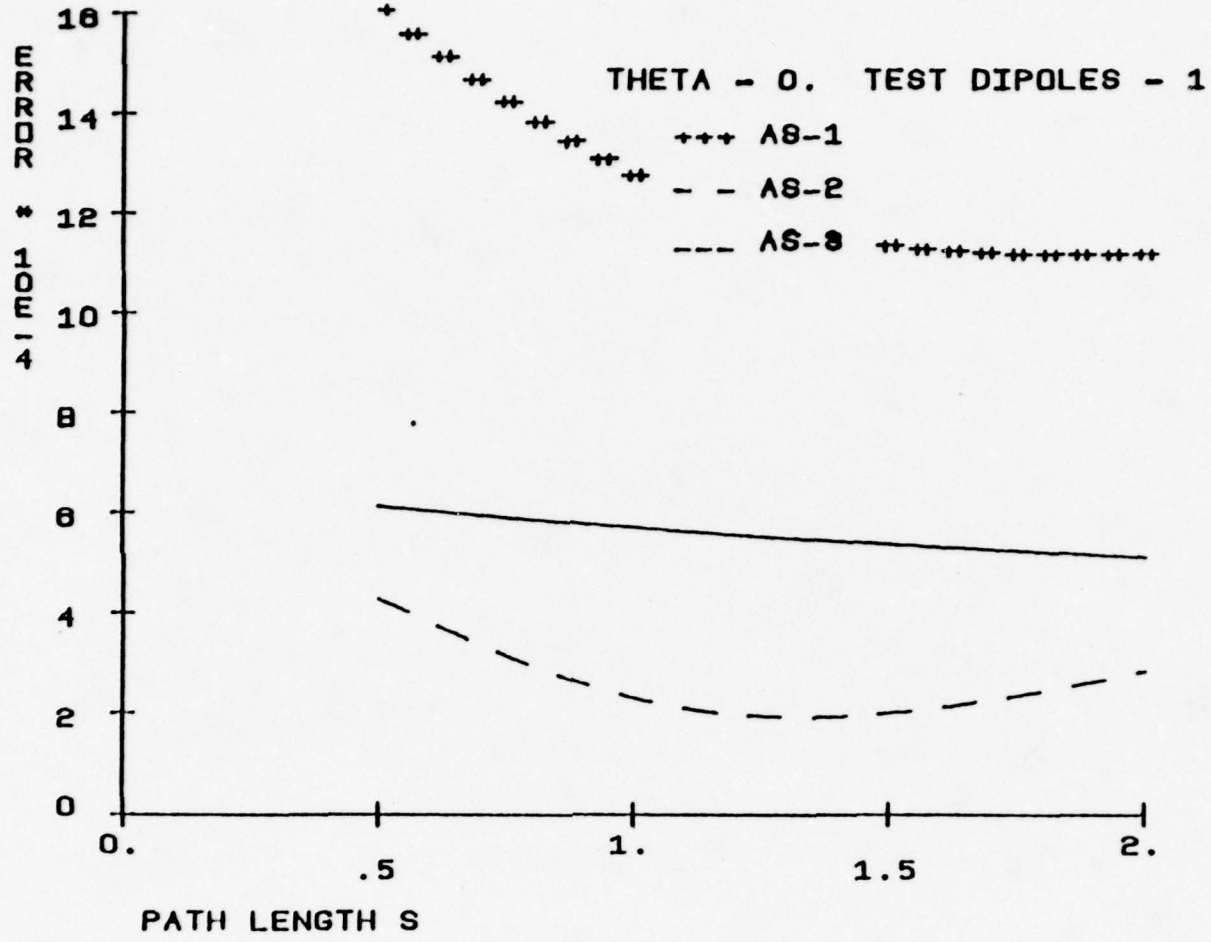

Figure 9 Results of Integral E-Field Test along $\theta = 0°$.

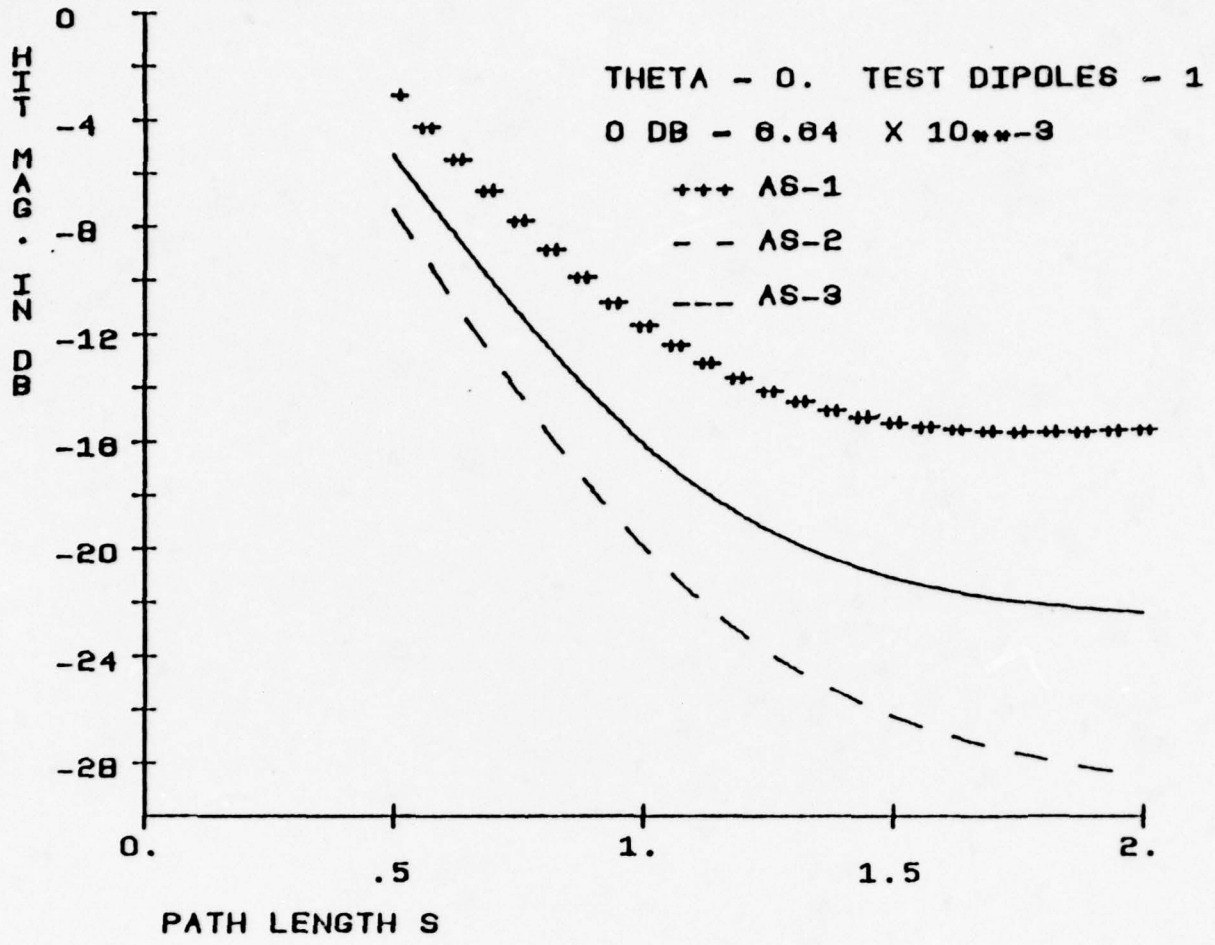

Figure 10 Iterated Magnitudes of the H_ϕ field along $\theta = 0°$.

Transform Approach to Electromagnetic Scattering

RAJ MITTRA, FELLOW, IEEE, WAI LEE KO, MEMBER, IEEE, AND YAHYA RAHMAT-SAMII, MEMBER, IEEE

Invited Paper

Abstract—In this paper, we present a comprehensive review of the Fourier transform technique as applied to the problem of high-frequency scattering and introduce the concepts of the spectral theory of diffraction (STD). In contrast to the more commonly employed ray-optical method for high-frequency scattering, viz. the geometrical theory of diffraction (GTD), the STD approach interprets the scattered field as the spectrum, or the Fourier transform of the induced current on the scatterer. Such an interpretation offers several important advantages: uniform nature of representation, capacity to improve and extend the ray-optical formulas in a systematic manner, and convenient accuracy tests for the results. Methods for combining integral equation methods with the Galerkin procedure and asymptotic techniques in the transform domain are described, and representative examples illustrating the application of the spectral approach are included.

NOMENCLATURE

STD	Spectral theory of diffraction.
UTD	Uniform theory of diffraction.
UAT	Uniform asymptotic theory.
u^i	Incident field.
u^s	Scattered field.
u^t	Total field.
E	Electric field.
H	Magnetic field.
J	Induced electric current.
F	Fourier transform operator.
F^{-1}	Inverse Fourier transform operator.
$\tilde{U}$	Transformed function.
$\tilde{J}$	Transformed function.
X	Spectral diffraction coefficient.
H^d	Edge diffracted field.
H^P	Physical optics field.
H^g	Geometrical optics field.
H_1	Field of edge 1.
H_2	Field of edge 2.
F	Fresnel function.
$\hat{F}$	Asymptotic term of Fresnel function.
J^b	Physical optics current.
J^{tr}	Truncated physical optics current.
J^1	Induced current on a semi-infinite half-plane.
H^D	Diffracted field in UTD formulation.
θ	Step function in Section III.
θ	Truncation operator in Section IV.
$\hat{\theta}$	Complimentary operator.
$\bar{\bar{G}}$	Dyadic Green's function.
$\tilde{J}_p$	Basis function.
$\tilde{W}_q$	Testing function.

Manuscript received December 4, 1978; revised July 5, 1979.

This work was supported in part by Joint Services Electronics Projects under Grant N00014-79-C-0424, and in part by Office of Naval Research under Grant N00014-75-C-0293.

R. Mitra and W. L. Ko are with the Electromagnetics Laboratory, Department of Electrical Engineering, University of Illinois, Urbana, IL 61801.

Y. Rahmat-Samii is with the Jet Propulsion Laboratory, California Institute of Technology, Pasadena, CA 91103.

0018-9219/79/1100-1486$00.75

I. Introduction

SPECTRAL-domain analysis, which makes use of the Fourier transform technique, has a long history of application in physics, applied mathematics, and engineering. An important attribute of the method is its ability to transform partial and ordinary differential equations into algebraic equations which are often easier to solve in the transform domain. Since the available references on this subject are too numerous to be listed here, we mention only four standard texts [1]-[4] for the readers interested in reviewing the general concepts of the transform technique. In electromagnetics, the Fourier transform technique has played a rather important role in solving many canonical problems, e.g., the half-plane and semi-infinite waveguide.

The conventional application [5]-[12] of the transform technique is rather limited, since it can only be used to construct solutions for a class of boundary value problems associated with specialized geometries. However, a number of extensions of the method to a modified version of these geometries have been published [10], [11]. These extensions, which often make use of function-theoretic methods, enable one to derive approximate analytical solutions to a wider class of problems than had been possible using the transform method alone.

Recently, the digital computer has opened up new vistas to researchers in electromagnetics and other disciplines, and has enabled them to attack a much wider class of problems than has been possible prior to the availability of high-speed computers. *In employing the computer as a problem-solving tool*, it is often tempting to let the computer do "all the work." In this event, one employs little or no analytical preparation prior to proceeding with the numerical steps on the computer. However, experience shows that the computer offers no panacea, at least when it is used in the manner indicated above. This is because for many practical problems, the requirements on storage, computational time, and cost can be prohibitively large if one uses a purely numerical approach. These limitations become particularly severe in the resonance region and above, where the geometrical dimensions of the object are on the order of two to three wavelengths or more. Below this region, the integral-equation formulation combined with matrix methods [13], [14] is well-suited for deriving numerically rigorous solutions to radiation and scattering problems involving objects of arbitrary shape.

For frequencies above the resonance region, the transform technique has been found useful for deriving efficient numerical solutions to radiation and scattering problems by combining integral-equation formulation with asymptotic techniques in the transform domain. The early application of the spectral technique had demonstrated its usefulness for a class of geometries involving open waveguides and scattering problems [15]-[21]. Recent studies have shown that the scope of application can be considerably enlarged while simultaneously improving the efficiency of computation by incorporating the existing high-frequency asymptotic solutions into the solution procedure. Consequently, this paper focuses mainly on this combination procedure which appears to offer the greatest potential for systematic and accurate solutions to radiation and scattering problems in the resonance region and above.

Turning now to a brief review of the asymptotic techniques, perhaps the most significant works on the subject are the two pioneering papers by Keller [22], [23] which introduced the concepts of the geometrical theory of diffraction (GTD) by augmenting the classical geometrical optics (GO) field expressions with the edge-diffracted fields from sharp corners. Keller's GTD and some of its extensions have been described in a number of review papers and book chapters [24]-[27]; an exhaustive set of useful references can be found in [28]. Although in the last fifteen years Keller's GTD has played a very significant and unique role in solving high-frequency scattering problems, its original form is known to break down at shadow boundaries,[1] reflection boundaries, and caustics. Two uniform theories have recently been developed [29]-[31] for circumventing the difficulties associated with Keller's GTD in the neighborhood of shadow boundaries. Each one of these theories is based on its own Ansatz and yields different forms for the expressions of the field in the transition region between the lit and shadow zones. Another totally different approach is based on a modification of physical optics (PO), called the physical theory of diffraction (PTD) developed by Ufimtsev and others [32], [33]. A comparative study of the various asymptotic techniques [34], [35] can be useful for evaluating the different methods for computing the edge-diffracted fields in the transition regions.

All of the aforementioned asymptotic techniques based on GTD, be they uniform or nonuniform, have two important and fundamental limitations.

a) it is difficult to estimate the accuracy of the solution;

b) there is no systematic procedure available for improving the solution. The addition of higher order multiply-diffracted terms in the asymptotic series can and often does lead to a divergent result. In contrast, the spectral approach to scattering, which was introduced in the literature [36] under the name of spectral theory of diffraction (STD), not only provides a built-in test for the satisfaction of the boundary condition, but is convenient for improving the GTD or other asymptotic solutions via Galerkin or iterative procedures also [35]-[42].

The principal motivation of this paper is to present a comprehensive review of the spectral approach for solving electromagnetic scattering and diffraction problems. In contrast to that in the ray approach or GTD, which is essentially geometric in nature, the scattered-field representation in the spectral approach is in terms of the Fourier transform of the induced surface current on the scatterer. Although the basic foundations of GTD and STD are different, the GTD solution, where valid, is indeed identifiable as the result obtained from an asymptotic evaluation of the transform-domain representation of the scattered field. In addition, the integral representation provides a uniform solution requiring no *a posteriori* correction [36]. This topic is discussed in Section III.

The important subject of systematic improvement of high-frequency asymptotic solutions via a combination of GTD methods and integral-equation formulation is described in Section IV, and some unique numerical advantages that accrue from the use of this procedure are also demonstrated. Finally, a few concluding remarks on the spectral approach are given in Section V. Possible extensions of this approach to a number of other important problems of practical interest are also mentioned in this section.

[1] For the definition of various terms such as *shadow boundaries* and *transition regions*, see [28].

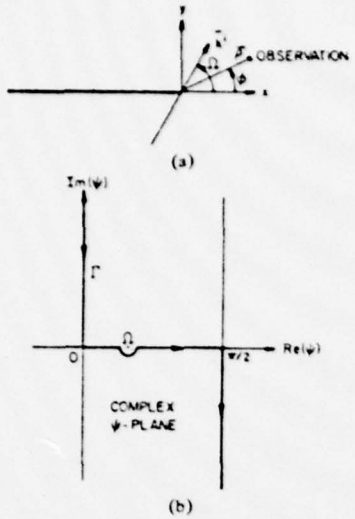

Fig. 1. (a) Diffraction of a plane wave by a half-plane, $0 \leqslant \Omega \leqslant \pi$ and $-\pi \leqslant \phi \leqslant \pi$. (b) Integration path Γ for integral representation (11).

II. Formalism for Transform Approach to High-Frequency Solution—STD

In this section we introduce the basic concepts of the STD via the half-plane problem. Since the canonical geometry of the half-plane is one of the cornerstones of the various nonuniform and uniform theories of high-frequency diffraction, we also choose this geometry to lay the foundations of STD.

The geometry of a perfectly conducting half-plane located at $y = 0$, $x \leqslant 0$ and illuminated by a plane wave is shown in Fig. 1(a). The Cartesian coordinates (x, y, z) and the cylindrical coordinates (ρ, ϕ, z) are erected at the edge of the half-plane. Angles are defined positively counterclockwise with the range $[-\pi, \pi]$. We let the direction of propagation of the incident plane wave be normal to the edge, i.e., $\vec{k}^i \cdot \hat{z} = 0$. This assumption changes the vector nature of the three-dimensional problem to a two-dimensional scalar problem. Furthermore, the problem may be classified according to the cases of E-wave (nonzero field components E_z, H_x, H_y), or H-wave (nonzero field components H_z, E_x, E_y) by simply letting the incident E-field or H-field be directed alternatively along the z-axis. Unless otherwise specified, the cases of E- and H-waves are treated simultaneously, with the help of two symbols u and τ such that

$$\text{for } E\text{-waves:} \quad u = E_z, \quad \tau = -1 \tag{1a}$$

$$\text{for } H\text{-waves:} \quad u = H_z, \quad \tau = +1. \tag{1b}$$

The total field u^t may be split into the incident field u^i and the scattered field u^s to give

$$u^t = u^i + u^s. \tag{2}$$

For a perfect electric conductor the total field u^t is subject to the boundary condition $u^t = 0$ or $\partial u^t/\partial y = 0$ for E-wave or H-wave cases, respectively, on the half-plane. If one defines the induced electric current on the half-plane as

$$\text{for } E\text{-wave:} \quad J_z = \left.\frac{\partial u^t}{\partial y}\right|_{0^+}^{0^-} \tag{3a}$$

$$\text{for } H\text{-wave:} \quad J_x = -\left.u^t\right|_{0^+}^{0^-} \tag{3b}$$

and uses the time convention $\exp(-i\omega_0 t)$, one can readily arrive at the following equations from Maxwell's equation [7], [12]:

$$\text{for } E\text{-wave:} \quad u^s = E_z^s = i\omega_0\mu \int_{-\infty}^{0} J_z(x') g_0(k|\vec{\rho} - x'\hat{x}|)\, dx' \tag{4a}$$

$$\text{for } H\text{-wave:} \quad u^s = H_z^s = \frac{\partial}{\partial y} \int_{-\infty}^{0} J_x(x') g_0(k|\vec{\rho} - x'\hat{x}|)\, dx' \tag{4b}$$

where $k = \omega_0\sqrt{\mu\epsilon}$, μ and ϵ are the permeability and permittivity of the medium, respectively, and $g_0(k\rho) = iH_0^1(k\rho)/4$ (H_0^1 is the Hankel function of first kind and zeroth order). The objective is to determine J and u^s for the half-plane illuminated by an incident plane wave. This is done by using the transform technique and employing the results given in [43].

A. Spectral Diffraction Coefficient and Total Field

Let us define the Fourier transform pair as

$$U(\alpha) = \int_{-\infty}^{\infty} u(x) \exp(i\alpha x)\, dx = \mathrm{F}[u(x)] \tag{5a}$$

and

$$u(x) = \frac{1}{2\pi} \int_{-\infty+i\Delta}^{\infty+i\Delta} U(\alpha) \exp(-i\alpha x)\, d\alpha = \mathrm{F}^{-1}[U(\alpha)] \tag{5b}$$

where Δ is a small positive number. The incident plane wave can be written as

$$u^i = \exp(i\vec{k} \cdot \vec{\rho}) = \exp(i(k_x x + k_y y)) = \exp(ik\rho \cos(\Omega - \phi)) \tag{6}$$

where $k_x = k \cos\Omega$, $k_y = k \sin\Omega$, and $0 \leqslant \Omega \leqslant \pi$ is the incident angle shown in Fig. 1(a). Transforming (4) into the spectral (Fourier) domain and applying the Wiener–Hopf construction [10], one arrives at the following:

$$\text{for } E\text{-wave:} \quad \mathrm{F}[J_z] = (i\omega_0\mu)^{-1} X(k_x, \alpha) \tag{7a}$$

$$\text{for } H\text{-wave:} \quad \mathrm{F}[J_x] = -\gamma^{-1} X(k_x, \alpha) \tag{7b}$$

where $X(k_x, \alpha)$ is

$$X(k_x, \alpha) = 2\frac{\sqrt{k + \tau k_x}\sqrt{k + \tau\alpha}}{\alpha + k_x} \tag{8}$$

and $\gamma = \sqrt{\alpha^2 - k^2}$ such that $Re\,\gamma \geqslant 0$, and $\alpha = -k \cos\psi$. In this work, unless otherwise stated, $\sqrt{\cdot}$ and $(\cdot)^{1/2}$ are defined with their proper branch cut slightly below the negative real axis. Using the transformed version of (4) and then incorporating (7), one finally obtains

$$U^s = \begin{Bmatrix} 1 \\ \operatorname{sgn}(y) \end{Bmatrix} X(k_x, \alpha) \frac{\exp(-\gamma|y|)}{2\gamma} \quad \text{for} \begin{Bmatrix} E\text{-wave} \\ H\text{-wave} \end{Bmatrix}. \tag{9}$$

Furthermore, one may notice that the following equation has

been used in the construction of (9)

$$F[g_0(k\rho)] = \frac{\exp(-\gamma|y|)}{2\gamma}. \tag{10}$$

Introducing the change of variables $x = \rho\cos\phi$, $y = \rho\sin\phi$, $k_x = k\cos\Omega$, $k_y = k\sin\Omega$, $\alpha = -k\cos\psi$, and $\gamma = -ik\sin\psi$ into (9) and substituting the result into (5b), one finally arrives at

$$u^s = \frac{i}{4\pi}\begin{Bmatrix}1\\ \operatorname{sgn}(\phi)\end{Bmatrix}\int_\Gamma \chi(\Omega,\psi)\exp(ik\rho\cos(\psi - |\phi|))\,d\psi \quad \text{for} \begin{Bmatrix}E\text{-wave}\\ H\text{-wave}\end{Bmatrix}. \tag{11}$$

In the preceding equation ψ is the complex angle defined on the path Γ, shown in Fig. 1(b), and $\chi(\Omega, \psi)$ is

$$\chi(\Omega,\psi) = X(k\cos\Omega, -k\cos\psi) = \chi_i(\Omega,\psi) + \tau\chi_r(\Omega,\psi) \tag{12}$$

where

$$\chi_{i,r}(\Omega,\psi) = \mp\csc\frac{\Omega \mp \psi}{2}. \tag{13}$$

We may notice that $\chi_i(\cdot)$ and $\chi_r(\cdot)$ have the same functional form, i.e., csc $(\cdot)$. This definition of χ_i and χ_r is closely related to the definition used by Deschamps in [24]. Clearly χ_i and χ_r are infinite at $\psi = \Omega$ and $\psi = -\Omega$, respectively. These two values of ψ correspond to the incident and reflection shadow boundaries appearing in the classical GTD expressions which are obviously "nonuniform" as a function of the observation angle. As a matter of fact, $\chi(\Omega, \psi)$ is precisely the angular part of Keller's diffraction coefficient, when ψ is replaced by the observation angle ϕ. Although χ tends to infinity at the shadow boundaries, it does not mean that the field itself is also infinite as Keller's GTD predicts. Instead, the correct value of the field is obtained from (11), which is always bounded. To distinguish it from Keller's coefficient, which is associated with the diffracted field, we will refer to $\chi(\Omega, \psi)$ as the *spectral diffraction coefficient* for the half-plane. This terminology is chosen since $\chi(\Omega, \psi)$ is associated with the spectrum, or equivalently, the Fourier transform, of the induced current and appears only inside the kernel of the plane-wave spectrum representation for the field and not directly in the form of a factor multiplying the incident field as in the case of Keller's representation.

We may further use (4) and (7) and introduce the spectral coefficient of the physical optics field X^{PO} as the Fourier transform of the physical optics induced current to arrive at

$$\text{for } E\text{-wave:} \quad X^{PO}(k_x,\alpha) = \frac{2k_y}{\alpha + k_x} \tag{14a}$$

$$\text{for } H\text{-wave:} \quad X^{PO}(k_x,\alpha) = \frac{2i\sqrt{\alpha^2 - k^2}}{\alpha + k_x}. \tag{14b}$$

The application of the change of variables used in (11) allows one to express (14) as

$$\chi^{PO}(\Omega,\psi) = \chi_i^{PO}(\Omega,\psi) + \tau\chi_r^{PO}(\Omega,\psi) \tag{15}$$

where

$$\chi_{i,r}^{PO}(\Omega,\psi) = \mp\operatorname{ctn}\frac{\Omega \mp \psi}{2}. \tag{16}$$

It is worthwhile to mention that χ^f, as defined in the following equation, is bounded at the shadow boundaries

$$\chi^f(\Omega,\psi) = \chi(\Omega,\psi) - \chi^{PO}(\Omega,\psi). \tag{17}$$

$\chi^f(\Omega, \psi)$ could be called the fringe diffraction coefficient.[2]

For the problem at hand, i.e., incident plane wave, the spectral integral (11) can be expressed exactly in terms of the Fresnel integral, viz.

$$u^s = -\exp(ik\rho\cos(\Omega - \phi))F(-\xi_i) + \tau\exp(ik\rho\cos(\Omega + \phi))F(\xi_r) \tag{18}$$

where the Fresnel integral F is defined as

$$F(\xi) = \frac{\exp(-i\pi/4)}{\sqrt{\pi}}\int_\xi^\infty \exp(it^2)\,dt \tag{19}$$

and

$$\xi_{i,r} = \mp\sqrt{2k\rho}\sin\frac{\Omega \mp \phi}{2}. \tag{20}$$

Using the analytic continuation argument, one can show that, for complex angles of incidence, equation (18) is still the proper solution of the diffraction problem. In this context Ω is replaced by the complex angle ψ which follows the path $\Gamma_i[(i\infty, 0) \cup (0, \pi) \cup (\pi, -i\infty)]$ in the complex ψ-plane to cover the infinite spectrum of incidence angles.

In reviewing the material presented in this section, we note that its principal contribution has been the introduction of the spectral diffraction coefficient, which is shown to be associated with the integral representation of the scattered field in terms of the Fourier transform of the induced current on the surface of the scatterer. The equivalence between the GTD results and those derived from the spectral representation for observation angles not close to the shadow boundaries can be easily established by substituting the asymptotic expansion of the Fresnel integral into (18).

One of the important attributes of the spectral approach is that it provides a uniform representation of the scattered field that is based on physical interpretation of the diffraction phenomenon in terms of radiation from the induced surface current. This feature allows one to generalize the formulas such that they apply to a wide range of scattering geometries. This point will be illustrated in subsequent sections with some representative examples.

III. Finite Bodies with Edges—Comparison of Spectral and Uniform Theories for a Typical Example—The Strip

In the previous section we introduced the concept of spectral-domain representation of the field scattered from a half-plane and showed how the difficulties with Keller's formulas in the transition regions could not only be interpreted but circumvented as well. Though the above result may be interesting from a theoretical point of view, the diffraction formula would be even more useful if it were applied to prac-

[2] The reader should be cautioned, however, that contrary to the popular belief, the fringe current (excess of physical optics current) is not confined to the very near vicinity of the diffracting edge and the assumption that the edge diffraction is a local phenomenon governed solely by the configuration of the tip of the edge can, in some cases, lead to substantial errors. An example of this occurring in a wedge-diffraction problem is given in Section V.

tical structures, which are obviously of finite extent. The classical GTD formulas, when applied to such finite structures, still contain spurious infinities,[3] notwithstanding the fact that the spectrum of the induced current, and hence the scattered field, must be necessarily finite. Thus in contrast to the half-plane problem for which it was necessary to express the scattered field in terms of the integral representation (11) because of the singularities in the diffraction coefficient, the far scattered field for the finite structure should be obtainable directly from the spectrum of the induced current by a straightforward application of the saddle point integration technique (which would merely require a substitution of variables) in the integral representation for the scattered field. If the transform or the spectrum of the induced current is properly computed, the far-field expression derived from it should be uniformly valid for all observation angles, including the transition regions, and consequently, no *a posteriori* correction would be needed for formulas derived in this manner. This is in contrast to conventional GTD formulas which are typically "repaired," after the fact, by employing one of the uniform theories, e.g., the uniform theory of diffraction (UTD) of Kouyoumjian and Pathak [30] or uniform asymptotic theory (UAT) of Lewis, Ahluwalia, and Boersma [29]. With this background in mind, we proceed in the following section to compare the various uniform theory formulas with the one derived from the spectral approach by considering a simple illustrative example, viz. the strip. We show that not only are the spectral formulas uniform in their original format, and therefore require no *a posteriori* correction, they are actually simpler and more accurate as well! The increased accuracy results from the inclusion of a term which arises naturally in the spectral formulas from a physical interpretation of the diffraction phenomenon, but is shown to be missing in the other uniform formulas which are based on the assumption that diffraction is a "local" phenomenon. We will see that the absence of this term can create nontrivial and nonphysical discontinuities in the scattered far field. This fact will be further illustrated in Section V, where we consider another wedge diffraction problem, viz. the diffraction by a rectangular cylinder.

Before closing this section it will be worthwhile to point out that the spectral approach does not achieve the characteristic advantages described above by abandoning the conventional and well-familiar formulas of Keller's GTD, which have unquestionably established themselves in the literature on high-frequency diffraction and proved their usefulness for computing the scattered field except in the vicinity of observation angles near the "trouble" regions. Interesting, the Keller coefficients blend in naturally in the STD formalism which makes explicit use of the GTD expressions in the representation of the scattered field. However, the interpretation of the Keller coefficients as well as the final form of the formulas in which they appear can be significantly different from those found in the ray-optical approach, as will be evident from the material presented in the following section.

A. Comparison of STD and UAT

The UAT of Lewis *et al.* [29] has been introduced to overcome some of the difficulties in GTD that occur at the transition regions associated with shadow and reflection boundaries.

[3] Except in special situations when the aggregate contribution of these infinities cancel.

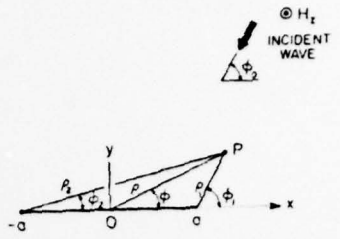

Fig. 2. Geometry of the strip problem.

In UAT, the fictitious infinities in Keller diffraction coefficients for edges are annihilated by the introduction of additional terms which themselves go to infinity at the shadow boundaries such that the singularities in the Keller coefficients are canceled out exactly.

We first present some uniform formulas based on UAT for some typical edge diffraction problems and then show that the UAT ansatz can not only be physically interpreted using the spectral approach, but can be improved and generalized also in a straightforward manner. To illustrate our point, we consider the problem of diffraction by a strip of width 2a which is illuminated by an H-polarized wave (see Fig. 2). The incident angle is ϕ_0, and other variables such as ρ_1, ϕ_1, ρ_2, and ϕ_2 are shown in the diagram.

Following the UAT prescription [28], we write the total field as

$$H^t = H^i[F(\xi_1^i) - \hat{F}(\xi_1^i)] + H^r[F(\xi_1^r) - \hat{F}(\xi_1^r)] + H_1^d - H^i + H^i[F(\xi_2^i) - \hat{F}(\xi_2^i)] + H^r[F(\xi_2^r) - \hat{F}(\xi_2^r)] + H_2^d - H^r \quad (21)$$

where H^i is the incident field given by

$$H^i = \exp(-ik\rho\cos(\phi - \phi_0)). \quad (22)$$

H^r is the reflected field (from an infinite plane) and has the form

$$H^r = \exp(-ik\rho\cos(\phi + \phi_0)). \quad (23)$$

F is the Fresnel integral defined in (19) and

$$\hat{F}(x) = \frac{1}{2x\sqrt{\pi}}\exp(i(x^2 + \pi/4)). \quad (24)$$

$\hat{F}$ is the asymptotic form of F for large positive argument. The subscripts 1 and 2 refer to the two edges which form the origins of the coordinate systems for the corresponding diffracted fields associated with these edges.

The diffracted fields H_1^d and H_2^d are derived from Keller's GTD formulas in a standard manner and are expressed as

$$H_1^d = \exp(-ika\cos\phi_0)\frac{\exp(i(k\rho_1 + \pi/4))}{\sqrt{8\pi k\rho_1}} \cdot \left(\frac{1}{\cos\left(\frac{\phi_0 + \phi_1}{2}\right)} - \frac{1}{\cos\left(\frac{\phi_1 - \phi_0}{2}\right)}\right) \quad (25a)$$

$$H_2^d = -\exp(ika\cos\phi_0)\frac{\exp(i(k\rho_2 + \pi/4))}{\sqrt{8\pi k\rho_2}} \cdot \left(\frac{1}{\cos\left(\frac{\phi_2 - \phi_0}{2}\right)} + \frac{1}{\cos\left(\frac{\phi_2 + \phi_0}{2}\right)}\right). \quad (25b)$$

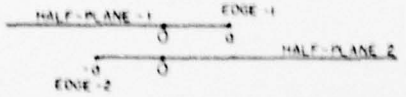

Fig. 3. Two half-planes corresponding to two edges of the strip.

Finally, $\xi_1^{i,r}$, $\xi_2^{i,r}$, the so-called "detour functions," are given by

$$\xi_1^i = -\sqrt{2k\rho_1}\sin\tfrac{1}{2}(\pi + \phi_0 - \phi_1), \qquad 0 \le \phi_1 \le \pi \quad (26a)$$

$$\xi_1^r = \sqrt{2k\rho_1}\sin\tfrac{1}{2}(\pi - \phi_0 - \phi_1), \qquad 0 \le \phi_1 \le \pi \quad (26b)$$

and similarly for the edge 2.

Note that we have deliberately added the term $-(H^i + H^r)$ to the UAT-prescribed formula in order to obtain the proper GO limit, although no direct allusion to such a modification is found in the UAT formulas.

Let us now concentrate on the upper hemisphere since the discussion pertaining to the lower hemisphere is expected to be very similar in view of the symmetry of the problem. For the region $y > 0$, $F(\xi_{1,2}^i) - \hat{F}(\xi_{1,2}^i) \approx 1$, and we can simplify (21) to obtain

$$H^t = H^i + H^r[F(\xi_1^r) - \hat{F}(\xi_1^r) + F(\xi_2^r) - \hat{F}(\xi_2^r) - 1] + H_1^d + H_2^d. \quad (27)$$

We note from (27) that the geometrical optics field has been replaced in the UAT formulation by

$$H^i + H^r[\{F(\xi_1^r) - \hat{F}(\xi_1^r)\} + \{F(\xi_2^r) - \hat{F}(\xi_2^r)\} - 1]$$

whereas the Keller GTD terms, viz. H_1^d and H_2^d, have remained unchanged. This is the essence of the UAT ansatz as interpreted by Lee [28].

We will now show that the UAT formula (27) can not only be physically interpreted, but improved and generalized as well.

To this end, we rewrite (27) as

$$H^t = H^i + (H_1^d - H_1^p) + (H_2^d - H_2^p) + \{H^r[F(\xi_1^r) - \hat{F}(\xi_1^r) + F(\xi_2^r) - \hat{F}(\xi_2^r) - 1] + H_1^p + H_2^p\} \quad (28)$$

where H_1^p and H_2^p are proportional to the Fourier transforms (or spectra) of the physical optics currents that would exist on *semi-infinite* half-planes erected at edges 1 and 2, respectively (see Fig. 3). These quantities are given by

$$H_1^p = \frac{\exp(i(k\rho_1 + \pi/4))}{\sqrt{8\pi k\rho_1}}(\sin\phi_1) \cdot 2\frac{\exp(-ika\cos\phi_0)}{\cos\phi_0 + \cos\phi_1} \quad (29a)$$

$$H_2^p = \frac{\exp(i(k\rho_2 + \pi/4))}{\sqrt{8\pi k\rho_2}}(\sin\phi_2) \cdot 2\frac{\exp(ika\cos\phi_0)}{\cos\phi_0 + \cos\phi_2} \quad (29b)$$

Note that $H_{1,2}^p$ have exactly the same singularities at the shadow boundaries ($\phi_{1,2} = \pi - \phi_0$) as the Keller coefficients. This is not unexpected, however, since it was pointed out in [36] that the singularities in Keller diffraction coefficients can indeed be identified as the contributions of the physical optics currents of semi-infinite extent. In fact, the two terms H_1^p and H_2^p have been deliberately introduced in the expression given in (28) so that we can provide a physical interpretation of the various terms. We can, for instance, identify $(H_1^d - H_1^p)$ as the spectrum or the far field associated with the J^1 current on the semi-infinite half-plane 1, J^1 being the difference between the total current and the physical optics current on the same half-plane. A similar interpretation can obviously be given to the companion term $(H_2^d - H_2^p)$. We now proceed to show that the terms appearing in the curly braces in (28) have a very simple physical interpretation, and can be replaced by a much simpler form that does not require the use of Fresnel integrals. Additionally, we find that the spectral-domain approach also provides an insight into the generalization of the formulas for curved surfaces.

In order to develop a physical interpretation of the UAT formula, we now turn to the spectral-domain interpretation of the scattered field. Unlike the ray-optical representation, which expresses the total field as a superposition of GO and diffracted fields, we use the conventional representation of the total field as

$$H^t = H^i + H^s \quad (30)$$

where H^s is the scattered field. The reason for choosing this form for the total field rather than its ray-optical counterpart

$$H^t = H^g + H^d \quad (31)$$

is that the geometrical optics field H^g is $O(k^0)$ and is obviously discontinuous at the shadow boundaries. Since the total field must be continuous everywhere in space, it follows that the exact H^d must also be discontinuous. Consequently, neither of these fields can be associated with physical induced currents on the surface of the scatterer for the obvious reason that these currents produce continuous fields everywhere in space external to the scatterer.

Thus we return to (30) and interpret the scattered field H^s as proportional to the spectrum or Fourier transform of the induced current J on the scatterer. The next step is to derive a high-frequency approximation of these currents under the same assumptions as employed in GTD. Basically, we know that for a single half-plane erected at edge 1, the induced current J can be thought of as a superposition of a physical optics current J^0 and a higher order ($k^{-1/2}$) component, which we call J^1. For the truncated half-plane, i.e., the strip, we can approximate J as

$$J = J^0 + J_1^{tr} + J_2^{tr} \quad (32)$$

where J^0 is the physical optics current on the strip and J_1^{tr}, J_2^{tr} are the $O(k^{-1/2})$ current components from edges 1 and 2, respectively, truncated over the strip. Thus we can write

$$J_{1,2}^{tr} = J_{1,2}^1 - J_{1,2}^t \quad (33)$$

where J_1^1 is the $O(k^{-1/2})$ current induced on the semi-infinite half-plane 1 and J_1^t is the portion of that current for $x < -a$. We can similarly interpret the quantities with subscript 2, which are associated with half-plane 2.

The final step is to invoke the Fourier transform relationship between the scattered field and the induced current, which reads

$$H^s = -ik\frac{\exp(i(k\rho + \pi/4))}{\sqrt{8\pi k\rho}}\sin\phi\tilde{J}_x\hat{z} \quad (34)$$

where $\tilde{J}_x$ is the transform or the spectrum of J_x. Thus from (32) and (33), we can write

$$H^t = H^i + H^s = H^i + (H_1^d - H_1^p) + (H_2^d - H_2^p) + H^0 - H_1^t - H_2^t \quad (35)$$

where we have again made use of the spectral-domain interpretation of the scattered field produced by I^1 and have expressed this field as the difference between the Keller diffracted field H^d and the field H^p which is proportional to the transform of the physical optics current on the half-plane. Also, we have used the symbol H^b for the scattered field due to the physical optics current on the strip. The expression for H^b is very straightforward, and is given by

$$H^b = -ik \frac{\exp(i(k\rho + \pi/4))}{\sqrt{8\pi k\rho}} (\sin\phi)\, 4a \cdot \frac{\sin[ka(\cos\phi_0 + \cos\phi)]}{ka(\cos\phi_0 + \cos\phi)}. \quad (36)$$

Let us now compare the UAT (28) and the STD expressions (35). To facilitate this comparison, we have numerically evaluated H^b and H^u where

$$H^u = H^r[F(\xi_1^r) - \hat{F}(\xi_1^r) + F(\xi_2^r) - \hat{F}(\xi_2^r) - 1] + H_1^p + H_2^p. \quad (37)$$

Shown in Fig. 4 are the plots of H^b and H^u for a 2λ wide strip and $\rho = 50\lambda$, which is the distance to the observation point from the origin of the coordinate system located at the center of the strip. It is evident that the two quantities are virtually indistinguishable. Thus we have a simple expression for H^b which is equivalent to the collection of several involved expressions that constitute H^u.

Next, we note a conspicuous absence of the $H_{1,2}^I$ terms in (28). Although these terms can make significant contributions to the scattered field, they are not present in any of the ray-optical expressions derived to date, perhaps because it is difficult to extract them from a ray-optical approach. We demonstrate a little later that the exclusion of these terms from the scattered field can introduce significant errors in some cases.

Returning to the comparison of (28) and (35), we draw the conclusion that the application of the STD concept provides us with a simpler and more accurate expression than the UAT. In particular, we note that the expressions of each of the terms H^d, H^p, and H^b in (35) are trigonometric in nature, whereas (28) requires the evaluation of the Fresnel integrals and cancellation of numbers which are equal, opposite, and infinitely large in the vicinity of the shadow boundaries. Next, we demonstrate that the same physical interpretation can also be applied to UTD, the Kouyoumjian–Pathak uniform formula [26]. The simplification in the expression for the scattered field is equally dramatic.

B. Comparison of STD with UTD

The UTD of Kouyoumjian–Pathak has also been introduced to overcome some of the difficulties in GTD that occur at the transition regions associated with shadow and reflection boundaries. However, in contrast to UAT, the fictitious infinities in Keller diffraction coefficients are eliminated in UTD by the introduction of multiplicative factors which go to zero at the shadow boundaries such that the product has a finite discontinuity that matches the discontinuity in the geometrical optics field. As a result, the total field computed by such a modified diffraction coefficient is continuous for all observation angles.

We first present the UTD solution of the problem of diffraction by a strip of width $2a$ illuminated by an H-polarized wave

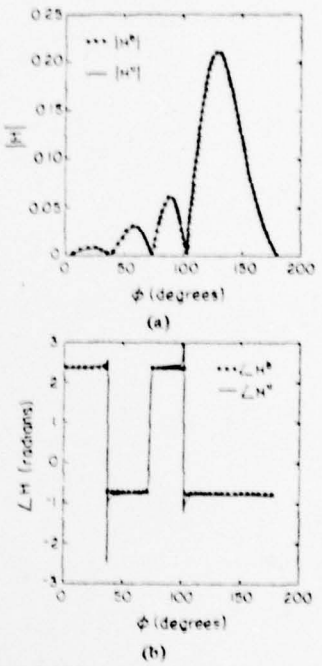

Fig. 4. Comparison of STD and UAT for a 2λ strip: (a) Magnitude of H^b (STD; cf. (36)) and magnitude of H^u (UAT; cf. (37)). (b) Phase of H^b (STD; cf. (36)) and phase of H^u (UAT; cf. (37)).

(see Fig. 2), and then show that the UTD ansatz can also be physically interpreted using the spectral approach. Furthermore, as in UAT, the UTD formulas can be improved and generalized for complex geometries in a straightforward manner.

Following the UTD formulation [26], we write the total field for $y > 0$ as

$$H^t = H^i + [\theta(-\epsilon_{r1}) + \theta(-\epsilon_{r2}) - 1]\, H^r + H_1^D + H_2^D \quad (38)$$

where H^i and H^r are given in (22) and (23), respectively; $\theta(\cdot)$ is the step function; ϵ_{r1} and ϵ_{r2} are the shadow indicators associated with half-planes 1 and 2, respectively. A shadow indicator has the value 1 in the shadow region, and 0 in the lit region. The $\theta(-\epsilon_{r1})$ and $\theta(-\epsilon_{r2})$ for this example can be written explicitly as

$$\theta(-\epsilon_{r1}) = \tfrac{1}{2} + \operatorname{sgn}[-(\pi - \phi_0) + \phi_1] \cdot \tfrac{1}{2} \quad (39a)$$

$$\theta(-\epsilon_{r2}) = \tfrac{1}{2} + \operatorname{sgn}(\pi - \phi_0 - \phi_2) \cdot \tfrac{1}{2} \quad (39b)$$

where

$$\operatorname{sgn}(x) = \frac{x}{|x|} = \begin{cases} 1, & \text{for } x > 0 \\ -1, & \text{for } x < 0 \end{cases} \quad (39c)$$

is simply a sign function.

The H_1^D and H_2^D in (38) are the diffracted fields calculated by the UTD formulas. With the modified diffraction coefficients, the Keller GTD diffracted fields $H_{1,2}^d$ as given in (25a) and (25b) can be made uniform according to UTD ansatz and become $H_{1,2}^D$, which are given below

$$H_1^D = \exp(-ika\cos\phi_0)\{-\exp(ik\rho_1)[F(k\rho_1; \phi_0 - \phi_1) \cdot \exp(-i2k\rho_1\cos^2\{(\phi_0 - \phi_1)/2\})\operatorname{sgn}(\pi - \phi_0 + \phi_1) + F(k\rho_1; \phi_1 + \phi_0)\exp(-i2k\rho_1\cos^2\{(\phi_1 + \phi_0)/2\}) \cdot \operatorname{sgn}(\phi_0 - \pi + \phi_1)]\} \quad (40a)$$

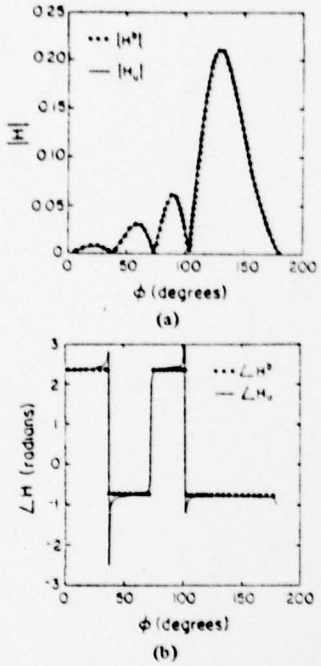

Fig. 5. Comparison of STD and UTD for a 2λ strip. (a) Magnitude of H^b (STD; cf. (36)) and magnitude of H_u (UTD; cf. (42)). (b) Phase of H^b (STD; cf. (36)), and phase of H_u (UTD; cf. (42)).

$$H_2^D = \exp(ika\cos\phi_0)\{-\exp(ik\rho_2)[F(k\rho_2;\phi_2-\phi_0)\cdot\exp(-i2k\rho_2\cos^2\{(\phi_2-\phi_0)/2\})\operatorname{sgn}(\pi+\phi_0-\phi_2)+F(k\rho_2;\phi_2+\phi_0)\exp(-i2k\rho_2\cos^2\{(\phi_2+\phi_0)/2\})\cdot\operatorname{sgn}(\pi-\phi_0-\phi_2)]\} \quad (40b)$$

where $\operatorname{sgn}(x)$ is defined in (39c) and $F(x)$ is defined in (19) with the argument given by

$$x = \sqrt{2k\rho}\left|\cos\frac{\phi\pm\phi_0}{2}\right| \quad (40c)$$

where $\rho = \rho_1$ or ρ_2, and $\phi = \phi_1$ or ϕ_2, accordingly.

In order to give a physical interpretation to the UTD formulation, we now rearrange the terms in (38) following the steps that are similar to the ones used in conjunction with (21). In UAT, these steps led to (28), which was then compared with the STD expression (35). To this end, we rewrite the total field given in (38) as

$$H^t = H^i + (H_1^d - H_1^p) + (H_2^d - H_2^p) + \{[\theta(-\epsilon_{r1}) + \theta(-\epsilon_{r2}) - 1]\cdot H^r + H_1^D - H_1^d + H_1^p + H_2^D - H_2^d + H_2^p\}. \quad (41)$$

Note that $H_{1,2}^d$ and $H_{1,2}^p$ have been added and subtracted from (38) in writing (41). H_1^d and H_2^d are given in (25a) and (25b), respectively. H_1^p and H_2^p are given in (29a) and (29b), respectively.

Following the same steps which led to H^u in (37), we obtain H_u, the UTD counterpart of H^u:

$$H_u = [\theta(-\epsilon_{r1}) + \theta(-\epsilon_{r2}) - 1]\, H^r + H_1^D - H_1^d + H_1^p + H_2^D - H_2^d + H_2^p \quad (42)$$

which may be identified as the collection of terms inside the braces { } in (41).

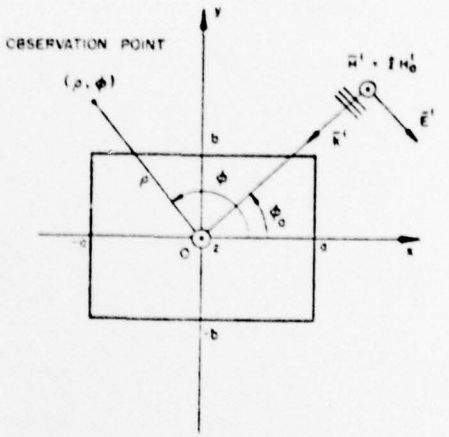

Fig. 6. Diffraction by a rectangular cylinder illuminated by an H-polarized plane wave incident at an angle ϕ_0.

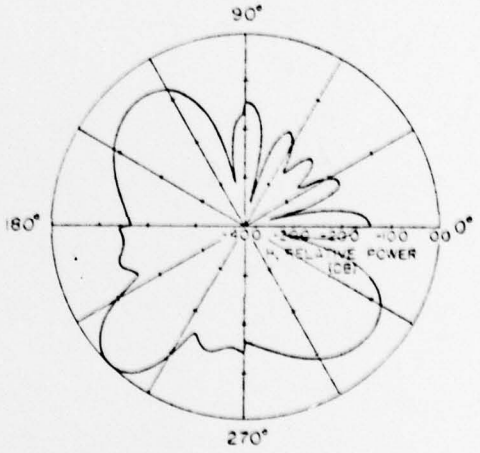

Fig. 7. GTD diffracted far-field pattern of the rectangular cylinder; $\phi_0 = \pi/4$, $a = b = 1\lambda$. Note that the discontinuities in the scattered field are on the order of 3 dB.

Shown in Fig. 5 are the plots of H^b given in (36) and H_u given in (42) for a 2λ wide strip, and $\rho = 50\lambda$, which is the distance of the observation point from the origin of the coordinate system located at the center of the strip. We have thus demonstrated that the Kouyoumjian–Pathak UTD can also be physically interpreted using the spectral concept. The simplification in the expression for the scattered field is equally dramatic, as evidenced by a comparison of H^b with H_u, the former being trigonometric and the latter involving the Fresnel integrals. Moreover, H^b is continuous throughout the entire region of observation, whereas H_u has terms with discontinuities in both the reflected and the diffracted parts of the expression.

C. Improvement of UAT and UTD

Next, we go on to show that the inclusion of $-(H_1^i + H_2^i)$ in the expression for the scattered field diffracted from edges can be very important for accurate evaluation of the field. To illustrate our point, we consider the example of a rectangular cylinder illuminated by a plane wave (see Fig. 6). Using conventional GTD uniform formulas, we obtain the scattering pattern shown in Fig. 7. The STD result (whose derivation will be presented in more detail in a later section in this

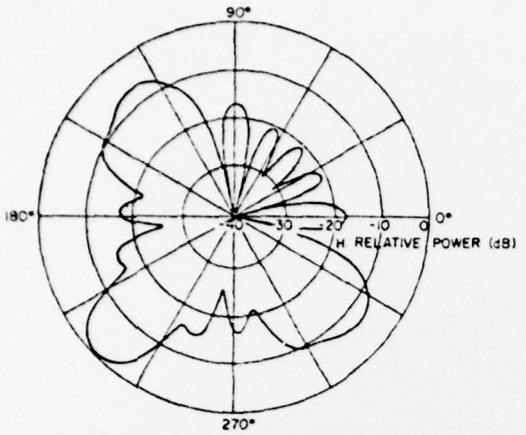

Fig. 8. Scattered far-field pattern of the rectangular cylinder using STD approach; $\phi_0 = \pi/4$, $a = b = 1\lambda$.

paper), which has been verified rigorously by comparison with the numerical computation of the scattered field, is shown in the companion diagram (Fig. 8). It is evident that the GTD results contain discontinuities (~3 dB) in the vicinity of angles $\phi = 0$, $\pi/2$, π, and $3\pi/2$, which, incidentially, are located far from the shadow boundaries. The investigation of the wedge problem also reveals that the generalization of the STD approach to wedge-type structures can be carried out in a very simple manner, and the resulting expressions are once again very simple, the Fresnel integrals being absent here, too.

In summary, we have demonstrated that the uniform GTD expressions for edge diffraction formulas can be simplified, physically interpreted, refined, and generalized using the STD concept.

IV. Systematic Improvement of Asymptotic Solutions

One of the most challenging problems in the solution of high-frequency scattering analyses is the establishment of the accuracy of the results and the refinement of the solution when the need for its improvement is clearly indicated. The difficulty in verifying whether the asymptotic expression, typically derived from the ray approach, does indeed solve the boundary value problem under consideration stems primarily from the fact that there is no obvious way to "build in" the boundary conditions in solution procedures based on ray methods. Another reason is that the high-frequency solutions are often constructed for the radiated far fields, whereas the application of the boundary conditions clearly requires the near-field information. In contrast, the integral-equation formulation for the scattering problem is based directly on the application of the boundary condition and, consequently, the boundary condition check is redundant for this approach. However, the conventional moment-method solution of integral equations is limited strictly to the low-frequency and resonance regions as the matrix size becomes unmanageably large beyond the resonance region.

In this section we will briefly outline a spectral-domain method for bridging the two approaches, viz. the integral-equation and asymptotic techniques. The hybrid method has the desirable feature that it not only verifies the accuracy of the ray solutions but provides a systematic means for improving the solution for a large class of problems of practical interest. This fact will be illustrated via a typical example, viz. plane-wave diffraction by a strip. Other cases have also been treated and may be found in [38], [39], [44], [45].

A. Development of Spectral-Domain Formulation of the Integral Equation and Its Iterative Solution

The key to combining the asymptotic solution with the integral-equation formulation lies in recognizing the fact that the Fourier transform of the induced current on a scatterer is directly related to the scattered far field and that a good approximation to this scattered field is often available from any asymptotic methods, e.g., GTD. To take advantage of these facts we choose to work with the "Fourier-transformed" or "spectral-domain" version of the integral equation rather than with the conventional spatial-domain counterpart. We begin, however, with the conventional electric-field integral equation (E-equation) for a perfectly conducting scatterer

$$(\bar{\bar{G}} * \bar{J})_t = -\bar{E}_t^i$$

$$\bar{\bar{G}} = \left(\bar{\bar{I}} + \frac{1}{k^2}\nabla\nabla\right) \exp(+ik|\bar{r} - \bar{r}'|/(4\pi|\bar{r} - \bar{r}'|) \quad (43)$$

where $\bar{\bar{G}}$ is the Green's dyadic, $\bar{\bar{I}}$ is the unit dyad, and $\bar{J}(\bar{r}')$ is the unknown induced surface current density. The subscript t signifies the tangential component of the field on the surface S of the scatterer, $\bar{E}^i$ is the incident electric field on the scatterer, and * symbolizes the convolution operation.

As a preamble to Fourier transforming (43), we first extend it over all space. To this end we define a truncation operator $\theta(\bar{A})$:

$$\theta(\bar{A}) = \int \bar{A}_t \delta(\bar{r} - \bar{r}_s)\, dr, \quad \bar{r}_s \in S \quad (44)$$

where δ is the Dirac delta function. Let $\hat{\theta}(\bar{A})$ be defined as the complementary operator

$$\hat{\theta}(\bar{A}) = \bar{A} - \theta(\bar{A}). \quad (45)$$

We can then rewrite (43)

$$\bar{\bar{G}} * \bar{J} = \theta(-\bar{E}^i) + \hat{\theta}(\bar{\bar{G}} * (\theta\bar{J})) \quad (46)$$

for all space. As indicated above, in contrast to (43), equation (46) is valid at all observation points whether on or off the surface S. Note that the integral equation (43) is embedded in (46) and that we have made use of the obvious identity $\theta\bar{J} = \bar{J}$. We have also dropped the subscript t in writing (46) because by referring to (44) we observe that the θ operator selects the tangential component of the function in its argument.

Next we Fourier transform (46) by introducing the transform relationships which are the three-dimensional versions of (5):

$$\tilde{F}(\bar{k}) = \int_{-\infty}^{\infty} F(\bar{r}) \exp(i\bar{k}\cdot\bar{r})\, d\bar{r} = \mathrm{F}[F(\bar{r})] \quad (47a)$$

and

$$F(\bar{r}) = \left(\frac{1}{2\pi}\right)^3 \int_{-\infty}^{\infty} \tilde{F}(\bar{k}) \exp(-i\bar{k}\cdot\bar{r})\, d\bar{k} = \mathrm{F}^{-1}[\tilde{F}(\bar{k})] \quad (47b)$$

with ~ on top denoting the transformed quantities.

The transformed version of (46) reads

$$\tilde{\bar{\bar{G}}}\,\tilde{\bar{J}} = -\tilde{\bar{E}}_I + \tilde{\bar{F}} \tag{48}$$

where $\tilde{\bar{F}} = \mathrm{F}[\hat{\theta}(\bar{\bar{G}} * (\theta\bar{J}))]$ and $\tilde{\bar{E}}_I$ is the transform of the tangential component of the incident field truncated on S. Note that the convolution operation in (46) is transformed into an algebraic product upon Fourier transformation.

A formal solution to (48) can now be written:

$$\tilde{\bar{J}} = \tilde{\bar{\bar{G}}}^{-1}(-\tilde{\bar{E}}_I + \tilde{\bar{F}}). \tag{49}$$

Equation (49) indicates that if we had available the Fourier transform of the scattered electric field, we could construct the solution for the induced surface current density in the transform domain by adding it to $-\tilde{\bar{E}}_I$, which is known, and by performing an algebraic division represented by $\tilde{\bar{\bar{G}}}^{-1}$. In practice, of course, $\tilde{\bar{F}}$ is not known and must be solved for along with $\tilde{\bar{J}}$ if (49) is to be used in the form as shown. However, instead of using this form, we proceed to derive an iterated form of the equation as shown below:

$$\tilde{\bar{J}}^{(n+1)} = \tilde{\bar{\bar{G}}}^{-1}(-\tilde{\bar{E}}_I + \tilde{\bar{F}}^{(n)}) \tag{50}$$

which indicates that the $(n+1)$th approximation of $\tilde{\bar{J}}$ can be derived from the nth approximation for $\tilde{\bar{F}}$. We next show how $\tilde{\bar{F}}^{(n)}$ itself can be derived from $\tilde{\bar{J}}^{(n)}$. To this end, we use the identity

$$\tilde{\bar{F}} = \mathrm{F}[\mathrm{F}^{-1}[\tilde{\bar{\bar{G}}}\tilde{\bar{J}}] - \theta(\mathrm{F}^{-1}[\tilde{\bar{\bar{G}}}\tilde{\bar{J}}])] \tag{51}$$

which may be verified by writing (51) as

$$\tilde{\bar{F}} = \mathrm{F}[\bar{\bar{G}} * \bar{J} - \theta(-\bar{E}^i)] \tag{52}$$

and using (46) to get

$$\tilde{\bar{F}} = \mathrm{F}[\hat{\theta}(\bar{\bar{G}} * (\theta\bar{J}))] \tag{53}$$

which, of course, is the definition of $\tilde{\bar{F}}$. We can now use (51) to derive the nth approximation $\tilde{\bar{F}}^{(n)}$ of $\tilde{\bar{F}}$ from the nth approximation of $\bar{J}$, i.e., $\bar{J}^{(n)}$. The relationship is written as

$$\tilde{\bar{F}}^{(n)} = \mathrm{F}[\mathrm{F}^{-1}[\tilde{\bar{\bar{G}}}\tilde{\bar{J}}^{(n)}] - \theta(\mathrm{F}^{-1}[\tilde{\bar{\bar{G}}}\tilde{\bar{J}}^{(n)}])]. \tag{54}$$

The desired iteration relating $\tilde{\bar{J}}^{(n+1)}$ and $\tilde{\bar{J}}^{(n)}$ may now be written. Using (50) and (54),

$$\tilde{\bar{J}}^{(n+1)} = \tilde{\bar{\bar{G}}}^{-1}[-\tilde{\bar{E}}_I + \mathrm{F}[\mathrm{F}^{-1}[\tilde{\bar{\bar{G}}}\tilde{\bar{J}}^{(n)}] - \theta(\mathrm{F}^{-1}[\tilde{\bar{\bar{G}}}\tilde{\bar{J}}^{(n)}])]]. \tag{55}$$

B. Procedure for Applying the Iterative Method

The step-by-step procedure for constructing the solution of the transformed surface current $\tilde{\bar{J}}$ will now be given.

1) Begin with an estimate of $\tilde{\bar{J}}^{(0)}$, which is the Fourier transform of the induced surface current, or equivalently, the scattered *far field* within a known multiplicative factor. That the far scattered field is directly related to the Fourier transform of the induced current is well known in electromagnetics and has been derived in several standard texts (see for instance [46, eq. (2.23b)]). Typically, the initial approximation for $\tilde{\bar{J}}$, viz. $\tilde{\bar{J}}^{(0)}$, can be obtained as follows:

a) Estimate $\tilde{\bar{F}}$, the Fourier transform of the scattered field $\bar{F}$ outside the scatterer, using GTD or other asymptotic solutions.[4]

b) Subtract $\tilde{\bar{E}}_I$, the Fourier transform of the tangential component of the incident electric field truncated to the surface of the scatterer.

c) Multiply the result of Step b) by $\tilde{\bar{\bar{G}}}^{-1}$. Note that $\tilde{\bar{\bar{G}}}^{-1}$ is known and the operation is algebraic. The Fourier transform is typically done numerically using the fast Fourier transform (FFT).

d) Take the inverse Fourier transform of the result of Step c), truncate it to the surface of the scatterer and then Fourier transform to obtain $\tilde{\bar{J}}^{(0)}$, the initial approximation for $\tilde{\bar{J}}$.

2) Multiply $\tilde{\bar{J}}^{(0)}$ by $\tilde{\bar{\bar{G}}}$, the known transform of the Green's Dyadic. Note this involves algebraic multiplication and not the usual time-consuming convolution operation.

3) Take the inverse Fourier transform of the product $\tilde{\bar{\bar{G}}}\tilde{\bar{J}}^{(0)}$ using both *visible and invisible ranges*.

4) Apply the truncation-projection operator θ to $\mathrm{F}^{-1}[\tilde{\bar{\bar{G}}}\tilde{\bar{J}}^{(0)}]$, which gives the approximation to the tangential component of the scattered electric field $\bar{E}_t^s$ on the surface S. The accuracy of the solution can be conveniently checked at this point by verifying the satisfaction of the boundary condition by the tangential component of $\bar{E}^s$, viz. $\{\bar{E}_t^s = -\bar{E}_t^i\}$ on S. As mentioned in the introduction, this is an important feature of the method.

5) Subtract $\theta(\mathrm{F}^{-1}[\tilde{\bar{\bar{G}}}\tilde{\bar{J}}^{(0)}])$ from the total $\mathrm{F}^{-1}[\tilde{\bar{\bar{G}}}\tilde{\bar{J}}^{(0)}]$ already evaluated.

6) Take the Fourier transform of the difference obtained in Step 5.

7) Subtract $\tilde{\bar{E}}_I$, the Fourier transform of the tangential component of the incident electric field truncated on the surface, from the result in Step 6.

8) Multiply the result obtained in Step 7 by $\tilde{\bar{\bar{G}}}^{-1}$. Note that $\tilde{\bar{\bar{G}}}^{-1}$ is also known and the operation is again algebraic as in Step 2. The result thus obtained is $\tilde{\bar{J}}^{(1)}$, which is the first iteration of the scattered far field.

9) Take the inverse Fourier transform of $\tilde{\bar{J}}^{(1)}$ obtained in Step 8 and evaluate it on S to get the desired induced surface current on the scatterer. In other words, perform the operation $\theta(\mathrm{F}^{-1}[\tilde{\bar{J}}^{(1)}])$. For an exact solution, this operation is redundant, since $\bar{J} = \theta\bar{J}$, and hence, $\theta(\mathrm{F}^{-1}[\mathrm{F}[\theta\bar{J}]]) = \theta\theta\bar{J} = \bar{J}$. However, the Fourier inversion of an nth approximate solution $\tilde{\bar{J}}^{(n)}$ will not give rise to a current distribution that is nonzero except on S. This step provides a test for the accuracy and for the convergence of the approximate solution by comparing the approximate $\tilde{\bar{J}}^{(0)}$ with $\mathrm{F}[\theta(\mathrm{F}^{-1}[\tilde{\bar{J}}^{(1)}])]$.

10) Take $\mathrm{F}[\theta(\mathrm{F}^{-1}[\tilde{\bar{J}}^{(1)}])]$ to derive an *improved* approximation for $\tilde{\bar{J}}^{(1)}$.

11) Repeat as necessary using, for instance, the *improved* $\tilde{\bar{J}}^{(1)}$ from Step 10 in the iteration (55) to generate the next higher order approximation $\tilde{\bar{J}}^{(2)}$.

[4] Note that GTD (Keller's) solutions may either have singularities or may be in error near shadow and reflection boundaries or at caustics, and the UTD [35] and the UAT [35] that are employed to repair GTD break down at caustics. The STD, on the other hand, is uniform for all observation angles. The criterion for choosing any of these asymptotic forms of solution is convenience of computation for desired accuracy. For a comparative evaluation of the accuracy of the GTD, UTD, UAT, and STD, the reader is referred to [35].

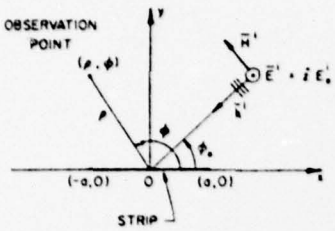

Fig. 9. Diffraction by a strip illuminated by an E-wave.

We now show in some detail the application of the iteration procedure just described to a two-dimensional scattering problem, viz. the diffraction by a strip.

C. Diffraction by a Strip

In the last section, we presented a general iteration method for obtaining solution of the integral equation in the transform domain with the GTD or other high-frequency solution as the zeroth-order approximation. This iteration method not only allows us to improve on the GTD or similar solutions but also provides a convenient means for testing the satisfaction of the boundary conditions on the surface of the scatterer. Furthermore, the method yields not only the far field but also the induced surface-current distribution, a feature not readily available in some other high-frequency techniques.

The application of the general procedure outlined in the last section is illustrated in this section by using it to solve the two-dimensional problem of a plane-wave diffraction by a finite screen or a strip. This problem was chosen for the following reasons: It is shown that when the angle of incidence is normal or near normal, the GTD solution accurately satisfies the boundary condition $\bar{E}_{\tan} = 0$ on the strip even when the multiple interaction between the two edges of the strip is neglected. However, it is found that when the angle of incidence is near grazing, the GTD solution is quite unsatisfactory, while the iterated solution generated by the hybrid technique does display the correct behavior.

The geometry of the electromagnetic scattering problem involving a perfectly conducting infinite strip of zero thickness illuminated by a uniform plane wave, whose electric intensity vector is oriented parallel to the edges of the strip, is depicted in Fig. 9. For convenience of analysis, an arbitrary incident wave can always be decomposed into two components with respect to the z-axis, namely, TM_z (E-wave) and TE_z (H-wave). In the following discussion we consider the E-wave case only; the H-wave case can be solved in a similar manner by considering $\bar{H}^i = \hat{z} H_0^i$.

The incident field is given by

$$E_z^i(\rho, \phi) = \exp(-ik(x \cos \phi_0 + y \sin \phi_0)) \tag{56}$$

where the $\exp(-i\omega t)$ time dependence is understood.

The integral-equation formulation [47] for the problem at hand takes the form

$$-E_z^i(x) = \int_{-a}^{a} J_z(x') G(x - x')\, dx', \quad x \in [-a, a] \tag{57}$$

where $J_z(x')$ is the algebraic sum of the induced surface current densities on the top and the bottom surfaces of the thin strip. The kernel G is the two-dimensional free-space Green's function given by

$$G(x - x') = \frac{i}{4} H_0^{(1)}(k_0 |x - x'|) \tag{58}$$

where $H_0^{(1)}$ is the Hankel function of the first kind of order zero, and $k_0 = 2\pi/\lambda$ is the free-space propagation constant. Note that (57) is the conventional integral equation which equates the integral representation of the tangential component of the scattered E-field radiated by the induced surface current density to the negative of the tangential component of the incident E-field on the surface of the perfectly conducting scatterer as required by the satisfaction of the boundary condition. Hence, equation (57) is valid on the strip only.

An extended integral equation that is valid for all x can be obtained by including the scattered fields outside the strip as well. If the scattered field on the interval $(-\infty, -a)$ is designated by $F_1(x)$ and the scattered field on the interval (a, ∞) is designated by $F_2(x)$, then the extended form of (57) becomes

$$\int_{-a}^{a} J_z(x') G(x - x')\, dx' = \theta(-E_z^i(x)) + F_1(x) + F_2(x) \tag{59}$$

where θ is defined in (44).

Since the Fourier transform of the induced surface current density can be related to the far field, equation (59) is Fourier transformed to give

$$\tilde{J}_z(\alpha)\, \tilde{G}(\alpha) = \widetilde{\theta(-E_z^i)}(\alpha) + \tilde{F}_1(\alpha) + \tilde{F}_2(\alpha) \tag{60}$$

where $\sim$ on top indicates the Fourier transform as defined in (47) with α as the one-dimensional transform variable replacing $\bar{k}$.

The Fourier transform of the two-dimensional Green's function in (60) takes the form

$$\tilde{G}(\alpha) = \frac{i}{2\sqrt{k_0^2 - \alpha^2}}. \tag{61}$$

Note that (60) is an algebraic equation in the spectral domain in contrast to the convolution form of the integral equation (59) in the spatial domain. The reason for working in the spectral domain will become clear when the method of solution for (60) is developed. Following the procedure discussed in the last section and in terms of the notations introduced in the present problem, we proceed as follows.

1) Obtain $\tilde{J}_z^{(0)}(\alpha)$, the initial approximation of the Fourier transform of the induced surface current density, or equivalently, the scattered *far field* within a known multiplicative factor, as follows.

1.1) Find the expressions for the first estimate of $\tilde{F}_1^{(0)}(\alpha) + \tilde{F}_2^{(0)}(\alpha)$. Note that GTD may be used to get closed-form expressions for $\tilde{F}_1^{(0)}(\alpha)$ and $\tilde{F}_2^{(0)}(\alpha)$ since these can be obtained from the GTD solutions to the two half-plane problems as shown in Fig. 10. The expressions for $\tilde{F}_1^{(0)}$ and $\tilde{F}_2^{(0)}$ as

Fig. 10. $F_1(x)$ can be approximated by the GTD solution to the half-plane problem (a) shown on the left-hand side; $F_2(x)$ can be approximated by the GTD solution to the half-plane problem (b) shown on the right-hand side.

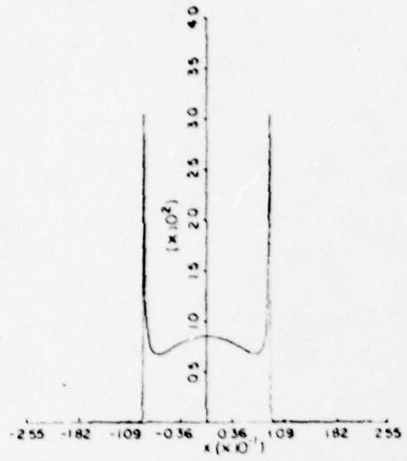

Fig. 11. Magnitude of the induced surface current density distribution normalized to $(ik_0Z_0)^{-1}$ on the strip of $ka = 4$ (1.273λ wide), $\phi_0 = 90°$.

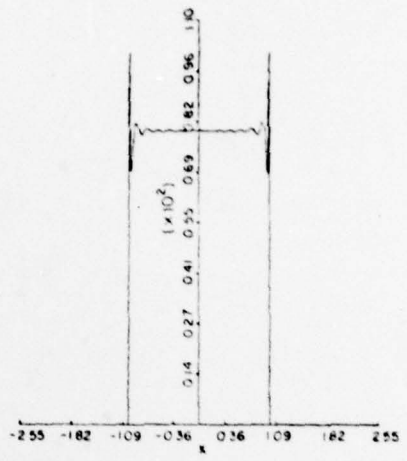

Fig. 12. Magnitude of the induced surface current density distribution normalized to $(ik_0Z_0)^{-1}$ on the strip of $ka = 40$ (12.73λ wide), $\phi_0 = 90°$.

obtained from GTD read

$$\tilde{F}_1^{(0)}(\alpha) = \frac{i}{2}\left[\exp(ika\cos\phi_0)\sqrt{8k}\sin\frac{\phi_0}{2}\right] \cdot \frac{\exp(ia\alpha)}{(\alpha + k\cos\phi_0)\sqrt{\alpha + k}} - \frac{i\exp(ia(\alpha + k\cos\phi_0))}{(\alpha + k\cos\phi_0)} \quad (62)$$

and

$$\tilde{F}_2^{(0)}(\alpha) = -\frac{i}{2}\left[\exp(-ika\cos\phi_0)\sqrt{8k}\cos\frac{\phi_0}{2}\right] \cdot \frac{\exp(-i\alpha a)}{(\alpha + k\cos\phi_0)\sqrt{k - \alpha}} + \frac{i\exp(-ia(\alpha + k\cos\phi_0))}{(\alpha + k\cos\phi_0)}. \quad (63)$$

Note that these expressions are free of singularities for all α.

1.2) Solve for the initial approximation of $\tilde{J}_z(\alpha)$, $\tilde{J}_z^{(0)}(\alpha)$, by carrying out the operations shown below:

$$\tilde{J}_z^{(0)}(\alpha) = F\left[\theta\left(F^{-1}\left[\frac{\widetilde{\theta(-E^i)}(\alpha) + \tilde{F}_1^{(0)}(\alpha) + \tilde{F}_2^{(0)}(\alpha)}{\tilde{G}(\alpha)}\right]\right)\right]. \quad (64)$$

2) Use (55) to further improve the solution as necessary.

The check for satisfaction of the integral equation can be applied very simply by computing $\tilde{J}(\alpha)\,\tilde{G}(\alpha)$, taking its inverse Fourier transform, and verifying how well it approaches $-E^i$ on the surface of the scatterer.

Fig. 11 shows the calculated induced surface current density distribution on the strip with $ka = 4$ (1.3λ wide) for normal incidence. Note that the current density becomes large at the edges, as it should for E-wave incidence, although no specific condition was enforced at the edges, nor any special care exercised. Note also that the approximate current is confined essentially on the surface of the strip and extends very little outside of this surface. Thus the solution in this case is very close to the true solution, and this is easily verified by truncating the current density, computing the scattered field it radiates on the strip, and verifying that the scattered field is indeed very nearly equal to $-E^i$.

Fig. 12 depicts the result for $ka = 40$, i.e., a 13λ strip. Note that the peak in the center is no longer present and the current

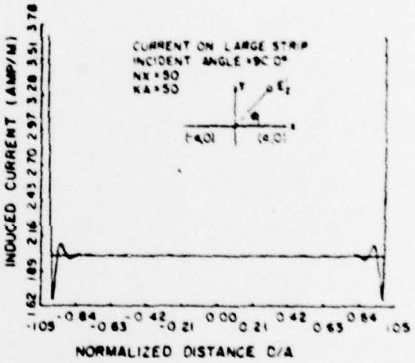

Fig. 13. Moment-method (applied in the spectral domain) solution of the magnitude of the induced surface current density distribution normalized to $1/Z_0$ on the strip of $ka = 50$ (15.92λ wide), $\phi_i = 90°$.

there approaches that given by the physical optics approximation. There are now more oscillations, however, and the current density has a sharp dip before rising to infinity at the edges.

Fig. 13 displays the moment method applied in the sprectral-domain solution [19] and the comparison with the one obtained here is quite favorable.

Fig. 14 exhibits the satisfaction of the boundary condition after one iteration. As mentioned before, such a test is not available in the conventional GTD approach.

Let us next turn to the interesting case of a near grazing incident where the zeroth-order current density has a long tail extending beyond the edge of the strip (see Fig. 15). This result is to be expected since the two half-plane GTD solutions used in the zeroth-order approximation represent a poor approximation for the induced current for shallow incidence angles. If this tail is truncated, the remaining portion of the current density on the strip produces a scattered field on the surface of the strip which is significantly different from $-E^i$, where $|E^i| = 1$, as may be seen from Fig. 16.

Fig. 17 shows the effect of one iteration on the zeroth-order GTD solution shown in Fig. 15. Note that the current density is significantly altered in the neighborhood of the shadowed

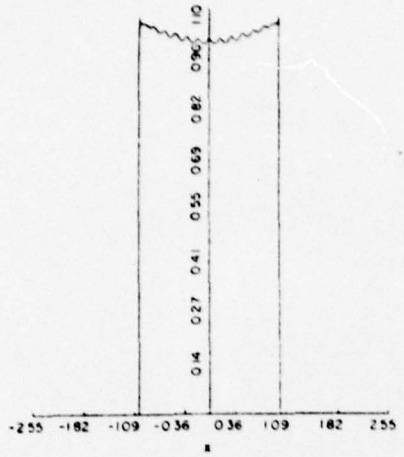

Fig. 14. Magnitude of the scattered E-field evaluated on the strip of $ka = 40, \phi_0 = 90^\circ$ (one iteration).

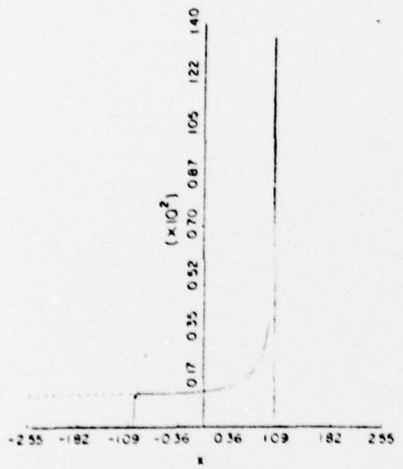

Fig. 15. Magnitude of the induced surface current density distribution normalized to $(ik_0Z_0)^{-1}$ on the strip of $ka = 40, \phi_0 = 10^\circ$ (no iteration).

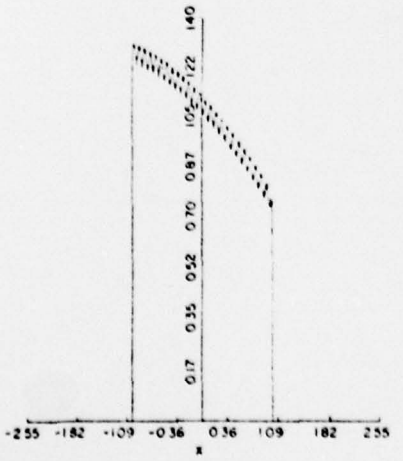

Fig. 16. Magnitude of the scattered E-field evaluated on the strip of $ka = 40, \phi_0 = 10^\circ$ (no iteration).

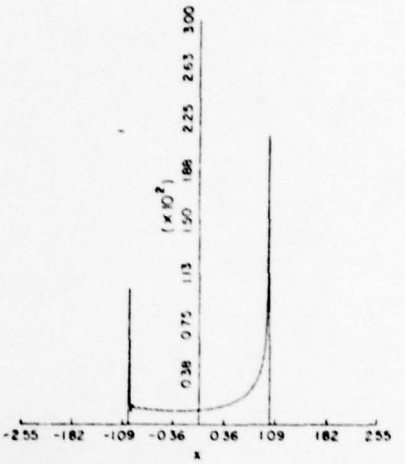

Fig. 17. Magnitude of the induced surface current density distribution normalized to $(ik_0Z_0)^{-1}$ on the strip of $ka = 40, \phi_0 = 10^\circ$ (one iteration).

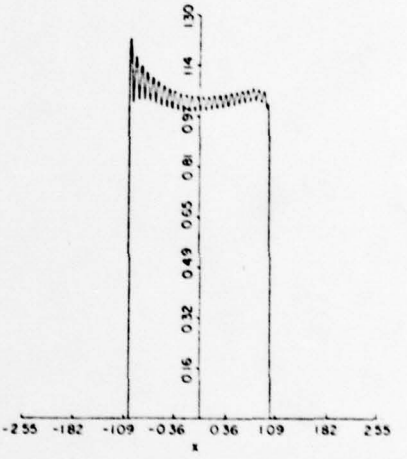

Fig. 18. Magnitude of the scattered E-field evaluated on the strip of $ka = 40, \phi_0 = 10^\circ$ (one iteration).

edge, demonstrating the fact that even with a relatively poor initial guess, the convergence is quite rapid in this case.

To see that this is indeed an improved solution, the truncated portion of it is used to calculate the scattered field. It is observed that the satisfaction of the boundary condition has been improved as shown in Fig. 18.

To verify the convergence of the solution numerically, one more iteration is performed and the result is depicted in Fig. 19. Note that the shape of the surface current density does not change much which indicates a settling down of the solution has occurred. Also, note that the tail extending outside of the strip has been reduced to an insignificant quantity, which, when truncated, will produce little effect on the scattered field on the surface of the strip.

To further validate the solution, the moment-method solution [19], of the same problem with slightly different parameters is shown in Fig. 20 for a comparison. Again, the agreement is good. However, in terms of computational efficiency, the present method is far superior to the moment-method solution for the accuracy realized.

To recapitulate, the strip problem has been solved by a combination of the integral equation and asymptotic high-

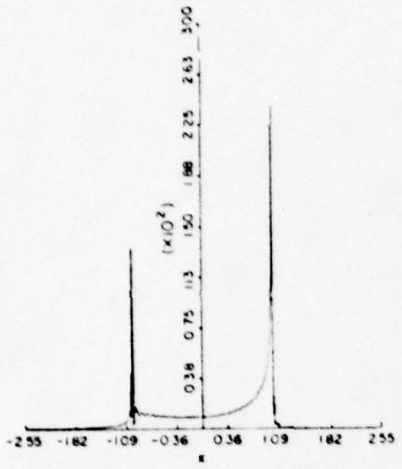

Fig. 19. Magnitude of the induced surface current density distribution normalized to $(ik_0Z_0)^{-1}$ on the strip of $ka = 40$, $\phi_0 = 10°$ (two iterations).

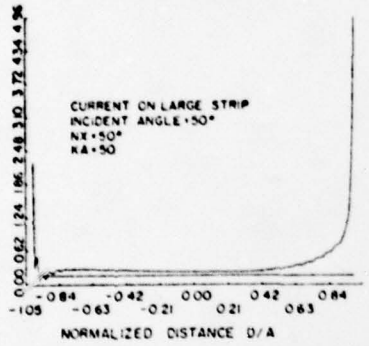

Fig. 20. Moment-method (applied in the spectral domain) solution of the magnitude of the induced surface current density distribution normlized to $1/Z_0$ on the strip of $ka = 50$, $\phi_0 = 5°$.

frequency techniques. Formulation of the intergral equation in the Fourier transform domain allows one to conveniently obtain the zeroth-order approximation to the transformed unknown surface current density from the solution of two half-plane problems.

Higher order solutions have been obtained via the iteration steps outlined above, and the numerical convergence has been demonstrated. The iteration process generates the proper edge singularities even when they are not present in the original approximation, e.g., physical optics. However, additional iterations are necessary in that case. Validity of the solution has been substantiated by numerically verifying the satisfaction of the boundary condition to within a close tolerance.

V. Diffraction by a Rectangular Cylinder

Next we consider a scattering problem involving multiple edges, e.g., a rectangular cylinder. This example is chosen for the purpose of illustrating the ease of application of the spectral-domain approach to problems of this type and to demonstrate the nonlocal behavior of the edge diffraction phenomenon. The solution to this problem has been constructed using the STD formula (35) given in Section III and the result obtained has been found to be very satisfactory. However, for the sake of illustrating the point alluded to in Section III regarding the potential of the STD approach with

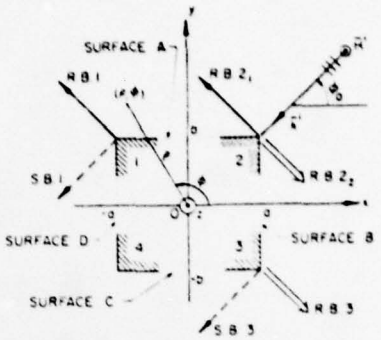

Fig. 21. For the angle of incidence ϕ_0 as shown, wedges 1, 2, and 3 are illuminated while wedge 4 is in the dark.

regard to the refinement of GTD solution, it will perhaps be more helpful to return to the conventional GTD expression for multiple edge diffraction, use it as a starting point, and then improve it via an iteration procedure based on the spectral approach.

The geometry of the problem is shown in Fig. 21. We note that the wedges 1, 2, and 3 and faces A and B are illuminated by the incident wave, while the faces C and D and the wedge 4 are in the shadow. Let us first consider the hemisphere above the face A. The contribution to the scattered field in this region comes from the two lit surfaces and rays diffracted by the wedges 1, 2, and 3. To derive a first approximation to the asymptotic expression for the far field scattered by the cylinder, we may use Keller's coefficients for the diffraction by the three wedges. From wedge 1 we have, for instance,

$$H_{z1}^{d} \sim \exp\left(-ik(-a\cos\phi_0 + b\sin\phi_0)\right)\frac{\exp(ik\rho)}{\sqrt{\rho}}\frac{\exp(i\pi/4)}{\sqrt{2\pi k}} \cdot \left\{\frac{2/3\sin 2\pi/3\exp(ika\cos\phi)\exp(-ikb\sin\phi)}{\cos 2\pi/3 - \cos 2/3(\phi - \phi_0)} + \frac{2/3\sin 2\pi/3\exp(ika\cos\phi)\exp(-ikb\sin\phi)}{\cos 2\pi/3 - \cos 2/3(\phi + \phi_0)}\right\} \tag{65}$$

where $0 \leq \phi_0 < \pi/2$ and $0 \leq \phi < 3\pi/2$. Similar expressions can be readily obtained for the wedges 2 and 3 [40]. Note that the scattered field from wedge 3 is restricted in the angular region $0 < \phi \leq \pi/2$ and $\pi \leq \phi \leq 2\pi$ for $0 \leq \phi_0 \leq \pi/2$. Hence, in the upper hemisphere only one-half of the angular range is illuminated by the scattered field from wedge 3, if Keller's formula for an *infinite* wedge is used to derive an approximation to this scattered field. Another rather important and common feature of the Keller expressions for the wedge-diffracted fields as given, for instance, by (65), is that these formulas predict fictitious infinities in the scattered fields at the shadow and reflection boundaries. One could, of course, completely eliminate these infinities by employing the spectral concepts and deriving the scattered far field from the transform of an approximation to the induced surface current, comprising the physical optics and fringe currents. This transform, being associated with a function with finite support, is always bounded and consequently free of the singular behavior present in (65).

As an alternative we may also employ one of the available uniform theories [30], [29] that provide smooth and bounded transition through the reflection and shadow boundaries. It is

fortuitous, however, that the aggregate contribution of the infinities from the individual wedges cancels out exactly when their contributions are superimposed. This occurs because of the unique symmetries of the geometry of the rectangular cylinder under consideration. Hence, no special care is required in this example at the transition regions. The diffracted far fields computed by using the Keller formulas for wedge diffraction are shown in Fig. 7. It is evident that the pattern is discontinuous at 0°, 90°, 180°, and 270°. As explained in Section III, this behavior is attributable to the assumption that the edge diffraction phenomenon is local which prompts the use of infinite wedge diffraction coefficients that yield a nonzero scattered field only in the region external to the wedge and, hence, produce discontinuous fields supported by induced surface currents that extend to infinity along the wedge surfaces.

To refine this far-field asymptotic solution, we may now proceed to apply the iterative procedure described by (55). To this end, we first introduce in Fourier transform the variable $\alpha = k \cos \phi$ and express the far scattered field in the hemispherical region defined by $0 < \phi < \pi$ in terms of α. We employ analytical continuation of the expressions for the wedge-diffracted fields to determine the Fourier transform in the range $|\alpha| > k$ by substituting appropriate complex values for ϕ. One of the chief advantages of using the available expressions for the asymptotic solution as a starting point for the iterative procedure is that the approximate analytical expression is convenient for estimating the scattered far field, both in the visible and invisible ranges. By Fourier inversion of the scattered E-field at infinity, we can derive the tangential E-field on a planar surface tangential to the face A. If this computed near field were to satisfy the boundary condition that the tangential E-field on surface A equal the negative of $\overline{E^i}$, and the similar situation is repeated for other faces, we would conclude that the solution so derived is an accurate one. However, we would not expect that to be true for the solution represented by (65), since, as pointed out earlier, this expression produces discontinuities at some angles of observation. Nevertheless, this solution provides a very good zeroth-order estimate for $\tilde{\bar{F}}^{(0)}$ which is readily derived by taking the transform of the near field derived in the plane of the surface A, after deleting the portion of the field that corresponds to the surface A of the scatterer, and repeating the same procedure for the other faces as well. In following this procedure, we effectively compute

$$F(F^{-1}[\tilde{\bar{G}}\tilde{\bar{J}}^{(0)}] - \Theta\{F^{-1}[\tilde{\bar{G}}\tilde{\bar{J}}^{(0)}]\})$$

which is an approximation to $\tilde{\bar{F}}$ derived by using $\tilde{\bar{J}}^{(0)}$. The next order of approximation to $\tilde{\bar{J}}$ is now readily obtained from (55). This quantity is Fourier inverted four times to calculate the tangential H-field on the four faces of the cylinder and the surface current on these faces is Fourier transformed again to derive the far-field pattern. The iterated far-field pattern $\tilde{\bar{J}}^{(1)}$ is shown in Fig. 8; the disappearance of the discontinuities at 0, $\pi/2$, $3\pi/2$, etc. is immediately evident from this plot. This result has also been verified by a few other workers who have followed different procedures than those outlined here [48]. Recall, however, that the method outlined here provides a convenient "built-in" check for the satisfaction of the boundary condition and an independent check is not altogether necessary to establish the accuracy of the solution.

VI. Application of Moment Method in the Transform Domain

A second approach to handling (48) would be to employ the Galerkin procedure in the transform domain [39]. One may write

$$\tilde{\bar{J}} \simeq \tilde{\bar{J}}^{(0)} + \sum C_p \tilde{\bar{J}}_p \tag{66}$$

where $\tilde{\bar{J}}^{(0)}$ is the transform of the approximate solution derived from a suitable asymptotic formula for the scattered field, and $\tilde{\bar{J}}_p$ represents a set of basis functions in the transform domain. Typically, there are certain angular regions in the far field where the asymptotic solutions require refinement. One may choose to concentrate the basis functions in these regions in the transform domain. Alternatively, the $\tilde{\bar{J}}_p$'s could be chosen as the transforms of a suitable set of basis functions in the space domain, and the location (support) of these subdomain basis functions may be selected to coincide with transition regions or corners, etc., where the canonical solution of the asymptotic solution may require refinement.

In either case, the problem of determining $\tilde{\bar{J}}$ may be reduced to that of finding the unknown coefficients C_p such that (66) satisfies (48). The Galerkin procedure provides a way for accomplishing this, as we will soon see. This technique also has the advantage that the other unknown in (48), viz. $\tilde{\bar{F}}$ is conveniently eliminated from this equation upon application of Galerkin's method. We demonstrate this fact in the manipulations presented below.

Substituting (66) in (48) and taking a scalar product of the resulting equation with a set of suitable testing functions $\tilde{\bar{W}}_q$, we arrive at

$$\sum C_p \langle \tilde{\bar{W}}_q, \tilde{\bar{\bar{G}}}\tilde{\bar{J}}_p \rangle = -\langle \tilde{\bar{W}}_q, \tilde{\bar{E}}_I \rangle + \langle \tilde{\bar{W}}_q, \tilde{\bar{F}} \rangle \tag{67}$$

where $\langle , \rangle$ is the scalar or inner product. If we now choose $\tilde{\bar{W}}_q$ to be transforms of functions which are nonzero only on the surface of the scatterer, then the scalar product $\langle \tilde{\bar{W}}_q, \tilde{\bar{F}} \rangle$ can be shown to vanish. To show this, one uses Parseval's theorem and transforms the scalar product of $\tilde{\bar{W}}_q$ and $\tilde{\bar{F}}$ in terms of a similar product of their counterparts in the space domain. Since the inverse transforms of $\tilde{\bar{W}}_q$ and $\tilde{\bar{F}}$ exist in complementary regions, viz. on the surface of the scatterer and in the region complementary to this surface, respectively, one finds that their scalar product is identically zero. One can now proceed in the usual manner to solve for the coefficients C_p by solving the matrix equation represented by (67) with the term $\langle \tilde{\bar{W}}_q, \tilde{\bar{F}} \rangle$ deleted. It is evident that the use of this method would be practical only when relatively few terms are needed in (66) to modify the available asymptotic solution; however, this is typically the situation for many problems. It should also be noted that (67) represents a direct check on the satisfaction of the boundary condition, in the sense of moments. The choice of $\tilde{\bar{W}}_p$'s is governed by the locations on the surfaces of the scatterer where these boundary conditions are applied. Typically these will be the zones where the asymptotic solution might be inaccurate, e.g., the transition region between the lit and shadow regions.

To illustrate the procedure we consider a smooth convex surface with no wedges—a circular cylinder. One of the important attributes of this canonical geometry is that it permits convenient comparison with the exact series solution available for the representation of scattered fields from this structure.

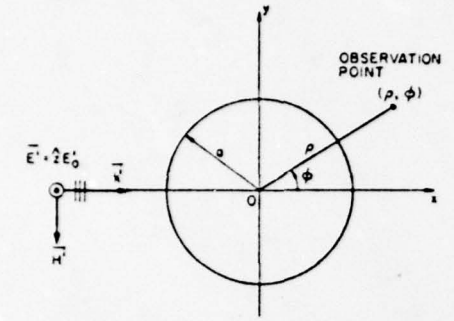

Fig. 22. Diffraction by a circular cylinder illuminated by an E-wave incident along the x-axis.

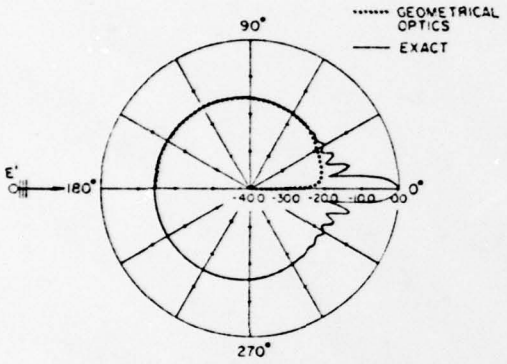

Fig. 23. Geometrical optics scattered far-field pattern in dB of a circular cylinder with radius $a = 3\lambda$.

The geometry of the problem is shown in Fig. 22. We consider the case of an E-polarized wave incident from $\phi = 180°$.

The first step in attacking the problem is to use a geometrical optical approach to derive the far scattered field. When this is done, one obtains the dotted curve in Fig. 23 which also exhibits the exact series solution for the scattered field as a solid curve. It is evident that in the range $-60° < \phi < 60°$ the GO solution is not adequate. This is not totally surprising since it is well known that creeping-wave contributions need to be included in the scattered field expression in the shadow and transition regions. Rather than following this procedure, we will now show how the Galerkin method can be readily and conveniently applied to this problem to derive an accurate solution.

To this end we consider, as a first step, the behavior of the scattered field on a surface erected in juxtaposition to the cylinder at the point $x = a$, the farthest point away from the incident field. Referring to Fig. 24, in the deep shadow region, say $|y| < 2$, we expect the scattered field $E_z^s = -E_z^i$ to be a very good approximation. On the other hand, when we go far onto the lit region on this surface, say for $|y| > 6$, we expect the E_z^s to be described adequately by the GO formulas. If we had a good estimate of the scattered field behavior in the transition region $2 < |y| < 6$, we would be able to get a good representation of the excess scattered field (over and above the GO field) on the entire surface at $x = a$. We should then be able to compute the field radiated in the rhs of the cylinder by this excess field using the concept of Huyghens' source and use this radiated field to fill in the gap between the GO pattern and the true pattern.

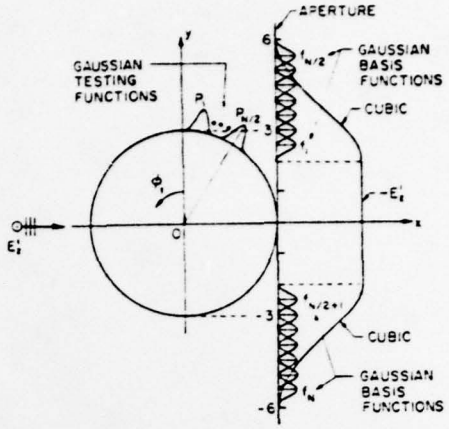

Fig. 24. Locations of the basis functions on the aperture and the testing functions on the surface of the obstacle.

To derive the E_z^s field in the transition region, we first interpolate the magnitude of this field from E^i at $|y| = 2$, to 0 at $y = 6$ and the phase from π at $|y| = 2$, to the GO phase at $|y| = 6$. Next we introduce a set of basis functions, with undetermined coefficients, to describe the correction to the interpolated E_z^s field at the plane $x = a$, $2 < |y| < 6$. To determine these coefficients, we apply the concept of Galerkin's method in the spectral domain as briefly outlined in the last section. In the example being considered here, the transforms of the basis functions play the role of $\tilde{J}_p$ in (66), and the zeroth-order scattered far-field $\tilde{\bar{f}}^{(0)}$ is obtained by adding the contributions of GO and the approximate excess E_z^s-field derived from the interpolation procedure just described.

The choice of the testing functions $\tilde{W}_q$ in (67) is suggested by the fact that the error in the high-frequency asymptotic solution is mostly concentrated around the transition region on the surface of the cylinder, i.e., in the neighborhood of the junction between the lit and shadow regions. Thus a suitable choice for the testing functions would be to locate them at the transition region as shown in Fig. 24, where the location of the basis functions is also shown. Note that we need not be restricted in our choice for the location of these functions by demanding that they have a common support, although this is almost always the case in the conventional moment or Galerkin methods. We may also note from Fig. 24 that the shape of the basis and testing functions are both Gaussian. Since we are dealing with transforms, this choice is not only convenient for deriving the Fourier transformations $\tilde{J}_p$ and $\tilde{W}_q$, but is also desirable from a numerical point of view because the transforms are not oscillatory as they would be for a pulse or triangular basis. This feature is important when numerically computing the scalar products $\langle \tilde{J}_p, \tilde{W}_q \rangle$ needed for the determination of the unknown coefficients C_p.

Only a few (3 to 7) unknowns C_p are needed to derive an accurate solution for both the radiated far field and the surface current on the cylinder. The accuracy itself can be verified by computing the tangential E-field on the surface via Fourier inversion of the hemispherical far-field pattern centered around the point to be tested. This procedure is also used to compute the surface current distribution from the knowledge of the scattered H-field at large distances. Of course an independent check is available for this problem via

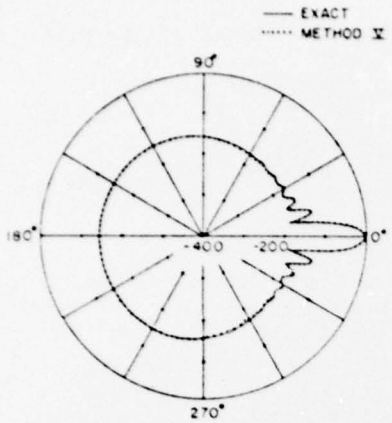

Fig. 25. Scattered far-field pattern in dB of a circular cylinder with radius $a = 3\lambda$ obtained by Galerkin's method.

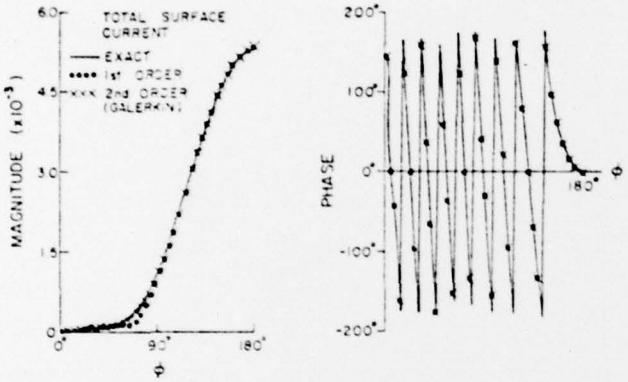

Fig. 26. Total surface current on a perfectly conducting circular cylinder with radius $a = 3\lambda$.

the exact series solution. A comparison of the Galerkin solution and the exact series solution is shown in Figs. 25 and 26 to illustrate the highly accurate nature of the Galerkin solution. In fact, the solution is almost identical to the exact solution except for a slight error in the transition region, even without the Galerkin refinement, as evidenced by the dotted curve in Fig. 26 which exhibits this case.

VII. Concluding Remarks

In addition to the representative problems discussed here, the spectral-domain approach has been found useful for other electromagnetic scattering and radiation problems of considerable interest [38], [49]. It has been applied to the problems of electromagnetic scattering by staggered half plane, a finite plate [38], a cylindrical shell [49] etc. The spectral-domain procedure for testing the accuracy of high-frequency solutions also has been applied to a number of problems of practical interest. One such example is the canonical problem of a corner in a thin plate for which an asymptotic solution was recently derived by Albertsen [50], using a multiple Wiener-Hopf procedure. Testing his solution for the satisfaction of the boundary condition that the tangential electric field be zero on the plate, one finds that the solution satisfies the boundary condition only approximately and contains some extraneous infinities that must be removed. Even so, the solution in its original form represents a good starting point for deriving improved, iterated solutions for the quarter-plane problem, and both the surface current and the far fields can be improved via the spectral-domain approach.

As another example, we quote the problem of constructing the Green's function for a magnetic dipole radiating in the presence of a smooth curved surface, e.g., a cylinder or a cone. The conventional GTD solution derived from applying Watson transformation to the modal series solution for the cylinder breaks down when the point of observation is close to the axial direction of the cylinder. This is because the effective wave number for propagation along the axis approaches zero, whereas the asymptotic solution requires that the wave number times the radius of the cylinder be large. Several different asymptotic solutions based on the modification of Fock's solution for the sphere problem have recently been presented for the axial region by a number of authors. The spectral-domain approach has been found useful not only for testing the relative accuracy of these solutions, but for iteratively improving them as well [45].

References

[1] E. C. Titchmarsh, *Introduction to the Theory of Fourier Integrals*. New York: Oxford, 1937.
[2] A. Papoulis, *The Fourier Integral and Its Applications*. New York: McGraw-Hill, 1962.
[3] R. N. Bracewell, *The Fourier Transform and Its Application*. New York: McGraw-Hill, 1965.
[4] I. N. Sneddon, *An Introduction to the Use of Integral Transforms*. New York: McGraw-Hill, 1972.
[5] A. Sommerfeld, *Partial Differential Equations in Physics*. New York: Academic, 1964.
[6] P. C. Clemmow, *The Plane Wave Spectrum Representation of Electromagnetic Fields*. London, England: Pergamon, 1966.
[7] D. S. Jones, *The Theory of Electromagnetism*. New York: Pergamon, 1964.
[8] M. Born and E. Wolf, *Principles of Optics*. New York: MacMillan, 1964.
[9] A. Banos, *Dipole Radiation in the Presence of Conducting Half-Space*. New York: Pergamon, 1966.
[10] B. Noble, *Methods Based on the Wiener-Hopf Techniques*. New York: Pergamon, 1958.
[11] R. Mittra and S. W. Lee, *Analytical Techniques in the Theory of Guided Waves*. New York: MacMillan, 1971.
[12] L. B. Felsen and N. Marcuvitz, *Radiation and Scattering of Waves*. Englewood Cliffs, NJ, Prentice-Hall, 1973.
[13] R. F. Harrington, *Field Computation by Moment Methods*. New York: MacMillan, 1968.
[14] R. Mittra, Ed., *Computer Techniques for Electromagnetics*. Oxford, England: Pergamon, 1973.
[15] Y. Rahmat-Samii, T. Itoh, and R. Mittra, "A spectral domain technique for solving microstrip line problems," *AEU Electron. Commun.*, Band 27, pp. 69-71, 1973.
[16] ——, "A spectral domain analysis for solving discontinuity problems," *IEEE Trans. Microwave Theory Tech.*, vol. MTT-22, pp. 372-378, Apr. 1974.
[17] T. Itoh and R. Mittra, "Spectral domain approach for calculating the dispersion characteristics of microstrip lines," *IEEE Trans. Microwave Theory Tech.*, vol. MTT-21, pp. 496-499, July 1973.
[18] J. B. Davies and D. Mirsnekar-Syahkal, "Spectral domain solution of arbitrary coplanar transmission line with multilayer substrate," *IEEE Trans. Microwave Theory Tech.*, vol. MTT-25, pp. 143-146, Feb. 1977.
[19] R. Mittra and T. S. Li, "A spectral domain approach to the numerical solution of electromagnetic scattering problems," *AEU Electron. Commun.*, Band 29, pp. 217-222, 1975.
[20] T. S. Li and R. Mittra, "Applications of the spectral domain approach for numerical solution of electromagnetic scattering from corner reflectors, prisms and rectangular plates," *AEU Electron. Commun.*, Band 29, pp. 323-333, 1975.
[21] N. N. Bojarski, "K-space formulation of the electromagnetic scattering problem," Tech. Rep. AFAL-TR-71-75, Mar. 1971.
[22] J. B. Keller, "Diffraction by an aperture," *J. Appl. Phys.*, vol. 28, pp. 426-444, 1957.
[23] ——, "Geometrical theory of diffraction," *J. Opt. Soc. Am.*, vol. 52, pp. 116-130, 1962.
[24] G. A. Deschamps, "Ray techniques in electromagnetics," *Proc. IEEE*, vol. 60, pp. 1022-1035, 1972.
[25] S. W. Lee, "Electromagnetic reflection from a conducting surface: Geometrical optics solution," *IEEE Trans. Antennas Propagat.*, vol. 23, pp. 184-191, 1975.

[26] R. G. Kouyoumjian, "The geometrical theory of diffraction and its application," in *Numerical and Asymptotic Techniques in Electromagnetics*. R. Mittra, Ed. New York: Springer-Verlag, 1975, ch. 6.

[27] H. Bach, "Engineering applications of the geometrical theory of diffraction," in *Modern Topics in Electromagnetics and Antennas*. E. J. Maanders and R. Mittra, Eds. London, England: Peter Peregrinus, 1977, ch. 5.

[28] S. W. Lee, "Uniform asymptotic theory of electromagnetic edge diffraction: A review," EM Rep. 77-1, Electromagnetics Lab., University of Illinois, Urbana, Il 1977. (This report includes some 300 references.)

[29] R. M. Lewis, D. S. Ahluwalia, and J. Boersma, "Uniform asymptotic theory of diffraction by a plane screen," *SIAM J. Appl. Math.*, vol. 16, pp. 783-807, 1968.

[30] R. G. Kouyoumjian and P. H. Pathak, "A uniform geometrical theory of diffraction for an edge in a perfectly conducting surface," *Proc. IEEE*, vol. 62, pp. 1448-1461, 1974.

[31] S. W. Lee and G. A. Deschamps, "A uniform asymptotic theory of electromagnetic diffraction by a curved wedge," *IEEE Trans. Antennas Propagat.*, vol. 24, pp. 25-34, Jan. 1976.

[32] P. Ya. Ufimtsev, *Method of Edge Waves in the Physical Theory of Diffraction*, Air Force Systems Command, Foreign Tech. Div. Document ID No. FTD-HC-23-259-71, 1971. (Translation from the Russian version published by Soviet Radio Publication House, Moscow, USSR, 1962.)

[33] K. M. Mitzner, "Studies in physical optics," Tech. Rep. AFAL-TR-74-22, Air Force Avionics Lab., Wright-Patterson Air Force Base, OH, 1974.

[34] S. W. Lee, "Comparison of uniform asymptotic theory and Ufimtsev's theory of electromagnetic edge diffraction," *IEEE Trans. Antennas Propagat.*, vol. 25, pp. 162-170, Mar. 1977.

[35] Y. Rahmat-Samii and R. Mittra, "Spectral analysis of high frequency diffraction of an arbitrary incident field by a half plane—Comparison with four asymptotic techniques," *Rad. Sci.*, vol. 13, pp. 31-48, Jan./Feb., 1978.

[36] R. Mittra, Y. Rahmat-Samii, and W. L. Ko, "Spectral theory of diffraction," *Appl. Phys.*, vol. 10, pp. 1-13, Jan. 1976.

[37] Y. Rahmat-Samii and R. Mittra, "A spectral domain interpretation of high frequency diffraction phenomena," *IEEE Trans. Antennas Progagat.*, vol. 25, pp. 676-687, Sept. 1977.

[38] W. L. Ko and R. Mittra, "A new approach based on a combination of integral equation and asymptotic techniques for solving electromagnetic scattering problems," *IEEE Trans. Antennas Propagat.*, vol. 25, pp. 187-197, Mar. 1977.

[39] R. Mittra and W. L. Ko, "An approach to high-frequency scattering from smooth convex surfaces," *IEEE Trans. Antennas Propagat.*, vol. 25, pp. 781-788, Nov. 1977.

[40] W. L. Ko and R. Mittra, "A new look at the scattering of a plane wave by a rectangular cylinder," *AEU Electron. Commun.*, pp. 494-500, Dec. 1977.

[41] Y. Rahmat-Samii and R. Mittra, "On the investigation of diffracted fields at the shadow boundaries of staggered parallel plates—A spectral domain approach," *Rad. Sci.*, vol. 12, pp. 659-670, Sept./Oct. 1977.

[42] R. Mittra and Y. Rahmat-Samii, "A spectral domain approach for solving high frequency scattering problems," in *Electromagnetic Scattering*, P.L.E. Uslenghi, Ed. New York: Academic, 1978.

[43] G. L. James, *Geometrical Theory of Diffraction for Electromagnetic Waves*. London, England: Peter Peregrinus, Ltd., 1976.

[44] M. Tew and R. Mittra, "Accuracy tests for asymptotic solutions to radiation from a cylinder," University of Illinois at Urbana-Champaign, EM Lab Tech. Rep. No. 77-22, Oct. 1977; see R. Mittra and M. Tew, "Accuracy tests for high frequency asymptotic solutions," *IEEE Trans. Antennas Propagat.* (to be published).

[45] —, "Reciprocity test for asymptotic solutions," National Radio Science Meeting, Boulder, CO, Jan. 1978; see R. Mittra and M. Tew, "An integral E-field accuracy test for asymptotic solutions" (to be published).

[46] R. E. Collin and F. J. Zucker, *Antenna Theory*. New York: McGraw-Hill, 1969.

[47] A. W. Maue, "Formulation of general diffraction problems through an integral equation," *Zeitschrift fur Physik*, vol. 126, pp. 601-619, 1949.

[48] W. D. Burnside, C. L. Yu, and R. J. Marhefka, "A technique to combine the geometrical theory of diffraction and the moment method," *IEEE Trans. Antennas Propagat.*, vol. AP-23, pp. 551-558, July 1975.

[49] W. L. Ko and R. Mittra, "High frequency scattering from smooth surfaces with edges—A spectral domain approach," presented at the National Radio Science Meeting at the University of Colorado (Boulder, CO, Nov. 1978).

[50] N. C. Albertsen, "A diffraction coefficient for the vertex of a quarter-plane," The Technical University of Denmark, Lyngby, Denmark, Applied Mathematical Physics Lab. Rep., 1976.